

MECHANISTIC STUDIES ON *E. COLI* DNA POLYMERASE III HOLOENZYME
AT THE REPLICATION FORK

by

QUAN YUAN

B.S., Peking University, 2004

A thesis submitted to the
Faculty of the Graduate School of the
University of Colorado in partial fulfillment
of the requirement for the degree of
Doctor of Philosophy
Department of Chemistry and Biochemistry
2013

This thesis entitled:
Mechanistic studies on *E. coli* DNA polymerase III holoenzyme at the replication
fork written by Quan Yuan
has been approved for the Department of Chemistry and Biochemistry

Charles McHenry

Robert Kuchta

Date _____

The final copy of this thesis has been examined by the signatories, and we
find that both the content and the form meet acceptable presentation standards
of scholarly work in the above mentioned discipline

Quan Yuan (Ph.D., Biochemistry)

Mechanistic studies on *E. coli* DNA polymerase III holoenzyme at the replication fork

Thesis directed by Professor Charles McHenry

The *E. coli* chromosome is replicated by a dimeric DNA polymerase III holoenzyme (Pol III HE) in a reaction where continuous leading and discontinuous lagging strand synthesis are coupled. Two models have been proposed to depict how a lagging strand polymerase dissociates from the preceding Okazaki fragment and cycle to the next primer. The collision model proposes that the polymerase collides with the 5'-end of the preceding Okazaki fragment and triggers release, whereas the signaling model suggests that the polymerase is signaled to cycle by synthesis of a new primer by primase. I developed a mini-circle DNA replication system with a highly asymmetric G:C distribution between DNA strands to differentiate these models. Specific perturbations of lagging strand synthesis by incorporation of ddGTP (chain termination) or dGDPNP (decreased elongation rate) on dCMP-containing lagging strand template confirm the signaling model and rule out the collision model. The lagging strand polymerase elongates much faster than the leading strand polymerase, explaining why gaps between Okazaki fragments are not found under physiological conditions. The presence of a primer, not primase, provides the signal to trigger cycling. Full-length Okazaki fragments (in the presence of dNTPs) and equivalent gaps between fragments (in the presence of dGDPNP) were obtained using reconstituted *E. coli* replicase regardless of the number of the τ DnaX subunits present in the clamp loader.

I characterized an intrinsic helicase-independent strand displacement activity of the DNA Pol III HE and found that Pol III is stabilized by an interaction with SSB on the

displaced strand by a Pol III- τ - ψ - χ -SSB interaction network. PriA, the initiator of replication restart on stalled replication forks, blocks the displacement reaction.

E. coli SSB functions as a homotetramer with each subunit possessing a C-terminus interacting with other proteins that function in DNA replication and repair. To assess how many C-termini of SSB are required for function in DNA replication, I carried out rolling circle DNA replication assays using concatemeric forms of SSB that possess only one or two C-termini. I discovered that SSB “tetramers” with one C-terminus cause a decrease in DNA synthesis and uncouples leading and lagging strand synthesis.

ACKNOWLEDGEMENTS

I would like to express my deepest gratitude to my advisor, Professor Charles McHenry, for his excellent guidance, great patience, and constant support. Without his advice and encouragement this dissertation would not have been possible.

I appreciate the guidance from my thesis committee: Professor Robert Kuchta, Professor James Goodrich, Professor Marcelo Sousa, and Professor Tom Perkins.

I appreciate all the help from my labmates over the years. In particular, I thank Dr. Paul Dohrmann and Dr. Garry Dallmann who have been a constant source of encouragement and wisdom throughout my years in the lab. They are excellent teachers who taught me almost all the techniques I used in the lab and helped me develop my background in biochemistry and molecular biology. Dr. Carol Manhart has been my labmate and classmate for the last 7 years and I am grateful for her support and company. Also, I thank Diane Hager for all of her help in everything.

I would like to thank my parents who always support me. Many thank to all my friends who helped me and encouraged me all the time.

Finally, I am indebted to my husband who has given me all his love in the past 13 years.

Table of Contents

CHAPTER

I. Introduction.....	1
1.1 Components in an <i>E. coli</i> DNA Replication System	2
1.1.1 Background of the <i>E. coli</i> polymerase III holoenzyme.....	3
1.1.2 <i>E. coli</i> Pol III α	3
1.1.3 DnaX complex clamp loader	5
1.1.4 Single-stranded binding proteins	7
1.1.5 Primosomal proteins	8
1.2 Initiation Complex Formation	9
1.3 DNA elongation	13
1.3.1 Mechanisms of lagging strand polymerase cycling	13
1.3.2 Processivity switch of Pol III HE	17
1.3.3 Do leading and lagging strand synthesis have the same rate?	19
1.3.4 Polymerase exchange at the replication fork	21
1.3.5 Strand displacement activity of Pol III HE	23
1.4 Research Goals.....	24
II. Strand Displacement by DNA Polymerase III Occurs through a τ-ψ-χ Link to	
SSB Coating the Lagging Strand Template	27
2.1 Abstract	27
2.2 Introduction	28
2.3 Materials and Methods	30

2.4 Results	36
2.5 Discussion	48
III. Cycling of the <i>E. coli</i> Lagging Strand Polymerase is Triggered Exclusively by the Availability of a New Primer at the Replication Fork	52
3.1 Abstract	52
3.2 Introduction	53
3.3 Materials and Methods	56
3.4 Results	59
3.4.1 Establishing an efficient <i>E. coli</i> rolling circle replication system on tailed mini-circular templates with an asymmetric G:C distribution	59
3.4.2 Specific blockage of Okazaki fragment synthesis before completion does not terminate overall lagging strand synthesis, consistent with predictions of the signaling model	63
3.4.3 Selectively slowing the rate of lagging strand synthesis with dGDPNP results in cycling to the next primer before Okazaki fragment completion, consistent with the signaling model	65
3.4.4 The presence of dGDPNP does not significantly influence the frequency of primer synthesis or primer utilization	67
3.4.5 The signal for cycling of the lagging strand polymerase is the availability of a new primer at the replication fork and is not dependent upon the presence or action of DnaG primase	68

3.4.6 Pol III HE functions equivalently in coupled replication with one to three τ subunits	71
3.5 Discussion	72
IV. Multiple C-terminal tails within a single <i>E. coli</i> SSB homotetramer coordinate	
DNA replication and repair	80
4.1 Abstract	80
4.2 Introduction	81
4.3 Materials and Methods	85
4.4 Results	93
4.4.1 Design of covalently linked SSB subunits with two or one C-termini per four OB-folds	93
4.4.2 DNA binding properties of covalently linked SSB proteins	97
4.4.3 An SSB with at least two C-terminal tails is required for <i>E. coli</i> survival .	102
4.4.4 SSB with fewer than four C-terminal tails exhibits decreased stimulation of the DNA polymerase on single-stranded templates	105
4.4.5 SSB containing only one C-terminal tail is defective in supporting rolling circle replicative reactions that mimic chromosomal replication forks	106
4.4.6 A one-tailed SSB tetramer does not support replication restart	108
4.4.7 <i>E. coli</i> cells expressing two-tailed SSB tetramer are more resistant to the effects of DNA damage, but accumulate more mutations	110
4.5 Discussion	115
References	121

APPENDIX

1. Supplementary material for Chapter III	138
S1.1 Supplemental Results	138
S1.1.1 Establishing a coupled rolling circle replication system on a mini-circle template	138
S1.1.2 Preincubation of reaction components minimizes the lag phase and permits synchronization of the rolling circle reaction	145
S1.1.3 Increasing concentrations of ddGTP result in decreased levels of radioactive nucleotide incorporation in the lagging strand, but permit maintenance of linear synthesis rates	146
S1.1.4 dGDPNP displays a higher apparent K_m for the DNA polymerase III holoenzyme-catalyzed reaction and can be used to modulate the elongation rate	147
S1.1.5 dGDPNP does not severely perturb the processivity of Pol III*	150
S1.2 Supplemental Materials and Methods	152
S1.3 Supplemental References	162
2. Supplementary material for Chapter IV	164
S2.1 Supplemental Materials and Methods	164
S2.2 Supplementary Table and Figures	174
S2.3 Supplemental References	181
3. Investigation on <i>E. coli</i> Pol III Exchange at the Replication Fork.....	183

S3.1 Introduction	183
S3.2 Results	184
S3.2.1 Exogenous D403E Pol III does not exchange with replicative Pol III at the replication fork	184
S3.2.2 Exogenous D403E E. coli Pol III* exchanges with replicative Pol III* at the replication fork	185
S3.2.3 The DnaX complex with inactive one ATPase is not competent for rolling circle DNA replication	187
S3.3 Materials and Methods	189
S3.4 References	191

Tables

Table 1.1 Subunits of <i>E. coli</i> DNA Pol III HE	2
Table 2.1 Steady state kinetic parameters for Pol III HE in single-stranded replication and strand displacement	38
Table 3.1 Determination of primer utilization and priming frequency	68
Table 4.1 Different <i>ssb</i> gene construct and phenotypes	105
Table S2.1 Plasmids used in this study (- <i>a</i> or - <i>t</i> denotes plasmids carrying resistance to either ampicillin or tetracycline respectively)	174

Figures

Figure 1.1 Diagram of Pol III HE at the replication fork.	3
Figure 1.2 Diagram of Pol III α	5
Figure 1.3 Contacts made by Pol III α , γ , and β on the primed template determined in cross-linking assays	9
Figure 1.4 Two pathways for initiation complex formation.	12
Figure 2.1 Requirements for Pol III HE components for strand displacement..	38
Figure 2.2 A Pol III- τ - ψ - χ complex is required for strand displacement.....	40
Figure 2.3 The C-terminal protein interaction sequence of SSB is required to support strand displacement.	42
Figure 2.4 The rate of strand displacement by Pol III HE is 150 nt/s.	43
Figure 2.5 Approximately one-third of the elongating Pol III HE dissociates upon encountering a flap and then displaces greater than 24 nucleotides processively.	44
Figure 2.6 Pol III HE adds 280 nucleotides processively during strand displacement ...	46
Figure 2.7 PriA inhibits the strand displacement reaction	47
Figure 2.8 Model for the strand displacement reaction with Pol III HE subunits.	50
Figure 3.1 Reactions conducted at high template concentration and substoichiometric helicase and Pol III* become dependent upon PriA and SSB.....	62

Figure 3.2 ddGTP halts Okazaki fragment synthesis before completion, but lagging strand synthesis continues.	64
Figure 3.3 Replacement of dGTP with dGDPNP leads to short Okazaki fragments followed by large gaps.....	67
Figure 3.4 The availability of primers signals the polymerase to cycle.	70
Figure 3.5 Pol III* reconstituted with DnaX complexes containing τ_3 , $\tau_2\gamma_1$, and $\tau_1\gamma_2$ produce the same length lagging strand products	72
Figure 3.6 Proposed sequence of events in cycling of lagging strand polymerase during Okazaki fragment synthesis.	79
Figure 4.1 Design of linked SSB tetramers.	95
Figure 4.2 Characterization of linked SSB tetramers.	96
Figure 4.3 ssDNA binding properties of linked SSB tetramers.....	101
Figure 4.4 SSB tetramers with only one C-terminal tail show decreased stimulation of DNA replication	108
Figure 4.5 SSB-LT-Drl does not support PriA-dependent replication restart pathway.	110
Figure 4.6 <i>In vivo</i> repair capabilities of E.coli strains carrying wt SSB or ssb-LD-Drl genes.....	113
Figure 4.7 Growth characteristics of E.coli cells carrying either four or two-tailed SSB tetramers.	114
Figure S1.1 Protein requirements for E. coli rolling circle reactions on 1 nM mini-circle DNA template	140

Figure S1.2 Protein requirements for <i>E. coli</i> rolling circle reactions on 10 nM mini-circle DNA template.....	142
Figure S1.3 Protein requirements for <i>E. coli</i> rolling circle reactions on 20 nM mini-circle DNA template.....	144
Figure S1.4 Preincubation of reaction components in the presence of ATP γ S supports formation of a preinitiation complex and elimination of a lag phase.....	146
Figure S1.5 A linear rate of Okazaki fragment synthesis is maintained as the concentration of ddGTP increases	147
Figure S1.6 dGDPNP can be used to modulate the rate of elongation on cytosine-containing templates	149
Figure S1.7 The processivity of Pol III* is about 2700 bp in the presence of dGTP and 1600 bp in the presence of dGDPNP	151
Figure S1.8 dGDPNP does not perturb the frequency of primer synthesis or the primer utilization	152
Figure S1.9 Important intermediate products and final product of mini-circle template preparation	155
Figure S1.10 Preparation of mini-circle DNA template	156
Figure S1.11 Conditions of the gap filling assay were explored	162
Figure S2.1 Schematic representation of the various SSB constructs used in this study	175
Figure S2.2 Sedimentation and quenching of SSB-LD and SSB-LT	176

Figure S2.3 Stability of linked SSB tetramers	177
Figure S2.4 Binding affinity of SSB to (dT) ₇₀ in NaBr	178
Figure S2.5 smFRET analysis showing diffusion and duplex melting activities of SSB tetramers	179
Figure S2.6 Interaction between SSB and χ monitored using ammonium sulfate precipitation analysis	180
Figure S2.7 Rate of spontaneous mutagenesis in <i>E. coli</i> cells carrying the SSB protein from <i>Deinococcus radiodurans</i> (Drad-SSB)	181
Figure S3.1 <i>E. coli</i> Pol III at the replication fork is resistant to inhibition of D403E Pol III	185
Figure S3.2 D403E Pol III* outcompetes the Pol III* at the replication fork	187
Figure S3.3 Pol III* with the DnaX complex ($\tau_2\gamma_1$) containing an inactive ATPase cannot support the rolling circle reaction as Pol III* with DnaX complex ($\tau_2\gamma_1$).	189

CHAPTER I

INTRODUCTION

1.1 Components in an *E. coli* DNA Replication System

1.1.1 Background of the *E. coli* polymerase III holoenzyme (Pol III HE)

The *E. coli* DNA Pol III HE is the replicative machinery responsible for both leading and lagging strand DNA synthesis (McHenry, 2003). Pol III HE is a tripartite assembly encompassing a replicative polymerase (Pol III), a sliding clamp processivity factor (β_2), and a clamp loader that assembles the sliding clamp around DNA (the DnaX complex) (McHenry, 2003). 10 different subunits (α , ϵ , θ , τ , γ , δ , δ' , χ , ψ , and β) form *E. coli* Pol III HE (Table 1.1). Pol III is composed of three subunits: the replicative polymerase α responsible for nucleotide incorporation, 3' to 5' exonuclease ϵ for proofreading, and θ with an unknown function. The DnaX complex is composed of seven subunits (DnaX₃ $\delta\delta'\chi\psi$). The DnaX subunits have two types, τ and γ . τ is the full length product of *dnaX*, and γ is a shorter one resulting from translational frameshifting (Flower and McHenry, 1990). The τ subunit can be subdivided into five domains (I-V), and the γ subunit shares the first three domains (I-III). Domain I and II of both τ and γ are ATP-binding domains. Domain III of τ and γ bind other DnaX subunits, δ , δ' , and ψ . Domain IV of τ binds DnaB helicase, stabilizing the replicase at the fork and accelerating the rate of replication fork progression (Kim et al., 1996b; Gao and McHenry, 2001c). Domain V of τ interacts with Pol III, so that two τ subunits dimerize both polymerases on the leading and lagging strands (Gao and McHenry, 2001b). The δ subunit interacts with β_2 to open the clamp (Jeruzalmi et al., 2001b). The δ' subunit remains rigid with limited conformational change (Jeruzalmi et al., 2001a). The N-

terminus of ψ wraps around the C-termini of the DnaX subunits to stabilize the complex (Glover and McHenry, 2000; Anderson et al., 2007; Simonetta et al., 2009). χ binds ψ and single-stranded binding proteins (SSB), stabilizing the interaction between SSB-coated template and polymerase via the Pol III- τ - ψ - χ -SSB network (Glover and McHenry, 1998; Yuan and McHenry, 2009) (Fig. 1.1).

A hexameric helicase, DnaB, precedes replisome and translocates along the lagging strand to unwind double stranded DNA in a 5' to 3' direction using the energy of ATP hydrolysis (LeBowitz and McMacken, 1986). Primase DnaG is recruited onto the lagging strand via DnaB to synthesize RNA primers that are elongated by Pol III HE to form Okazaki fragments. SSB coats the exposed single-stranded DNA of the lagging strand (Fig. 1.1) (McHenry, 2011b). Subsequently, RNA primers are excised and resulting gaps are filled by DNA polymerase I. The nicks between Okazaki fragments are sealed by a DNA ligase (Kornberg and Baker, 1992).

Subunit	Structural gene	M.W. (kD)	Function	Subassembly	
α	dnaE	129.9	Polymerase	Pol III	Pol III*
ϵ	dnaQ	26.9	3'→5' exonuclease		
θ	hoIE	8.8	Unknown		
τ	dnaX	71.0	Dimerizes pol, chaperones pol to β , interacts with DnaB and ψ , ATPase, loads β with auxiliary subunits	DnaX complex	
γ	dnaX	47.4	ATPase, loads β with auxiliary subunits		
δ	hoIA	38.7	Binds β		
δ'	hoIB	36.9	Bridge between DnaX and β		
χ	hoIC	16.6	Binds DnaX and SSB		
ψ	hoID	15.0	Bridge between DnaX and χ		
β	dnaN	40.6	Processivity factor		

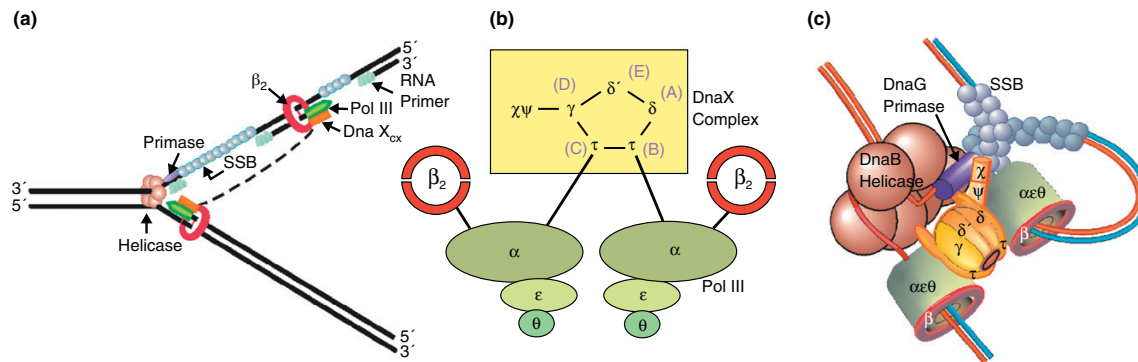
Table 1.1 Subunits of *E. coli* DNA Pol III HE

Figure 1.1 Diagram of Pol III HE at the replication fork. (A) Helicase translocates on the lagging strand to split the parental duplex preceding the leading strand polymerase. SSB coats on the single stranded lagging strand. Primase associates with the helicase and synthesizes RNA primers elongated by lagging strand polymerase. A DnaX complex is shared by leading and lagging strand polymerase at the replication fork (dotted line). (B) Three subassemblies, Pol III, β_2 , and DnaX complex, form Pol III HE. Interactions among 10 subunits in *E. coli* DNA Pol III HE are shown. (C) A cartoon of the replication fork. DnaB helicase interacts with DnaG primase and τ . τ also binds two polymerases. SSB associates with DnaG primase and χ (McHenry, 2011a).

1.1.2 *E. coli* Pol III α

The N-terminus of *E. coli* Pol III α includes a polymerase domain and a PHP (Polymerases and Histidinol Phosphatase) domain, while the C-terminus includes a β_2 binding domain, an OB-fold domain, and a τ -binding domain (Fig. 1.2).

The polymerase domain of Pol III α contains palm, thumb, and fingers subdomains, forming a cupped right hand shape. The palm domain provides the active site for polymerization catalysis with three aspartates (D401, D403, D555) that bind the magnesium ions needed for the catalytic triad mechanism (Pritchard and McHenry, 1999) (Fig. 1.2). The fingers domain binds the incoming nucleotide and the ssDNA

template, and the thumb domain binds the duplex DNA. The PHP domain, located in the extreme N-terminus of Pol III α , functions as a coediting exonuclease with Zn^{2+} -dependent 3' \rightarrow 5' proofreading activity targeting mispaired nucleotides (Stano et al., 2006), and also interacts with the classical Mg^{2+} -dependent exonuclease ϵ to presumably provide a channel for the transfer of 3' mismatched terminus from polymerase to exonuclease ϵ (Wieczorek and McHenry, 2006).

The β_2 binding domain of Pol III α resides in the internal C-terminus. This C-terminal domain also possesses dsDNA binding ability through a helix-hairpin-helix (HhH) motif and flanking loops. The extreme end of the C-terminus contains a τ -binding site rather than a β_2 binding domain as once proposed (Leu et al., 2003). Mutations in that binding site only cause 2-fold decrease in β_2 binding but 400-fold decrease in τ binding (Dohrmann and McHenry, 2005). This τ -binding site is loosely packed against the Oligonucleotide Binding (OB) fold (Bailey et al., 2006), which was close to the primer terminus in a crystal structure of the complex of Pol III α -primed template (Wing et al., 2008a) (Fig. 1.2).

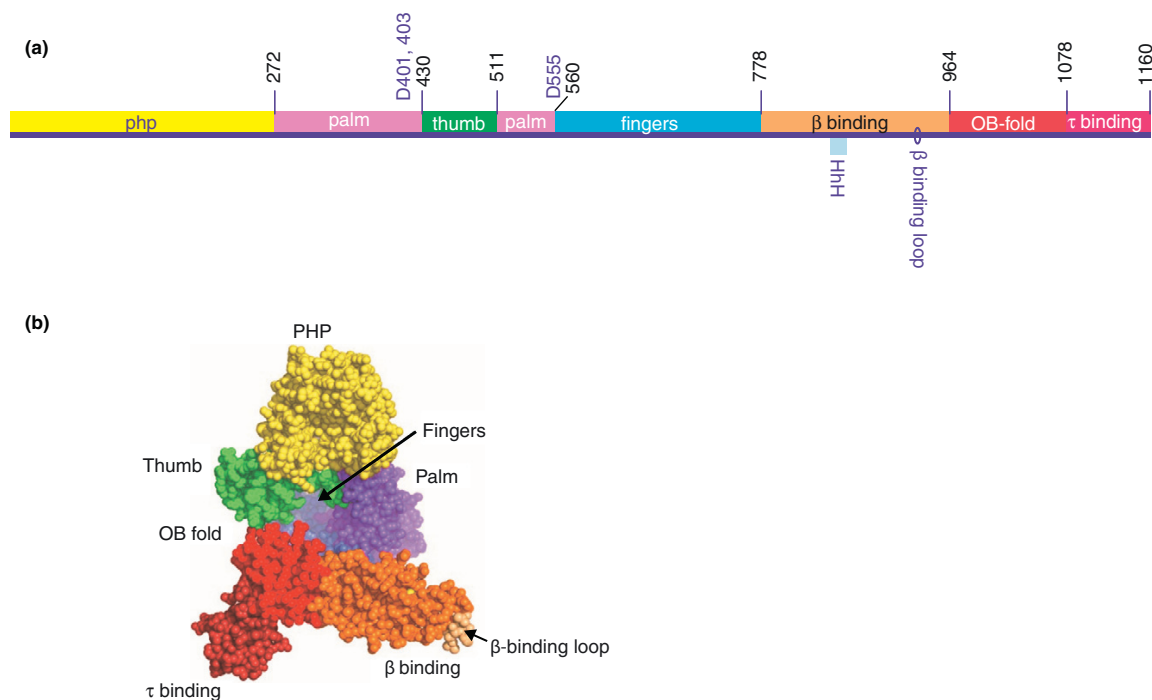


Figure 1.2 Diagram of Pol III α . (A) Domain organization of *E. coli* Pol III α (McHenry, 2011b). The numbers above the bar are domain borders. The three aspartates are the catalytic ones in the active site. The dsDNA binding HhH motif and β -binding loop in the β binding domain are also labeled. (B) A space-filling representation of the *Taq* Pol III α structure. The colors of domains are identical to (A). (McHenry, 2011a)

1.1.3 DnaX complex clamp loader

The DnaX complex is composed of the DnaX subunits (τ or γ), δ , and δ' , but the complex composition can change depending on the number of τ or γ subunits that reside. Although it can be reconstituted as a τ - or γ -only complex ($\tau_3\delta\delta'\chi\psi$ or $\gamma_3\delta\delta'\chi\psi$) *in vitro*, $\tau_2\gamma\delta\delta'\chi\psi$ is believed to be the composition of the DnaX complex in cells, because purified Pol III HE from overproducer strains contains both τ and γ subunits (McHenry, 1982; Cull and McHenry, 1995; Pritchard et al., 2000). Some researchers suspected that there were no γ subunits in the cellular DnaX complex and the γ -sized protein was a proteolyzed form of the τ subunit cleaved by OmpT (outer membrane protein T)

(McInerney et al., 2007). To date, we have found several lines of evidence to prove that this notion is wrong. First of all, it was confirmed that the misleading γ -sized fragment of τ proteolyzed by protease was two amino acids shorter than the authentic γ subunit. In *ompT* mutant strains, the proteolyzed product did not appear. In addition, proteolysis can be avoided with careful cell lysis handling preventing potential γ -sized proteins (Pritchard et al., 1996). Second, a mutant DnaX complex overproducer that cannot frameshift yields only τ -containing DnaX complex (Pritchard et al., 1996). Third, our lab discovered that either in *ompT* mutant strains or wild-type (wt) strains, Pol III HE contains the same amount of γ (unpublished data). Fourth, γ has been determined in cross-linking experiments to have a specific position next to τ in authentic DnaX complexes (Glover and McHenry, 2000). We believe based on all available evidence that native DnaX complex is composed of $\tau_2\gamma\delta\delta'\chi\psi$.

The crystal structure of the γ complex ($\gamma_3\delta\delta'$) bound to a primer-template and a segment of ψ confirmed the composition of the γ complex. The ATP analogue, ADP•BeF₃, binds to each of the three γ subunits in the crystal structure. The AAA+ modules of δ' and the three γ were organized in a symmetrical right-handed spiral shape wrapping around the DNA template via interactions with the phosphate backbone. δ disengages from the spiral structure probably because of the lack of clamp binding that should provide extra interactions as a scaffold. The template's ssDNA 5' overhang exits the central cavity of the complex from the gap between δ and δ' . The primer has no interactions with the complex, except the last base interacts with δ Tyr316. The fragment of ψ subunit winds through the collar domains of the three γ subunits making

different contacts with each subunit, preventing more ψ subunits from binding (Simonetta et al., 2009).

The τ subunit is a multi-functional protein in the DnaX complex. Besides its role as an ATPase, τ has been found to be required to dimerize the leading and lagging strand polymerase and couple the synthesis on two strands via domain V (Kim et al., 1996b). BIAcore experiment results show that domain IV of τ interacts with DnaB, and more than one τ subunit is required to bind DnaB for a physiological affinity (Gao and McHenry, 2001b). It is proposed that τ couples DnaB and polymerase, leading to acceleration of both DnaB and polymerase movement to the physiological magnitude (400 nt/s) (Kim et al., 1996a). It is also found that τ protects β from unloading by the γ complex (Kim et al., 1996c; Turner et al., 1999). Furthermore, τ plays a passive role in bridging Pol III and SSB via interaction of τ - ψ - χ (Glover and McHenry, 1998; Yuan and McHenry, 2009). Recently our lab proposed that the τ -containing DnaX complex loads clamps onto DNA and chaperones the associated Pol III onto the newly loaded clamp (Downey and McHenry, 2010).

1.1.4 Single-stranded binding proteins (SSB)

SSB are homotetramers bound with ssDNA. SSB itself has no known catalytic function, but it plays significant roles in protecting ssDNA from digestion by exonucleases, eliminating secondary structures on ssDNA that otherwise impede DNA replication, recombination and repair, and mediating many protein interactions (Meyer and Laine, 1990). Each protomer comprises two domains. The N-terminal domain is the DNA binding domain containing an oligonucleotide/oligosaccharide binding (OB)-fold

(residues 1-112) (Raghunathan and Kozlov, 2000). The majority of the C-terminal domain is disordered, except the extreme C-terminus possesses a conserved sequence (DDDIPF) responsible for interacting with more than a dozen of proteins, including χ , PriA, primase, exonuclease I (Shereda et al., 2008). Recently our lab discovered that SSB facilitated τ to chaperone Pol III using a region other than the conserved C-terminus (Downey and McHenry, 2010). Future experiments are required to determine the new binding site.

SSB can bind ssDNA in different modes, mainly (SSB)₃₅, (SSB)₅₅, and (SSB)₆₅, where the subscript is the number of nucleotides an SSB tetramer occludes (Bujalowski and Lohman, 1986). High salt concentration and low ratio of SSB to DNA favor the (SSB)₆₅ binding mode, by which SSB binds ssDNA with high affinity but low cooperativity (Lohman et al., 1986a). With this mode, SSB can randomly diffuse along DNA and thus transiently destabilize hairpins (Zhou et al., 2011). This mode is thought to mediate DNA repair and DNA recombination. In contrast, (SSB)₃₅ is usually seen with low salt concentration and with high ratio of SSB to DNA. The (SSB)₃₅ binding mode exhibits highly positive cooperation and facilitates the formation of clusters or filaments on ssDNA (Lohman et al., 1986a), which is proposed to be adopted in DNA replication (Lohman and Ferrari, 1994).

1.1.5 Primosomal proteins

Primosomal proteins are a series of proteins that reload the replicative machinery at a stalled replication fork. Restart primosomes include PriA, PriB, PriC, DnaT, DnaB, DnaC, and DnaG, all of which were originally discovered as necessary for the single-

stranded Φ 174 bacteriophage replication initiation (Schekman et al., 1975). The assembly of the primosomes in the restart pathway initiates from PriA binding to a replication fork in a structure-specific fashion, such as the three-stranded structure or a D loop, followed by the assembly of PriB and DnaT. Helicase DnaB is loaded in assistance with helicase loaders, DnaC, and primase DnaG is assembled subsequently (Liu and Marians, 1999; Heller and Marians, 2005). Pol III HE is then assembled to the fork, and leading and lagging strand DNA synthesis start coordinately. I established a rolling circle replication system using the primosomal proteins and Pol III HE, which was widely exploited in the studies described in this thesis.

1.2 Initiation Complex Formation

Prior to DNA elongation, a stable initiation complex forms on the primed DNA template in the presence of ATP (Johanson, 1982). A footprint experiment has revealed that an initiation complex occupies the upstream 30 nucleotides of a primer (Reems and McHenry, 1994). The linear arrangement of an initiation complex relative to a primer explored using site-specific photo cross-linking experiments exhibits that Pol III α contacts the upstream -13 of the primer, particular -9; the γ subunit contacts the upper -13 to -22, particularly -18; the β subunit binds at -22 (Reems et al., 1995) (Fig 1.3).

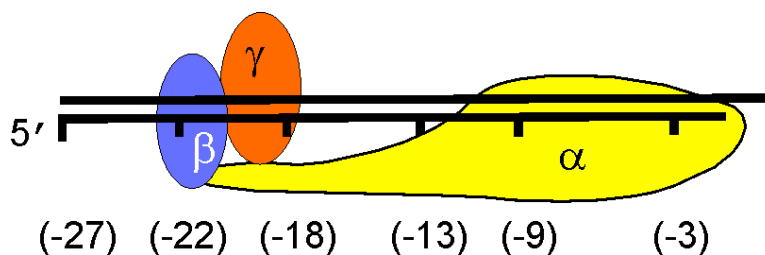


Figure 1.3 Contacts made by Pol III α , γ , and β on the primed template determined in cross-linking assays.

Initiation complex formation requires ATP binding and hydrolysis to modulate affinity among the γ complex, β and DNA. All five subunits of the pentameric complex are members of the AAA+ family of ATPases (ATPases associated with diverse cellular activities). The DnaX subunits τ and γ are active ATPases. δ and δ' are structurally homologous to the DnaX subunits but lack of active ATP binding sites (Jeruzalmi et al., 2001a; Bullard et al., 2002). ATP binding sites are positioned at the interface of domains I and II of the DnaX subunits. Arginine fingers from δ' , γ_1 , and γ_2 interact with the ATP bound on γ_1 , γ_2 , and γ_3 respectively, triggering ATP hydrolysis (Jeruzalmi et al., 2001a).

A structural study on the nucleotide-free $\gamma_3\delta\delta'$ complex suggests that binding of ATP to the γ subunit adjacent to δ causes δ to swing out of the sequestration of δ' , so that δ can interact with β and open the clamp (Jeruzalmi et al., 2001a). ATP binding not only enhances the affinity of the clamp loader for the clamp, but also for the primed template, thereby bringing all components together (Ason et al., 2000). Once the DnaX complex binds the primed template, bound ATP hydrolyzes immediately (Hingorani and O'Donnell, 1998; Ason et al., 2003). Bloom's kinetic study on the initiation complex formation with the γ complex shows that the rate of binding of the γ complex to the primed DNA template is slower than that to β_2 clamps unless the γ complex is preincubated with ATP, because the former interaction is limited by the slow ATP-induced conformational change, while the latter one is only determined by the rate of diffusion of proteins (Thompson et al., 2009). Because β binding to γ complex does not trigger ATP hydrolysis efficiently, the ordered binding may reduce the chance of ATP consumption without opening clamps, saving energy source for the cell (Ason et al., 2003).

Upon ATP hydrolysis, the affinity of the clamp loader for DNA and clamps decreases. Bloom's other kinetic study shows that upon ATP hydrolysis, the γ complex dissociates from DNA first, and then from β_2 (Anderson et al., 2009). It has been proposed that release of β_2 is the slowest step for a single clamp loading reaction (Anderson et al., 2009). However, at which step β_2 is closed is still unknown. For several continuous clamp loading cycles, dissociation of bound ADP from the released inactive DnaX complex has been determined to be the rate limiting step (Ason et al., 2003).

It has been proposed that three ATPs binding and hydrolysis occur in a synchronous wave (Johnson and O'Donnell, 2003). In order to test how many active ATPases are required for initiation complex formation, our lab generated a mutation on a Walker A motif (K53E) of both τ and γ , and reconstituted 10 types of DnaX complexes containing either wt or mutant τ or γ . Exploiting the reconstituted DnaX complexes, our lab has discovered that only one active ATPase is sufficient for initiation complex formation on ssDNA (Wieczorek et al., 2010). However, our pre-steady-state kinetics study shows that losing one active ATPase decreases the rate of initiation complex formation by 30 fold, which indicates three active ATPases support the physiologically relevant rate (Wieczorek et al., 2010; Downey et al., 2011).

In the past, assembly of the initiation complex was artificially divided into two stages: first, the DnaX complex loads β_2 onto DNA using ATP in the absence of polymerase. Second, after the DnaX complex dissociates from the template and β_2 , Pol III associates with the loaded β_2 to form a highly processive complex (Stukenberg et al., 1991). In fact, most studies on clamp loading were conducted in the absence of Pol III. Our lab discovered that the wild-type Pol III bound to the τ complex could resist

inhibition of D403E Pol III that only binds, not elongates, primers. This indicates that the clamp loader chaperones the associated replicative polymerase onto the clamp that was newly loaded onto DNA by the same DnaX complex in a coupled manner. That is, in the presence of τ and Pol III, initiation complex formation occurs in a tightly coupled fashion rather than two separated steps (Downey and McHenry, 2010). In this process, the DnaX complex dissociates from the primed DNA template after β_2 loading, but remains bound to Pol III because of the tight interaction between τ and α (Fig. 1.4). Compared to the unchaperoned pathway, chaperoning increases the rate of initiation complex formation by 100 fold and decreases the Pol III concentration required for efficient assembly (Downey and McHenry, 2010), which is much more in accordance with the physiological rate of Okazaki fragment synthesis (1-2 s).

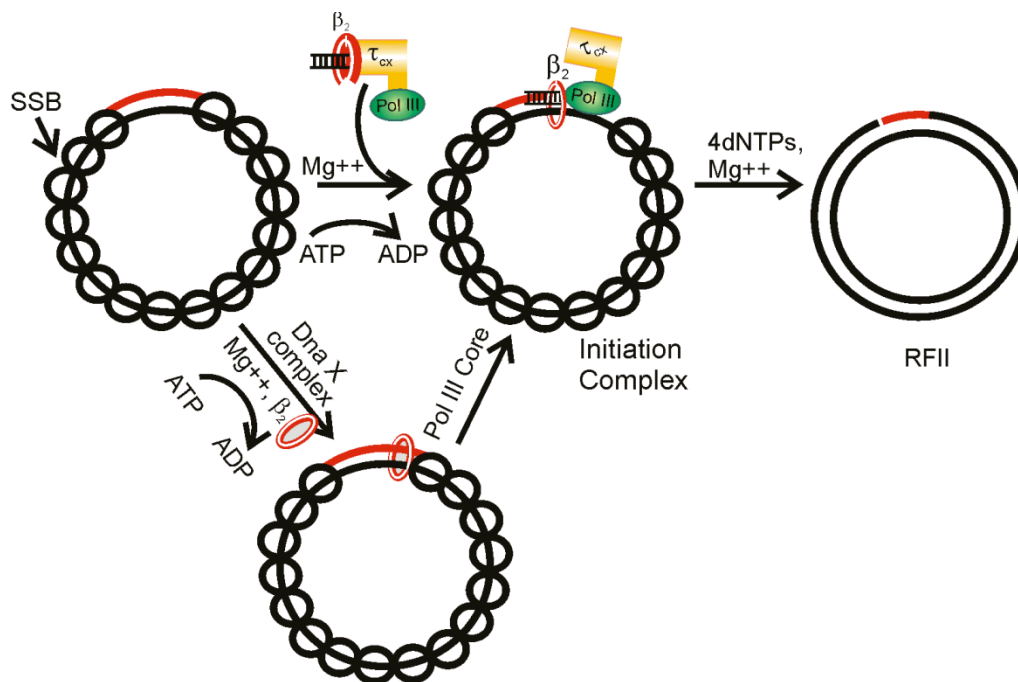


Figure 1.4 Two pathways for initiation complex formation. The top pathway is the chaperone pathway, whereby the DnaX complex containing τ loads β_2 and chaperones the Pol III to the same β_2 . The bottom pathway is the two-stage reaction, whereby the

DnaX complex (composed of either the γ or τ forms of DnaX or any combination) loads β_2 onto DNA first, and then Pol III can associate with the assembled β_2 after the DnaX complex dissociates.

Our lab has also discovered that Pol III and β_2 can form an initiation complex only on the leading strand in the presence of ATP γ S. Upon the addition of ATP, β_2 , and SSB, the ATP γ S-initiation complex can be assembled with the lagging strand. When ATP γ S is added to an isolated ATP-initiation complex, only the lagging strand half of the initiation complex dissociates. Furthermore, an initiation complex forms in an order and disassembles in a reversed order. In a rolling circle replication system with exogenous primers, the presence of ATP γ S cannot support lagging strand synthesis (Johanson and McHenry, 1984; Glover and McHenry, 2001). These results indicate Pol III HE is an asymmetrical dimer with distinguishable leading and lagging strand halves. This intrinsic structural asymmetry of Pol III HE reveals its functional asymmetry, which associates with distinct leading and lagging strand functions.

1.3 DNA elongation

1.3.1 Mechanisms of lagging strand polymerase cycling

The leading strand polymerase proceeds in the same direction as the replication fork movement, while the lagging strand polymerase moves in the opposite direction. To preserve directionality, the lagging strand must be synthesized discontinuously.

Therefore, while the leading strand polymerase proceeds continuously, the lagging strand polymerase must dissociate from a complete Okazaki fragment and bind to a new primer for another Okazaki fragment synthesis. Pol III HE has very high processivity. It can replicate at least 150,000 bp before dissociation (Mok and Marians,

1987). Thus, dissociation of the lagging strand polymerase from the preceding Okazaki fragment and cycling to a new primer must be regulated for the DNA replication process to proceed rapidly.

There are two competing but nonexclusive models of lagging-strand polymerase cycling, the collision model and the signaling model. The collision model was originally proposed by Albert for the T4 system (Alberts et al., 1983), and later extended to the *E. coli* system. The collision model suggests that the polymerase releases the primer and cycles to a new primer when the last nucleotide is replicated, or the synthesis of the current Okazaki fragment is almost complete (Leu et al., 2003; Georgescu et al., 2009). On the other hand, the signaling model posits that synthesis of a new primer signals polymerase to release and associate to the new primer, even though synthesis of the current Okazaki fragment is not complete yet (Wu et al., 1992).

The signaling model was first proposed by Marians (Wu et al., 1992). Gaps between Okazaki fragments were detected when Pol III was diluted below approximately 1 nM in replication fork reconstitution experiments (Wu et al., 1992). To further test the signaling model, primase was added to isolated rolling circle DNA with extremely long leading strand and replisome to bypass the existence of primers. Under this condition, all lagging strand products remained 2 kb, which suggested that primase induced cycling of lagging strand polymerase even at the first primer. Otherwise, more than 9 kb-long product should have been produced by free polymerase. In *E. coli*, primase concentration determines the frequency of priming and the length of Okazaki fragments, which led to the proposal that primase set the timing of events at the replication fork and provided the signal of lagging strand polymerase release and

recycling to the next primer (Tougu and Mariani, 1996b). When Exogenous primers were annealed to long rolling circle DNA to bypass the requirement of primase, distinct bands with the characteristic distance between primers were observed. This result was used to support the collision model since no primase existed in the system to be a signal (Li and Mariani, 2000). Actually, primase itself or some event involving primase may not be necessarily the signal that triggers cycling. The presence of primers serving as a signal to trigger the cycling could be an alternative interpretation for the products observed in the assay without primase. In Chapter III, I carefully tested this issue and determined that the availability of primers indeed signals lagging strand polymerase cycling.

In the bacteriophage T4 system, clear results suggested that the signaling model was predominant. Low concentration of dCTP added to reactions selectively decreased the rate of lagging strand synthesis on the rolling circle template when used with a dC-deficient leading strand. Shortened Okazaki fragments and ssDNA gaps between them was consistent with prediction of the signaling model, whereby the signal that presumably exhibited at a constant pace induced the lagging strand polymerase to release from the Okazaki fragment that it was currently elongating and left a ssDNA gap. If the collision model were correct, slow lagging strand synthesis would require more time to complete an Okazaki fragment while the replication fork was proceeding at a constant rate. As a consequence, the next primer elongated at the replication fork must be further away from the preceding one as several primers are skipped by polymerase, leading to longer Okazaki fragments (Yang et al., 2006). It was also observed that diluted clamp and clamp loader resulted in longer Okazaki fragments. Thus, Yang et al.

proposed that loading a clamp onto a new primer (primer utilization), instead of primer synthesis, might serve as a signal. Otherwise, the change of clamp and clamp loader concentration should have not affect the length of Okazaki fragment since primers were laid on the lagging strand evenly (Yang et al., 2006).

In the bacteriophage T7 system, Hamdan et al. utilized single-molecule techniques to visualize lagging strand loop formation (DNA shortening) and loop release (DNA lengthening) in a coordinated leading and lagging strand synthesis system by monitoring the moving distance of a bead that was attached on one end of the lagging strand. The lag time between preceding loop release and subsequent loop formation was also determined. They observed that reduced rNTP concentration causes longer loop length and longer lag time. In T7, primer synthesis starts with condensation of the ATP and CTP to form pppAC, and then two more ribonucleotides are incorporated at a much slower rate. In the presence of the reduced ATP and CTP concentration, adding premade pAC to bypass the condensation step restores the loop length to the original length produced with optimal amount of ATP and CTP, but the lag time did not change. This result suggests that condensation of pppAC triggers loop release and the lag time includes the slow primer synthesis step in addition to primer handoff to polymerase. (Hamdan et al., 2009).

The evidence behind the collision model was primarily based on modulation of binding affinities. Although the observation of decreased affinity of polymerase for DNA and β in several studies using equilibrium measurements seems to support the collision model (Leu et al., 2003; Georgescu et al., 2009), our lab has proved that the collision model is not a competent mechanism for lagging-strand polymerase cycling kinetically.

Since dNTP incorporation takes most of the time, polymerase dissociation and cycling must occur within a very short time period (<0.1 s) upon collision with the preceding Okazaki fragment. A surface plasmon resonance study was conducted to investigate the kinetics of polymerase dissociation from a mimicked Okazaki fragment. A blocking oligonucleotide mimicking the preceding Okazaki fragment was annealed downstream 10 nt away from the primer. The off rate of polymerase dissociation was about 2-5 min when the gap was filled with the last dNTP, whereas it shortened to 30 s when ATP and an exogenous primed template were also present. Nonetheless, the off rate is still too slow to support the collision model compared with the expected physiological value (Dohrmann et al., 2011). Furthermore, strand displacement occurred for most of the primed template after the gap was filled in these experiments, which at least implied that collision was not a precise mechanism for polymerase dissociation (Dohrmann et al., 2011).

1.3.2 Processivity switch of Pol III HE

Although high processivity is necessary for *E. coli* to replicate the whole genome, a processivity switch is required for the lagging strand polymerase to rapidly dissociate from the lagging strand. Several subunits or subunit elements have been proposed to function as a sensor to modulate binding affinities among the polymerase, template and β_2 . A mechanism in which τ sensed the conversion of a gap to a nick and competed with the β processivity factor for binding to the C-terminus of the Pol III α subunit was proposed. τ was thought to be able to recognize the change of DNA structure from a single nucleotide gap to a nick, and enhance the Pol III α to bind primed template rather

than a nick (Leu et al., 2003; López de Saro et al., 2003a, 2003b). In fact, a cross-linking experiment showed that τ did not bind downstream of a single-stranded template and hence could not act as a DNA structure sensor or regulate the interaction according to the DNA structure. Furthermore, it has been proven that a proposed C-terminal β binding site at 1154-1160 aa within α interacted with τ much more significantly than β . Therefore, there is no apparent competition between τ and β for binding α (Dohrmann and McHenry, 2005). In contrast, through the cross-linking experiment, it has been determined that Pol III α is the protein that immediately collides with the preceding Okazaki fragment and the template (Dohrmann et al., 2011).

The OB fold of Pol III α has also been proposed to be the processivity switch. Because the ssDNA binding portion of Pol III was localized to a C-terminal region of α that contains the OB fold element (McCauley et al., 2008) and the OB fold seems to be positioned close to the ssDNA template in advance of the primer terminus in the crystal structure, it was proposed that upon completing synthesis of an Okazaki fragment, the OB fold lost the contact with ssDNA and consequently triggered the release of Pol III α from β (Wing et al., 2008b). To test this hypothesis, three basic residues on the β_1 - β_2 loop of the OB fold (a region known to contribute to ssDNA binding) were mutated to serine, which caused loss of affinity of the OB fold for ssDNA oligonucleotide (Georgescu et al., 2009). Pol III containing the OB mutation became less processive than wt Pol III core, but the presence of τ restored the processivity (Georgescu et al., 2009). The recovery by τ seems to suggest that the OB fold is not an indispensable processivity sensor. Furthermore, because the K_d of OB fold bound to ssDNA was close to the detection limit of fluorescence anisotropy, the result of no binding of the

mutant OB fold to ssDNA became less reliable. It is also possible that the three mutations may not be the critical ones for sensing the switch (McHenry, 2011b).

Considering extensive conformational changes of Pol III α upon substrate binding, it was also posited that the entire polymerase active site might be the processivity switch (Dohrmann et al., 2011). When Pol III α binds DNA, the β_2 binding domain rotates 20°, thereby permitting the dsDNA binding motif (HhH) to interact with DNA and placing the β_2 binding domain close to the β clamp (Wing et al., 2008b). When the last nucleotide is inserted, the active site of α may lose affinity for the substrate, which triggers a reversed conformational change and diminished contact between α and β . It has been found that mutation of the β binding domain, which eliminates its ability of β binding, leads to decreased processivity of Pol III*, consistent with this hypothesis (Kim and McHenry, 1996b).

In Chapter III, I proposed that the DnaX complex serves as a sensor. More details are discussed there.

1.3.3 Do leading and lagging strand synthesis have the same rate?

A model system with bacteriophage T7 was used to determine the rate of leading and lagging strand synthesis. A single molecule experiment demonstrated that the lag time between the lagging strand loop release and the next loop formation was about 12 s. It was postulated that primer synthesis, lagging strand polymerase release, and association on a new primer occurred during such a long lag time (Pandey et al., 2009). Since all these steps require a large amount of extra time in addition to lagging strand synthesis, how to coordinate leading and lagging strand synthesis becomes an issue.

Lee et al. conducted single molecule replication assays and found that the leading strand synthesis made a transient pause of 6 s before each lagging strand loop formation, and meanwhile the two strands were synthesized with the same rate. They proposed T7 primase might function as a brake to halt leading strand synthesis while a new primer was synthesized or the lagging strand polymerase was hopping to a new primer (Lee et al., 2006) In contrast, Pandey et al. detected no pausing event on the leading strand or slowing of leading strand synthesis in T7 in their single molecule FRET and kinetic study. Furthermore, they proposed that new primers were synthesized during ongoing leading strand synthesis prior to the lagging strand polymerase association with it, and that the nascent lagging strand with the newly synthesized primer formed a priming loop close to the replication fork to facilitate primer handoff from primase to polymerase. The rate of T7 polymerase preceeding on the SSB-covered primed ssDNA template was found to be faster than that of T7 replisome movement based on ensemble kinetic assays, which suggested that the lagging strand polymerase synthesized Okazaki fragment faster than the replication fork movement and a few seconds were spared for lagging strand cycling (Pandey et al., 2009).

Lia et al observed that in living *E. coli* the intensity of fluorescence protein fused on SSB displayed bursts, meaning the amount of SSB bound on the lagging strand was not constant during DNA replication. If the rate of the replication fork movement were equivalent to the rate of lagging strand polymerase, no burst of fluorescence should have been observed. The increasing fluorescent intensity indicated that more ssDNA was exposed through helicase translocation than dsDNA synthesized by lagging strand polymerase. It is likely that lagging strand polymerase was undergoing cycling during

that period. While the decreasing fluorescent intensity indicated that lagging strand polymerase synthesized Okazaki fragments faster than replication fork movement (Lia et al., 2012). My finding about the rate of leading and lagging strand synthesis will be discussed in Chapter III.

1.3.4 Polymerase exchange at the replication fork

Yang et al. found that a wild-type DNA polymerase (wt gp43) in the bacteriophage T4 system demonstrates high processivity by maintaining the amount of dNTP incorporation, the length of Okazaki fragments, and polymerase dissociation rate upon polymerase dilution. However, they also discovered that wt gp43 within the replisome can be readily replaced by an exogenous mutant gp43 (gp43-D408N). Mutating the aspartate 408 to asparagine in the palm domain of gp43 causes it to lose capability of elongating primers and thus inhibit both leading and lagging strand synthesis in a coupled DNA replication reaction, while retaining the ability to form the initiation complex at the replication fork. Therefore, gp43-D408N can serve as a trap protein and compete with wt gp43. It was observed that both leading and lagging strand synthesis in a coupled reaction initiated by wt gp43 were inhibited by the addition of gp43-D408N within a time period shorter than the dissociation rate of gp43. This inhibition exhibits dependence on the concentration of gp43-D408N. Another C-terminal mutant polymerase, gp43 Δ 10, that abolishes interaction between the polymerase and the clamp without affecting nucleotidyl transfer and DNA binding, does not show any inhibition. These results suggest that gp43-D408N actively displaces wt gp43 via the interaction between the polymerase C-terminus and the clamp, rather than passively

binding template after dissociation of wt gp43. Yang proposed that the C-terminus of the incoming polymerases might bind the interdomain loop of one subunit of the clamp and temporarily displace the polymerase at the replication fork under some regulated mechanism (Yang et al., 2004).

Similarly, in a bacteriophage T7 system, a complex of wild-type DNA polymerase (gp5) and its processivity factor, *E. coli* thioredoxin (gp5/trx), can readily exchange with excess mutant gp5-thioredoxin complexes (gp5-Y526F/trx) without affecting high processivity in a strand displacement reaction or coupled DNA replication reaction. Replacing tyrosine 526 with phenylalanine in the nucleotide binding site confers the mutant gp5 the ability to incorporate ddNTPs but does not affect its abilities of binding with other protein components and elongating primers. Both strand displacement synthesis and leading strand synthesis in a coupled reaction initiated by gp5-Y526F/trx are inhibited upon addition of gp5/trx and ddNTPs, which indicates that wild-type polymerase exchanges with the mutant ones at the replication fork. Interestingly, the exchange activity was not observed in a ssDNA replication reaction where helicase was not included. To explain why the polymerase retains high processivity and yet exchanges with other polymerases at the same time, Johnson et al proposed that more than one copy of polymerase bound to different subunits of helicase await exchange with the polymerase at the replication fork that dissociates from DNA template transiently (Johnson et al., 2007).

E. coli Pol III α proteins labeled with single fluorescence molecules diffuse slowly enough to be detected by a whole-cell single molecule localization technique. Lia et al. observed repetitive bursts of fluorescence localization of labeled Pol III α in living cells

with expressed fluorescent fusion of Pol III α , which indicates that polymerases exchange at the replication fork. Otherwise, no signal would be seen after photobleaching. They proposed that free polymerases labeled with fluorescence exchange with the polymerase on the lagging strand either via direct replacement of the one previously on the lagging strand, or via binding to an empty τ subunit without Pol III bound and then to the Okazaki fragment (Lia et al., 2012).

1.3.5 Strand displacement activity of Pol III HE

In addition to the well-characterized processive replication reaction catalyzed by the Pol III HE on ssDNA, the enzyme possesses an intrinsic strand displacement activity on flapped templates. During processive replication of long single-stranded templates, the Pol III HE typically stops synthesis upon encountering a duplex (O'Donnell and Kornberg, 1985). The elongation reaction is very rapid (400-700 nt/s) and exhibits processivity that may enable replication of the entire *E. coli* chromosome without dissociation (McHenry, 2003). However, a more feeble strand displacement activity of the DNA polymerase III holoenzyme has been observed under a variety of conditions (Canceill and Ehrlich, 1996; Stephens and McMacken, 1997; Yao et al., 2000; Xu and Marians, 2003).

Canceill and Ehrlich observed that Pol III HE could replicate through a 30-nt stem (Canceill and Ehrlich, 1996). A mechanism was proposed where the enzyme could non-processively elongate a few nucleotides when base pairing is transiently disrupted. Stephens and McMacken observed more extensive strand displacement synthesis on flapped templates using native Pol III HE in a reaction that was dependent upon SSB

(Stephens and McMacken, 1997). Marians and colleagues, in studies of replicative resolution of recombination intermediates, observed a background strand displacement reaction in the absence of helicase (Xu and Marians, 2003). O'Donnell and colleagues have also observed strand displacement of oligonucleotides containing large internal secondary structures (Yao et al., 2000).

Although observed by different research groups, strand displacement was never carefully studied. Besides, this activity introduces an undesirable background to the helicase-dependent DNA replication. Thus, in Chapter II, I systematically investigated the strand displacement activity, and determined conditions to defeat it. I found that the interaction network, Pol III- τ - ψ - χ -SSB, was essential to strand displacement, and PriA inhibits it.

Recently, Jergic et al. further investigated this reaction and discovered that strand displacement activity is ϵ -dependent. The C-terminus of ϵ interacts with one side of the β dimer through clamp binding motifs, which stabilizes the replisome on the replication fork. This function of ϵ is independent of its proofreading activity. The interaction between ϵ - β is weaker than α - β , so that alternative polymerases can presumably replace ϵ to β when necessary and ϵ can undergo proofreading in a timely manner. But the ϵ - β contact is quickly rebuilt for DNA polymerization (Jergic et al., 2013).

1.4 Research Goals

Whether the collision model or the signaling model depicts the cycling of the *E. coli* lagging strand polymerase has been a controversial topic for decades. To ascertain

whether the signaling model or the collision model is sufficient to explain *E. coli* polymerase cycling on the lagging strand, I establish an *E. coli* rolling circle DNA replication system with an asymmetric G:C distribution containing 17 purified proteins and mini-circle templates. Strand displacement reaction catalyzed by Pol III in the absence of helicase is an unfavorable background reaction to the authentic rolling circle reaction. In order to eliminate the background reaction, I systematically study the strand displacement activity of Pol III and determined experimental conditions to defeat that reaction. The results of these experiments will be discussed in Chapter II.

Chapter III describes how I determine the mechanism of lagging strand polymerase cycling. The highly asymmetric G:C distribution between DNA strands is a valuable feature of the rolling circle DNA replication system, which allows me to separately monitor the synthesis of two strands, and particularly perturb the lagging strand synthesis. I use ddGTP chain terminator to block Okazaki fragment synthesis before completion; I also use dGDPNP to selectively slow down the rate of lagging strand synthesis so that Okazaki fragment cannot be completely elongated before receiving the next signal. In both cases, shorter Okazaki fragments with gaps in between were observed, which indicates that Pol III still cycles to the next primer even though the Okazaki fragment synthesis is not complete. Because both results are consistent with prediction of the signaling model, I seek to determine what is the signal that triggers cycling of the lagging strand polymerase. Furthermore, I investigate how composition of the DnaX complex affects the cycling of the lagging strand polymerase by exploiting reconstituted DnaX complexes with different numbers of τ or γ subunits.

In Chapter IV, to determine how many C-terminal tails of SSB are required to maintain a normal DNA replication level, I study how cross-linked SSB with one or two C-terminal tails in both affect ssDNA replication reaction and rolling circle replication reaction. In Appendix 3, to investigate whether Pol III can be exchanged at the replication fork, I conduct rolling circle replication assays with exogenous mutant Pol III and Pol III*.

CHAPTER II

STRAND DISPLACEMENT BY DNA POLYMERASE III OCCURS THROUGH A τ - ψ - χ LINK TO SSB COATING THE LAGGING STRAND TEMPLATE

2.1 Abstract

In addition to the well-characterized processive replication reaction catalyzed by the DNA polymerase III holoenzyme on single-stranded DNA templates, the enzyme possesses an intrinsic strand displacement activity on flapped templates. The strand displacement activity is distinguished from the single-stranded (ss) DNA-templated reaction by a high dependence upon single-stranded DNA binding protein and an inability of γ complex to support the reaction in the absence of τ . However, if γ complex is present to load β_2 , a truncated τ protein containing only domains III-V will suffice. This truncated protein is sufficient to bind both the α subunit of Pol III and $\chi\psi$. This is reminiscent of the minimal requirements for Pol III to replicate short single-stranded DNA binding protein coated templates where τ is only required to serve as a scaffold to hold Pol III and χ in the same complex (Glover and McHenry, 1998). I propose a model in which the strand displacement by DNA polymerase III holoenzyme depends upon a Pol III- τ - ψ - χ -SSB binding network where SSB is bound to the displaced strand, stabilizing the Pol III-template interaction. The same interaction network is likely important for stabilizing the leading strand polymerase interactions with authentic replication forks. The specificity constant (k_{cat}/K_m) for the strand displacement reaction is *ca.* 300-fold less favorable than reactions on single-stranded templates and proceeds with a slower rate (150 nucleotide/s) and only moderate processivity (*ca.* 300 nucleotides). PriA, the initiator of replication restart on collapsed or misassembled

replication forks, blocks the strand displacement reaction, even if added to an ongoing reaction.

2.2 Introduction

All cellular replicases are tripartite assemblies, consisting of a replicative polymerase (Pol III in bacteria, Pol δ or ϵ in eukaryotes), a sliding clamp processivity factor (β_2 in bacteria, PCNA in eukaryotes) and a clamp loader composed of a five protein core of AAA+-like proteins that assembles the sliding clamp around DNA (DnaX complex in bacteria, RFC in eukaryotes) (Kelman and O'Donnell, 1995; McHenry, 2003; Burgers, 2009). The *E. coli* DnaX complex comprises three copies of DnaX, and one each of δ , δ' and $\chi\psi$ (Pritchard et al., 2000; Jeruzalmi et al., 2001b). *E. coli* and many other bacteria contain two forms of DnaX, the full length τ translation product and a shorter protein, γ , that results from translational frameshifting (Blinkowa and Walker, 1990; Flower and McHenry, 1990; Tsuchihashi and Kornberg, 1990). Both τ and γ contain the three domains that are required for ATP-dependent β_2 loading onto DNA (Jeruzalmi et al., 2001b). The third domain of τ and γ is responsible for binding other DnaX subunits, as well as δ , δ' and $\chi\psi$ (Gao and McHenry, 2001a; Glover et al., 2001; Simonetta et al., 2009). τ contains two additional domains that interact with the DnaB replicative helicase (domain IV) and Pol III (domain V) (Gao and McHenry, 2001b, 2001c).

The primary determinant of processivity of the *E. coli* replicase is the interaction of Pol III with β_2 (LaDuca et al., 1986; Kong et al., 1992). However, other interactions stabilize the interaction of Pol III with the replication fork. Two τ protomers bind the

DnaB helicase, further stabilizing the replicase at the fork (Kim et al., 1996a, 1996c). Pol III alone is unable to replicate ssDNA coated by SSB. To accomplish this feat, τ , ψ and χ must be present if β_2 is absent (Glover and McHenry, 1998). τ does not serve its prototypical role as the clamp loader in this minimal system, but apparently only serves as a bridge, tethering $\psi\chi$ in the same complex with Pol III, enabling an otherwise weak Pol III-template interaction to be stabilized by a χ -SSB contact (Glover and McHenry, 1998).

During processive replication of long single-stranded templates, the Pol III HE typically stops synthesis upon encountering a duplex (O'Donnell and Kornberg, 1985). The elongation reaction is very rapid (400-700 nt/s) and exhibits processivity that may enable replication of the entire *E. coli* chromosome without dissociation (McHenry, 2003). However, a more feeble strand displacement activity of the DNA polymerase III holoenzyme has been observed under a variety of conditions (Canceill and Ehrlich, 1996; Stephens and McMacken, 1997; Yao et al., 2000; Xu and Marians, 2003).

Canceill and Ehrlich observed that Pol III HE could replicate through a 30-nt stem (Canceill and Ehrlich, 1996). A mechanism was proposed where the enzyme could non-processively elongate a few nucleotides when base pairing is transiently disrupted. Stephens and McMacken observed more extensive strand displacement synthesis on flapped templates using native Pol III HE in a reaction that was dependent upon SSB (Stephens and McMacken, 1997). Marians and colleagues, in studies of replicative resolution of recombination intermediates, observed a background strand displacement reaction in the absence of helicase (Xu and Marians, 2003). O'Donnell and colleagues

have also observed strand displacement of oligonucleotides containing large internal secondary structures (Yao et al., 2000).

Observations of the strand-displacement activity of Pol III HE have occurred peripheral to studies conducted for other purposes. No investigation has been made aimed at understanding the reaction, its protein requirements and how it might differ from the well-characterized reaction that occurs on single-stranded templates. This study was directed toward remediating these deficiencies in knowledge. I found that an interaction of the leading strand polymerase with the lagging strand template, mediated by a Pol III- τ - ψ - χ -SSB bridge, was essential for efficient strand displacement. This interaction network likely stabilizes the replicase at the fork, in addition to the characterized Pol III- β_2 and τ -DnaB interactions.

2.3 Materials and Methods

Proteins: *E. coli* DNA Pol III HE protein subunits were purified as previously described: SSB (Griep and McHenry, 1989), β (Johanson et al., 1986), DnaG (Griep and McHenry, 1989), Pol III* (Pol III₃ $\tau_3\delta\delta'\chi\psi$) (Pritchard et al., 2000), Pol III (McHenry and Crow, 1979), τ (Dallmann and McHenry, 1995), $\chi\psi$ (Olson et al., 1995), τ complex (Glover and McHenry, 2000), γ complex (Glover and McHenry, 2000), τ_{III-V} (Gao and McHenry, 2001b) and τ_{IV-V} (Gao and McHenry, 2001c). Complexes of τ derivatives with $\chi\psi$ (τ - ψ - χ , τ_{III-V} - ψ - χ and τ_{IV-V} - ψ - χ) were made by the incubation of equimolar τ , τ_{III-V} or τ_{IV-V} with $\chi\psi$ for 20 min at 30 °C. SSB-c Δ 42 (Roy et al., 2007) and SSB-c Δ 8 (Hobbs et al., 2007) were obtained from the laboratories of Tim Lohman (Washington University) and Mike Cox (University of Wisconsin), respectively.

Oligonucleotides: The sequence of the 32-mer primer was 5'-T-dU(5-biotin)-GAACGGTGTACAGATCACGCGCATAGGCTG-3'. The sequence of the 50-mer flap was 5'-TTTTTTTTTTTTTTTTTTTTTTTTTTTTTCTGTGTTTTGTTGTCTT-GTTCCCTG-3'. The sequence of the 67-mer primer was 5'-T-dU(5-biotin)-GAACGGTGTACAGATCACGCGCATAGGCTGCCTTTTCTCGTGTTGGCCTGGGGTC CGCTGTCTCT-3'. The sequence of the 91-mer template was 5'- biotin linked by a phosphodiester and a 6-carbon spacer to CAGGGAACAAGACAACA-AAACACAAGAGACAGCGGACCCCAGGCCAACACGAGAAAAGGCAGCCTATGCGC GTGATCTGTACACCGTTCAA -3'.

DNA templates: M13Gori ssDNA, M13Gori template with a 30 nt primer and activated calf thymus DNA were prepared as previously described (Johanson et al., 1986; Kim and McHenry, 1996c; Glover and McHenry, 2001). pUCNICK tail DNA was generated from plasmid pUCNICK (2,716 bp) (Jones et al., 2004) and purified by Qiagen plasmid Maxi prep. Purified plasmid DNA (30 µg, 1 µg/µl) was nicked at the single recognition site with Nb.BbvCI nicking enzyme (New England Biolabs, 300 units) at 37 °C for 4 h. Nb.BbvCI was thermally inactivated (80 °C, 20 min). A 1% agarose gel showed that the nicking reaction was >90% complete. The nicked plasmid was precipitated by the addition of 0.5 volume of 5 M ammonium acetate and 1.5 volumes of isopropanol, and the pellet was washed with 70% ethanol and dissolved in 10 mM Tris-HCl buffer (pH 8) to 0.2 µg/µl final concentration. Glycerol was added to 13% final concentration. This solution was incubated with 200 µM dATP, dGTP, and dTTP and Klenow fragment (exo+, 2U/ µg DNA) at 37 °C for 30 min, so that the 61 nt long C-less DNA flap was formed. EDTA was added to a final concentration of 20 mM. Tailed

pUCNICK (2,777 nt) was precipitated with isopropanol and dissolved in 10 mM Tris-HCl (pH 8) at a concentration of 1 $\mu\text{g}/\mu\text{l}$. Tailing efficiency, determined by Pvu II digestion and 1.8% agarose gel electrophoresis, was >90% complete.

^{32}P -dTTP labeled pUCNICK tail template was prepared with the same protocol used for preparation of unlabeled pUCNICK tail, except that 0.5 Ci/L [α - ^{32}P]-dTTP was added with the other dNTPs. Unincorporated [α - ^{32}P]-dTTP was removed by the tandem use of a Microspin G-25 spin column and a NAP-5 column (GE Healthcare). The pooled solution was precipitated with 95% ethanol, the pellet washed with 70% ethanol and the DNA dissolved in 10 mM Tris-HCl (pH 8). The 32-mer and 67-mer were 5'-end labeled with [γ - ^{32}P]-ATP using T4 polynucleotide kinase. Unincorporated [γ - ^{32}P]-ATP was removed by a Microspin G-25 spin column. The 32-mer and 91-mer were mixed in 10 mM Tris-HCl (pH 7.5), 5 mM MgCl_2 , and 200 mM NaCl in a 1:1 ratio for the template 32/91, heated to 95 °C for 5 min, incubated at 65 °C for 1 h, slowly cooled to 25 °C over 2 h, and incubated at 25 °C for 30 min. The 32-mer or 67-mer primer, 50-mer, and 91-mer were incubated at a 1:2:1 ratio to ensure all templates contained a blocking, flapped oligonucleotide. Native polyacrylamide gel electrophoresis confirmed that no 32/91 or 67/91 existed as contaminants in 32/50/91 or 67/50/91. 10-fold excess streptavidin was incubated with 32/91, 32/50/91, and 67/50/91 in 10 mM Tris-HCl (pH 8) at room temperature to form bumpers to prevent loaded β_2 from sliding off.

Single-stranded replication assays: Single-stranded replication assays contained 2.3 nM M13Gori DNA, 0.6 μM SSB₄, 6 nM β_2 , 40 nM DnaG, 10 nM Pol III and 4 nM τ complex. The reaction mixture was incubated with 0.2 mM UTP, CTP and GTP, 0.3 mM ATP, 18 μM [^3H]-dTTP (ca. 100 cpm/pmol total nucleotide), 48 μM dATP, 48 μM dGTP,

and 48 μM dCTP for 5 min at 30 °C in 25 μl . All replication reactions were quenched by 100 μl of 0.2 M sodium pyrophosphate and 500 μl of 10% TCA unless stated otherwise. Precipitated product was quantified by scintillation counting. All reactions with M13Gori templates were conducted with the single-stranded replication buffer: 10 mM magnesium acetate, 50 mM Hepes (pH 7.5), 100 mM potassium glutamate, 20% glycerol, 200 $\mu\text{g/ml}$ BSA, 0.02% NP40, and 10 mM DTT.

Strand displacement assays: 4 nM pUCNICK tail, 100 μM ATP, 0.75 μM SSB₄, 25 nM β_2 , 51 nM Pol III, 17 nM τ complex, 300 μM dNTPs, and ca. 130 cpm/pmol ³H-TTP were incubated for 5 min at 30 °C in 25 μl . The strand displacement buffer was the same as the single-stranded replication buffer except it contained 20 mM NaCl. Incorporation was expressed in terms of total nucleotide by multiplying the total dTTP incorporated by 4 (pUCNICK contains 24.7% T).

Determination of the rate of strand displacement: Initiation complexes between Pol III HE and flapped templates were formed by incubating 5 nM pUCNICK tail, 125 μM ATP, 0.94 μM SSB₄, 31 nM β_2 , and 25 nM Pol III* at 30 °C for 1 min. Then 375 μM dNTPs and 5 $\mu\text{Ci/reaction}$ [α -³²P]-dTTP were added to initiate strand displacement. Aliquots of the 20 μl reaction were quenched by 100 mM EDTA (final concentration) at various time points. The samples were loaded along with alkaline agarose gel loading buffer (30 mM NaOH, 2 mM EDTA, 1% glycerol, and 0.02% bromophenol blue) to 0.5% alkaline agarose gels in a running buffer of 30 mM NaOH and 2 mM EDTA. Gels were run at 22 V for 18.5 h, fixed in 5% TCA, dried, and scanned by a phosphorimager. The molecular weights (MW) of the longest reaction products were determined by measuring

their relative mobilities (Rf) [compared to ^{32}P -labeled DNA size marker] on the alkaline agarose gel.

Determination of the processivity of Pol III HE on a short-flapped template:

Challenge assays were performed to determine processivity. In these assays, a large excess of activated calf thymus DNA (challenge) was added to elongating complexes to trap dissociated polymerase so that products represented a single processive association-elongation-dissociation event. Solutions containing strand displacement buffer (125 μM ATP, 0.31 μM SSB₄, 31 nM β_2 , and 10 nM Pol III*) were prewarmed and mixed with 1.5 nM [γ - ^{32}P]-labeled 32/91, 32/50/91, or 67/50/91 at 30 °C for 15 s to form the initiation complexes. To block ϵ -catalyzed primer degradation, 10 μM dGTP were added for 32/91 and 32/50/91 templates and 10 μM dTTP and dCTP for 67/50/91 during incubation. Then 375 μM dNTPs (final concentration) and 20 μg activated calf thymus DNA were added to allow the reaction to occur. After 10 s, 55% formamide, 50 mM EDTA, 0.0083% bromophenol blue, and 0.0083% xylene cyanol (final concentrations) were added to quench the 20 μl reaction. The solution was fractionated on 12% polyacrylamide gel with 8.2 M urea for 3 h at 95 W. The gel was scanned with a phosphorimager and quantified with ImageQuant 5.2 software (Amersham Biosciences). Controls to show the challenge was effective followed the same procedure except activated calf thymus DNA was added with the templates before the addition of Pol III HE.

Determination of the processivity of Pol III HE on a rolling circle template: In this assay, pre-warmed 1 nM pUCNICK tail, 100 μM ATP, 0.75 μM SSB₄, 25 nM β_2 , and 10 nM Pol III* were assembled to form holoenzyme initiation complexes for 20 s at 30 °C.

Then 300 μM dNTPs (final concentration) and 5 μg activated calf thymus DNA were added to initiate the reaction. This 25 μl reaction was carried out at 30 $^{\circ}\text{C}$ for various time periods and stopped by 83 mM EDTA (final concentration). Each reaction sample was precipitated by addition of 0.5 volume 5 M ammonium acetate, 20 μg glycogen, and then 2.5 volumes of 95% ethanol. The pellet was washed by 70% ethanol and dissolved in 20 μl of 10 mM Tris-HCl buffer (pH 8). DNA was then digested by 75 U EcoRI at 37 $^{\circ}\text{C}$ for 18 h. Unchallenged strand displacement assays followed the same procedure except activated calf thymus DNA was added just prior to EcoRI digestion to ensure uniformity in sample workup. After digestion, all samples were treated at 95 $^{\circ}\text{C}$ for 5 min with alkaline agarose gel loading buffer, then loaded onto 1.5% alkaline agarose gels in a running buffer of 30 mM NaOH and 2 mM EDTA. Gels were run at 100 V for 2 h, then fixed in 5% TCA, dried and scanned by a phosphorimager. The product bands were quantified by ImageQuant 5.2 software (Amersham Biosciences). Because the reaction products were diffuse, the center of the product in each lane (r_{AVG}) was defined as the average length of the product. The whole product was sliced into pieces about every hundred nucleotides. $r_{\text{AVG}} = \sum (r_i * P_i) / \sum P_i$, where r_i was the average length of product slice i and P_i was the pixel of product slice i . The processivity of Pol III* was calculated by subtracting the primer length, 67 nt, from r_{AVG} .

PriA inhibition assay: To test whether PriA could inhibit strand displacement before the initiation complex formed, 10 nM pUCNICK tail, 0.94 μM SSB₄, 31 nM β_2 , 125 μM ATP, 375 μM dNTPs, and 100 cpm/pmol ³H-TTP were mixed first, and then incubated with 10 nM Pol III* and varying amounts of PriA for 5 min at 30 $^{\circ}\text{C}$ in 20 μl . To test whether PriA could inhibit strand displacement after initiation complex formation,

the same procedure was followed, except that protein components were first incubated with pUCNICK tail in the presence of ATP at 30 °C for 2 min, and then dNTPs were added with PriA. For assays on ssDNA templates, PriA was added following the same sequence as described above either before or after the initiation complex formed. Every other component contained the same concentration as described above under Single-stranded replication assay, except that 10 nM Pol III* replaced Pol III and τ complex. To examine whether PriA could inhibit ongoing strand displacement, 8 nM pUCNICK tail was incubated with 100 μ M ATP, 0.75 μ M SSB₄, 25 nM β_2 , and 8 nM Pol III* at 30 °C for 1 min to form initiation complexes. 300 μ M dNTPs and ³H-TTP were then added to start strand displacement. At 45 s after the reaction started, 20 nM, 60 nM or no PriA was added. At different time points, aliquots of the 25 μ l reaction solution were quenched by 20 mM EDTA (final concentration).

2.4 Results

An initial characterization of the strand displacement activity of Pol III HE was performed on a circular template with a 61-nt flap. Protein components were titrated and compared to the requirement for standard processive assays on long single-stranded templates (Fig. 2.1). Approximately twice as much Pol III was required for the strand displacement reaction, likely a consequence of the decreased processivity of Pol III HE in the strand displacement reaction (see below). Both τ complex and β_2 were required to support the strand displacement reaction at protein levels approximately the same as required on single-stranded templates. Strikingly, the γ form of DnaX could not be substituted for τ in the strand displacement reaction, in contrast to reactions on single-

stranded DNA templates. Another significant difference was observed in the SSB requirement. As is typically observed, SSB stimulated the Pol III HE marginally (ca. 2-fold) on preprimed single-stranded templates; the dependence was nearly absolute for strand displacement.

Another profound difference became apparent upon varying dNTP concentrations (Fig. 2.1F). In the ssDNA reaction, a low mM K_m was measured. However, nearly 100-fold higher concentrations of dNTPs were required to drive the strand displacement reaction. To obtain a comparison of the specificity differences of the two reactions, I calculated k_{cat}/K_m that revealed a 330-fold preference of Pol III HE for synthesis on an ssDNA template compared to a duplex, during strand displacement (Table 2.1). A possible explanation for the high K_m for strand displacement could be the need for a rapid second-order nucleotide association reaction being required to trap an intermediate that lies on the elongation pathway and competes with steps that lead to dissociation. It is also possible that association of the polymerase with a displaced strand or loss of ssDNA template contacts might place it into an alternative conformation with a distorted active site that interacts with dNTPs less favorably.

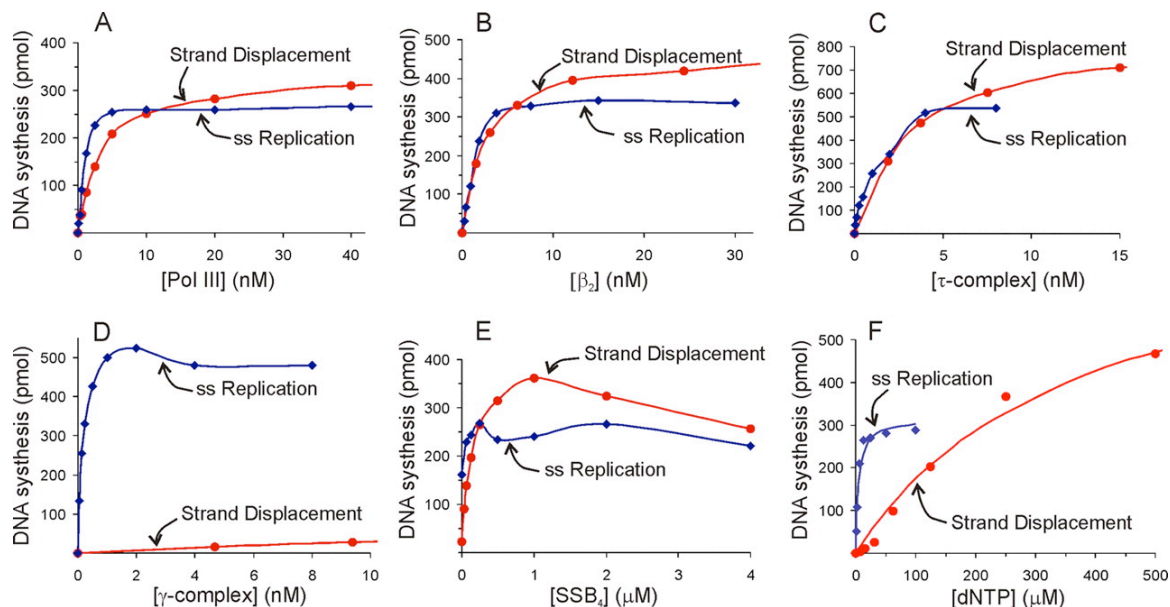


Figure 2.1 Requirements for Pol III HE components for strand displacement. Pol III HE protein subunits were titrated in single-stranded (ss) replication reactions (\blacklozenge) and strand displacement reactions (\bullet) in the presence of other protein subunits at optimal saturating levels as described under “Experimental Procedures.” (A) titration with Pol III. (B) titration with β_2 . (C) titration with τ complex. (D) titration with γ complex. (E) titration with SSB_4 . In this single experiment, an M13Gori template primed by annealing a 30-nt primer was used instead of DnaG primase-primed template, so the elongation requirement of SSB_4 could be determined separately from the absolute requirement for DnaG-catalyzed primer formation. (F) titration with dNTPs.

	Single-stranded replication	Strand displacement
K_m (μ M)	4.5	380
k_{cat} (s^{-1})	570	150
k_{cat}/K_m ($s^{-1} \cdot \mu$ M $^{-1}$)	130	0.39

Table 2.1 Steady state kinetic parameters for Pol III HE in single-stranded replication and strand displacement. The dNTP titration curves were fit to the Michaelis-Menton kinetic function, $1/v = (K_m/v_{max}[S]) + (1/v_{max})$, by nonlinear least-squares regression to determine both v_{max} and K_m . $[S]$ was the concentration of dNTPs, and v was the rate of dNTP incorporation ($\mu\text{mol}/\text{min}$). The value for k_{cat} at 30 °C for the strand displacement reaction was taken from the data reported in Fig. 2.4; that for the ssDNA reaction was taken from Ref (Johanson, 1982).

Next, I asked whether the τ requirement was a manifestation of a unique role for τ in loading β_2 onto DNA or whether τ performed another function, separate from β_2 loading. To address this issue, I loaded β_2 onto the DNA templates with γ complex and determined the contribution of various forms of τ . Adding τ alone had little effect, but adding a complex of τ - ψ - χ , which alone is inactive in β_2 loading, stimulated the strand displacement reaction significantly (Fig. 2.2A). τ and γ , in the absence of other proteins exchange very slowly. The presence of δ , δ' and $\chi\psi$ blocks exchange, eliminating the possibility that τ , added briefly to reactions, exchanges into γ complex (Pritchard and McHenry, 2001). Furthermore, if the result obtained were due to such an exchange reaction, $\chi\psi$ would not be required since it is already present in the γ complex.

In earlier work, we observed an effect of τ in enabling Pol III to replicate ssDNA coated with SSB, which required only its function of binding $\chi\psi$. In this example, τ held χ in the same complex with Pol III, enabling it to bind template-bound SSB and stabilizing an otherwise weak interaction (Glover and McHenry, 1998). Thus, I added a protein that comprises domains III-V of DnaX, τ_{III-V} . DnaX domain III binds $\chi\psi$ and domain V binds the α subunit of Pol III (Gao and McHenry, 2001a, 2001b). If the only function of τ is to link Pol III and χ , this truncated protein should suffice to stimulate strand displacement

when γ complex is present to load β_2 . Indeed, τ_{III-V} stimulated strand displacement the same amount as full-length τ bound to $\chi\psi$, although higher concentrations were required (Fig. 2.2B). Addition of an equimolar mixture of τ_{IV-V} and $\chi\psi$ did not stimulate the reaction. τ_{IV-V} binds the a subunit of Pol III, but not $\chi\psi$.

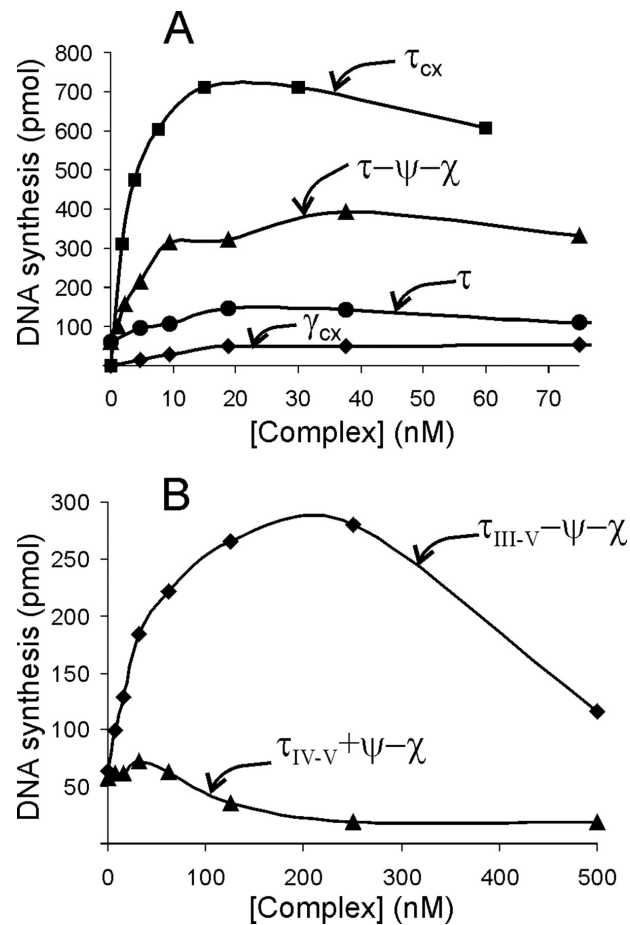


Figure 2.2 A Pol III- τ - ψ - χ complex is required for strand displacement. Strand displacement reactions were conducted using 4 nM pUCNICK tail, 0.75 μ M SSB₄, 25 nM β_2 , 50 nM γ complex, 100 μ M ATP, 300 μ M dNTPs, and [³H]TTP. Reactions were assembled on ice with τ -containing complexes of the specified composition. Pol III (final concentration, 51 nM) was added last (25 μ l final volume). Reactions were carried out at 30 °C for 5 min. The form of τ -containing complexes in the various complexes was as follows: τ complex ($\tau_{3\delta\delta'\psi\chi}$) (■), γ complex ($\gamma_{3\delta\delta'\psi\chi}$) (◆), τ (●), and τ - ψ - χ (▲) (A); τ_{III-V} - ψ - χ (◆) and τ_{IV-V} - ψ - χ (▲) (B).

The above results are consistent with a critical χ -SSB contact required to stabilize the strand displacement reaction. χ interacts with the C-terminal tail of SSB (Kelman et al., 1998; Witte et al., 2003). To further test the existence and importance of this interaction in the strand displacement reaction, I replaced wild-type SSB with two C-terminal SSB proteins that had 8 and 42 aa deleted from their C-terminus (Hobbs et al., 2007; Roy et al., 2007). I observed that neither supported strand displacement (Fig. 2.3A) consistent with our hypothesis. As a control experiment, I tested the effect of both on the Pol III HE single-strand template reaction and observed an inhibition even though there is not much of a requirement for SSB in the normal reaction (Fig. 2.3B). Thus, deletion of the C-terminus of SSB creates a gain of an inhibitory function for SSB, presumably because the protein interacting tail is not available for modulation of binding state (Roy et al., 2007) or displacement from the template.

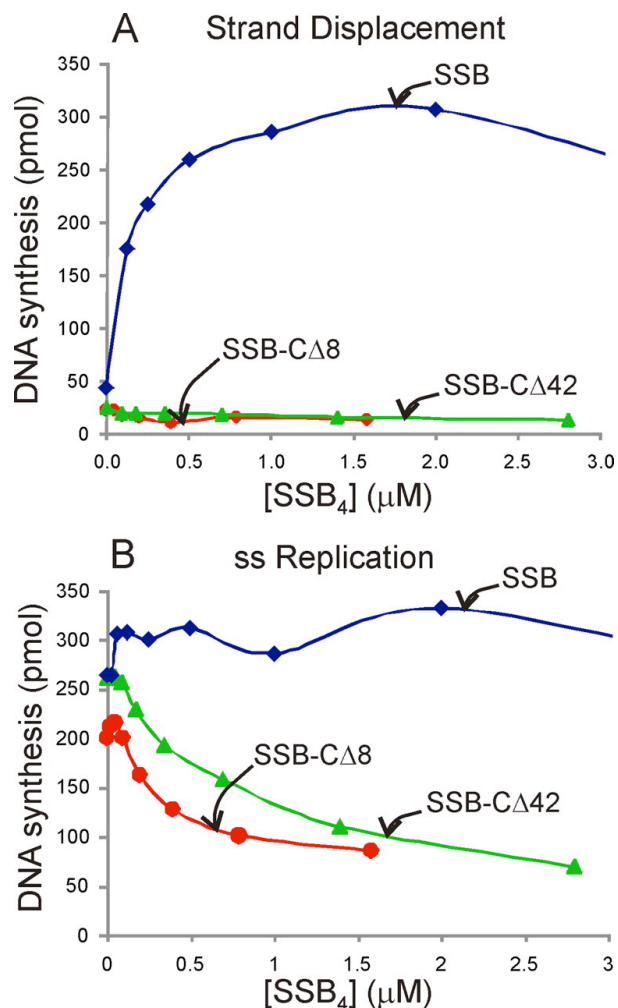


Figure 2.3 The C-terminal protein interaction sequence of SSB is required to support strand displacement.

SSB₄ titrations in the strand displacement reaction (A) and single-stranded (ss) templated reaction (B) were conducted as described for Fig. 2.1(E) except the SSB-cΔ42 (▲) and SSB-cΔ8 (●) proteins were substituted for wild-type SSB (◆) in the designated reactions.

I also determined the rate of elongation for the strand displacement reaction by determining the length of the longest products visible on a denaturing gel starting with labeled primer (Fig. 2.4). I observed a rate of 150 nt/s, slower than the 400-700 nt/s typically observed for the elongation reaction catalyzed by Pol III HE on ssDNA.

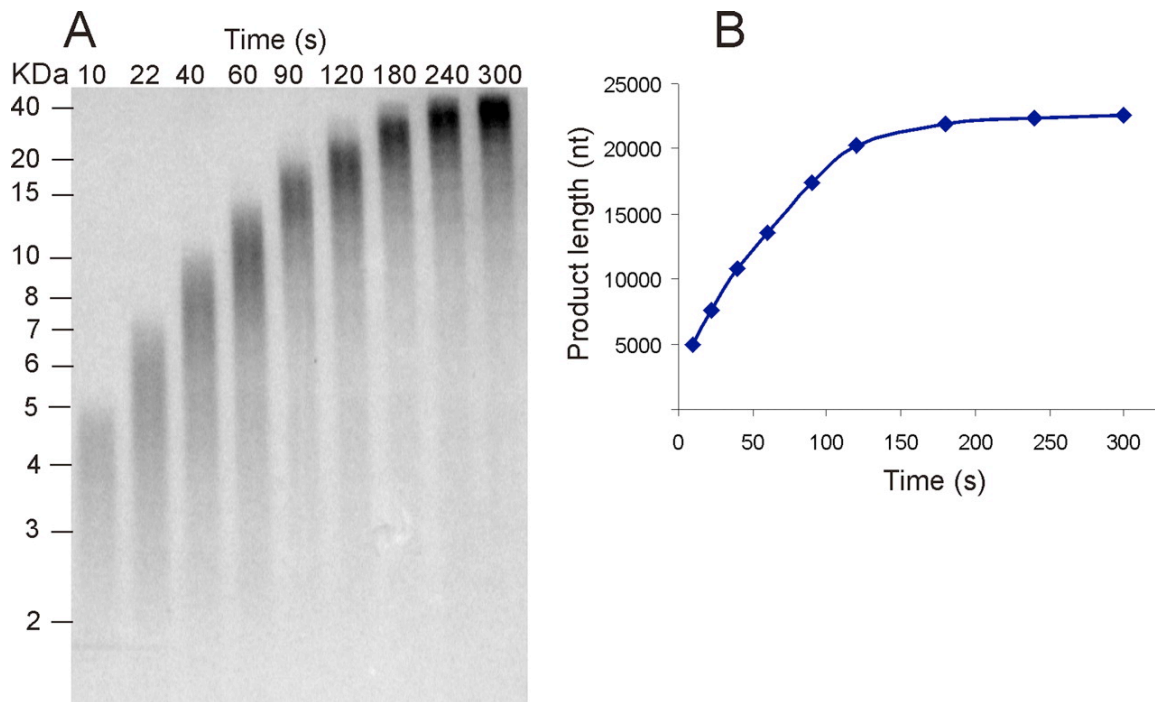


Figure 2.4 The rate of strand displacement by Pol III HE is 150 nt/s. (A) ^{32}P -labeled products of strand displacement using labeled primer were monitored on a 0.5% alkaline agarose gel. (B) the longest product at each time point was plotted as a function of time, and the rate was determined by the slope of a line intersecting the first five points.

Based on an initial expectation of low processivity, I made a series of synthetic templates with a common 91 nt segment (Fig. 2.5). One was simply primed at the 3'-end of the template with no other oligonucleotides annealed (template a). Two contained flapped blocking oligonucleotides, one with a 35 nt gap between the primer terminus and the flap (template b) and the other with the primer terminus abutting the flap junction (template c). Processivity was determined by first forming initiation complexes and then adding an excess of challenge DNA to capture any polymerase that dissociated during elongation. The efficacy of the challenge template was demonstrated by complete inhibition if added with the template before the addition of enzymes (Fig. 2.5, lanes 4-6). In the absence of a challenge, all templates were nearly

completely elongated to the expected full-length 91 nt product (lanes 7-9). If initiation complexes were formed prior to addition of the challenge template concomitant with dNTPs, again most of the primer was elongated to full-length product (lanes 10-12), indicating a processivity greater than 24 for strand displacement. However, 30% of the elongated product on template b terminated when the Pol III HE encountered the flap (lane 11), even though little product of a length intermediate between 67-mer and 91-mer was detected (<2%).

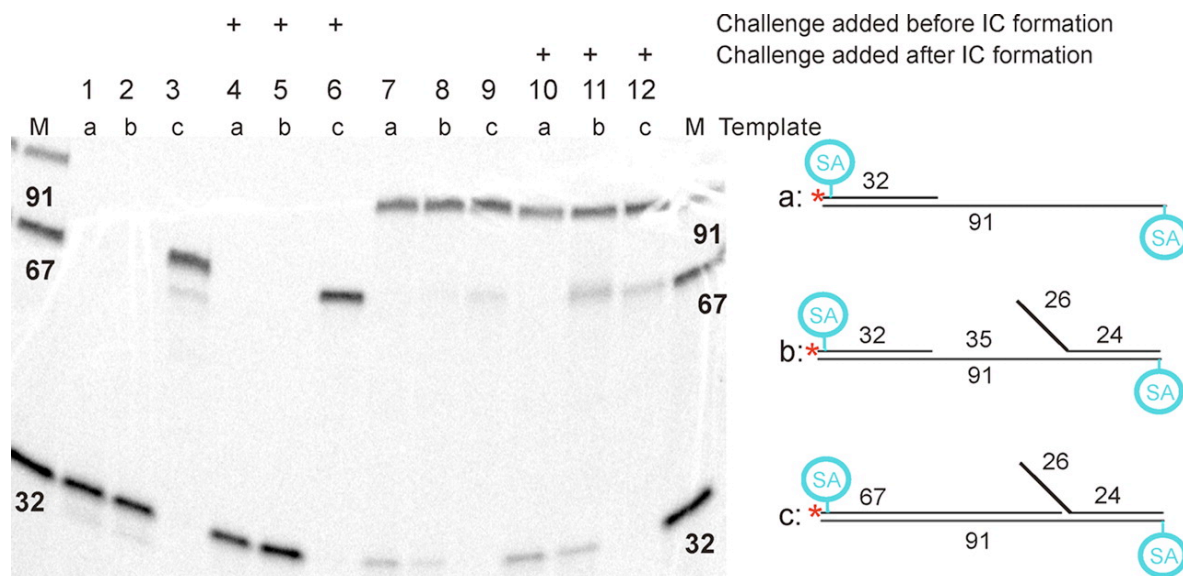


Figure 2.5 Approximately one-third of the elongating Pol III HE dissociates upon encountering a flap and then displaces greater than 24 nucleotides processively. *Left*, a 12% polyacrylamide denaturing gel showing the products of processivity determination experiments. *Lanes 1–3*, untreated templates showing the positions of unextended labeled primers; *lanes 4–6*, challenge DNA was added before initiation complex (IC) formation; *lanes 7–9*, DNA replication assays conducted without challenge DNA; *lanes 10–12*, challenge DNA was added after the initiation complex formation. *M*, the markers of the 32-, 67-, and 91-mer. The percentages of 32-mer (relative to other bands in the same lane) were 20, 8.3, 34, and 14% for *lanes 7, 8, 10, and 11*, respectively; percentages of 67-mer were 0.2, 7.6, 26, and 19% for *lanes 8, 9, 11, and 12*, respectively; and percentages of 91-mer were 80, 92, 92, 66, 61, and 81% for *lanes 7–12*, respectively. *Right*, the three DNA templates (a–c) with ^{32}P -labeled primers (indicated by an asterisk) made as described under “Experimental Procedures.” SA, positions of streptavidin attachment.

Since the processivity was too high to estimate on short, linear templates, I turned to longer flapped templates. Initial experiments failed to resolve the product of processive synthesis from the 2,777 nt starting material, indicating limited processivity. To permit resolution, I labeled the primer for the template during creation of the flap, limiting the position of radioactive nucleotides to the 3'-terminal 61 nt. After elongation, this permitted cleavage with restriction endonuclease *EcoRI*, generating a product of 67 nt plus the number of nt added during the elongation event. This permitted better product resolution. Using this longer template, a challenge experiment was conducted, similar to the one performed on the short, synthetic template above. The presence of a challenge template mixed with the labeled template prior to enzyme addition inhibited the elongation reaction (Fig. 2.6, lanes 8-9). Pre-formation of initiation complexes followed by addition of the challenge template with dNTPs limited synthesis (Fig. 2.6, lanes 10-13) relative to the unchallenged controls (lanes 4-7), indicating limited processivity. Since processivity is an intrinsic property of an enzyme, the length of a processive product should not be affected by incubation time. I observed that the product length remained unchanged beyond the initial 5 s time point. Thus, the 10-20 s products from the elongation experiment (Fig. 2.6, lanes 11-13) were used to calculate processivity. The population of products as a function of length was quantified and an average processivity of 280 nt was calculated.

the only other protein present. I observed that PriA blocked the strand displacement reaction whether or not an initiation complex was formed between the Pol III HE and DNA prior to PriA addition. In contrast, PriA had no effect on the Pol III HE-catalyzed reaction on ssDNA templates (Fig. 2.7A). I also investigated whether PriA could halt an ongoing elongation reaction (Fig. 2.7B). Initiation complexes were formed on flapped templates and, 45 s after initiation, PriA was added, resulting in an immediate block in the presence of 60 nM PriA.

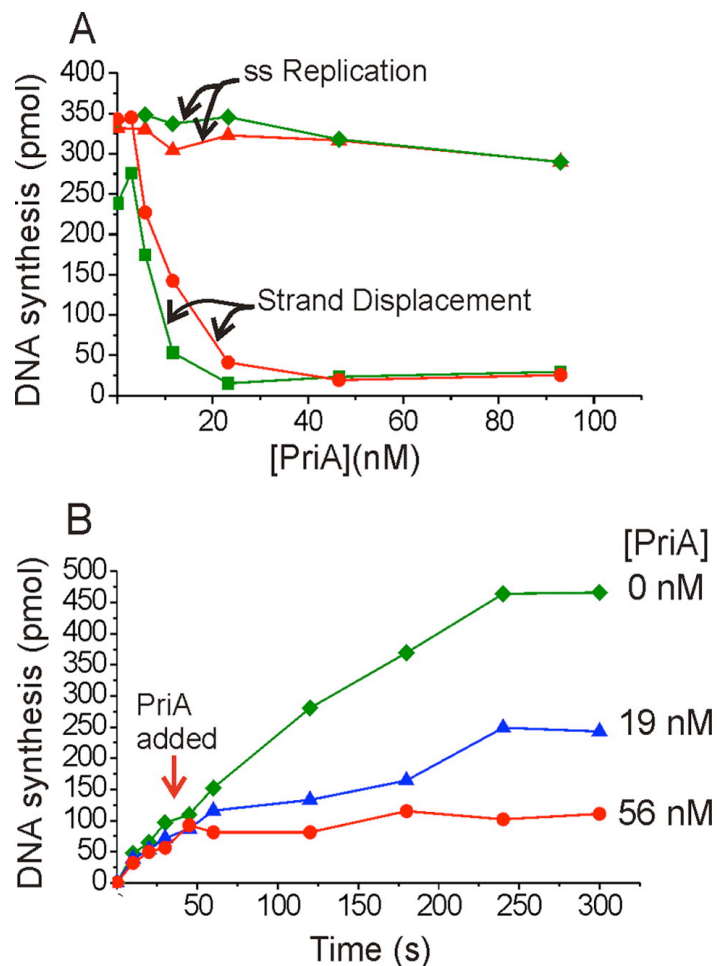


Figure 2.7 PriA inhibits the strand displacement reaction. (A) PriA was titrated before (*red*) the holoenzyme initiation complex formed with pUCNICK tail (●) and M13Gori (▲) and after (*green*) the initiation complex formed with pUCNICK tail (■) and M13Gori (◆) in the presence of the optimal amounts of Pol III HE components as described under “Experimental Procedures.” (B) time course of PriA inhibition of ongoing strand

displacement. 0 nM PriA (◆), 19 nM PriA (▲), or 56 nM PriA (●) was added at 45 s after the strand displacement reaction initiated. ss, single-stranded.

2.5 Discussion

I observed that the Pol III HE has an intrinsic strand displacement reaction that has markedly different properties than the well-studied synthesis reaction catalyzed on ssDNA templates. Both reactions require Pol III, β_2 and a clamp loader. However, unlike the ssDNA-templated reaction, SSB is nearly absolutely required for strand displacement. It only modestly stimulates reactions on ssDNA templates when the complete Pol III HE is present. Even more striking is the observation that γ complex alone is not effective— τ must be present for strand displacement to occur. However, the unique requirement for τ is not a consequence of its β_2 clamp loading activity. If γ complex is provided to load β_2 , a truncated τ protein that lacks the critical domains required for ATP binding and hydrolysis (domains I-II) will serve to drive strand displacement. The truncated τ must contain domain III, the $\chi\psi$ binding domain (Gao and McHenry, 2001b). The C-terminal tail of SSB that is involved in a variety of protein interactions (Shereda et al., 2008) is required.

These observations are reminiscent of the minimal Pol III that is required for modest replication on SSB-coated ssDNA templates, Pol III- τ - ψ - χ , where τ only serves as a tether to hold χ and Pol III in the same complex (Glover and McHenry, 1998). The explanation of activity in this system was that χ contacted SSB when bound to ssDNA, increasing binding of the polymerase. The molecular interactions behind this protein network are well understood. Pol III binds τ in an interaction between the C-terminus of

Pol III and domain V of τ (Kim and McHenry, 1996c; Gao and McHenry, 2001a; Dohrmann and McHenry, 2005). One ψ protomer binds a trimeric assembly of DnaX proteins through their domain III (Gao and McHenry, 2001b; Simonetta et al., 2009). ψ binds χ and χ binds to SSB through its C-terminal domain (Glover and McHenry, 1998; Kelman et al., 1998; Witte et al., 2003).

In the strand displacement reaction, however, the only ssDNA available for SSB binding is the displaced strand. Thus, I propose the model depicted in Fig. 2.8, where a Pol III- τ - ψ - χ -SSB interaction stabilizes the interaction of Pol III with the template sufficiently to permit moderately processive strand displacement. It is interesting that the β_2 -Pol III interaction alone is inadequate to stabilize the Pol III-template interaction sufficiently to enable strand displacement. Perhaps limited ssDNA template-Pol III contacts make additional stabilizing interactions necessary. The interaction network shown in Fig. 2.8 could be important for stabilizing interaction of the leading strand polymerase at the replication fork, through an interaction of the DnaX complex with the lagging strand template. Normally, a τ_2 -DnaB₆ interaction will further stabilize the replisome, but there may be situations—for example, when difficult structures are encountered during mismatch repair—where the Pol III- τ - ψ - χ -SSB interaction network becomes critical for function. In unusual cases, such as blockage of the leading strand polymerase by a lesion or other obstruction when the helicase continues to progress, single-stranded DNA would be created on the leading strand template and bound by SSB, enabling stabilization of Pol III HE interactions, perhaps providing a tether to localize Pol III HE during polymerase switching.

The Pol III HE strand displacement reaction exhibits only modest (*ca.* 300 nt) processivity as compared with the proposed megabase processivity of the Pol III HE on ssDNA and the >100,000 base processivity observed on reconstituted replication forks. Thus, even a combination of the Pol III- β_2 interaction and the τ -mediated χ -SSB contact cannot provide sufficient stability for the highest levels of processivity. It is interesting that approximately one-third of Pol III HE dissociates upon encountering a flap while actively polymerizing, yet appears to dissociate at the very low frequency required for 300 nt processivity at other positions. The enzyme presumably encounters the same structure prior to the addition of each nucleotide. It is possible that formation of the χ -SSB contact with the lagging strand template (displaced strand in Fig. 2.8) is on the same order as the rate of nucleotide addition and, upon encountering a flap, a portion of the enzymes fails to form the contact in adequate time and dissociates due to weak interactions.

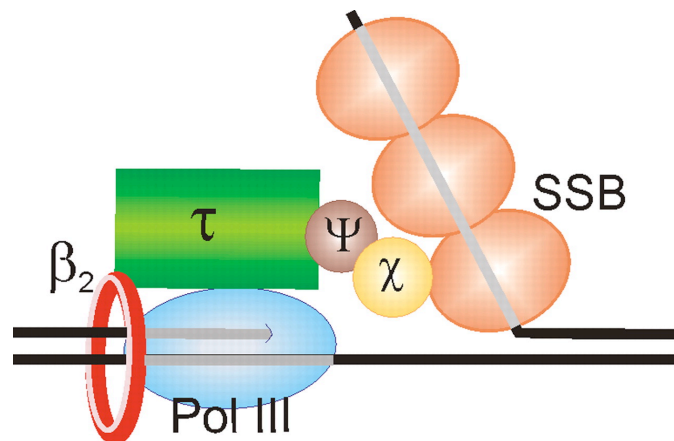


Figure 2.8 Model for the strand displacement reaction with Pol III HE subunits. The flap is covered by SSB, and the primer is bound with polymerase. χ connects polymerase to SSB via a τ - ψ link. Thus, SSB- χ - ψ - τ forms a bridge to stabilize interaction of Pol III with the strand displacement template and, presumably, natural replication forks where the flap would represent the lagging strand template and the polymerase shown, the leading strand half of the replicase.

As first pointed out by Marians (Xu and Marians, 2003), a Pol III HE-catalyzed DnaB-independent strand displacement reaction could present problems for the cell and, under some circumstances, is negatively regulated by PriA. They proposed PriA could act by binding to the 3'-end of a primer juxtaposed to a fork and block binding by the Pol III HE. Interestingly, gp59, a T4 bacteriophage encoded protein that has multiple functions, some of which overlap with PriA, can block the action of T4 DNA polymerase by forming a ternary complex with it on DNA where gp59 site-specifically contacts the polymerase and locks it into a conformation where exonuclease and polymerase activities are inhibited (Xi et al., 2005). Our studies cannot yet resolve which of these two mechanisms are used by *E. coli* PriA in blocking the Pol III HE strand displacement reaction.

Our studies have an additional practical benefit. Rolling circle DNA replication systems that mimic the action of the replisome at an *in vivo* replication fork typically employ the PriA protein to initiate a series of interactions that result in the biologically relevant assembly of an active DnaB helicase at a replication fork. However, fork systems are sometimes assembled that lack the natural helicase loaders and researchers instead add large excesses of DnaB to drive self-assembly. Such systems, lacking the PriA checkpoint protein, could be complicated by the strand displacement activities of Pol III HE, especially if conducted in the presence of τ and high Pol III and dNTP concentrations. The understanding of the properties of the intrinsic Pol III HE strand displacement reaction will permit artifacts, driven by its action, to be avoided in such systems in the future.

CHAPTER III

**CYCLING OF THE *E. COLI* LAGGING STRAND POLYMERASE IS TRIGGERED
EXCLUSIVELY BY THE AVAILABILITY OF A NEW PRIMER AT THE REPLICATION
FORK**

3.1 Abstract

Two models have been proposed for the mechanism whereby a lagging strand replicase is triggered to release from the preceding Okazaki fragment and cycle to the primer for the next. Collision with the 5'-end of the preceding fragment and synthesis of a new primer by primase have been posited as the triggers for the collision and signaling models, respectively. I developed a minicircle replication system with a highly asymmetric G:C distributions between strands to distinguish these models. Specific perturbation of lagging strand synthesis with ddGTP or dGDPNP yielded results that confirmed the signaling model and ruled out the collision model. I demonstrated that the presence of a primer, not primase *per se*, provides the signal that triggers cycling. Lagging strand synthesis proceeds much faster than leading strand synthesis, explaining why gaps between Okazaki fragments are not found under physiological conditions. Reconstitution of the *E. coli* replicase with forms of the clamp loader containing one, two or three copies of the τ form of DnaX all yield full length Okazaki fragments in the presence of dNTPs and equivalent gaps between fragments when lagging strand synthesis is specifically slowed with dGDPNP.

3.2 Introduction

The *E. coli* chromosome is replicated by a dimeric DNA polymerase III holoenzyme (Pol III HE) in a reaction where replication is coupled between the leading and lagging strands (McHenry, 1982; Wu et al., 1992; Kim et al., 1996b). Like all replicases, the Pol III HE is tripartite with a specialized replicative polymerase (Pol III, $\alpha\epsilon\theta$), a sliding clamp processivity factor (β_2) and a clamp loader (DnaX complex, $\text{DnaX}_{\delta\delta'\chi\psi}$) (McHenry, 2011b). The leading strand is highly processive, capable of synthesizing products of at least 150,000 bases *in vitro* without dissociating (Mok, 1987; Mok and Marians, 1987; Tanner et al., 2009). In a coupled reaction, the lagging strand polymerase must cycle rapidly during the synthesis of a series of Okazaki fragments. Thus, a signal must exist that triggers the lagging strand polymerase to switch from a highly processive state to one that can rapidly cycle to the next primer synthesized at the replication fork.

Two models have been proposed for the source of the signal that triggers cycling. In the 'signaling' model, it was proposed that synthesis of a new primer by primase triggers the lagging strand polymerase to cycle, even if the Okazaki fragment being synthesized is incomplete (Wu et al., 1992). Evidence for this model first arose in early replication fork reconstitution experiments that demonstrated that if Pol III was diluted below approximately 1 nM that gaps were detected between Okazaki fragments (Wu et al., 1992). This suggested that the signal that triggered cycling was not dependent upon Okazaki fragment completion. DnaG primase synthesizes primers by reversible association with the DnaB helicase (Tougu and Marians, 1996b). Thus, primase concentration determines the frequency of priming and the length of Okazaki

fragments. Coupling of these observations led to the proposal that primase set the timing of events at the replication fork and provided the signal of lagging strand polymerase release and recycling to the next primer (Tougu and Marians, 1996b).

Further support for the signaling model derived from the observation that long leading strands could be synthesized, providing long templates for lagging strand synthesis, in the absence of primase. Upon addition of primase, the first Okazaki fragment could have been up to 100 Kb, yet it was of normal length, again suggesting a signal that was independent of Okazaki fragment completion (Li and Marians, 2000).

An alternative model, the 'collision model' proposed that the *E. coli* lagging strand polymerase was triggered to recycle by colliding with the preceding Okazaki fragment (Leu et al., 2003) or by approaching the preceding Okazaki fragment (Georgescu et al., 2009). A mechanism in which τ sensed the conversion of a gap to a nick and competed with the β processivity factor for binding to the C-terminus of the Pol III α subunit was proposed (López de Saro et al., 2003a, 2003b). However, it is now realized that the C-terminus of the Pol III α subunit does not contain the binding site required for a processive interaction with β either in vitro or in vivo (Dohrmann and McHenry, 2005). Instead, the β binding site is internal (Kim and McHenry, 1996b; Dalrymple et al., 2001; Dohrmann and McHenry, 2005; Bailey et al., 2006). The C-terminus of Pol III α provides the τ -binding site (Dohrmann et al., 2011; Liu et al., 2013).

An alternative proposal was made that the OB fold within α might sense the disappearance of single-stranded DNA in advance of the primer terminus (Georgescu et al., 2009). Consistent with this hypothesis, the ssDNA binding portion of Pol III was localized to a C-terminal region of α that contains the OB fold element (McCauley et al.,

2008) and the OB fold may be near the template in a crystal structure of a complex Pol III α with primed template (Wing et al., 2008b). A test of the importance of the OB fold motif was made using a mutant in which three basic residues located in the β 1- β 2 loop were changed to serine (Georgescu et al., 2009). The processivity of the mutant polymerase was decreased by the β 1- β 2 loop mutations, an effect that was rescued by the presence of the τ complex (Georgescu et al., 2009). The latter observation would seem to suggest that although the OB fold contributes to ssDNA affinity and processivity, it is not the processivity sensor, or at least that the residues mutated are not the key interactions.

The evidence behind the collision model was primarily based on modulation of binding affinities. The relevant issue is whether the processes are kinetically competent to support physiological rates of DNA replication. Determinations of the rates and extents of Pol III dissociation upon completion of an Okazaki fragment (Dohrmann et al., 2011) agreed with models that dissociation is enhanced upon adding the last nucleotide to convert a gap to a nick (Leu et al., 2003), but not with models that posit that just reducing the size of the gap between Okazaki fragments is sufficient (Georgescu et al., 2009). However, the half-life of Pol III HE on nicks upon Okazaki fragment completion is approximately two minutes, approximately 1000-fold too slow to support physiological rates of cycling during lagging strand DNA replication (Dohrmann et al., 2011). Thus, the collision model might be involved in slow release reactions that occur at sites other than the replication fork, such as long patch DNA repair or mismatch repair, but is too slow to support DNA replication at the fork.

In this study, I sought a rigorous test of the signaling model in a coupled rolling fork replication system that was reconstituted in the presence of high template concentrations so that DnaB and Pol III concentrations could be set as substoichiometric and limiting. This eliminated the possibility that exogenous polymerase or helicase were acting on products after their initial synthesis.

3.3 Materials and Methods

Proteins: DnaB₆ (Marians, 1995a), DnaG (Griep and McHenry, 1989), SSB₄ (Griep and McHenry, 1989), and β_2 (Johanson et al., 1986), Pol III (Kim and McHenry, 1996c), four different DnaX complexes with stoichiometries of $\tau_3\delta\delta'\chi\psi$, $\tau_2\gamma_1\delta\delta'\chi\psi$, $\tau_1\gamma_2\delta\delta'\chi\psi$, and $\gamma_3\delta\delta'\chi\psi$ (Glover and McHenry, 2000; Pritchard et al., 2000) were purified as described. PriA, PriB, DnaT, and DnaC were expressed in *E. coli* BL21 DE3 pLysS and purified by modifications of procedures of Marians (Marians, 1995a) that are described under *Supplemental Experimental Procedures* in Appendix 1.

Pol III* was expressed in *E. coli* strain BLR (*F ompT hsdS_B(r_B⁻ m_B⁻) gal dcm Δ (*srl-recA*)306::Tn10 (Tet^R)*) containing the plasmid pHOC 2.6.1 and the purification described under *Supplemental Experimental Procedures*. This plasmid contained the structural genes for the components of Pol III* expressed behind an IPTG inducible P_{A1} promoter in the order: *dnaQ*, *holE*, *dnaE*, *holC*, *holD*, *holB*, *holA*, *dnaX*. The spacing between genes was kept to a minimum and, where possible, translational terminators were overlapped with translational initiators to permit translational coupling. The parent plasmid was pDRK-N(M) (Kim and McHenry, 1996c). pDRK-N(M) contains the IPTG

inducible P_{A1} promoter, a *colE1* replication origin, and an ampicillin resistant gene. The *dnaQ*, *holE*, and *dnaE* genes came from the plasmid pHN4 (Kim and McHenry, 1996a).

Pol III* (Pol III₃ $\tau_3\delta\delta'\chi\psi$) was assembled from purified Pol III and DnaX complex ($\tau_3\delta\delta'\chi\psi$) at a molar ratio of 5:1. Pol III* (Pol III₃ $\tau_2\gamma_1\delta\delta'\chi\psi$) was assembled from purified Pol III and DnaX complex ($\tau_2\gamma_1\delta\delta'\chi\psi$) at a molar ratio of 4:1. Pol III* (Pol III₃ $\tau_1\gamma_2\delta\delta'\chi\psi$) was assembled from purified Pol III and DnaX complex ($\tau_1\gamma_2\delta\delta'\chi\psi$) at a molar ratio of 4:1. Assembly was performed at room temperature for 5 min. The assembled complexes were desalted on NAP-25 columns and purified by Mono-S columns as described (Dohrmann et al., 2011).

Optimized rolling circle reaction: 20 nM mini-circle DNA template, 0.5 μ M SSB₄, 100 nM β_2 , 12 nM DnaB₆, 100 nM DnaG, 2.5 nM Pol III*, 160 nM PriA, 50 nM PriB₂, 333 nM DnaT₃, and 108 nM DnaC were incubated with 5 μ M ATP γ S, 200 μ M CTP, 200 μ M UTP, and 200 μ M GTP for 5 min at 30°C. The concentration of DnaG used was on the plateau of the titration, four-fold greater than the optimum selected. It was used to adjust the length of Okazaki fragments to the physiological range of 1-2 kb.

The reaction buffer was 10 mM magnesium acetate, 70 mM KCl, 50 mM HEPES (pH 7.5), 100 mM potassium glutamate, 20 % glycerol, 200 μ g/ml bovine serum albumin, 0.02% Nonidet P-40, and 10 mM dithiothreitol. 1 mM ATP and 100 μ M dNTPs were added to start the reaction. After 3 min, α -[³²P] dCTP or dGTP were added to allow quantification of leading and lagging strand synthesis, respectively. The reaction was quenched with either 83 mM EDTA for scintillation counting or an equal volume of stop mix (40 mM Tris-HCl (pH 8.0), 0.2% SDS, 100 mM EDTA, and 50 μ g/ml proteinase

K) for gel electrophoresis after 5 min. For the analysis of the size of lagging strand products, samples subjected to alkaline agarose gel electrophoresis.

Nucleotide analogs: dGDPNP was custom synthesized for this project by TriLink Biotechnologies.

Quantification of DNA synthesis: DNA products were quantified by TCA precipitation and scintillation counting as described for strand displacement replication assays (Yuan and McHenry, 2009).

Alkaline Agarose Gel Electrophoresis: For the analysis of the size of lagging strand products, samples were digested with protease K (30 min, 37 °C, 25 µg/ml) mixed with 30 mM NaOH, 2 mM EDTA, 2% glycerol, and 0.02% bromophenol blue and fractionated on 0.6% alkaline agarose gels for approximately 18 h at 24 V in a running buffer of 30 mM NaOH and 2 mM EDTA. Gels were fixed in 8% (w/v) trichloroacetic acid, dried onto DEAE paper, autoradiographed on storage phosphor screens, and scanned with a PhosphorImager.

Determination of Okazaki Fragment Length: The lengths of Okazaki fragment (L) were determined by a method that removed the bias of more radioactivity being incorporated into longer products using $L = \sum(L_i \cdot n_i) / \sum n_i$. n_i is the relative molar amount of the Okazaki fragments with a certain length L_i . $n_i = \text{density}_i / L_i$, where density_i is the pixel density at L_i in a lane determined using ImageQuant. Thus, $L = \sum \text{density}_i / \sum (\text{density}_i / \text{length}_i)$. To exclude leading strand product, only density below 8 kb was used for calculation of average Okazaki fragment length unless otherwise indicated specifically.

Determination of primer utilization and the numbers of GMP+UMP per Okazaki fragment: Rolling circle reactions were carried out in the presence of α -[³²P] GTP and α -

[³²P] UTP (specific activity 12,000 cpm/pmol) or α -[³²P] dCTP (specific activity 400 cpm/pmol). The sample was loaded to 20% denatured polyacrylamide gel with 50% w/v urea. γ -[³²P] ATP labeled 12-mer RNA and 20-mer DNA were loaded as markers. The gel was prerun at 14 W for 30 min and then run at 12 W for 3.5 h. The gel was dried on DEAE paper, exposed to a phosphorimage screen for 18 hours, and scanned with a PhosphorImager. 10-14 mer was quantified as free primers, and the dark bands at the top of the gel were quantified as elongated primers.

Considering the count from scintillation counting was directly proportional to the pixel density from phosphorimaging, the specific activity measured using scintillation counting was employed to substitute for the specific activity in pixel density. 1 μ l of α -[³²P] G/UTP and 1 μ l of α -[³²P] dCTP were spotted on a GFC filter paper and the counts were determined with a scintillation counter. The specific activity of α -[³²P] G/UTP and α -[³²P] dCTP were calculated by the count divided by the amount of each nucleotide in a reaction. A relative amount of α -[³²P] G/UTP and α -[³²P] dCTP incorporation was calculated by the pixel density of bands divided by the specific activity of the corresponding radioactive material. This term was directly comparable among different bands.

3.4 Results

3.4.1 Establishing an efficient *E. coli* rolling circle replication system on tailed mini-circular templates with an asymmetric G:C distribution

I chose to establish a complete PriA-dependent replication system that used defined minicircle templates to exploit multiple significant advantages such systems

afford (Lee et al., 1998, 2002; Yang et al., 2003). (i) Employing defined templates permits creating an asymmetric nucleotide composition between the two strands, enabling quantitation of the levels of synthesis of each strand by measuring nucleotide incorporation. (ii) Extreme asymmetry in strand nucleotide composition permits selective modulation of the rates of lagging strand synthesis. (iii) Use of small DNA substrates allows higher template concentrations to be used, allowing substoichiometric helicase and polymerase concentrations. This helps avoid side reactions resulting from excess helicase acting on reaction products and excess polymerase extending unused primers at sites remote from the replication fork. (iv) Use of the full PriA/ PriB/ DnaT/ DnaC-dependent helicase loading system avoids the necessity of using vast excesses of helicase and permits blocking of a helicase-independent background reaction catalyzed by the strand displacement activity of Pol III HE in the presence of SSB (Xu and Marians, 2003; Yuan and McHenry, 2009).

I established the system using a tailed 409 bp circle initially developed for *B. subtilis* rolling circle replication (Sanders et al., 2010). This DNA substrate contained a 50:1 ratio of C:G in the template for lagging strand synthesis. This template is longer than those commonly employed in minicircle systems and was chosen to minimize potential steric issues at the replication fork. Modifying our previous scheme to create this template to include a PCR amplification step permitted very large quantities to be made (Fig. S1.10).

Each individual component of the reconstituted rolling circle reaction was titrated to its optimum, except DnaB₆ helicase and Pol III* which were deliberately maintained at limiting, substoichiometric concentrations (Fig. S1.1-3). Titrations performed at standard

low (1 nM) vs. high (20nM) template concentrations revealed significant differences. I was unable to obtain efficient replication with substoichiometric helicase and polymerase in the presence of 1 nM template, presumably because I was working under K_D s required for reaction components to efficiently interact (Fig. S1.1). An acceptably efficient reaction could be reconstituted with 12 nM DnaB₆ and 2.5 nM Pol III* on 20 nM templates (Fig. S1.3). I observed significant differences in the requirement for SSB between the low and high template concentration systems. In the presence of 20 nM template, SSB stimulated the reaction four-fold. No SSB dependence was observed in the presence of 1 nM template (Fig. 3.1A,B).

The effect of PriA on reactions performed at low and high template concentrations also differ in potentially important ways. As the first step of our optimization, I titrated PriA into an otherwise complete reaction that lacked DnaB₆ to determine the level of PriA required to completely block a background reaction catalyzed by the strand displacement activity of the Pol III HE (Fig. 3.1C,D). Reactions containing higher template concentrations required higher concentrations of PriA for inhibition of intrinsic strand displacement activity of Pol III HE. PriA was then titrated into a complete reaction that contained DnaB₆. In reactions conducted at low template concentrations, I observed a high background level of leading strand synthesis in the absence of PriA (Fig. 2.1E). Addition of PriA restored stoichiometric leading and lagging strand synthesis. At high template concentration, which permitted use of substoichiometric DnaB₆ and Pol III*, equivalent levels of leading and lagging strand synthesis were observed at all levels of PriA (Fig. 3.1F). Instead of the inhibition, I observed, due to suppression of a nonphysiological background reaction, stimulation on

1 nM template with an optimum near the point where helicase-independent strand displacement is abolished. These characteristics led us to have a higher level of confidence in reactions conducted using 20 nM template and substoichiometric DnaB₆ and Pol III* and these conditions were used for further study.

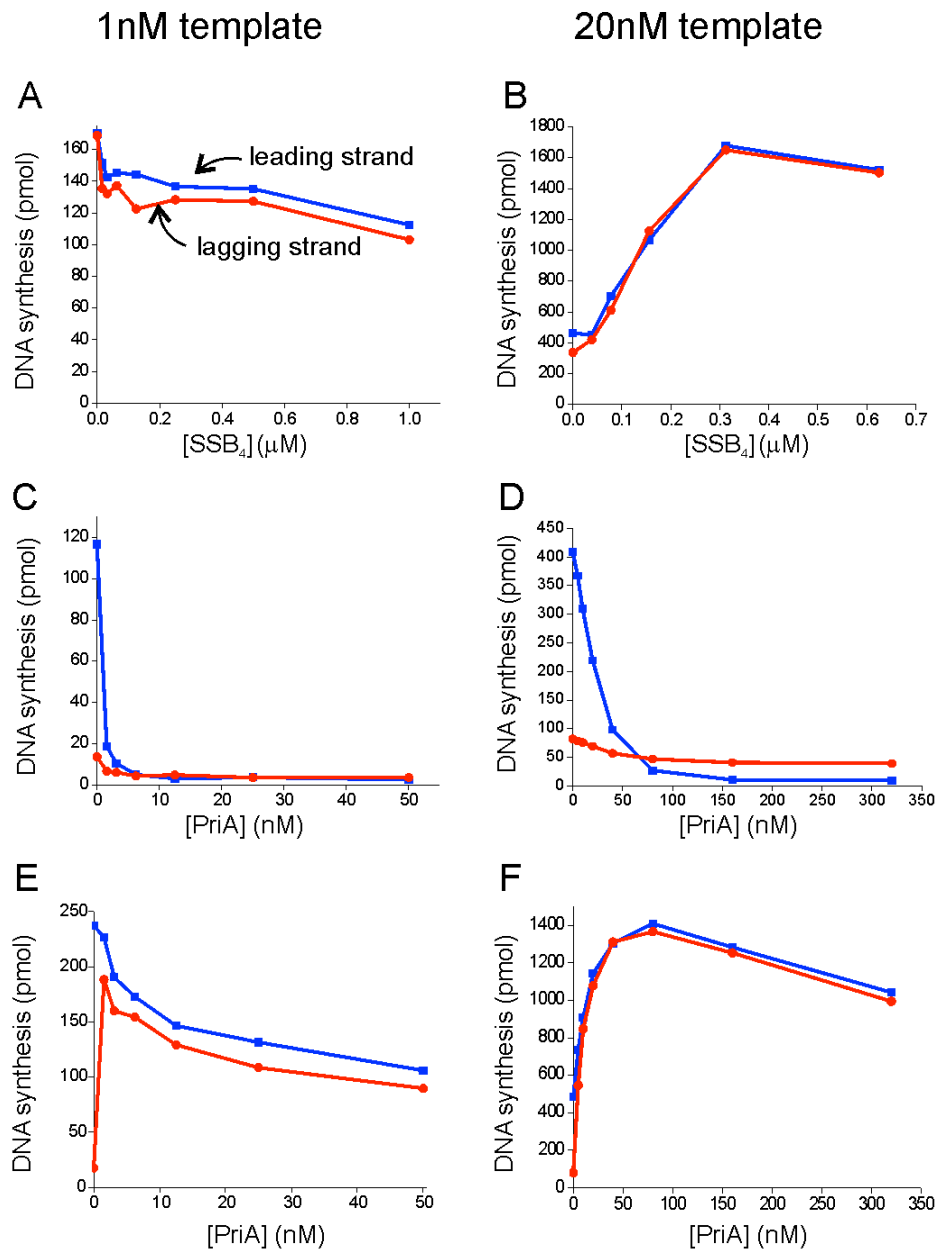


Figure 3.1 Reactions conducted at high template concentration and substoichiometric helicase and Pol III* become dependent upon PriA and SSB. (A, B) SSB titration in the presence of 1 nM and 20 nM DNA under optimal conditions.

(C, D) PriA titration in the presence of 1 nM and 20 nM DNA under optimal conditions but without DnaB.

(E, F) PriA titration in the presence of 1 nM and 20 nM DNA under optimal conditions.

In the presence of low helicase and Pol III* concentrations, helicase loading and initiation complex formation are rate-limiting. I discovered these barriers could be overcome by pre-incubation of all components with ATP γ S and CTP, UTP and GTP (Fig. S1.4). ATP γ S supports loading of the helicase if the other primosomal proteins are present (Manhart and McHenry, 2013) and initiation complex formation by the leading strand half of the dimeric replicase (Glover and McHenry, 2001). The absence of ATP prevents translocation of loaded helicase.

3.4.2 Specific blockage of Okazaki fragment synthesis before completion does not terminate overall lagging strand synthesis, consistent with predictions of the signaling model

The asymmetry in G:C composition between the leading and lagging strand templates permits specifically perturbing lagging strand synthesis by the addition of ddGTP. This chain terminator would be expected to terminate synthesis before Okazaki fragment synthesis is complete. The signaling model would predict efficient cycling of the lagging strand polymerase upon new primer synthesis at the fork. The collision model would predict an abrupt cessation of lagging strand synthesis, because the polymerase would never collide with the 5'-end of the preceding Okazaki fragment and be induced to cycle. Addition of increasing concentrations of ddGTP decreases the length of the Okazaki fragments observed (Fig. 3.2A). In a control reaction, the rate of leading strand synthesis was shown to be unperturbed (Fig. 3.2B).

I next measured the rate of nucleotide incorporation into the leading and lagging strands in the presence and absence of ddGTP. I observed a nearly undiminished rate of leading strand synthesis and a drop in lagging strand nucleotide incorporation to about one-half (Fig. 3.2C). In the presence of ddGTP, the length of Okazaki fragments is reduced (Fig. 3.2A), explaining much of the reduction of synthesis. If the collision model was the dominant model on the time scale of the experiment, one Okazaki fragment would be synthesized in less than two seconds and synthesis would stop, leading to a complete abolishment of Okazaki fragment synthesis. When these reactions were conducted in the presence of increasing ddGTP concentrations, the level of Okazaki fragment synthesis decreased, but synthesis continued at a remarkably linear rate (Fig. S1.5). Much of the decrease is due to shortening of the Okazaki fragments at increasing ddGTP concentrations. Thus, the molar level of Okazaki fragment synthesis does not decrease to the same extent that nucleotide incorporation does.

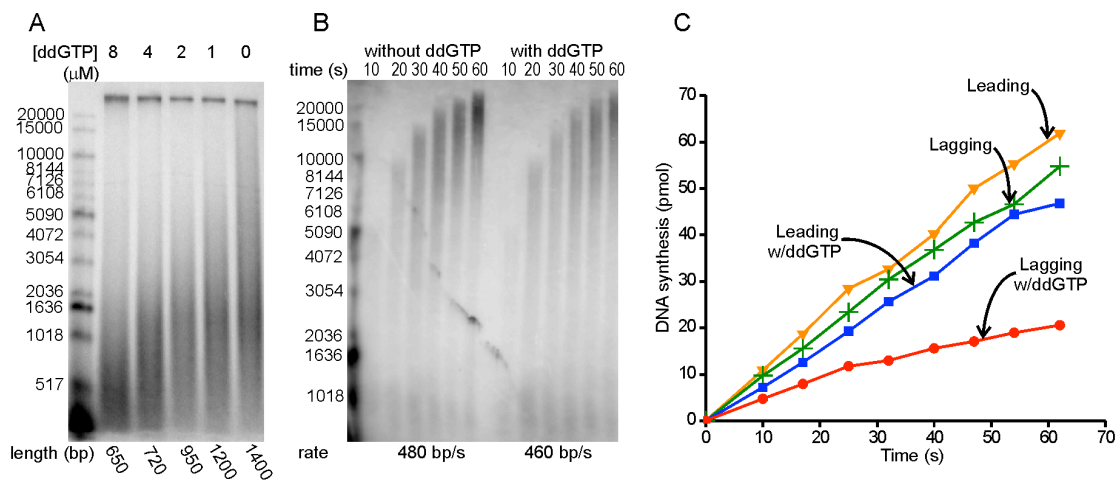


Figure 3.2 ddGTP halts Okazaki fragment synthesis before completion, but lagging strand synthesis continues.

(A) Reactions were carried out under conditions of the optimized rolling circle reaction with ddGTP added at the same time as radiolabeled nucleotide. Okazaki fragments

incorporating α - ^{32}P] dGTP(10,000 cpm/pmol) were monitored by alkaline agarose gel electrophoresis. Lengths were determined with the cutoff to exclude leading strand products of 20 kb.

(B) In the presence and absence of 4 μM ddGTP, an optimized rolling circle reaction was conducted as in panel A except that α - ^{32}P] dCTP (20,000 cpm/pmol) and ddGTP were added at the same time as dNTPs and ATP. The 3 min elongation step in the presence of non-radioactive dNTPs before the addition of radioactive nucleotide was skipped so that the products would be short enough for accurate length quantification. Radiolabeled leading strand products were monitored on an alkaline agarose gel. The products of 10s, 20s, and 30s reactions were used to calculate the rate of leading strand synthesis.

(C) The amount of leading and lagging strand synthesis in the absence (leading-orange; lagging-green) and presence (leading-blue; lagging-red) of 1 μM ddGTP.

3.4.3 Selectively slowing the rate of lagging strand synthesis with dGDPNP results in cycling to the next primer before Okazaki fragment completion, consistent with the signaling model

The signaling model would predict that the Okazaki fragments synthesized in the presence of ddGTP would have gaps between them that corresponded proportionally to the amount that they were shortened. I was unable to find a suitable polymerase that could exonucleolytically remove incorporated ddGMP that did not strand displace to test this hypothesis. So, I switched to the use of another perturbant of lagging strand synthesis, dGDPNP, that offered its own unique advantages. dGDPNP exhibits a much higher K_m than dGTP (40 μM vs. 2 μM respectively) (Fig. S1.6A,B). This allowed us to adjust the rate of lagging strand synthesis by decreasing the concentration of dGDPNP without going below the concentration of the normal dNTPs in the reaction and creating a danger of artifacts from nucleotide depletion.

Measurement of the rates of primer extension on M13 templates were used as a surrogate for a template that required the incorporation of dGMP for elongation, like the

lagging strand template in our model minicircle system. Substitution of 240 μM dGDPNP for saturating dGTP led to a 10-fold decrease in elongation rate, suggesting slowing of the chemistry step of the polymerase reaction in addition to the K_m effect (Fig. S1.6C). Reduction of dGDPNP to 30 μM decreased the elongation rate *ca.* 25-fold relative to dGTP. Control reactions for the rate of leading strand synthesis indicated the lack of a significant perturbation (Fig. S1.6D).

Reduction in the concentration of dGDPNP in the presence of the other three normal dNTPs resulted in a marked decrease in the length of Okazaki fragments produced (Fig. 3.3). Deproteinization and treatment of the rolling circle reaction products with Pfusion DNA polymerase results in extension of all of the shortened Okazaki fragments to approximately the same length (Fig. 3.3). In control experiments, I demonstrated that this polymerase does not significantly strand-displace (Fig. S1.11). The results suggest that Okazaki fragments synthesized during balanced synthesis have negligible gaps between them while those synthesized in the presence of 30 μM dGDPNP have *ca.* 400 nt gaps between them. Length quantification in these experiments used a normalization procedure that removed the bias of longer products containing more radioactive nucleotide. Thus, the numbers presented represent the molar mean length.

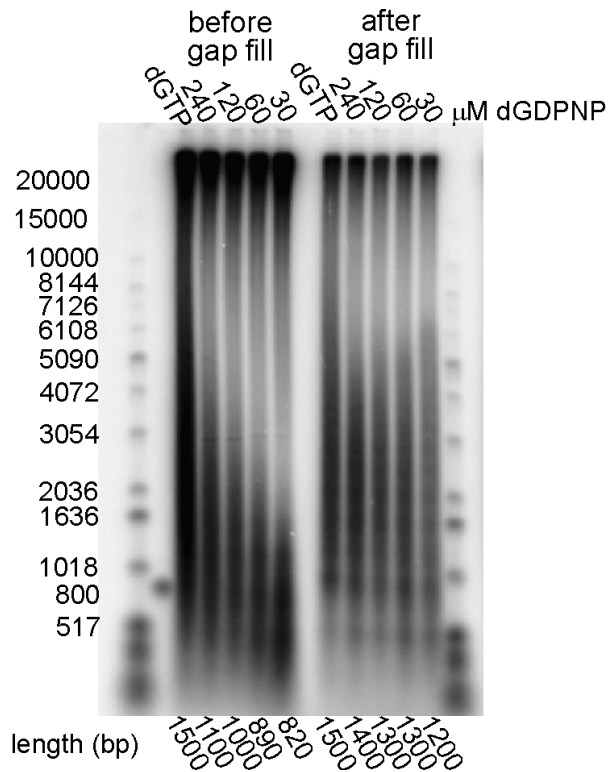


Figure 3.3 Replacement of dGTP with dGDPNP leads to short Okazaki fragments followed by large gaps. An optimized rolling circle reaction with 20 mM template was carried out in the presence of 100 μ M dGTP or indicated concentration of dGDPNP. Products were extracted with phenol-chloroform, precipitated by isopropanol, and incubated with 100 μ M dNTPs, 0.2 U Phusion polymerase, and α - 32 P dATP (12,000 cpm/pmol) at 72 $^{\circ}$ C for 15 min. The products before and after the gap fill assay were monitored by alkaline agarose gel electrophoresis.

3.4.4 The presence of dGDPNP does not significantly influence the frequency of primer synthesis or primer utilization

It is possible that the length of Okazaki fragments could be reduced by more frequent primer synthesis or an increased rate of primer utilization. I investigated this possibility using gel assays to quantify the percentage of unelongated primers to determine primer utilization (Zechners et al., 1992) (Fig. S1.8). Incorporation assays, quantifying the ratios of radiolabeled GMP and UMP incorporated relative to dCMP were used as a measure of priming frequency. I observed a modest decrease in primer

utilization (from 66% to 50%) upon substitution of dGDPNP for dGTP (Table 3.1). The number of GMP and UMP residues/ Okazaki fragment increased from eight to ten (Table 3.1). Thus, the decrease in Okazaki fragment size in the presence of dGDPNP cannot be attributed to perturbations in priming.

	Corrected G+U in elongated primers	Corrected G+U in unelongated primers	Corrected dC in rolling circle product	Utilization efficiency ^a	Average utilization efficiency	G+U in elongated primer/dNTP in rolling circle ^b	Gap-filled Okazaki Fragment (bp) ^c	# of G+U/ Okazaki Fragment (bp) ^d
100 μ M dGTP	650	380	54,000	63%		0.0054		
	630	290	53,000	68%	66 \pm 3%	0.0053	0.005 1 \pm 0.0005	1500
	810	380	82,000	68%		0.0044		8 \pm 1
240 μ M dGDPNP	460	470	44,000	49%		0.0047		
	820	330	45,000	71%	60 \pm 11%	0.0081	0.0059 \pm 0.0020	1400
	600	420	57,000	59%		0.0048		8 \pm 3
30 μ M dGDPNP	360	410	23,000	47%		0.0070		
	380	400	23,000	49%	50 \pm 4%	0.0074	0.0081 \pm 0.0016	1200
	540	420	25,000	56%		0.0098		10 \pm 2

^a Utilization efficiency = Corrected G+U in elongated primers/(Corrected G+U in elongated primers + Corrected primers)
^b G+U in elongated primer/ dNTP in rolling circle = Corrected G+U in elongated primers/(Corrected dC in rolling circle/%dC in rolling circle)
^c Values taken from Figure 3.
^d # of G+U/OF = G+U in elongated primer/dNTP in rolling circle x Gap filled Okazaki Fragment (bp)

Table 3.1 Determination of primer utilization and priming frequency

3.4.5 The signal for cycling of the lagging strand polymerase is the availability of a new primer at the replication fork and is not dependent upon the presence or action of DnaG primase

Coupled with the previous observation that the rate of release of the Pol III HE upon collision with the 5'-end of the preceding Okazaki fragment does not provide a kinetically competent pathway (Dohrmann et al., 2011), the preceding experiments

suggest that cycling of the lagging strand polymerase is regulated by synthesis of a new primer at the replication fork as initially proposed by Marians (Wu et al., 1992). With the new tools developed for this work, I sought to determine whether this signal was provided by the action of DnaG or whether just the availability of an annealed primer at the fork was sufficient. Previous work demonstrated that priming at the replication fork can occur through exogenously provided primers (Li and Marians, 2000). These reactions require large excesses of oligonucleotides, presumably because the annealing reaction at the fork is kinetically driven.

I determined that by omitting primase and substituting a 120 nM 15-mer complementary to a unique position within the 409 nt template, that Okazaki fragments with an average length of *ca.* 1800 nt could be obtained, comparable to the lengths observed if primers are synthesized by DnaG (Fig. 3.4A). A banding pattern, separated by approximately 400 nt was consistent with priming occurring at a unique location (Fig. 3.4A).

To determine if these exogenously provided primers could signal cycling, I titrated ddGTP into the reaction. The logic for this reaction was the same as explained for the experiment performed with DnaG-primed synthesis reported in Figure 3.2. If lagging strand cycling occurs through the collision model, synthesis should abort after initial Okazaki fragments incorporate ddGMP before encountering the 5'-end of the preceding Okazaki fragment. When ddGTP is added to the reaction Okazaki fragments become progressively smaller just as they do in the primase-primed reaction (Fig. 3.4A). Comparison of the rates of leading strand synthesis in the presence and absence of ddGTP shows similar rates of synthesis indicating no significant perturbation of the

rates of leading strand synthesis (Fig. 3.4B). I observe robust synthesis of Okazaki fragments in the presence of synthetic primers, both in the presence and absence of ddGTP. (Fig. 3.4C). Okazaki fragment synthesis remains linear for over a minute in the presence of ddGTP.

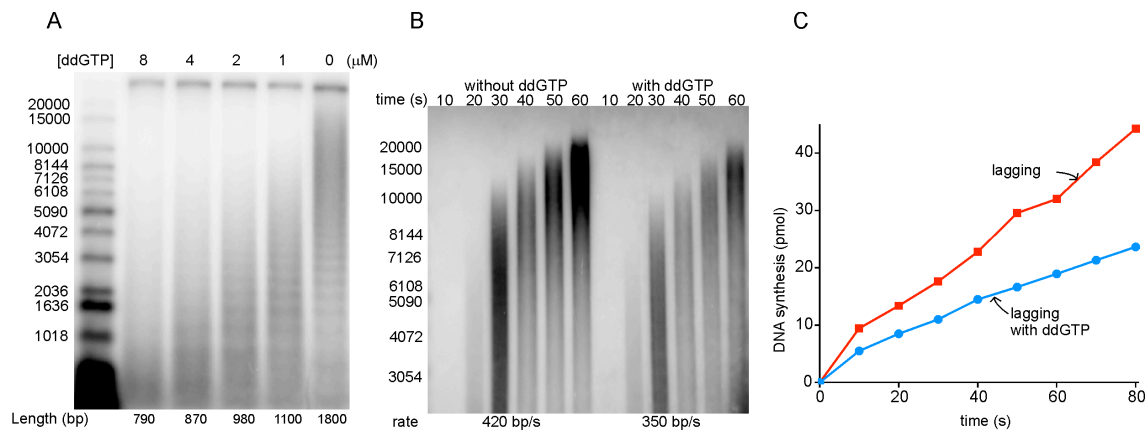


Figure 3.4 The availability of primers signals the polymerase to cycle.

(A) Optimized rolling circle reactions were carried out as described except synthetic 15-mer primers substituted for primase and GTP, CTP and UTP. ddGTP was added to the designated concentration at the same time radiolabeled nucleotide was added. Okazaki fragments incorporating α - ^{32}P dGTP (5000 cpm/pmol) were monitored by alkaline agarose gel electrophoresis. Lengths were determined with the cutoff to exclude leading strand products of 20 kb.

(B) In the presence and absence of 4 μM ddGTP, optimized rolling circle reactions were conducted as in panel A except α - ^{32}P dCTP or dGTP (3000 cpm/pmol) were added at the same time with ATP and dNTPs. The 3 min elongation step in the presence of non-radioactive dNTPs before the addition of radioactive nucleotide was skipped so that the products would be short enough for accurate length quantification. Leading strand products incorporating α - ^{32}P dCTP (20,000 cpm/pmol) were monitored by alkaline agarose gel electrophoresis. The products of 20s, 30s, and 40s were used to calculate the rate of leading strand synthesis.

(C) The amount of lagging strand synthesis in the presence of 1 μM ddGTP was quantified.

3.4.6 Pol III HE functions equivalently in coupled replication with one to three τ subunits

The DnaX complex of the *E. coli* replicase contains two distinct proteins, τ and the shorter γ protein that results from translational frameshifting. In the preceding experiments, I used Pol III* expressed and assembled from an artificial operon expressing both the γ and τ forms of DnaX. Thus, the Pol III* should reflect normal cellular stoichiometry which I believe to be dominated by the $\tau_2\gamma\delta\delta'\chi\psi$ form of the DnaX complex (McHenry, 2011b).

Because DnaX complexes containing three subunits that can be either γ or τ , four different stoichiometries are possible: $\tau_3\delta\delta'\chi\psi$, $\tau_2\gamma\delta\delta'\chi\psi$, $\tau\gamma_2\delta\delta'\chi\psi$, and $\gamma_3\delta\delta'\chi\psi$. These four forms have been reconstituted and resolved by high resolution chromatographic methods (Wieczorek et al., 2010). I tested the function of all four DnaX complexes in our minicircle replication system that permits the use of substoichiometric Pol III* (DnaX complex + Pol III). I found that all three τ -containing DnaX complexes functioned equivalently in terms of equivalent levels of leading and lagging strand synthesis (Fig. 3.5A). Interestingly, all three τ -containing DnaX complexes synthesized Okazaki fragments of the same length in the presence of the four natural dNTPs (Fig. 3.5B, lanes labeled dGTP). The extent to which Okazaki fragments were shortened when lacking strand synthesis was specifically slowed down by substituting dGDPNP for dGTP and lowering its concentration below its K_m was the same for all three τ -containing DnaX forms (Fig. 3.5B). DnaX complex lacking τ (γ complex) was unable to function under the experimental conditions used (Fig. 3.5 A,B).

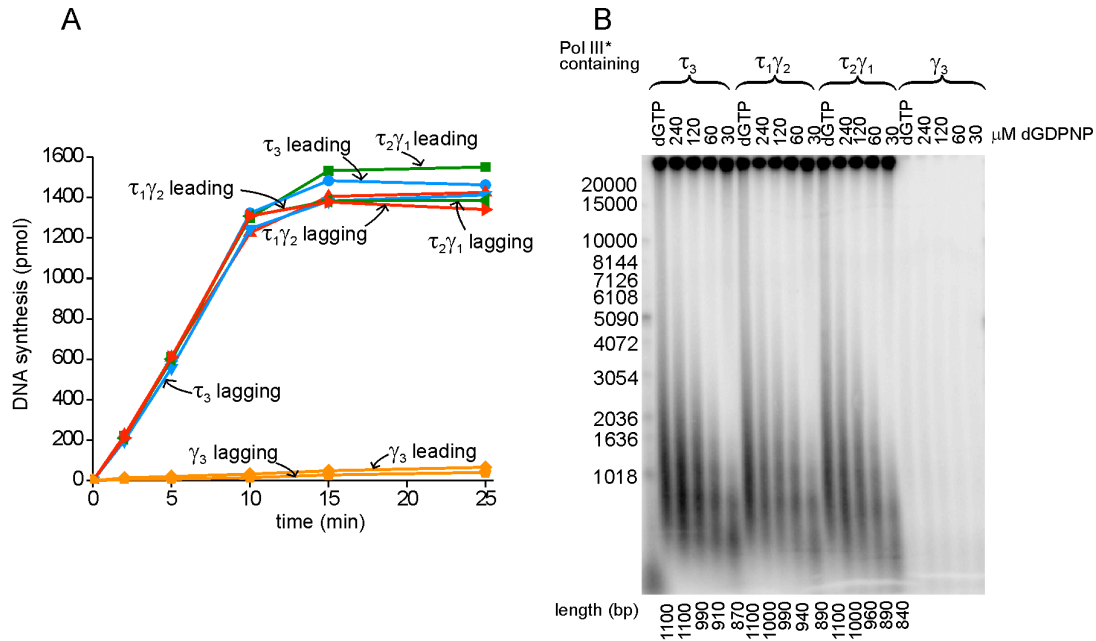


Figure 3.5 Pol III* reconstituted with DnaX complexes containing τ_3 , $\tau_2\gamma_1$, and $\tau_1\gamma_2$ produce the same length lagging strand products.

(A) An optimized rolling circle reaction was conducted with Pol III* reconstituted with the designated DnaX complexes, using α - ^{32}P dCTP or dGTP (3000 cpm/pmol) labeled the leading and lagging strands, respectively.

(B) Optimized rolling circle reactions were conducted in the presence of either 100 μM dGTP or the indicated amount of dGDPNP. α - ^{32}P dATP (2000 cpm/pmol) was used to label both leading and lagging strands which could be distinguished by their length after alkaline agarose gel electrophoresis.

3.5 Discussion

Two models have been proposed for providing the trigger to convert an otherwise highly processive replicase to rapidly cycle during Okazaki fragment synthesis. In the collision model, it had been posited that collision with the 5'-end of the preceding Okazaki fragment provided the signal. We recently eliminated the collision model showing that it is kinetically incompetent—the Pol III HE takes nearly two minutes to release and recycle upon collision with the 5'-end of model Okazaki fragments

(Dohrmann et al., 2011). The alternative signaling model proposed that synthesis of new primers by DnaG primase provided the signal for cycling (Wu et al., 1992).

To provide a rigorous test for the signaling model under conditions of balanced ongoing replication, I set up a large (409 nt) 5'-flapped minicircle system with highly asymmetric (50:1) G:C composition. That not only allowed convenient monitoring of leading and lagging strand synthesis by quantifying radiolabeled dGMP or dCMP incorporation, but provided a means to selectively perturb lagging strand synthesis without affecting leading strand replication. Also, as demonstrated in the bacteriophage T7 system (Lee et al., 1998, 2002), use of minicircles allows high template concentrations to be achieved so that substoichiometric helicase and replicase can be used, avoiding artifacts arising from action of these enzymes, if present in excess, on the initial replication products. Indeed, rolling circle replication reconstituted under these conditions did behave differently showing a dependence on SSB and a dependence on PriA for leading strand replication.

As our first test of the signaling model, I prematurely terminated synthesis of lagging strands by adding increasing concentrations of the chain terminator ddGTP to reactions containing the four normal dNTPs. I observed shortening of Okazaki fragments because of incorporation of the ddGMP chain terminator. Yet, the rate of Okazaki fragment synthesis remained linear. This observation was only consistent with the signaling model whereby a stalled replicase on a prematurely terminated Okazaki fragment was induced to cycle to the next primer at the replication fork. An alternative explanation might have been that the Pol III HE stalled on a ddNMP terminated chain somehow had a decreased affinity and released more rapidly. That possibility was

eliminated by direct experimental measurements of the rate of Pol III HE release from dNMP- and ddNMP-terminated chains (Dohrmann et al., 2011). The rate of release of Pol III HE from a ddCMP terminated chain within a gap varies from 6-11 minutes, several hundred-fold longer than the time required for synthesis of an Okazaki fragment.

To provide a further test of the signaling model, I substituted dGTP in reactions with dGDPNP. The chemistry step for insertion of this nucleotide is slowed and it also exhibits a higher K_m than dGTP. Thus, the rate of Okazaki fragment elongation can be 'dialed in' to the desired rate by decreasing dGDPNP concentrations. Using long single-stranded M13 templates, I was able to slow the elongation rate of Pol III HE from 570 nt/s (with 48 μM dGTP) to 23 nt/s (in the presence of 30 μM dGDPNP). The model M13 template contained *ca.* 25% C. Our lagging strand minicircle template contained 46% C. Thus, I would expect the rate of lagging strand synthesis on the minicircle to be decreased even further, but direct measurements were not experimentally accessible. Under these conditions leading strand synthesis on the minicircle template only decreased to 420 nt/s. Thus, dGDPNP could be used to selectively slow the rate of lagging strand synthesis. I observed shortened Okazaki fragments in the presence of dGDPNP, consistent with the elongating lagging strand replicase being induced to release and recycle to the next primer synthesized at the replication fork before completion of Okazaki fragment synthesis.

If the collision mechanism was used, to any significant level, even together with the signaling mechanism, it would take longer for an Okazaki fragment to be completed in the presence of dGDPNP. During this longer time, the replicase would have advanced, causing each Okazaki fragment to become increasingly longer. This

outcome would be the opposite of our experimental observations. This provides additional evidence, in the context of a complete replication system in the context of natural replication forks, that the collision model is not operational. This result is consistent with our earlier studies on model lagging strands that showed the collision model was kinetically incompetent.

If Pol III HE is signaled to cycle prematurely because of slow elongation in the presence of dGDPNP, one would expect gaps between the resulting Okazaki fragments. I tested this prediction by elongation of the putative incomplete Okazaki fragments with a thermophilic polymerase that does not strand displace, a representation made by the manufacturer that I experimentally verified. All shortened Okazaki fragments, regardless of their length were elongated to approximately the same length, consistent with a regular spacing of primers synthesized during rolling circle replication. I also experimentally verified that the rate of primer synthesis or utilization was not affected significantly by dGDPNP.

I note that Okazaki fragments synthesized in the presence of dGDPNP are not shortened to the same extent as would be predicted based on the slowing of replication on model M13 templates. In the presence of dGTP, Okazaki fragment length is only shortened 45% in the presence of 30 μ M dGDPNP. Based on the difference in elongation rates on M13 templates, I would expect the length of Okazaki fragments to be shortened 25-fold. I have experimentally determined that the rate of leading strand replication is not slowed. So, the rate of lagging strand synthesis using dGDPNP in coupled replication forks is much faster than expected. Thus, the rate of polymerization is somehow accelerated significantly within the lagging strand polymerase, at least with

dGDPNP. If the lagging strand polymerase rate is similarly accelerated using natural nucleotides, that would provide an explanation of why gaps in Okazaki fragments are rarely observed, even though the collision model is not operational. If the lagging strand polymerase is much faster than the leading strand polymerase, it will complete its synthesis first and wait for the synthesis of a new primer before cycling (Fig. 3.6). This model is consistent with whole cell single-molecule microscopy experiments. Using fluorescently-tagged SSB, waves of occupancy at the replication fork have been observed (Lia et al., 2012). As initially pointed out, if the rates of leading and lagging strand replication were equivalent, SSB occupancy at the replication fork would remain constant. It was concluded from these studies that the rate of lagging strand polymerase elongation was significantly faster than leading strand elongation (Lia et al., 2012). Faster rates of lagging strand elongation have been proposed for bacteriophage T7 replication as well (Pandey et al., 2009).

A single-molecule total reflection fluorescence microscopy study concluded that lagging strand synthesis that proceeded using DnaX complexes with a $\tau_2\gamma\delta\delta'\chi\psi$ composition contained gaps but that replicases with a $\tau_3\delta\delta'\chi\psi$ composition did not (Georgescu et al., 2011). Because the resolution of the CCD camera used in the experiments was 600 nt/pixel, lagging strand replication needed to be perturbed by decreasing DnaG primase to very low levels to obtain > 20,000 nt Okazaki fragments (Georgescu et al., 2011). I reinvestigated this finding using our coupled system with physiological Okazaki fragment size and observed no difference regardless of whether the experiments are conducted with $\tau_3\delta\delta'\chi\psi$, $\tau_2\gamma\delta\delta'\chi\psi$ or $\tau_1\gamma_2\delta\delta'\chi\psi$. DnaX complexes with

a $\gamma_3\delta\delta'\chi\psi$ composition (the classical γ complex that has long served as a prototype for DnaX complexes) is inert in our system.

It is believed that the natural Pol III HE from *E. coli* contains two τ subunits which dimerizes the leading and lagging strand halves of the replicase (McHenry, 2011b). However, τ also interacts with DnaB helicase (Kim et al., 1996a; Gao and McHenry, 2001b). It is possible that weak τ -DnaB interactions may provide some redundancy in replisome organization and permit $\tau\gamma_2\delta\delta'\chi\psi$ to function in our *in vitro* system.

Having established that the signaling model and not the collision model operates at the replication fork, I sought to identify the signal. Clearly some event associated with synthesis of a new primer is involved, as proposed in the initial model (Wu et al., 1992). I sought to distinguish whether the signal emanated from primase (or its interaction with helicase or some other replisome component) or merely from the availability of a new primer. It has been previously demonstrated that high concentrations of exogenous synthetic primers can be used to drive Okazaki fragment synthesis (Li and Marians, 2000). I applied the ddGTP technique used to demonstrate the use of the signaling model by the replisome with DnaG primase-synthesized primers to the replication system driven by exogenous primers and obtained the same result. Using a level of exogenous primer that gives approximately the same Okazaki fragment length as that obtained with primase, I titrated ddGTP and obtained about two-fold shortening with 4 μ M ddGTP with both systems. Thus, it is just the presence of primers that provides the signal.

How might the signal be sensed? We have recently demonstrated that the DnaX complex not only loads β_2 in an ATP-dependent reaction, but also chaperones the

associated polymerase onto the recently loaded β_2 (Downey and McHenry, 2010). Is it possible that the chaperoning reaction might be reversible with the ability to escort the polymerase off of an Okazaki fragment when appropriately signaled? When we found that Pol III HE took nearly two minutes to release when it collided with the preceding Okazaki fragment in a model system, we sought factors that might accelerate release. We only found one combination: τ -containing DnaX complex, exogenously provided primed-template and ATP (Dohrmann et al., 2011). ATP γ S could not substitute for ATP, so, presumably, ATP hydrolysis is required. β_2 is not required for polymerase release but is presumably associated with DnaX under these conditions in cells since its association is faster than the ATP-driven conformational change required for DNA binding (Thompson et al., 2009).

The acceleration was only four-fold and the rates achieved were not adequate to support the kinetics of Okazaki fragment synthesis. However, when properly oriented by interaction with helicase and perhaps other components at the replication fork, it could serve as a sensor. Thus, I incorporate DnaX complex as the sensor as a speculative feature of our cycling model (Fig. 3.6). I note that the Benkovic laboratory observed that the concentration of clamp and clamp loader affected primer utilization and Okazaki fragment size at the T4 bacteriophage replication fork, raising the possibility that the clamp loader might play a role in cycling of the lagging strand polymerase as well (Yang et al., 2006). Thus, the features of this evolving signaling model for triggering lagging strand replicase cycling during Okazaki fragment synthesis might be generally applicable.

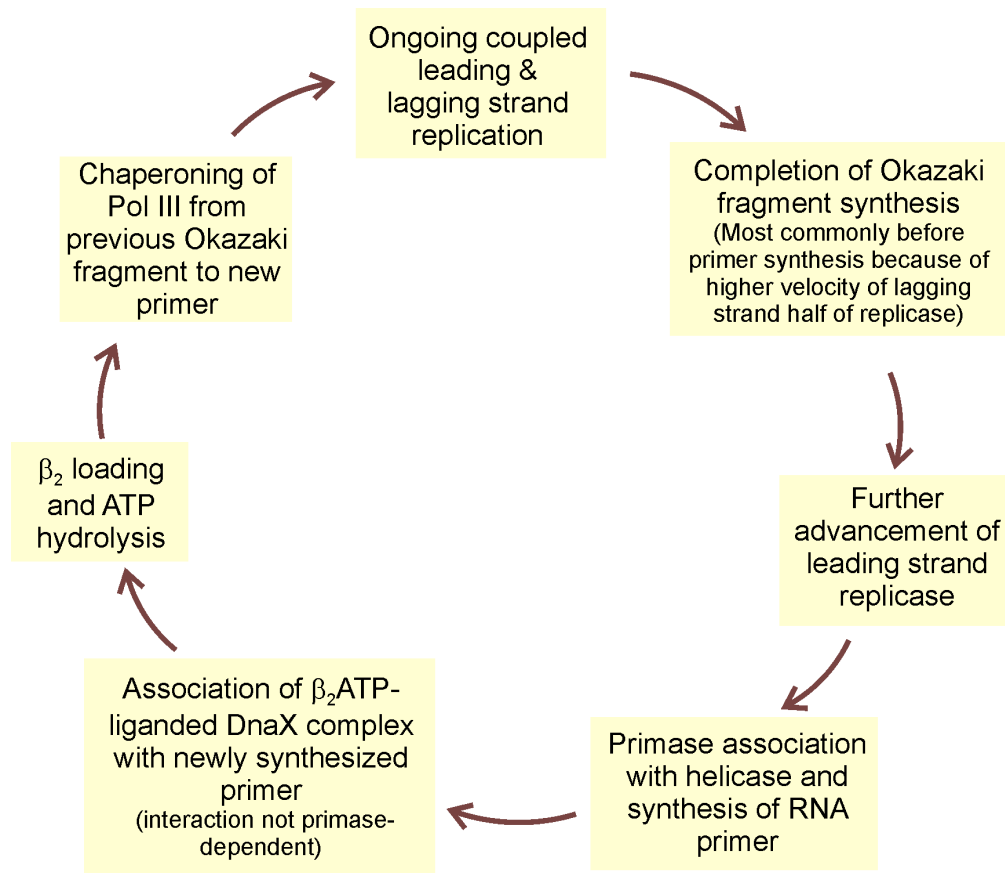


Figure 3.6 Proposed sequence of events in cycling of lagging strand polymerase during Okazaki fragment synthesis.

CHAPTER IV¹

MULTIPLE C-TERMINAL TAILS WITHIN A SINGLE *E. COLI* SSB HOMOTETRAMER COORDINATE DNA REPLICATION AND REPAIR²

4.1 Abstract

E. coli single strand DNA binding protein (SSB) plays essential roles in DNA replication, recombination and repair. SSB functions as a homotetramer with each subunit possessing a DNA binding domain (OB-fold) and an intrinsically disordered C-terminus, the last nine amino acids of which provides the site for interaction with at least a dozen other proteins that function in DNA metabolism. To examine how many C-termini are needed for SSB function we engineered covalently linked forms of SSB that possess only one or two C-termini within a four OB-fold "tetramer". Whereas *E. coli* expressing SSB with only two tails can survive, expression of a single tailed SSB is dominant negative. *E. coli* expressing only the two-tailed SSB recovers faster from exposure to DNA damaging agents, but accumulate more mutations. A single tailed SSB shows defects in coupled leading and lagging strand DNA replication and is inactive in supporting replication restart *in vitro*. This provides a plausible explanation for the lethality observed *in vivo*. These results indicate that a single SSB tetramer interacts with multiple protein partners simultaneously during its essential roles in genome maintenance.

¹ My experimental work is the *in vitro* single-stranded replication and rolling circle assay presented in Fig. 4.4 of this chapter and described in section 4.3 "In Vitro Single-stranded Replication Assays" and "In Vitro Rolling Circle Replication Assays". The remaining experimental work was performed by the co-authors of the corresponding submitted publication (Antony, E., Weiland, E., Yuan, Q., Manhart, C. M., Nguyen, B., Kozlov A, McHenry, C. S., and Lohman, T. M. Multiple C-terminal tails within a single *E. coli* SSB homotetramer coordinate DNA replication and repair).

² The contents of this chapter are submitted in collaboration with Tim Lohman's lab at Washington University and are presented here with few modifications.

4.2 Introduction

Single strand DNA binding (SSB) proteins are essential in all kingdoms of life and function in part by binding to the single stranded (ss) DNA intermediates that form transiently during all aspects of genome maintenance (Lohman et al., 1988). SSB proteins both protect the ssDNA and remove secondary structures, such as hairpins, that can inhibit replication, recombination and repair of DNA (Williams et al., 1983). In most bacteria, including *E. coli*, SSB protein functions as a homotetramer with each subunit (177 amino acids) possessing two domains: a DNA binding domain containing an oligonucleotide/oligosaccharide binding (OB)-fold (residues 1-112) and an intrinsically disordered C-terminal tail (65 residues) (Williams et al., 1983; Lohman and Ferrari, 1994; Raghunathan et al., 1997; Raghunathan and Kozlov, 2000). The last nine amino acids of the C-terminal tail (MDFDDDIPF in *E. coli*) contain the site of direct interaction between SSB and more than a dozen other proteins that SSB recruits to their sites of function in DNA replication, repair and recombination (Shereda et al., 2009).

Due in part to its homo-tetrameric nature, *E. coli* (*Ec*) SSB can bind to long ssDNA in several DNA binding modes. The dominant binding modes observed *in vitro* are referred to as (SSB)₆₅, (SSB)₅₅ and (SSB)₃₅, where the subscript denotes the average number of nucleotides occluded per SSB tetramer (Chrysogelos and Griffith, 1982; Griffith et al., 1984; Lohman et al., 1985; Bujalowski and Lohman, 1986). In the (SSB)₆₅ mode, favored at high monovalent salt and divalent cation concentrations, ssDNA wraps around all four subunits of the tetramer with a topology resembling the seams of a baseball (Lohman et al., 1985; Raghunathan and Kozlov, 2000). In contrast,

in the (SSB)₃₅ binding mode, ssDNA is only partially wrapped around the tetramer, interacting with an average of only two subunits (Lohman et al., 1985; Bujalowski and Lohman, 1986; Raghunathan and Kozlov, 2000). The ssDNA binding properties of these two major binding modes differ significantly. In the (SSB)₆₅ mode, an SSB tetramer binds with high affinity, but with little cooperativity (Lohman et al., 1986b), yet can undergo a random diffusion along ssDNA, a feature that is important for its ability to transiently destabilize DNA hairpins and facilitate RecA filament formation on natural ssDNA (Roy et al., 2009; Zhou et al., 2011). The (SSB)₃₅ mode, favored at low salt and high protein to DNA ratios, displays extensive positive inter-tetramer cooperativity and thus can form protein clusters or filaments on ssDNA (Griffith et al., 1984; Lohman et al., 1986b; Ferrari et al., 1994). In this mode, SSB can undergo a direct transfer between ssDNA molecules or distant segments of the same DNA without proceeding through a free protein intermediate (Kozlov and Lohman, 2002 *Biochemistry* 41, 11611-11627). Based on these differences, it has been suggested that the (SSB)₃₅ binding mode may function in DNA replication, whereas the (SSB)₆₅ binding mode might mediate DNA repair and/or recombination (Bujalowski et al., 1988; Lohman et al., 1988; Lohman and Ferrari, 1994).

In eukaryotes, the hetero-trimeric Replication Protein A (RPA) is the SSB analog that functions in genomic DNA replication (Braun et al., 1997). However, eukaryotes also encode a homo-tetrameric mitochondrial SSB protein with a DNA binding core that is structurally similar to *E. coli* SSB, but does not possess the unstructured C-termini of bacterial SSB (Tiranti et al., 1993; Li and Williams, 1997; Yang et al., 1997). Organelle-specific homotetrameric SSB proteins are also found in eukaryotic parasites such as

Plasmodium falciparum (*Pf*) and *Toxoplasma gondii* (*Tg*) and localize to the apicoplast where they presumably function in apicoplast DNA maintenance (Prusty et al., 2010; Antony et al., 2012a, 2012b). Although both *Pf*-SSB and *Tg*-SSB proteins also possess C-terminal tails, the sequences of these tails differ considerably from those of bacterial SSB proteins.

DNA replication is a complex process mediated by a replisome containing multiple proteins and enzymes (McHenry, 2011b) and *Ec*-SSB is a central component of these complexes. The DNA polymerase III holoenzyme (Pol III HE) consists of a DNA Pol III core (α - ϵ - θ), the multi-subunit DnaX complex clamp loader (τ , γ , δ , δ' , χ and ψ subunits) and the β clamp, a processivity factor. SSB binds to the $\chi\psi$ complex within the clamp loader (Kozlov et al., 2010a; Naue and Curth, 2012) and has been shown to contribute to processive replication (Glover and McHenry, 1998; Kelman et al., 1998). A second interaction with a Pol III HE site, other than χ , contributes to rapid initiation complex formation in a process where DnaX complex chaperones Pol III onto β_2 loaded in the same reaction cycle (Downey and McHenry, 2010). Recent studies also show that leading and lagging strand DNA replication is uncoupled when the SSB- χ interaction is lost (Marceau et al., 2011). The interaction between SSB and χ is critical as mutations within the protein interaction domain in SSB (e.g., *ssb-113*) are conditionally lethal (Quiñones and Neumann, 1997; Kelman and Hurwitz, 1998). Furthermore, strand displacement synthesis catalyzed by the Pol III HE in the absence of helicase is dependent on SSB (Yuan and McHenry, 2009). SSB may play a role in primer hand-off and the detachment of primase from RNA primers formed on the lagging strand, although aspects of this model have been brought into question (Marceau et al., 2011).

SSB directly interacts with primase (DnaG) (Yuzhakov et al., 1999) as well as with PriA (Cadman and McGlynn, 2004; Kozlov et al., 2010a). This latter interaction is critical to restart of DNA replication at stalled forks and is further enhanced by recruitment of PriB onto DNA (Cadman and McGlynn, 2004; Cadman et al., 2005).

Ec-SSB also binds a variety of DNA repair proteins including RecQ (a DNA helicase) (Lecoite et al., 2007; Shereda et al., 2007), RecJ (Han et al., 2006) and ExoI nucleases (Lu et al., 2011), and the recombination mediator RecO (Umezu and Kolodner, 1994). These proteins are involved at various stages in DNA recombination and perturbation of the interaction between SSB and these proteins leads to severe DNA repair defects (Kowalczykowski et al., 1994; Shereda et al., 2009). SSB also interacts with Uracil DNA glycosylase (Handa et al., 2001), a key component of the base excision repair pathway. Interactions between SSB and two repair specific polymerases, DNA Pol II and Pol V, have also been identified highlighting a role for SSB in translesion DNA synthesis (Molineux and Gefter, 1974; Arad et al., 2008).

Extremophilic bacteria such as *Thermus aquaticus* and *Deinococcus radiodurans* (*Dr*) have a dimeric version of SSB (Bernstein et al., 2004; Fedorov et al., 2006) in which each subunit contains two OB-folds, hence the DNA binding core still possesses four OB-folds and thus is structurally similar to the homotetrameric SSB. In fact, comparisons of the crystal structures and DNA binding properties of the *Dr*-SSB and *Ec*-SSB suggest that they share similar mechanisms of DNA binding and wrapping (Bernstein et al., 2004; Witte et al., 2005; Kozlov et al., 2010b; George et al., 2012). However, one consequence of the dimeric nature of *Dr*-SSB is that it possesses only two C-terminal tails that can mediate protein-protein interactions.

Whether *E. coli* SSB requires all four C-terminal tails for its functions *in vivo* is not known. To investigate this we examined the functional consequences of having an SSB with less than four C-terminal tails. We engineered and characterized SSB variants in which either two or all four OB-folds were covalently linked, thus forming a four OB-fold "tetramer" possessing either only two C-terminal tails (linked SSB dimers (SSB-LD)) or only one C-terminal tail (linked SSB tetramer (SSB-LT)). We find that a two-tailed SSB "tetramer" (SSB-LD-Drl) is functional *in vivo* and is competent for DNA replication *in vitro*, but it shows defects in DNA repair and consequently *E. coli* accumulates significantly more mutations. However, we find that a single tailed SSB "tetramer" (SSB-LT or SSB-LT-Drl) is unable to complement wild-type SSB and thus cannot carry out one or more essential functions *in vivo*. This single-tailed SSB also shows defects in coupling leading and lagging strand DNA replication and in replication restart *in vitro*.

4.3 Materials and Methods Results

Cloning of linked SSBs: The *wt ssb* gene was cloned into a pET-21a protein expression vector (EMD, Germany) with NdeI and BamHI restriction sites flanking its coding region. The detailed methodology to generate the linked SSBs is described in the Supplemental Information section.

Protein purification: The *wt* SSB, *ssb-S1* and deletion constructs were purified as previously described for *wt* SSB (Lohman, 1986; Bujalowski and Lohman, 1991) and all the buffers included a 1x final concentration of the protease inhibitor cocktail (Sigma, MO). The linked SSBs were purified using a slightly modified procedure as described in the supplemental materials. DNA replication β_2 (Johanson et al., 1986), DnaB₆ (Marians,

1995b), and DnaG (Griep and McHenry, 1989) were purified as described. DNA Polymerase III* (Pol III_{3τ2γδδ'χψ}) was purified as described (Fay et al., 1982) from overexpressing cells that contained a plasmid bearing an artificial operon containing all of the Pol III* subunit genes. Primosomal proteins PriA, PriB₂, DnaT₃, and DnaC were obtained using a published strategy (Marians, 1995b) with modifications (Yuan and McHenry; in preparation for publication).

DNA: The oligodeoxynucleotides, (dT)₃₅ and (dT)₇₀, were synthesized and purified as described (Ferrari et al., 1994). Poly(dT) was purchased from Midland Certified Reagent Co, (Midland, TX) and dialyzed extensively against buffer using a 3500 Da molecular weight cut-off dialysis membrane (Spectrum Inc., Houston, TX). All ssDNA concentrations were determined spectrophotometrically using the extinction coefficient $e_{260} = 8.1 \times 10^3 \text{ M}^{-1} (\text{nucleotide}) \text{ cm}^{-1}$ for oligo(dT) and poly(dT) (Kowalczykowski et al., 1981). Mini-circle DNA templates were 409-nucleotide duplex circles with a 396-nucleotide single-stranded tail that served as the initial lagging strand template (Sanders et al., 2010). The leading and lagging strands had a 50:1 asymmetric G:C distribution, allowing quantification of leading and lagging strand synthesis by ³²P-dCTP and dGTP incorporation, respectively. DNA was prepared as described (Sanders et al., 2010) with modifications (Yuan and McHenry; unpublished).

Analytical Sedimentation: Sedimentation velocity and equilibrium experiments were performed using an Optima XL-A analytical ultracentrifuge equipped with an An50Ti rotor (Beckman Coulter, Fullerton, CA) at 25 °C. For sedimentation velocity experiments in Figure 4.2C, we measured the sedimentation properties of 1 μM SSB (4-OB folds) in 30 mM Tris-Cl, pH 8.0, 10 % glycerol, 0.2 M NaCl and 1 mM EDTA. 380 μl

of the sample and 392 μl of the buffer were loaded into their appropriate sectors of an Epon charcoal-filled two-sector centerpiece and centrifuged at 42000 rpm (25 °C) while the absorbance was monitored at 280 nm. The continuous sedimentation coefficient $c(s)$ was calculated using the program SEDFIT (Schuck, 1998; Dam and Schuck, 2004). For sedimentation equilibrium experiments (Fig. 4.2D & 2E), 120 μL of protein solution was loaded into each of the three channels of an Epon charcoal-filled six-channel centerpiece with 130 μl of buffer in each reference channels. Protein concentration was monitored by absorbance at 280 nm (SSB-LD-Drl) and 230 nm (SSB-LT-Drl) at three different protein concentrations ([SSB-LD-Drl] = 3.6 μM , 2.3 μM and 1 μM ; [SSB-LT-Drl] = 2.2 μM , 1.2 μM and 0.6 μM). Data were collected with a spacing of 0.001 cm with an average of ten scans per step at three rotor speeds: 9500, 11500, 14000 and 17000 rpm. At each speed sedimentation equilibrium was determined when successive scans measured over a 2 hour time window were superimposable. Data sets were edited and extracted using SEDFIT (Schuck, 1998; Dam and Schuck, 2004) followed by analysis by nonlinear least squares (NLLS) using the program SEDPHAT (Vistica et al., 2004). Apparent molecular weights were obtained by fitting the data to eq 1:

$$A_T = \sum_{i=1}^n \exp(\ln A_{0,i} + \sigma_i (r^2 - r_{ref}^2)/2) + b \quad (1)$$

where A_T is the total absorbance at radial position r , $A_{0,i}$ is the absorbance of component i at the reference radial position (r_{ref}), b is the baseline offset, $\sigma_i = [M_i(1-\bar{v}_i\rho)\omega^2]/RT$, M_i and \bar{v}_i are the molecular mass and partial specific volume of component i , respectively (calculated using SEDENTREP (Laue et al., 1992)). For Pf-SSB the \bar{v}_i value (0.7191 mL g^{-1} at 25 °C) was calculated based on its amino acid composition (residues 77-284). The

solution density ρ for buffer $H^{0.1M}$ was 1.0026 (calculated using SEDENTREP). ω is the angular velocity, R is the ideal gas constant and T is the absolute temperature. A global NLLS fit to eq 1 of the nine absorbance files was used to calculate the molecular weight.

Fluorescence titrations: Equilibrium binding of SSB to oligodeoxynucleotides Poly (dT) and (dT)_L, was performed by monitoring the quenching of intrinsic SSB tryptophan fluorescence upon addition of DNA (PTI-QM-2000 spectrofluorometer, PTI Inc., Lawrenceville, NJ) [I_{ex} = 296 nm (2 nm band-pass), and I_{em} = 345 nm (2-5 nm band-pass)] with corrections applied as described (Lohman, 1992; Ferrari et al., 1994). Experiments were carried out at 25 °C in Buffer T: 10 mM Tris-Cl, pH 8.1, 0.1 mM EDTA and [NaCl] varied as noted in the text.

Wrapping Experiment: Wrapping of ssDNA around the SSB tetramer was measured on a deoxyoligonucleotide 65 nt in length with a Cy5.5 fluorophore at the 5' end and a Cy3 fluorophore at the 3' end. 50 nM of the DNA was incubated with increasing [SSB] and the enhancement of Cy5.5 fluorescence was monitored at 700 nm by exciting the Cy3 probe at 515 nm. These experiments were performed at 25 °C.

In Vivo Bumping Experiments: Bumping experiments were performed as described previously (Porter et al., 1990). *RPD317* is a strain where the chromosomal *SSB* gene has been deleted, but the strains survive using a copy of the *SSB* gene on a helper plasmid with a *Tet^r* cassette. We transformed these cells with our test-SSB containing plasmid carrying the *Amp^r* cassette. We selected transformants that grew on the LB agar plates with ampicillin (Amp, 100 µg/ml) and kanamycin (Kan, 50 µg/ml) and passaged them six times in 5 ml LB media containing Amp+Kan. For each passage the cells were grown overnight for 16 hours at 37 °C with shaking at 250 rpm. After the final

passage, the cells were diluted 1:1000 and plated onto LB agar containing Kan+Amp or Kan+Tet (34 g/ml tetracycline). Strains that can complement loss of *SSB-WT* grew only on the plates with Amp+Kan whereas those that did not complement grew on plates with either Kan+Amp or Kan+Tet because they could not bump the functional version of the *SSB-WT* protein. For all the experiments, a plasmid containing *SSB-WT* was used as a control to monitor the efficiency of bumping. All the bumping results were repeated at least twice and identical results were obtained.

In Vitro Single-stranded Replication Assays: 0.8 mM *SSB*₄ was incubated with 2.3 nM M13Gori ssDNA annealed with a 30-nt primer, 15 nM β_2 , and 2 nM Pol III* in the presence of 0.1 mM ATP, 18 μ M [³H] dTTP (100 cpm/pmol total nucleotide), 48 μ M dATP, 48 μ M dGTP, and 48 μ M dCTP at 30 °C for indicated time periods. The single-stranded DNA replication buffer contains 10 mM magnesium acetate, 200 mM NaCl, 50 mM Hepes (pH 7.5), 100 mM potassium glutamate, 20 % glycerol, 200 μ g/ml bovine serum albumin, 0.02% Nonidet P-40, and 10 mM dithiothreitol. Reactions were quenched, and products were quantified by scintillation counting as previously described (Yuan and McHenry, 2009).

In Vitro Rolling Circle Replication Assays: 20 nM mini-circle DNA template, the designated level of *SSB*₄, 100 nM β_2 , 12 nM DnaB₆, 100 nM DnaG, 2.5 nM Pol III*, 160 nM PriA, 50 nM PriB₂, 333 nM DnaT₃, and 108 nM DnaC were incubated with 5 μ M ATP_gS, 200 μ M CTP, 200 μ M UTP, and 200 μ M GTP for 5 min at 30 °C. The reaction buffer was the same as in the single-stranded replication assay except 50 or 25 mM NaCl (contributed by 0.8 μ M or 0.4 μ M *SSB*₄, respectively) was used instead of 200 mM. 1 mM ATP and 100 μ M dNTPs were added to start the reaction. After 3 min, [α -³²P]

dCTP or dGTP were added to allow quantification of leading and lagging strand synthesis, respectively. The reaction was quenched with an equal volume of stop mix (40 mM Tris-HCl (pH 8.0), 0.2% SDS, 100 mM EDTA, and 50 μ g/ml proteinase K) after 5 min. DNA product was quantified as in the single-stranded replication assays (Yuan and McHenry, 2009). For the analysis of the size of lagging strand products, samples were mixed with 30 mM NaOH, 2 mM EDTA, 2% glycerol, and 0.02% bromophenol blue and fractionated on 0.6% alkaline agarose gels for approximately 18 h at 24 V in a running buffer of 30 mM NaOH and 2 mM EDTA. Gels were fixed in 8% (w/v) trichloroacetic acid, dried onto DEAE paper, imaged on storage phosphor screens, and scanned with a PhosphorImager. The lengths of Okazaki fragment (L) were determined by a method that removed the bias of more radioactivity being incorporated into longer products using $L = \sum(L_i \cdot n_i) / \sum n_i$. n_i is the relative molar amount of the Okazaki fragments with a certain length L_i . $n_i = \text{density}_i / L_i$, where density_i is the pixel density at L_i in a lane determined using ImageQuant. Thus, $L = \sum \text{density}_i / \sum (\text{density}_i / \text{length}_i)$.

FRET Replication Restart Assay: This assay was conducted as previously described (Manhart and McHenry, 2013): 20 nM substrate constructed from FT₉₀, QT₉₀, and P_{10g} was combined with 100 nM trap oligo (45-mer complimentary to duplex region of FT₉₀), 200 nM streptavidin, and protein components in a buffer containing 50 mM HEPES (pH 7.5), 10 mM magnesium acetate, 10 mM dithiothreitol, 20% (v/v) glycerol, 0.02% (v/v) Nonidet-P40 detergent, 200 mg/mL bovine serum albumin, 100 mM potassium glutamate, and 10 mM ATP in a round-bottomed black 96-well plate in a final volume of 50 μ L. Samples were incubated at 30 °C for 15 min. Fluorescence emission was detected at 535 nm using an Envision plate reader with an excitation of 485 nm.

Using concentrations of un-annealed fluorescent leading strand template that are in the linear range of the assay, fluorescent units were converted to molarity using a standard curve.

DNA damage experiments:

Effect of HU and HN2: A 5 ml culture of *RDP317* cells with either *wt ssb* or *ssb-LD-Drl* under the control of the native SSB promoter was grown to an OD_{600} of 0.2 in the presence of 50 $\mu\text{g/ml}$ kanamycin and 100 $\mu\text{g/ml}$ ampicillin. HU was added to the cultures (final concentration 100 mM) and grown for an additional 5 hours at 37 °C. The cells were harvested and washed five times with 5 ml of ice-cold PBS. After the final wash, the cells were resuspended in 10 ml of 1X PBS and five serial dilutions were generated. 4 μl from each dilution in the series were plated onto LB and grown overnight at 37 °C. To quantitate the effect of nitrogen mustard (HN2), cells carrying either the *wt-SSB* or *SSB-LD-Drl* genes were grown as for the HU experiment and 2 mM HN2 (final concentration) was added to the cells when the OD_{600} reached 0.5. The cells were grown for another hour at 37 °C and 1 ml of this culture was directly diluted into 10 ml of M9 media. Serial dilutions were generated and immediately plated onto LB agar media containing 100 $\mu\text{g/ml}$ of ampicillin and 50 $\mu\text{g/ml}$ of kanamycin.

UV Sensitivity: *RDP317* cells with either *wt ssb* or *ssb-LD-Drl* under the control of native SSB promoter were grown overnight and 5-fold serial dilutions of these cells were made and 4 μl of the dilutions were spotted on a LB plate carrying 50 $\mu\text{g/ml}$ Kanamycin. The plates were dried for 30 min at 37 °C and exposed to UV.

RecA Western Blot: *RDP317* cells with either *wt ssb* or *ssb-LD-Drl* under the control of native SSB promoter were grown to an OD_{600} of 0.5 in the presence of both

100 µg/ml ampicillin and 50 µg/ml kanamycin. Nalidixic acid was added to the cultures (final concentration was 100 µg/ml) followed by growth at 37 °C. 1 ml of the sample was removed at the appropriate time intervals (30, 60, 90 and 120 min), spun down using a table top centrifuge and the cells were washed three times with 1.5 ml of ice cold phosphate buffered saline. 50 µg of the total cell lysate collected at each time point were resolved on a 10% SDS-PAGE gel followed by western blotting. We used a 1:15000 ration of the anti-RecA antibody (MD-03-3; MBL Corp. MA, USA) and detected the levels of RecA using chemiluminiscence.

Rifampicin resistance: To measure the rate of spontaneous mutagenesis of the RDP317 cells carrying either the *wt ssb* or the *ssb-LD-Drl* genes, overnight cultures of these cells were grown in the presence of 100 µg/ml ampicillin and 50 µg/ml kanamycin. The cultures were then plated onto LB agar media and 20 colonies were picked for each strain and 5 ml cultures for each colony were grown overnight at 37 °C. The cultures were then plated onto LB agar media containing 10 µg/ml rifampicin (Sigma, MO, USA). The plates were incubated overnight at 37°C and the numbers of colonies were counted. The experiment was repeated three times and the mutagenesis of 20 individual colonies were screened during each trial.

Growth Curves: To measure the growth kinetics of RDP317 cells carrying either the *wt ssb* or *ssb-LD-Drl* genes, we selected 8 colonies for each plate and either grew and overnight culture or to an OD₆₀₀ of 0.6. We diluted 1 µl from each of these starting conditions to 1 ml of fresh LB with 100 µg/ml ampicillin and 50 µg/ml of kanamycin. 200 µl of this diluted culture was added into a 96-well Greiner cell culture plate (USA Scientific, Cat # 655180) and the cells grown in a Tecan infinite M200 pro plate reader

(Tecan Systems, CA, USA) with constant shaking at 250 rpm. The OD_{600} was measured every 10 minutes and plotted versus time to generate the growth curves.

4.4 Results

4.4.1 Design of covalently linked SSB subunits with two or one C-termini per four OB-folds

Wild-type *Ec*-SSB tetramers contain four-OB folds and four C-termini. To probe the functionality of the four C-terminal tails we engineered a set of covalently-linked-SSB proteins that maintain the four OB-folds but possess either only one or two C-termini (Fig. 4.1A). Our first attempt was to clone two or four *ssb* genes in tandem and remove the appropriate stop codons, generating SSB-Linked-Dimers (SSB-LD) and SSB-Linked-Tetramers (SSB-LT), respectively (Fig. S2.1). In these constructs, the amino acid linker between two covalently linked OB-folds consisted of the full length wild-type C-terminal tail linked directly to the N-terminus of the next OB-fold. We were able to express and purify these recombinant proteins. However, unlike the wt SSB protein that is a monodisperse homotetramer in solution (Lohman and Ferrari, 1994) both the SSB-LD and SSB-LT proteins formed a mixture of higher order oligomers (Fig. S2.2A). Sedimentation velocity analysis of the purified proteins showed multiple broad peaks whose apparent molecular weights corresponded to complexes containing 4-OB folds, 8-OB folds, 12-OB folds and higher (Fig. S2.2A) suggesting the formation of species in which two or more OB-folds that are covalently linked could be shared to form higher order non-covalent complexes. Even though both the SSB-LD and SSB-LT proteins can bind tightly to ssDNA (Fig. S2.2B), we modified the length and composition

of the amino acid linkers between the subunits in an attempt to prevent the formation of these higher order oligomers.

The SSB protein encoded by *D. radiodurans* (*Dr*) is a homodimer with each subunit containing two-OB-folds connected by a 23 amino acid linker (Fig. 4.1B) with the sequence: QLGTQPELIQDAGGGVRMSGAGT (Bernstein et al., 2004). Since this is a naturally occurring linker, and because the DNA binding domains of *Ec*-SSB and *Dr*-SSB are structurally similar (Fig. 4.1B), we used this linker to connect the *Ec*-SSB subunits and generated linked dimer (SSB-LD-Drl) and linked tetramer (SSB-LT-Drl) constructs (Fig. 4.1A & S2.1). Upon expression and purification (Fig. 4.2A), we found that more than 70-80% of these proteins were single tetramers and after fractionation over an S200 size exclusion column, we obtained stable versions of both the dimeric SSB-LD-Drl and monomeric SSB-LT-Drl proteins. Sedimentation velocity experiments show that both the dimeric SSB-LD-Drl and monomeric SSB-LT-Drl proteins form single species with apparent molecular weights consistent with the presence of four-OB folds in each construct (Fig. 4.2B). Further analysis by sedimentation equilibrium revealed a single species for both proteins with average molecular masses of $M_r = 65070 \pm 612$ Da and $M_r = 61626 \pm 112$ Da for SSB-LD-Drl and SSB-LT-Drl, respectively (Fig. 4.2C & 4.2D). These values agree with the predicted molecular masses of 67343 Da for the SSB-LD-Drl (4-OB folds + 2 C-tails) and 61266 Da for the SSB-LT-Drl (4-OB folds + 1 C-tail) based on their amino acid sequences. Once purified, these linked SSB proteins (with either the long or 'drl' linker) showed no subunit exchange even after incubation for 3-10 days at room temperature (Fig. S2.3).

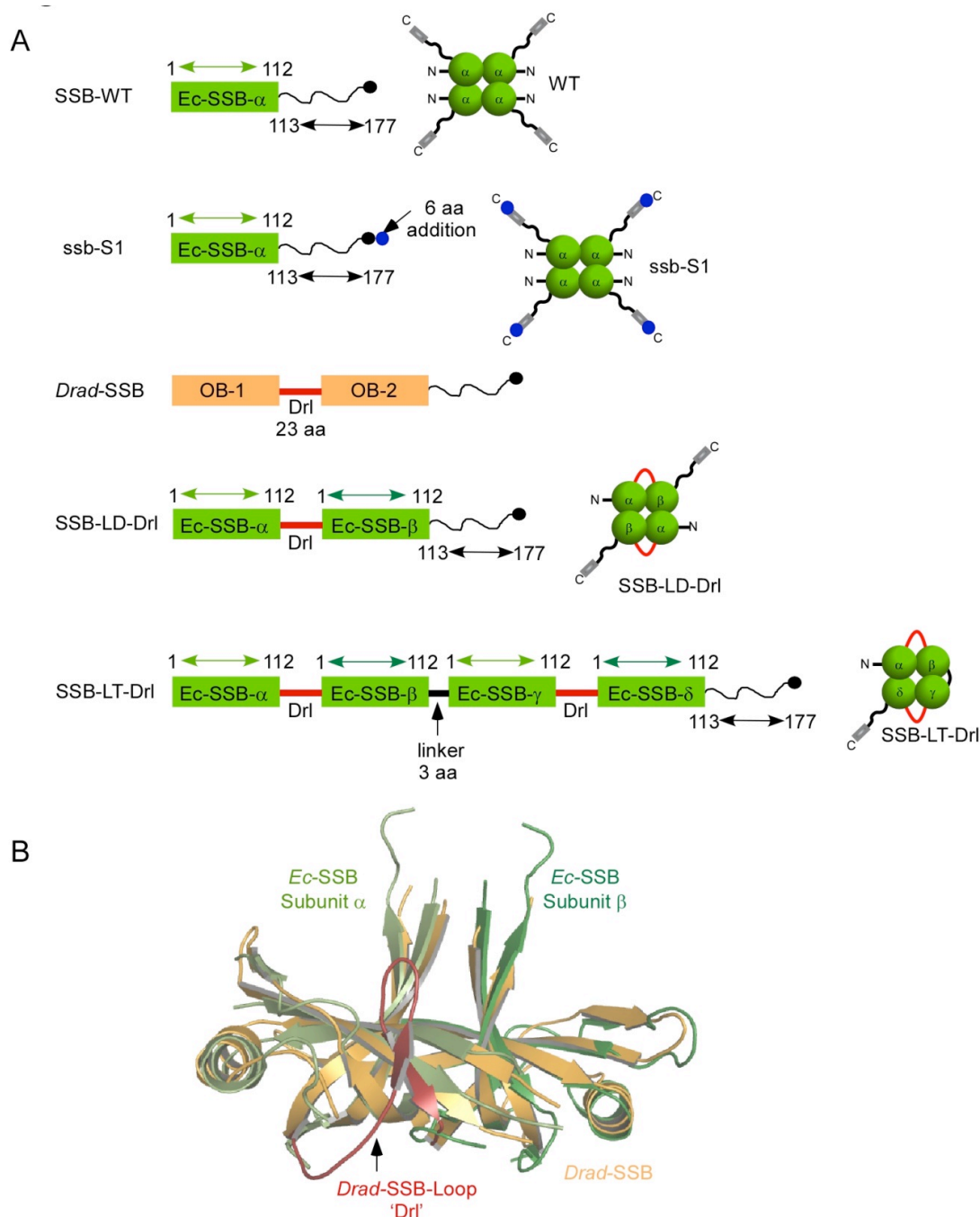


Figure 4.1 Design of linked SSB tetramers. (A) Schematic of the linker design used to generate the linked SSB dimer (SSB-LD-Drl) and the linked SSB tetramer (SSB-LT-Drl) resulting in two and one C-terminal tail per 4-OB folds respectively. (B) Superimposition of one *Dr*-SSB monomer containing two OB-folds and two *Ec*-SSB subunits containing one OB-fold per subunit. The linker observed between the two OB-folds in the *Dr*-SSB protein is shown in red and is the linker used to design the SSB-LD-Drl and SSB-LT-Drl proteins.

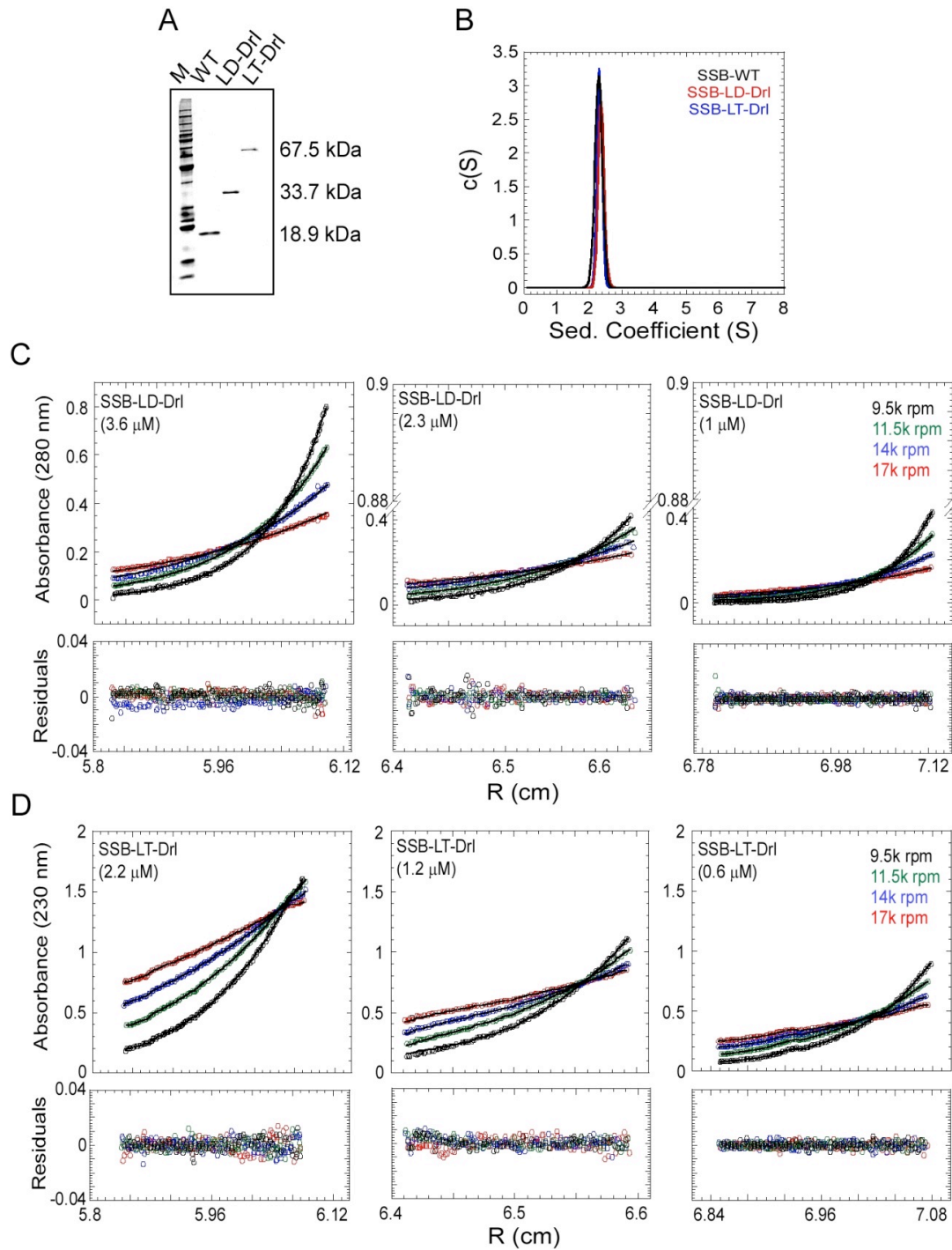


Figure 4.2 Characterization of linked SSB tetramers. (A) SDS-PAGE analysis of recombinantly purified SSB WT, SSB-LD-Drl and SSB-LT-Drl proteins. (B) Sedimentation velocity analysis of SSB WT, SSB-LD-Drl and SSB-LT-Drl proteins at 42000 rpm show the presence of a single species in solution for all three proteins. The SSB-LD-Drl (C) and SSB-LT-Drl (D) proteins sediment as tetramers in equilibrium centrifugation experiments with molecular weights corresponding to a single tetramer with 4-OB folds (LD-Drl: 65070 Da and LT-Drl: 61626 Da). The experiments were done

using three different protein concentrations (as noted) and at four rotor speeds (9500, 11500, 14000 and 17000 rpm). These experiments were performed at 25 °C in buffer containing 30 mM Tris-Cl, pH 8.0, 10 % glycerol, 0.2 M NaCl and 1 mM EDTA.

4.4.2 DNA binding properties of covalently linked SSB proteins

We next examined the ssDNA binding properties of the linked SSB proteins. WT SSB binds tightly to ssDNA and can bind in a number of distinct DNA binding modes *in vitro*, depending on solution conditions, especially salt concentration and type (Lohman and Ferrari, 1994). On poly(dT), three major ssDNA binding modes are observed at 25°C, denoted (SSB)₃₅, (SSB)₅₅ and (SSB)₆₅, where the subscript denotes the average number of nucleotides occluded per tetramer (Lohman et al., 1985; Bujalowski and Lohman, 1986; Lohman and Ferrari, 1994). We therefore measured the average occluded site sizes for the SSB-LD-Drl and SSB-LT-Drl proteins in Buffer T at 25°C by monitoring the quenching of the intrinsic SSB tryptophan fluorescence upon titrating with poly(dT) as a function of [NaCl]. Both SSB-LD-Drl and SSB-LT-Drl can form the same three distinct DNA binding modes, (SSB)₃₅, (SSB)₅₅ and (SSB)₆₅, that are observed for wt SSB (Fig. 3A). However, the transitions between the binding modes shift to higher [NaCl] as the number of C-terminal tails decreases from four to two to one. This effect is consistent with previous observations that showed a shift in the (SSB)₃₅ to (SSB)₆₅ transition to higher [NaCl] when all four C-terminal tails were truncated by chymotrypsin cleavage (Roy et al., 2007). These results indicate that the covalently linked SSB proteins are able to bind and wrap ssDNA to form the same complexes as the wt SSB protein, although the relative stabilities of the different modes are affected.

We also compared the ssDNA binding properties of wt SSB, SSB-LD-Drl and SSB-LT-Drl in the same buffer that we used in the DNA replication assays discussed

below [50 mM Hepes, pH 7.5, 100 mM NaCl, 10 mM Mg(CH₃CO₂)₂, 100 mM potassium glutamate and 20 % (v/v) glycerol] at 25°C. Under these conditions we measure similar occluded site sizes of 64 ± 3 , 59 ± 4 and 58 ± 3 nucleotides on poly(dT) for the wt SSB, SSB-LD-Drl and SSB-LT-Drl proteins (per 4 OB-folds), respectively (Fig. 4.3B). All three proteins also show the same maximum Trp fluorescence quenching. We also examined binding of these proteins to (dT)₇₀ by monitoring SSB Trp fluorescence quenching. WT SSB, SSB-LD-Drl and SSB-LT-Drl all bind tightly to (dT)₇₀ with a stoichiometry of one (dT)₇₀ molecule per 4-OB folds with the same Trp fluorescence quenching consistent with DNA interacting with all four OB-folds with similar wrapping (Fig. 4.3C). These results indicate that the number of C-terminal tails does not affect the ability of these SSB proteins to form a fully-wrapped ssDNA complex. Since SSB binding to (dT)₇₀ is stoichiometric under these conditions for all three proteins (i.e., $K_{\text{obs}} > 10^9 \text{ M}^{-1}$), an accurate estimate of the binding affinities could not be obtained. In order to lower the equilibrium binding constants to the (dT)₇₀ substrate to a measureable range, we performed titrations in buffer containing high NaBr concentrations (Bujalowski and Lohman, 1989b) (10 mM Tris-Cl, pH 8.1, 0.1 mM EDTA and 1.6 M NaBr) at 25 °C. Under these conditions, the binding affinities for wt SSB, SSB-LD-Drl and SSB-LT-Drl are $K_{\text{obs}} = (9 \pm 1.6) \times 10^7 \text{ M}^{-1}$, $(9.6 \pm 1.4) \times 10^6 \text{ M}^{-1}$ and $(6.6 \pm 0.4) \times 10^6 \text{ M}^{-1}$, respectively (Fig. S2.4). Hence both linked proteins bind with ~10-fold weaker affinities compared to WT-SSB. These results suggest that the DNA binding activity is affected slightly due to the covalent linking of the OB-folds. However, as stated above, under the buffer conditions used to examine DNA replication, all three SSB proteins (wt, LD-Drl and LT-Drl) bind with affinities that are too high to measure and thus ssDNA binding is not compromised.

We also compared the extent to which ssDNA wraps around the 4-OB folds in wt SSB, SSB-LD-Drl and SSB-LT-Drl by examining their binding to a (dT)₆₅ labeled with a fluorescence donor (3'-Cy3) and acceptor (5'-Cy5.5) at either end. As shown previously (Kozlov and Lohman, 2002; Roy et al., 2007), when this ssDNA forms a fully wrapped 1:1 molar complex with an SSB tetramer (i.e., in the (SSB)₆₅ mode), the two fluorophores are brought into close proximity resulting in a large Fluorescence Resonance Energy Transfer (FRET) signal (monitored as a Cy5.5 fluorescence increase). Upon addition of higher SSB concentrations, two SSB tetramers can bind per DNA, each in the (SSB)₃₅ binding mode, resulting in an increase in the distance between the Cy3 and Cy5.5 fluorophores and thus a decrease in FRET signal. Figure 3D shows that we observe the highest FRET signal at a stoichiometry of one (dT)₆₅ per "tetramer" (4 OB-folds) for all three proteins. At higher SSB concentrations a second "tetramer" of wt SSB, SSB-LD-Drl and SSB-LT-Drl proteins can bind to the DNA resulting in the expected decrease in FRET.

WT SSB is able to bind two molecules of (dT)₃₅ per tetramer, but with negative cooperativity such that the second molecule of (dT)₃₅ binds with lower affinity (Lohman and Bujalowski, 1988; Bujalowski and Lohman, 1989a, 1989b). Figure 4.3E compares the binding of (dT)₃₅ to wt SSB, SSB-LD-Drl and SSB-LT-Drl proteins in our DNA replication buffer [50 mM Hepes, pH 7.5, 100 mM NaCl, 10 mM Mg(CH₃CO₂)₂, 100 mM potassium glutamate and 20 % (v/v) glycerol]. Under these conditions, the first (dT)₃₅ binds with very high affinity (stoichiometrically), precluding an accurate estimate of the binding constant, whereas the second (dT)₃₅ binds with lower binding constants with values of $(2.34 \pm 0.29) \times 10^5 \text{ M}^{-1}$ and $(1.66 \pm 0.71) \times 10^5 \text{ M}^{-1}$ for SSB-LD-Drl and SSB-

LT-Drl proteins (Fig. 4.3E), respectively compared to $(1.60 \pm 0.16) \times 10^7 \text{ M}^{-1}$ for wt SSB (Fig. 4.3E). The lower affinities for the binding of the second $(\text{dT})_{35}$ for the linked proteins is consistent with the higher stability of the $(\text{SSB})_{35}$ binding mode at higher $[\text{NaCl}]$ for these proteins on poly(dT) (Fig. 4.3A).

Recent single molecule fluorescence studies have shown that an *Ec*-SSB tetramer is able to diffuse along ssDNA (Roy et al., 2007) and can use this property to transiently melt a double stranded DNA hairpin and that this activity of SSB can facilitate formation of a RecA filament on natural ssDNA (Roy et al., 2009). Using these same single molecule approaches we show (Fig. S2.5) that the covalently linked SSB proteins are also able to diffuse along ssDNA and transiently melt a DNA hairpin.

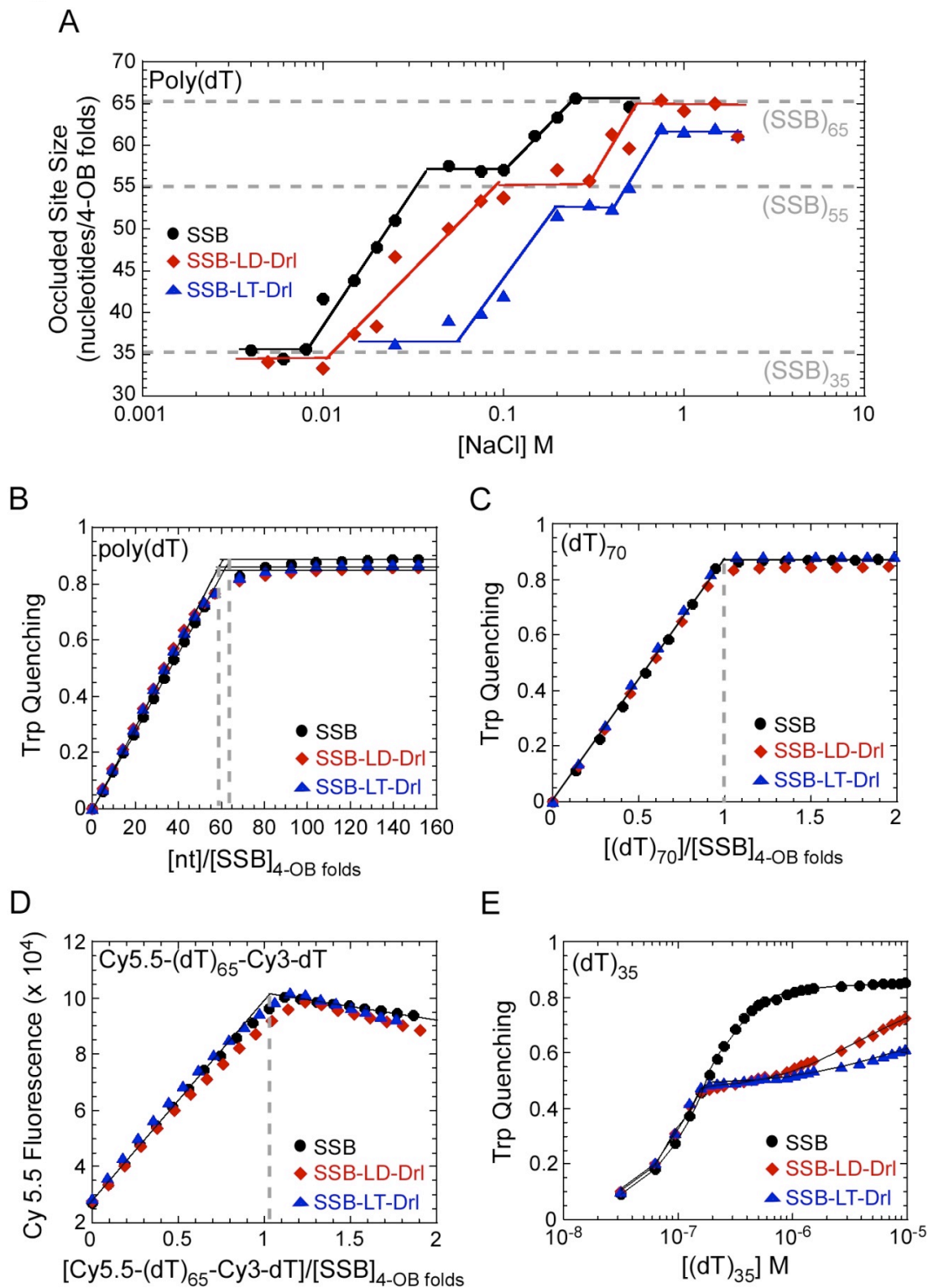


Figure 4.3 ssDNA binding properties of linked SSB tetramers. (A) Occluded site-size measurements as a function of increasing $[\text{NaCl}]$ for the SSB WT and linked SSB proteins on poly(dT) ssDNA show the presence of three distinct DNA binding modes $(\text{SSB})_{35}$, $(\text{SSB})_{55}$, and $(\text{SSB})_{65}$ for all three proteins. (B) Measurement of occluded site

size in replication buffer show that all three proteins bind to ssDNA in the (SSB)₆₅ binding mode. (C) Quenching of intrinsic SSB Trp fluorescence upon binding to a (dT)₇₀ oligonucleotide shows that all three proteins bind stoichiometrically. (D) Wrapping of ssDNA around SSB WT and linked SSB proteins measured using an oligonucleotide with Cy5.5 and Cy3 fluorophores positioned at the 5' and 3' ends respectively, and monitoring enhancement of Cy5.5 fluorescence at 700 nm by exciting the Cy3 probe at 515 nm. (E) Binding of (dT)₃₅ to SSB WT and linked SSB tetramers show binding of two (dT)₃₅ molecules to SSB WT ($K_1 > 10^{15} \text{ M}^{-1}$ and $K_2 = 1.60 \pm 0.16 \times 10^7 \text{ M}^{-1}$) whereas both the SSB-LD-Drl and SSB-LT-Drl tetramers bind to one (dT)₃₅ with high affinity ($K_1 > 10^{15} \text{ M}^{-1}$ for both SSB-LD-Drl and SSB-LT-Drl) whereas the second (dT)₃₅ binding is weaker ($K_2 = 1.66 \pm 0.71 \times 10^5 \text{ M}^{-1}$ and $2.34 \pm 0.29 \times 10^5 \text{ M}^{-1}$ for SSB-LD-Drl and SSB-LT-Drl respectively). These experiments were done at 25 °C in buffer containing 50 mM Hepes pH 7.5, 10 mM Mg(OAc)₂, 100 mM NaCl, 100 mM KC₅H₈NO₄, and 20 % glycerol.

4.4.3 An SSB with at least two C-terminal tails is required for *E. coli* survival

We next examined the ability of the covalently linked SSB proteins, SSB-LD-Drl and SSB-LT-Drl, to function in *E. coli* by testing whether they can complement the loss of wt SSB protein *in vivo* using a “bumping” assay developed by Porter (Porter and Black, 1991). *E. coli* strain RDP317 lacks a chromosomal copy of the wild-type *ssb* gene and thus can survive only if it also carries a plasmid expressing a version of an *ssb* gene that can functionally complement the *wt ssb* gene. We first grew RDP317 cells containing a plasmid expressing the *wt ssb* gene (pEW-WT-*t*) that also contains a tetracycline resistance cassette (*tet*^R). The *ssb* mutant gene to be tested for complementation was then cloned into a second compatible plasmid containing ampicillin resistance (*amp*^R) (pEW-X-*a*; where ‘X’ denotes the SSB variant to be tested and ‘a’ denotes the resistance to ampicillin; Table S2.1). We cloned each *ssb* gene under control of the natural *ssb* promoter to regulate expression levels of all SSB constructs (Yamaguchi and Yamaguchi; Sugiura et al., 1993; Wadood et al., 1997). RDP317 cells containing the pEW-WT-*t* (*ssb*⁺, *tet*⁺) were then transformed with the test plasmid (pEW-X-*a*). The transformed cells were then passaged (sub-cultured

successively) five to six times, selecting for cells possessing ampicillin resistance (100 µg/ml Ampicillin). If the test *ssb-x* gene is able to complement wt *ssb*, the plasmid containing the wt *ssb* gene along with its *tet^R* cassette can be lost (bumped) from RDP317. However, if the test gene is unable to complement wt *ssb*, then the original (*ssb⁺*, *tet⁺*) plasmid will be retained in RDP317. Consequently, if a test *ssb-x* gene complements the wt *ssb* gene, then cells containing the test *ssb-x* gene will possess only ampicillin resistance, whereas if the test *ssb-x* gene does not complement the wt *ssb* gene, then cells containing the *test ssb-x* gene will be resistant to both ampicillin and tetracycline. Our results indicate that the *ssb-LD-Drl* gene expressing SSB with only two C-tails was able to functionally complement the loss of wt *ssb* gene *in vivo*; however, the *SSB-LT-Drl* showed a dominant negative phenotype (Table 4.1; discussed below).

The last 9 amino acids of the SSB C-tail provides the site of interaction with more than one dozen SSB interacting proteins (SIPs) and this site is critical for SSB function as *ssb* genes with deletions of the last 8 amino acids (*ssb-ΔC8*) (Curth et al., 1996) or that contain an additional 6 amino acid extension (*ssb-S1*) do not complement loss of the wt *ssb* gene (Table 4.1). The genes encoding for covalently linked SSB proteins possessing only two C-tails (*ssb-LD* and *ssb-LD-Drl*) complement the wt *ssb* gene (Table 4.1). To check the integrity of the genes encoding the linked SSB proteins, we isolated plasmid DNA after the final passage. Sequencing of the gene showed the expected sequence with no evidence for any mutations or recombination. Hence two functional C-terminal tails within an SSB construct containing 4-OB folds are sufficient to support growth. However, neither of the single C-terminal tailed genes encoding *ssb-LT* and *ssb-LT-Drl* were able to complement and in fact were toxic. We therefore interpret

these to have a dominant negative phenotype (Table 4.1). We were able to successfully clone these constructs into plasmids under control of a T7 promoter, but multiple parallel attempts to clone them under control of the native SOS promoter were unsuccessful. For both the *ssb-LT* and *ssb-LT-Drl* constructs, only a few colonies appeared after transformation, but in every case (total of 9 colonies from 8 attempts) the genes contained mutations that introduced premature stop codons within the open reading frame. These results suggest that an SSB tetramer with one free tail is toxic to *E. coli* when under the control of the SOS promoter and expressed constitutively.

Since the *ssb-LD-Drl* gene was able to support cell growth, we also tested whether the *Dr-ssb* gene (which encodes a naturally occurring two C-tail protein in *Deinococcus radiodurans*) can functionally complement *wt* SSB. The C-terminal 9 amino acids of the *Dr*-SSB protein are PPEEDDLPF which is similar to the MDFDDDIPF sequence found in the *Ec*-SSB protein. In fact, *Dr*-SSB is able to complement *wt* SSB protein *in vivo* (Witte et al., 2005) and Table S2.1), providing additional evidence that an SSB with only two C-terminal tails is sufficient to allow *E. coli* survival and growth

Construct	Phenotype
<i>Un-Linked monomers</i>	
WT	Complements
ssb- Δ C8	No Complementation
ssb-S1	No Complementation
SSB- Δ 120-166	Complements
SSB- Δ 130-166	Complements
SSB- Δ 151-166	Complements
SSB- Δ 162-166	Complements
<i>Linked Dimers</i>	
SSB-LD	Complements
SSB-LD-Drl	Complements
<i>Linked Tetramers</i>	
SSB-LT	Dominant Negative
SSB-LT-Drl	Dominant Negative

TABLE 4.1 Different ssb gene construct and phenotypes

4.4.4 SSB with fewer than four C-terminal tails exhibits decreased stimulation of the DNA polymerase III holoenzyme on single-stranded templates.

We next examined whether the linked SSB constructs with either two or one C-tails could function in *E. coli* DNA replication. We initially examined a simple reaction—the conversion of primed single-stranded DNA to a duplex (Fig. 4.4A). This reaction requires the ability of the Pol III HE to form an ATP-dependent initiation complex on a primer and to processively elongate it approximately 8000 nucleotides. The reaction is independent of SSB under low salt conditions, but becomes partially (~3-4-fold) dependent upon SSB at elevated salt concentrations (200 mM NaCl). We observe full

stimulation of the reaction by wild-type SSB and incrementally decreased stimulation by SSB-LD-Drl and SSB-LT-Drl, respectively (Fig. 4.4A). The level of DNA synthesis observed in reactions containing one-tailed SSB-LT-Drl is only slightly above that observed in the absence of SSB.

Ssb-S1, an SSB homo-tetramer that possesses four C-terminal tails but contains a 6 amino acid extension after the 9 amino acid SIP interaction motif, severely inhibits the reaction (Fig. 4.4A). Extensions beyond the C-terminal phenylalanine has been shown to block SIP interactions (Kozlov et al., 2010a)(Naue et al., 2013) and the ssb-S1 protein does not interact with χ (Fig. S2.6). We have previously observed inhibition by other SSB derivatives that lack portions of the C-terminal tail (Yuan and McHenry, 2009).

4.4.5 SSB containing only one C-terminal tail is defective in rolling circle replication reactions that mimic chromosomal replication forks

Duplex circles containing a 5'-flap on one strand provide a substrate for reconstitution of replication forks that exhibit the same characteristics of replication forks *in vivo* (Kim et al., 1996a). Replication is dependent upon restart primosomal proteins (PriA, PriB, DnaT) that direct the assembly of the DnaB helicase in the presence of the DnaC helicase loader and SSB. Once the helicase is loaded on the lagging strand template, it uses its ATP-dependent DNA helicase activity to unwind the duplex DNA at the replication fork, permitting the dimeric Pol III HE (associated with DnaB through an interaction with the τ subunit of Pol III HE) (Kim et al., 1996a; Gao and McHenry, 2001a) to follow. Primers are provided on the lagging strand by a reversible interaction between the DnaG primase and DnaB (Tougu and Marians, 1996a). The lagging strand primers

are extended by the lagging strand half of the dimeric Pol III HE in a coupled reaction (Kim et al., 1996b).

I find that SSB-LD-Drl functions equivalently to *wt* SSB in this system. However, SSB-LT-Drl, containing only one C-tail, exhibits a two-fold decrease in the level of leading strand synthesis (Fig. 4.4B). The levels of lagging strand synthesis are decreased even further, suggesting that leading and lagging strand DNA replication reactions become uncoupled.

To determine whether the decrease in lagging strand synthesis relative to leading strand is due to a defect in primer formation, I examined Okazaki fragment length by electrophoresis of labeled lagging strand products in alkaline agarose gels (Fig. 4.4C). I observe similar product lengths with all three proteins (*wt* SSB, SSB-LD-Drl and SSB-LT-Drl) suggesting that the replication defect is not associated with formation of primers. Uniform Okazaki fragment length is an indication that primers are synthesized with the same frequency and spacing in the presence of all three SSB proteins (Zechner et al., 1992b).

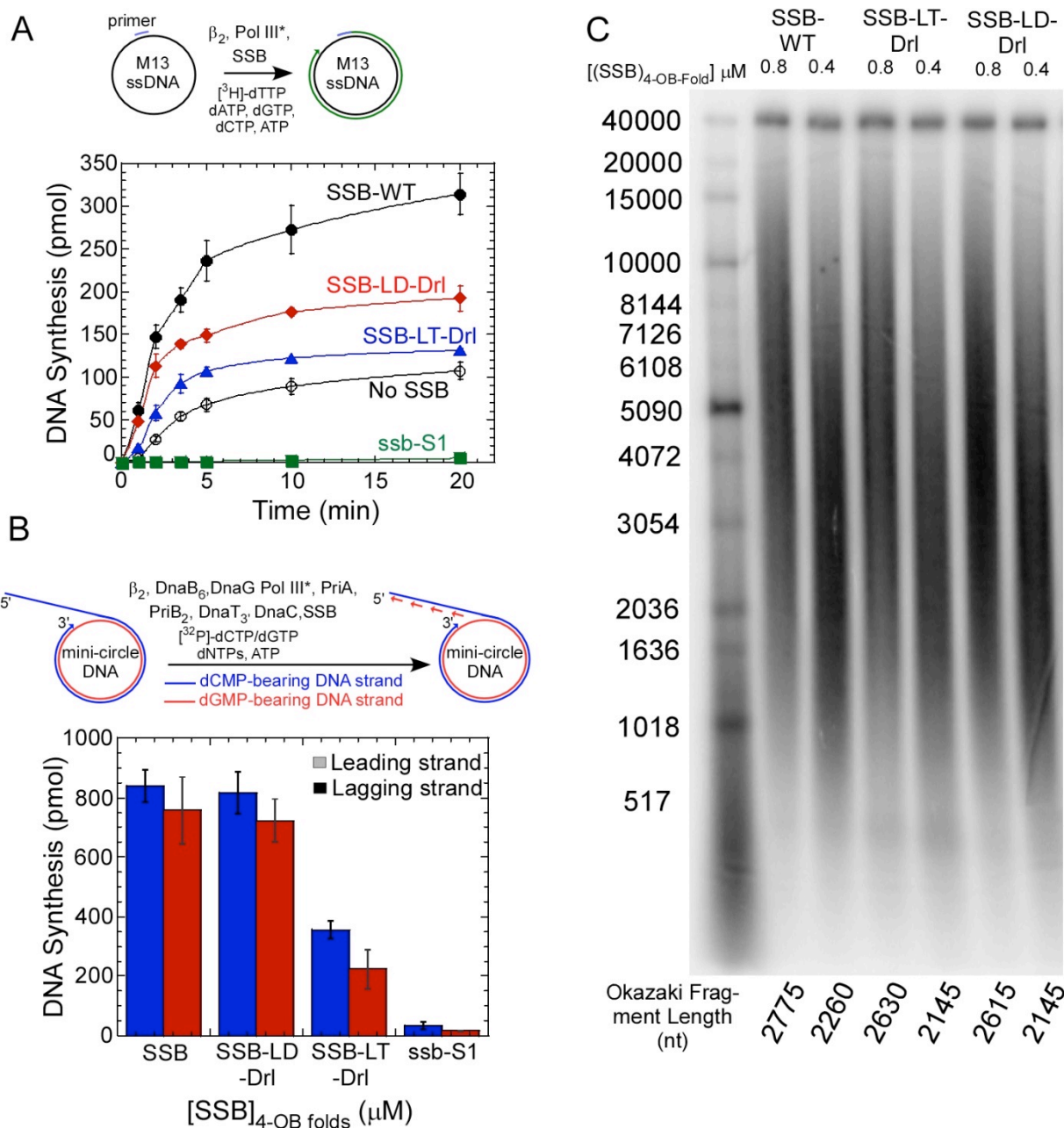


Figure 4.4 SSB tetramers with only one C-terminal tail show decreased stimulation of DNA replication. (A) *In-vitro* single-stranded DNA replication assays were carried out in the presence of indicated SSB derivative. (B) *In-vitro* rolling circle DNA replication assays were carried out in the presence of indicated SSB. (C) The products from the rolling circle replication reactions were fractionated on an alkaline agarose gel and the length of Okazaki fragments were determined. (From left to right: 2775, 2260, 2630, 2145, 2615, and 2145 nt.)

4.4.6 A one-tailed SSB tetramer does not support replication restart

In the rolling circle replication reactions described above, the initial PriA-dependent helicase assembly occurred during a five-minute pre-incubation of components in the presence of ATPγS. This precluded use of the rolling circle reactions to examine the effect of the SSB variants with variable numbers of tails on the kinetics of the replication restart reaction. To enable this determination, we used a recently developed FRET assay that monitors PriA- and SSB-dependent helicase assembly on model forks (Manhart and McHenry, 2013). Unwinding activity in this experiment is a direct measure of DnaB helicase loading onto the leading strand. The presence of the streptavidin-biotin complex on the 5' end of the lagging strand prevents helicase loading at that site. SSB is required for the loading of the helicase onto the leading strand primer-template. Using this assay under conditions where DNA unwinding is proportional to the time of the reaction we observe a modest decrease in DNA unwinding when SSB-LD-Dri is substituted for SSB. However, substitution by the one-tailed SSB-LT-Dri results in a severe inhibition of the unwinding reaction indicating an inability of the single tailed SSB to load the DnaB helicase. The level of inhibition is nearly equivalent to that observed with the *ssb-S1* derivative (Fig. 4.5).

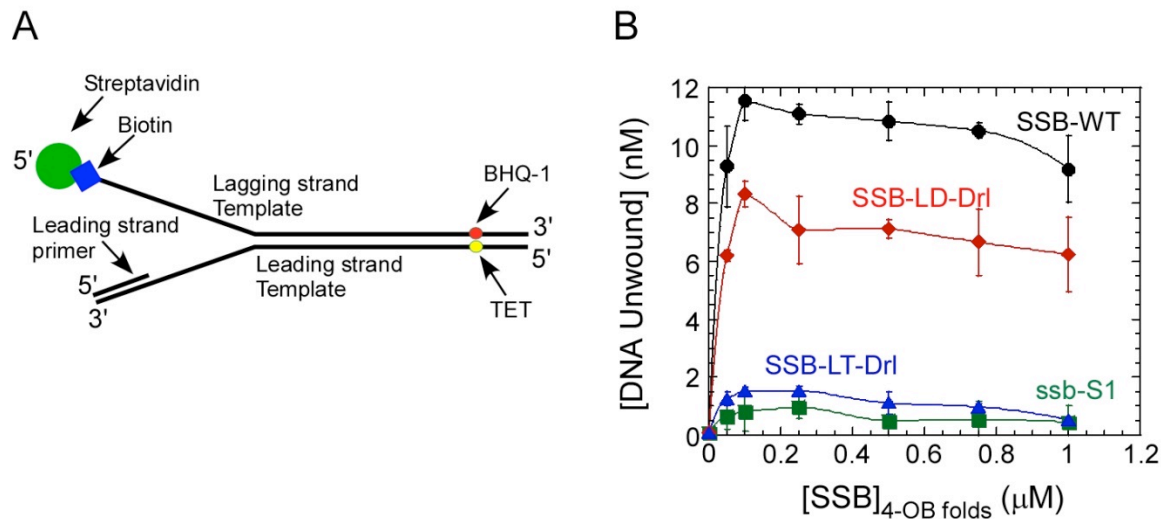


Figure 4.5 SSB-LT-Drl does not support PriA-dependent replication restart pathway. (A) DNA substrate used in unwinding reactions. The fluorescence of TET on the 5' terminus increases when separated by helicase action from a quencher (BHQ-1) on the lagging strand template. Streptavidin binding to biotinylated thymidine on the 5'-end of the lagging strand template blocks helicase self-loading by threading over a free 5'-end. There is a 10 nt gap between the 3'-OH of the leading strand primer and the duplex region of the fork. (B) SSB forms titrated individually in triplicate in the presence of 150 nM PriA, 50 nM PriB₂, 50 nM DnaT₃, 12 nM DnaB₆, 50 nM DnaC.

4.4.7 *E. coli* cells expressing two-tailed SSB tetramers are more resistant to the effects of DNA damage, but accumulate more mutations.

Since *Ec*-SSB interacts with several SIPs that are involved in DNA repair (Lecoïnte et al., 2007; Shereda et al., 2008; Costes et al., 2010), we tested whether the number of C-tails associated with a single SSB tetramer affects the ability of cells to recover from DNA damage. *E. coli* cells expressing either wt SSB or SSB-LD-Drl were grown in the presence of the DNA damaging agents: hydroxyurea (HU), nitrogen mustard (N(CH₂CH₂Cl)₃ or HN3), or exposed to UV irradiation. HU is an inhibitor of ribonucleotide reductase and treatment of *E. coli* results in depletion of dNTP pools leading to DNA double strand breaks near replication forks (Rosenkranz and Levy,

1965; Rosenkranz et al., 1966), whereas HN3 inhibits DNA replication by covalently crosslinking the two DNA strands (Biesele et al., 1950). Exposure of cells to UV irradiation leads to formation of DNA breaks and UV-sensitivity (Bonura and Smith, 1975). To assess the ability of a four-tailed versus two-tailed SSB to respond to DNA damage, we grew cells carrying these genes in the presence of either HU (100 mM) or HN3 (2 mM). We then compared the relative abilities of the cells to grow after exposure to these DNA damaging agents. Surprisingly, cells expressing the two-tailed SSB-LD-Drl recover faster from exposure to both DNA damaging agents as indicated by faster cell growth observed across the serial dilutions (Fig. 4.6A & B).

To test the ability of the RDP317 cells carrying either the *wt ssb* or *ssb-LD-Drl* genes to recover from UV induced damage, we grew overnight cultures, plated serial dilutions of these cells and exposed them to varying levels of UV irradiation. *E. coli* cells expressing either *wt* SSB or SSB-LD-Drl display comparable sensitivities to low levels of UV irradiation (0 – 25 J/m²) as indicated by the growth of the colonies across the serial dilutions (Fig. 4.6C). However, after exposure to higher UV levels (150 J/m²), the cells expressing SSB-LD-Drl show a slight recovery, compared to the failure of cells expressing *wt* SSB to recover from these high UV doses (Fig. 4.6D).

Since one of the major proteins expressed in response to DNA damage is RecA, we hypothesized that the ability of the cells expressing SSB-LD-Drl to better recover from the effects of DNA damage might be due to expression of higher levels of RecA. To test this, we treated cells with nalidixic acid (a DNA damaging agent) and quantified the expression levels of RecA using an anti-RecA antibody. However, Western blots

(Fig. 4.6E) show a similar level of induction of RecA protein in the presence of nalidixic acid for cells expressing either wt SSB or SSB-LD-Drl.

Another possible explanation for the faster recovery of the SSB-LD-Drl cells after DNA damage is that the DNA lesions are not repaired, but bypassed. If this were the case, then an elevated rate of mutagenesis should occur in these cells. We thus compared the rate of mutagenesis in *E. coli* expressing wt SSB or SSB-LD-Drl using the rifampicin resistance assay (Ezekiel and Hutchins, 1968). *E. coli* grown in the presence of rifampicin can survive through spontaneous mutations in the rifampicin binding site on the β subunit of RNA polymerase. We observe a 30-fold increase in the number of *Rif^r* colonies in the SSB-LD-Drl cells compared to the wt SSB cells (Fig. 4.7A). These results suggest that the better recovery from the effects of the DNA damaging agents are due to a lower level of repair of DNA mutations in cells expressing SSB-LD-Drl. Repair of mutations after DNA damage results in slower cell growth (Rosenberg, 2001). Since cells expressing SSB-LD-Drl are deficient in repairing mutations, we would expect these cells to display faster growth kinetics. The data in Figure 4.7 (panels B and C) show this to be the case as cells expressing SSB-LD-Drl enter exponential growth phase significantly faster than cells expressing wt SSB. When cell growth is initiated from overnight cultures, cells expressing SSB-LD-Drl reach the mid-log phase about 70 min faster than cells expressing wt SSB (Fig. 4.7B). When cell growth is initiated from cells in log-phase, the SSB-LD-Drl cells reach mid-log about 120 min faster than the wt SSB cells (Fig. 4.7C). These results support the conclusion that the SSB-LD-Drl protein with two C-tails per tetramer shows defects in DNA repair, but is able to support DNA replication.

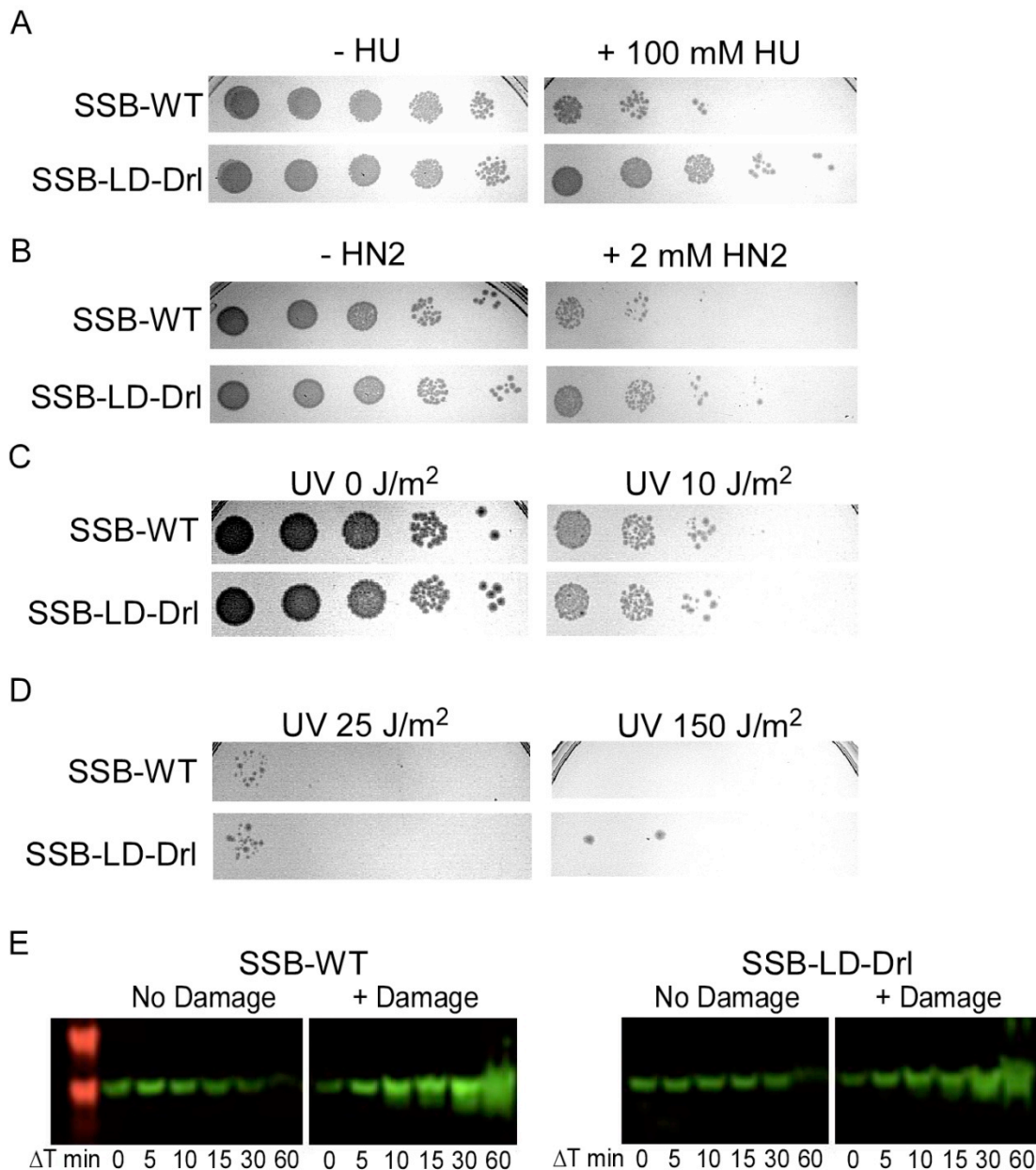


Figure 4.6 *In vivo* repair capabilities of *E. coli* strains carrying *wt* SSB or *ssb-LD-Drl* genes. Serial dilutions of cells in the absence or presence of 100 mM hydroxyurea (A) or 2 mM nitrogen mustard (B). Cells harboring the *ssb-LD-Drl* gene recover better compared to the *wt* cells in the presence of the either DNA damaging agent. Both strains tolerate lower levels of UV to similar extents (C). However at a higher dose of UV (D), only the cells carrying the *ssb-LD-Drl* gene is able to grow. E) Western blot detection of RecA levels in the absence or presence of 100 mM Nalidixic acid. Both strains are capable of inducing RecA expression in the presence of DNA damage.

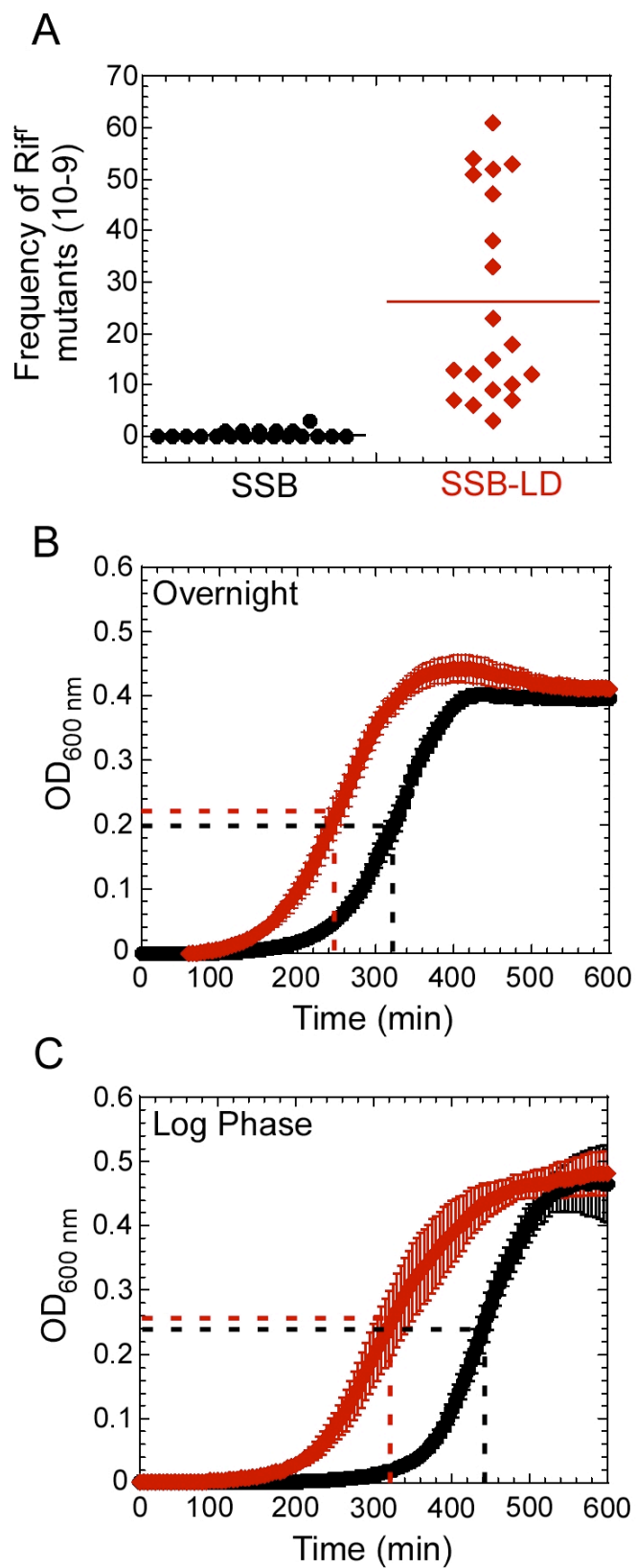


Figure 4.7 Growth characteristics of *E. coli* cells carrying either four or two-tailed SSB tetramers. (A) Rifampicin resistance assay showing the frequency of mutations in strains carrying the *wt SSB* or the *SSB-LD-Drl* genes. Growth analysis of *E. coli* cells with the *wt SSB* gene or *SSB-LD-Drl* gene shows faster recovery of the two-tailed SSB strain when the cultures are started from an overnight passage (B) or from a log phase starter culture (C).

4.5 Discussion

In addition to its role in binding ssDNA, *E. coli* SSB protein serves as an important recruitment platform during DNA replication, repair and recombination in that it binds more than a dozen proteins (SIPs) via its unstructured C-terminal tails. Each SSB homotetramer has four potential SIP binding sites and we show here that a reduction in the number of C-terminal tails associated with each tetramer has deleterious effects on many of its biological functions. We find that *E. coli* cells are unable to survive when expressing an SSB construct that contains four OB-folds ("tetramer") but only one C-terminal tail (SSB-LT-Drl), whereas *E. coli* expressing an SSB "tetramer" with only two tails (SSB-LD-Drl or *Drad* SSB) is able to survive. Furthermore, whereas a two-tailed SSB "tetramer" is able to coordinate leading and lagging strand DNA replication *in vitro*, a single-tailed "tetramer" is deficient *in vitro*. In addition, the single-tailed SSB does not support the loading of the DnaB helicase in a model replication restart assay, whereas a two-tailed SSB can function in this capacity. However, even though the two-tailed SSB "tetramer" can support cell growth, this variant shows defects in DNA repair and as a consequence mutations accumulate at a high frequency. These results indicate that more than one tail is needed within a single SSB tetramer for it to properly function in at least one essential process *in vivo*. Our experiments *in vitro* suggest that at least two essential functions are impaired: the

coupling of leading and lagging strand DNA synthesis as well as replication restart. However, an SSB with only two tails is also unable to coordinate some aspects of mutational repair. Therefore, either a single SSB tetramer is required to bind to at least two SIP proteins simultaneously or one essential SSB-SIP interaction requires two C-terminal tails on a single SSB tetramer.

Although our covalently linked SSB variants with two and one tail per "tetramer" bind and wrap ssDNA similarly to wt SSB, there is a quantitative difference in their affinity for (dT)₇₀ and their ability to bind to two (dT)₃₅ molecules (Fig. 4.3). Whereas the SSB variant proteins can form the (SSB)₃₅, (SSB)₅₆ and (SSB)₆₅ binding modes on poly(dT), there is also a shift in the salt dependence of the relative stabilities of the three binding modes. However, under the buffer conditions used in the replication studies reported here *in vitro*, all of the SSB proteins bind in a fully-wrapped mode and with high affinity. Although it is not known whether all three of the binding modes are functional *in vivo*, we cannot rule out that there may be some effects on SSB function due to these differences.

With respect to DNA repair, even though the levels of RecA protein are similar in cells expressing SSB-LD-Drl and wt SSB proteins upon exposure to DNA damage, the mutation frequency is 30-fold higher in cells expressing SSB-LD-Drl, the two-tailed SSB variant (Fig. 4.7A). This may be due to an effect of the number of tails on SSB binding to the recombination mediator RecO. RecO, a part of the RecFOR mediator complex, binds directly to SSB and the RecFOR complex regulates the formation of the RecA nucleoprotein filament on ssDNA (Sakai and Cox, 2009; Morimatsu et al., 2012). Apart from defective HR, the loss of interactions with other repair proteins such as RecQ,

uracil DNA glycosylase (UDG) and Exol affect other pathways such as Base Excision repair and Mismatch Repair. Consequently, the lesions on the DNA are not being repaired leading to the higher frequency of mutagenesis. We propose that the inability of the SSB-LD-Drl tetramer at the replication fork to communicate the presence of the DNA lesion and deliver the DNA repair machinery might result in the absence of DNA repair. The results presented here highlight the significance of SSB and its SIP interacting C-terminal tails in mediating DNA replication and repair. It is interesting to note that *E. coli* cells carrying the *Dr*-SSB protein instead of the native wt Ec-SSB protein also show a higher frequency of spontaneous mutagenesis (Fig. S2.7). The *Dr*-SSB protein is not engineered and shows the same repair properties as the linked SSB-LD-Drl protein *in vivo*. This again suggests that the number of C-terminal tails on SSB influences coordination of DNA replication and repair in bacteria.

In an attempt to reconcile the lethal dominant negative phenotype of *ssb-LT-Drl* with *in vitro* biochemical observations, we examined the consequence of substituting wt SSB with the SSB-LD-Drl and SSB-LT-Drl derivatives in DNA replication assays. In a relatively simple assay where the processive activity of Pol III HE is required for efficient conversion of an 8000 nt single-stranded circle to a duplex, we observed a decrease in the ability of the SSB derivatives with one or two tails to stimulate this reaction. The defect with the one-tailed SSB-LT-Drl was most severe, giving little stimulation above the level observed in the absence of SSB. In these reactions, the extent of the reaction was most severely reduced (Fig. 4.4). The reduced velocities can be explained by fewer DNA molecules participating in the reaction. Thus, at least part of the defect appears to be in the initiation phase of the reaction. The χ subunit of the Pol III HE interacts with

the C-terminal tail of SSB and facilitates binding to and elongating templates that are coated with SSB (Glover and McHenry, 1998; Kelman and Hurwitz, 1998; Kozlov et al., 2010b; Naue and Curth, 2012). We have observed that an interaction between Pol III HE component other than χ and the C-terminal tail of SSB is required for the optimal efficiency of initiation complex formation under conditions where Pol III associated with τ -containing DnaX complexes is chaperoned onto newly assembled β_2 (Downey and McHenry, 2010). During initiation complex formation in the presence of single-tailed SSB-LT-Drl it is possible that a portion of the Pol III HE interacts through χ precluding stimulation by the second interaction site or even trapping the enzyme in a non-productive complex.

In a more complex rolling circle replication reaction, we observe no difference upon substituting the two-tailed SSB (SSB-LD-Drl) for wt SSB; however, a two-fold decrease in leading strand synthesis and a further decrease in lagging strand synthesis is observed upon substituting the one-tailed SSB, SSB-LT-Drl. In this assay, a dimeric Pol III HE simultaneously replicates the leading and lagging strand in a reaction that is coupled, in part, through an interaction with the DnaB helicase (Kim et al., 1996a, 1996b; Gao and McHenry, 2001a). The decrease in leading strand synthesis could be explained by a defect in interaction of the Pol III HE through χ to SSB coating the lagging strand. This interaction has been shown to be important for stabilizing leading strand replication during the extensive elongation that takes place on rolling circle templates (Marceau et al., 2011) and in stabilizing leading strand Pol III HE in strand displacement reactions (Yuan and McHenry, 2009).

To determine whether the additional lagging strand defect was due to slower lagging strand specific elongation or a defect in priming, we examined the length of Okazaki fragments produced. The length of Okazaki fragments is very sensitive to Pol III HE elongation rates and the frequency of primer synthesis and utilization (Zechner et al., 1992a). However, we see the same average lengths in the presence of all SSB forms, eliminating these possibilities.

The additional decrease in lagging strand synthesis may be due to an occasional defect in DNA replication initiation on RNA primers. This defect is not absolute. Approximately 60 Okazaki fragments are made in the reaction with wt SSB during the five minute reaction (~ 2500 nt Okazaki fragments synthesized at ~ 500 nt/s). Thus, repeated cycles of initiation, elongation and recycling to new primers occurs, even in the presence of the one-tailed SSB-LT-Drl. But, failure to reinitiate lagging strand synthesis likely leads to uncoupling of the reaction and possible replication fork collapse.

Intuitively, the replication defects observed do not appear to be sufficiently severe to result in the dominant lethal phenotype observed for *ssb-LT-Drl*. Mechanisms exist in *E. coli* for reinitiation at collapsed initiation forks. The principal pathway proceeds through a PriA-dependent reaction. PriA recognizes collapsed forks and through a reaction dependent on sequential interactions with PriB, DnaT, and DnaC, leads to the reassembly of the DnaB helicase at forks and the ensuing re-entry of Pol III HE, re-establishing replication forks (Marians, 2000). The PriA-dependent reaction is absolutely dependent upon SSB (Manhart and McHenry, 2013). Thus, we sought to determine whether this replication restart reaction is impaired in the presence of SSB with less than the full complement of C-terminal tails.

We employed a FRET assay that monitors the separation of two strands by the DnaB helicase on artificial replication forks. Sterically blocking the 5'-end of the lagging strand template precludes helicase self-assembly by a threading reaction, making helicase PriA-, PriB-, DnaT-, DnaC- and SSB-dependent (Manhart and McHenry, 2013). In the presence of SSB-LD-Drl the reaction decreases approximately 30%. However, in the presence of SSB-LT-Drl, the reaction is nearly completely inhibited.

An interaction between SSB and PriA is important to support PriA function (Cadman and McGlynn, 2004; Kozlov et al., 2010a). SPR studies of PriA binding to synthetic replication forks suggest multiple copies of PriA interact (Yuan and McHenry, unpublished result). It is possible that multiple PriA monomers must interact with multiple C-terminal tails in a single SSB tetramer. The replication restart primosomal reaction involves sequential interactions of the PriA, PriB, DnaT and DnaC/DnaB proteins in a possible handoff reaction (Liu et al., 1996; Lopper et al., 2007). Thus, an SSB with multiple C-terminal tails could be required to bind to a partner downstream of PriA facilitating complex stability or requisite handoffs.

E. coli priA mutants yield very small slow growing colonies and exhibit a low viability upon dilution and re-plating (Marians, 2000). Viability could be due to a percentage of cells that do not experience replication fork collapse in sequential divisions. SSB-LT-Drl supports decreased levels of replication at reconstituted replication forks in reactions that likely lead to uncoupling and increased frequencies of replication fork collapse. That defect superimposed on the inability of cells to reinitiate by the PriA-dependent replication restart pathway provides a plausible explanation for the lethality observed with *ssb-LT-Drl*.

In bacterial cells, SSB functions at the interface of multiple biological processes including DNA replication, repair, recombination and replication restart. The number of C-terminal tails associated with each SSB tetramer appears to be a critical factor in determining when and how these processes are coupled.

REFERENCES

- Alberts, B.M., Barry, J., Bedinger, P., Formosa, T., Jongeneel, C. V, and Kreuzer, K.N. (1983). Studies on DNA replication in the bacteriophage T4 in vitro system. *Cold Spring Harbor Symposia on Quantitative Biology* 47 Pt 2, 655–668.
- Anderson, S.G., Thompson, J. a, Paschall, C.O., O'Donnell, M., and Bloom, L.B. (2009). Temporal correlation of DNA binding, ATP hydrolysis, and clamp release in the clamp loading reaction catalyzed by the Escherichia coli gamma complex. *Biochemistry* 48, 8516–8527.
- Anderson, S.G., Williams, C.R., O'donnell, M., and Bloom, L.B. (2007). A function for the psi subunit in loading the Escherichia coli DNA polymerase sliding clamp. *The Journal of Biological Chemistry* 282, 7035–7045.
- Antony, E., Kozlov, A.G., Nguyen, B., and Lohman, T.M. (2012a). Plasmodium falciparum SSB tetramer binds single-stranded DNA only in a fully wrapped mode. *Journal of Molecular Biology* 420, 284–295.
- Antony, E., Weiland, E.A., Korolev, S., and Lohman, T.M. (2012b). Plasmodium falciparum SSB tetramer wraps single-stranded DNA with similar topology but opposite polarity to E. coli SSB. *Journal of Molecular Biology* 420, 269–283.
- Arad, G., Hendel, A., Urbanke, C., Curth, U., and Livneh, Z. (2008). Single-stranded DNA-binding protein recruits DNA polymerase V to primer termini on RecA-coated DNA. *The Journal of Biological Chemistry* 283, 8274–8282.
- Ason, B., Bertram, J.G., Hingorani, M.M., Beechem, J.M., Donnell, M.O., Goodman, M.F., and Bloom, L.B. (2000). A model for Escherichia coli DNA polymerase III holoenzyme assembly at primer/template ends. *The Journal of Biological Chemistry* 275, 3006–3015.
- Ason, B., Handayani, R., Williams, C.R., Bertram, J.G., Hingorani, M.M., O'Donnell, M., Goodman, M.F., and Bloom, L.B. (2003). Mechanism of loading the Escherichia coli DNA polymerase III beta sliding clamp on DNA: Bona fide primer/templates

preferentially trigger the gamma complex to hydrolyze ATP and load the clamp. *The Journal of Biological Chemistry* 278, 10033–10040.

Bailey, S., Wing, R.A., and Steitz, T.A. (2006). The structure of *T. aquaticus* DNA polymerase III is distinct from eukaryotic replicative DNA polymerases. *Cell* 893–904.

Bernstein, D.A., Eggington, J.M., Killoran, M.P., Misic, A.M., Cox, M.M., and Keck, J.L. (2004). Crystal structure of the *Deinococcus radiodurans* single-stranded DNA-binding protein suggests a mechanism for coping with DNA damage. *Proceedings of the National Academy of Sciences of the United States of America* 101, 8575–8580.

Biesele, J., Philips, F., Thiersch, J., Burchenal, J., Buckley, S., Stock, C., Loveless, A., and Ross, W.C. (1950). Chromosome alteration and tumour inhibition by nitrogen mustards; the hypothesis of crosslinking alkylation. *Nature* 166, 1112–1114.

Blinkowa, A.L., and Walker, J.R. (1990). Programmed ribosomal frameshifting generates the *Escherichia coli* DNA polymerase III γ subunit from within the τ subunit reading frame. *Nucleic Acids Research* 18, 1725–1729.

Bonura, T., and Smith, K.C. (1975). Quantitative evidence for enzymatically-induced DNA double-strand breaks as lethal lesions in UV irradiated *pol+* and *polA1* strains of *E. coli* K-12. *Photochemistry and Photobiology* 22, 243–248.

Braun, K.A., Lao, Y., He, Z., Ingles, C.J., and Wold, M.S. (1997). Role of protein-protein interactions in the function of replication protein A (RPA): RPA modulates the activity of DNA polymerase alpha by multiple mechanisms. *Biochemistry* 36, 8443–8454.

Bujalowski, W., and Lohman, T. (1991). Monomers of the *Escherichia coli* SSB-1 mutant protein bind single-stranded DNA. *Journal of Molecular Biology* 217, 63–74.

Bujalowski, W., and Lohman, T.M. (1986). *Escherichia coli* single-strand binding protein forms multiple, distinct complexes with single-stranded DNA. *Biochemistry* 25, 7799–7802.

Bujalowski, W., and Lohman, T.M. (1989a). Negative co-operativity in *Escherichia coli* single strand binding protein-oligonucleotide interactions. II. Salt, temperature and oligonucleotide length effects. *Journal of Molecular Biology* 207, 269–288.

Bujalowski, W., and Lohman, T.M. (1989b). Negative co-operativity in *Escherichia coli* single strand binding protein-oligonucleotide interactions. II. Salt, temperature and oligonucleotide length effects. *Journal of Molecular Biology* 207, 269–288.

Bujalowski, W., Overman, L.B., and Lohman, T.M. (1988). Binding mode transitions of *Escherichia coli* single strand binding protein-single-stranded DNA complexes. Cation, anion, pH, and binding density effects. *The Journal of Biological Chemistry* 263, 4629–4640.

Bullard, J.M., Pritchard, A.E., Song, M.-S., Glover, B.P., Wieczorek, A., Chen, J., Janjic, N., and McHenry, C.S. (2002). A three-domain structure for the delta subunit of the DNA polymerase III holoenzyme delta domain III binds delta' and assembles into the DnaX complex. *The Journal of Biological Chemistry* 277, 13246–13256.

Burgers, P.M.J. (2009). Polymerase dynamics at the eukaryotic DNA replication fork. *The Journal of Biological Chemistry* 284, 4041–4045.

Cadman, C.J., Lopper, M., Moon, P.B., Keck, J.L., and McGlynn, P. (2005). PriB stimulates PriA helicase via an interaction with single-stranded DNA. *The Journal of Biological Chemistry* 280, 39693–39700.

Cadman, C.J., and McGlynn, P. (2004). PriA helicase and SSB interact physically and functionally. *Nucleic Acids Research* 32, 6378–6387.

Canceill, D., and Ehrlich, S.D. (1996). Copy-choice recombination mediated by DNA polymerase III holoenzyme from *Escherichia coli*. *Proceedings of the National Academy of Sciences of the United States of America* 93, 6647–6652.

Caruthers, J.M., and McKay, D.B. (2002). Helicase structure and mechanism. *Current Opinion in Structural Biology* 12, 123–133.

Chrysogelos, S., and Griffith, J. (1982). *Escherichia coli* single-strand binding protein organizes single-stranded DNA in nucleosome-like units. *Proceedings of the National Academy of Sciences of the United States of America* 79, 5803–5807.

Costes, A., Lecointe, F., McGovern, S., Quevillon-Cheruel, S., and Polard, P. (2010). The C-terminal domain of the bacterial SSB protein acts as a DNA maintenance hub at active chromosome replication forks. *PLoS Genetics* 6, e1001238.

Cull, M.G., and McHenry, C.S. (1995). Purification of *Escherichia coli* DNA polymerase III holoenzyme. *Methods in Enzymology* 262, 22–35.

Curth, U., Genschel, J., Urbanke, C., and Greipel, J. (1996). In vitro and in vivo function of the C-terminus of *Escherichia coli* single-stranded DNA binding protein. *Nucleic Acids Research* 24, 2706–2711.

Dallmann, H.G., and McHenry, C.S. (1995). DnaX complex of *Escherichia coli* DNA polymerase III holoenzyme. *The Journal of Biological Chemistry* 270, 29563–29569.

Dalrymple, B.P., Kongsuwan, K., Wijffels, G., Dixon, N.E., and Jennings, P. a (2001). A universal protein-protein interaction motif in the eubacterial DNA replication and repair systems. *Proceedings of the National Academy of Sciences of the United States of America* 98, 11627–11632.

Dam, J., and Schuck, P. (2004). Calculating sedimentation coefficient distributions by direct modeling of sedimentation velocity concentration profiles. *Methods in Enzymology* 384, 185–212.

Dohrmann, P.R., Manhart, C.M., Downey, C.D., and McHenry, C.S. (2011). The rate of polymerase release upon filling the gap between Okazaki fragments is inadequate to support cycling during lagging strand synthesis. *Journal of Molecular Biology* 414, 15–27.

Dohrmann, P.R., and McHenry, C.S. (2005). A bipartite polymerase-processivity factor interaction: only the internal beta binding site of the alpha subunit is required for processive replication by the DNA polymerase III holoenzyme. *Journal of Molecular Biology* 350, 228–239.

Downey, C.D., Crooke, E., and McHenry, C.S. (2011). Polymerase chaperoning and multiple ATPase sites enable the *E. coli* DNA polymerase III holoenzyme to rapidly form initiation complexes. *Journal of Molecular Biology* 412, 340–353.

Downey, C.D., and McHenry, C.S. (2010). Chaperoning of a replicative polymerase onto a newly assembled DNA-bound sliding clamp by the clamp loader. *Molecular Cell* 37, 481–491.

Ezekiel, D.H., and Hutchins, J.E. (1968). Mutations affecting RNA polymerase associated with rifampicin resistance in *Escherichia coli*. *Nature* 220, 276–277.

Fay, P.J., Johanson, K.O., McHenry, C.S., and Bambara, R.A. (1982). Size classes of products synthesized processively by two subassemblies of *Escherichia coli* DNA polymerase III holoenzyme. *The Journal of Biological Chemistry* 257, 5692–5699.

Fedorov, R., Witte, G., Urbanke, C., Manstein, D.J., and Curth, U. (2006). 3D structure of *Thermus aquaticus* single-stranded DNA-binding protein gives insight into the functioning of SSB proteins. *Nucleic Acids Research* 34, 6708–6717.

Ferrari, M.E., Bujalowski, W., and Lohman, T.M. (1994). Co-operative binding of *Escherichia coli* SSB tetramers to single-stranded DNA in the (SSB)₃₅ binding mode. *Journal of Molecular Biology* 236, 106–123.

Flower, A.M., and McHenry, C.S. (1990). The gamma subunit of DNA polymerase III holoenzyme of *Escherichia coli* is produced by ribosomal frameshifting. *Proceedings of the National Academy of Sciences of the United States of America* 87, 3713–3717.

Gao, D., and McHenry, C.S. (2001a). Tau binds and organizes *Escherichia coli* replication proteins through distinct domains. Domain III, shared by gamma and tau, binds delta delta' and chi psi. *The Journal of Biological Chemistry* 276, 4447–4453.

Gao, D., and McHenry, C.S. (2001b). Tau binds and organizes Escherichia coli replication proteins through distinct domains. Domain IV, located within the unique C terminus of tau, binds the replication fork, helicase, DnaB. *The Journal of Biological Chemistry* 276, 4441–4446.

Gao, D., and McHenry, C.S. (2001c). Tau binds and organizes Escherichia coli replication through distinct domains. Partial proteolysis of terminally tagged tau to determine candidate domains and to assign domain V as the alpha binding domain. *The Journal of Biological Chemistry* 276, 4433–4440.

George, N.P., Ngo, K. V, Chitteni-Pattu, S., Norais, C.A., Battista, J.R., Cox, M.M., and Keck, J.L. (2012). Structure and cellular dynamics of Deinococcus radiodurans single-stranded DNA (ssDNA)-binding protein (SSB)-DNA complexes. *The Journal of Biological Chemistry* 287, 22123–22132.

Georgescu, R.E., Kurth, I., and O'Donnell, M.E. (2011). Single-molecule studies reveal the function of a third polymerase in the replisome. *Nature Structural & Molecular Biology* 19, 113–116.

Georgescu, R.E., Kurth, I., Yao, N.Y., Stewart, J., Yurieva, O., and O'Donnell, M. (2009). Mechanism of polymerase collision release from sliding clamps on the lagging strand. *The EMBO Journal* 28, 2981–2991.

Glover, B.P., and McHenry, C.S. (1998). The chi psi subunits of DNA polymerase III holoenzyme bind to single-stranded DNA-binding protein (SSB) and facilitate replication of an SSB-coated template. *The Journal of Biological Chemistry* 273, 23476–23484.

Glover, B.P., and McHenry, C.S. (2000). The DnaX-binding subunits delta' and chi are bound to gamma and not tau in the DNA polymerase III holoenzyme. *The Journal of Biological Chemistry* 3017–3020.

Glover, B.P., and McHenry, C.S. (2001). The DNA polymerase III holoenzyme: an asymmetric dimeric replicative complex with leading and lagging strand polymerases. *Cell* 105, 925–934.

Glover, B.P., Pritchard, A.E., and McHenry, C.S. (2001). Tau binds and organizes Escherichia coli replication proteins through distinct domains: domain III, shared by gamma and tau, oligomerizes DnaX. *The Journal of Biological Chemistry* 276, 35842–35846.

Griep, M.A., and McHenry, C.S. (1989). Glutamate overcomes the salt inhibition of DNA polymerase III holoenzyme. *The Journal of Biological Chemistry* 264, 11294–11301.

Griffith, J.D., Harris, L.D., and Register, J. (1984). Visualization of SSB-ssDNA complexes active in the assembly of stable RecA-DNA filaments. *Cold Spring Harbor Symposia on Quantitative Biology* 49, 553–559.

Hamdan, S.M., Loparo, J.J., Takahashi, M., Richardson, C.C., and Van Oijen, A.M. (2009). Dynamics of DNA replication loops reveal temporal control of lagging-strand synthesis. *Nature* 457, 336–339.

Han, E.S., Cooper, D.L., Persky, N.S., Sutera, V.A., Whitaker, R.D., Montello, M.L., and Lovett, S.T. (2006). RecJ exonuclease: substrates, products and interaction with SSB. *Nucleic Acids Research* 34, 1084–1091.

Handa, P., Acharya, N., and Varshney, U. (2001). Chimeras between single-stranded DNA-binding proteins from *Escherichia coli* and *Mycobacterium tuberculosis* reveal that their C-terminal domains interact with uracil DNA glycosylases. *The Journal of Biological Chemistry* 276, 16992–16997.

Heller, R.C., and Marians, K.J. (2005). The disposition of nascent strands at stalled replication forks dictates the pathway of replisome loading during restart. *Molecular Cell* 17, 733–743.

Hingorani, M.M., and O'Donnell, M. (1998). ATP binding to the *Escherichia coli* clamp loader powers opening of the ring-shaped clamp of DNA polymerase III holoenzyme. *The Journal of Biological Chemistry* 273, 24550–24563.

Hobbs, M.D., Sakai, A., and Cox, M.M. (2007). SSB protein limits RecOR binding onto single-stranded DNA. *The Journal of Biological Chemistry* 282, 11058–11067.

Jergic, S., Horan, N.P., Elshenawy, M.M., Mason, C.E., Urathamakul, T., Ozawa, K., Robinson, A., Goudsmits, J.M.H., Wang, Y., Pan, X., et al. (2013). A direct proofreader-clamp interaction stabilizes the Pol III replicase in the polymerization mode. *The EMBO Journal* 32, 1322–1333.

Jeruzalmi, D., O'Donnell, M., and Kuriyan, J. (2001a). Crystal structure of the processivity clamp loader gamma (gamma) complex of *E. coli* DNA polymerase III. *Cell* 106, 429–441.

Jeruzalmi, D., Yurieva, O., Zhao, Y., Young, M., Stewart, J., Hingorani, M., O'Donnell, M., and Kuriyan, J. (2001b). Mechanism of processivity clamp opening by the delta subunit wrench of the clamp loader complex of *E. coli* DNA polymerase III. *Cell* 106, 417–428.

Johanson, K.O. (1982). The beta subunit of the DNA polymerase III holoenzyme becomes inaccessible to antibody after formation of an initiation complex with primed DNA. *The Journal of Biological Chemistry* 257, 12310–12315.

Johanson, K.O., Haynes, T.E., and McHenry, C.S. (1986). Chemical characterization and purification of the beta subunit of the DNA polymerase III holoenzyme from an overproducing strain. *The Journal of Biological Chemistry* 261, 11460–11465.

Johanson, K.O., and McHenry, C.S. (1984). Can support the formation of an initiation complex between the DNA polymerase III holoenzyme and primed DNA. *The Journal of Biological Chemistry* 259, 4589–4595.

Johnson, A., and O'Donnell, M. (2003). Ordered ATP hydrolysis in the gamma complex clamp loader AAA+ machine. *The Journal of Biological Chemistry* 278, 14406–14413.

Johnson, D.E., Takahashi, M., Hamdan, S.M., Lee, S.-J., and Richardson, C.C. (2007). Exchange of DNA polymerases at the replication fork of bacteriophage T7. *Proceedings of the National Academy of Sciences of the United States of America* 104, 5312–5317.

Jones, C.E., Green, E.M., Stephens, J. a, Mueser, T.C., and Nossal, N.G. (2004). Mutations of bacteriophage T4 59 helicase loader defective in binding fork DNA and in interactions with T4 32 single-stranded DNA-binding protein. *The Journal of Biological Chemistry* 279, 25721–25728.

Kelman, Z., and Hurwitz, J. (1998). Protein-PCNA interactions: a DNA-scanning mechanism? *Trends in Biochemical Sciences* 23, 236–238.

Kelman, Z., and O'Donnell, M. (1995). DNA polymerase III holoenzyme: Structure and function of a chromosomal replicating machine. *Annual Review of Biochemistry* 64, 171–200.

Kelman, Z., Yuzhakov, A., Andjelkovic, J., and O'Donnell, M. (1998). Devoted to the lagging strand-the chi subunit of DNA polymerase III holoenzyme contacts SSB to promote processive elongation and sliding clamp assembly. *The EMBO Journal* 17, 2436–2449.

Kim, D.R., and McHenry, C.S. (1996a). Biotin tagging deletion analysis of domain limits involved in protein-macromolecular interactions. *Biochemistry* 271, 20690–20698.

Kim, D.R., and McHenry, C.S. (1996b). Identification of the beta-binding domain of the alpha subunit of *Escherichia coli* polymerase III holoenzyme. *The Journal of Biological Chemistry* 271, 20699–20704.

Kim, D.R., and McHenry, C.S. (1996c). In vivo assembly of overproduced DNA polymerase III. *The Journal of Biological Chemistry* 271, 20681–20689.

Kim, S., Dallmann, H.G., McHenry, C.S., and Marians, K.J. (1996a). Coupling of a replicative polymerase and helicase: a tau-DnaB interaction mediates rapid replication fork movement. *Cell* 84, 643–650.

Kim, S., Dallmann, H.G., McHenry, C.S., and Marians, K.J. (1996b). Tau couples the leading- and lagging-strand polymerases at the *Escherichia coli* DNA replication fork. *The Journal of Biological Chemistry* 271, 21406–21412.

Kim, S., Dallmann, H.G., McHenry, C.S., and Marians, K.J. (1996c). Tau protects beta in the leading-strand polymerase complex at the replication fork. *The Journal of Biological Chemistry* 271, 4315–4318.

Kong, X.P., Onrust, R., O'Donnell, M., and Kuriyan, J. (1992). Three-dimensional structure of the beta subunit of *E. coli* DNA polymerase III holoenzyme: a sliding DNA clamp. *Cell* 69, 425–437.

Kornberg, A., and Baker, T.A. (1992). *DNA Replication*.

Kowalczykowski, S., Lonberg, N., Newport, J., and Von Hippel, P. (1981). Interactions of bacteriophage T4-coded gene 32 protein with nucleic acids. I. Characterization of the binding interactions. *Journal of Molecular Biology* 145, 75–104.

Kowalczykowski, S.C., Dixon, D.A., Eggleston, A.K., Lauder, S.D., and Rehrauer, W.M. (1994). Biochemistry of homologous recombination in *Escherichia coli*. *Microbiological Reviews* 58, 401–465.

Kozlov, A.G., Cox, M.M., and Lohman, T.M. (2010a). Regulation of single-stranded DNA binding by the C termini of *Escherichia coli* single-stranded DNA-binding (SSB) protein. *The Journal of Biological Chemistry* 285, 17246–17252.

Kozlov, A.G., Jezewska, M.J., Bujalowski, W., and Lohman, T.M. (2010b). Binding specificity of *Escherichia coli* single-stranded DNA binding protein for the chi subunit of DNA pol III holoenzyme and PriA helicase. *Biochemistry* 49, 3555–3566.

Kozlov, A.G., and Lohman, T.M. (2002). Stopped-flow studies of the kinetics of single-stranded DNA binding and wrapping around the *Escherichia coli* SSB tetramer. *Biochemistry* 41, 6032–6044.

LaDuca, R.J., Crute, J.J., McHenry, C.S., and Bambara, R.A. (1986). The beta subunit of the *Escherichia coli* DNA polymerase III holoenzyme interacts functionally with the catalytic core in the absence of other subunits. *The Journal of Biological Chemistry* 261, 7550–7557.

Laue, T., Shah, B.D., Rldgeway, T.M., and Pelletier, S.L. (1992). Computer-aided interpretation of analytical sedimentation data for proteins. Royal Society of Cambridge, Cambridge, UK 1.

LeBowitz, J.H., and McMacken, R. (1986). The *Escherichia coli* dnaB replication protein is a DNA helicase. *The Journal of Biological Chemistry* 261, 4738–4748.

Lecoite, F., Sérèna, C., Velten, M., Costes, A., McGovern, S., Meile, J.-C., Errington, J., Ehrlich, S.D., Noirot, P., and Polard, P. (2007). Anticipating chromosomal replication fork arrest: SSB targets repair DNA helicases to active forks. *The EMBO Journal* 26, 4239–4251.

- Lee, J., Chastain, P.D., Griffith, J.D., and Richardson, C.C. (2002). Lagging strand synthesis in coordinated DNA synthesis by bacteriophage T7 replication proteins. *Journal of Molecular Biology* 316, 19–34.
- Lee, J., Chastain, P.D., Kusakabe, T., Griffith, J.D., and Richardson, C.C. (1998). Coordinated leading and lagging strand DNA synthesis on a minicircular template. *Molecular Cell* 1, 1001–1010.
- Lee, J.-B., Hite, R.K., Hamdan, S.M., Xie, X.S., Richardson, C.C., and Van Oijen, A.M. (2006). DNA primase acts as a molecular brake in DNA replication. *Nature* 439, 621–624.
- Leu, F.P., Georgescu, R., and O'Donnell, M. (2003). Mechanism of the *E. coli* tau processivity switch during lagging-strand synthesis. *Molecular Cell* 11, 315–327.
- Li, K., and Williams, R.S. (1997). Tetramerization and single-stranded DNA binding properties of native and mutated forms of murine mitochondrial single-stranded DNA-binding proteins. *The Journal of Biological Chemistry* 272, 8686–8694.
- Li, X., and Marians, K.J. (2000). Two distinct triggers for cycling of the lagging strand polymerase at the replication fork. *The Journal of Biological Chemistry* 275, 34757–34765.
- Lia, G., Michel, B., and Allemand, J.-F. (2012). Polymerase exchange during Okazaki fragment synthesis observed in living cells. *Science* 335, 328–331.
- Liu, B., Lin, J., and Steitz, T. a (2013). Structure of the PolIII α - τ -DNA complex suggests an atomic model of the replisome. *Structure (London, England : 1993)* 21, 658–664.
- Liu, J., and Marians, K.J. (1999). PriA-directed assembly of a primosome on D loop DNA. *The Journal of Biological Chemistry* 274, 25033–25041.
- Liu, J., Nurse, P., and Marians, K.J. (1996). The ordered assembly of the phiX174-type primosome. III. PriB facilitates complex formation between PriA and DnaT. *The Journal of Biological Chemistry* 271, 15656–15661.
- Lohman, M., Overman, L.B., and Datta, S. (1986a). Salt-dependent changes in the DNA binding co-operativity of *Escherichia coli* single strand binding protein. *Journal of Molecular Biology* 187, 603–615.
- Lohman, T. (1986). Kinetics of protein-nucleic acid interactions: use of salt effects to probe mechanisms of interaction. *CRC Critical Reviews in Biochemistry* 19, 191–245.
- Lohman, T., Bujalowski, W., and Overman, L. (1988). *E. coli* single strand binding protein: a new look at helix-destabilizing proteins. *Trends in Biochemical Sciences* 13, 250–255.

Lohman, T.M. (1992). Escherichia coli DNA helicases: mechanisms of DNA unwinding. *Molecular Microbiology* 6, 5–14.

Lohman, T.M., and Bujalowski, W. (1988). Negative cooperativity within individual tetramers of Escherichia coli single strand binding protein is responsible for the transition between the (SSB)₃₅ and (SSB)₅₆ DNA binding modes. *Biochemistry* 27, 2260–2265.

Lohman, T.M., and Ferrari, M.E. (1994). Escherichia coli single-stranded DNA-binding protein: multiple DNA-binding modes and cooperativities. *Annual Review of Biochemistry* 63, 527–570.

Lohman, T.M., Overman, L.B., and Datta, S. (1986b). Salt-dependent changes in the DNA binding co-operativity of Escherichia coli single strand binding protein. *Journal of Molecular Biology* 187, 603–615.

Lohman, T.M., Overman, L.B., Gm, S.G., Welch, R.A., and Grant, F. (1985). Two binding modes in Escherichia coli single strand binding protein-single stranded DNA complexes. *The Journal of Biological Chemistry* 3594–3603.

López de Saro, F.J., Georgescu, R.E., Goodman, M.F., and O'Donnell, M. (2003a). Competitive processivity-clamp usage by DNA polymerases during DNA replication and repair. *The EMBO Journal* 22, 6408–6418.

López de Saro, F.J., Georgescu, R.E., and O'Donnell, M. (2003b). A peptide switch regulates DNA polymerase processivity. *Proceedings of the National Academy of Sciences of the United States of America* 100, 14689–14694.

Lopper, M., Boonsombat, R., Sandler, S.J., and Keck, J.L. (2007). A hand-off mechanism for primosome assembly in replication restart. *Molecular Cell* 26, 781–793.

Lu, D., Myers, A.R., George, N.P., and Keck, J.L. (2011). Mechanism of Exonuclease I stimulation by the single-stranded DNA-binding protein. *Nucleic Acids Research* 39, 6536–6545.

Manhart, C.M., and McHenry, C.S. (2013). The PriA replication restart protein blocks replicase access prior to helicase assembly and directs template specificity through its ATPase activity. *The Journal of Biological Chemistry* 288, 3989–3999.

Marceau, A.H., Bahng, S., Massoni, S.C., George, N.P., Sandler, S.J., Marians, K.J., and Keck, J.L. (2011). Structure of the SSB-DNA polymerase III interface and its role in DNA replication. *The EMBO Journal* 30, 4236–4247.

Marians, K.J. (1995a). phi X 174-type primosomal proteins: purification and assay. *Methods in Enzymology* 262, 507–521.

- Marians, K.J. (1995b). Phi X174-type primosomal proteins: purification and assay. *Methods in Enzymology* 262, 507–521.
- Marians, K.J. (2000). PriA-directed replication fork restart in *Escherichia coli*. *Trends in Biochemical Sciences* 25, 185–189.
- McCauley, M., Shokri, L., Sefcikova, J., Venclovas, C., Beuning, P., and Williams, M.C. (2008). Distinct double- and single-stranded DNA binding of *E. coli* replicative DNA polymerase III alpha subunit. *ACS Chem. Biol.* 3, 577–587.
- McHenry, C., and Crow, W. (1979). DNA polymerase III of *Escherichia coli*. *The Journal of Biological Chemistry* 254, 1748–1753.
- McHenry, C.S. (1982). Purification and Characterization of DNA Polymerase III' : Identification of tau as a subunit of the DNA polymerase III holoenzyme. *The Journal of Biological Chemistry* 257, 2657–2663.
- McHenry, C.S. (2003). Chromosomal replicases as asymmetric dimers: studies of subunit arrangement and functional consequences. *Molecular Microbiology* 49, 1157–1165.
- McHenry, C.S. (2011a). Bacterial replicases and related polymerases. *Current Opinion in Chemical Biology* 15, 587–594.
- McHenry, C.S. (2011b). DNA replicases from a bacterial perspective. *Annual Review of Biochemistry* 80, 403–436.
- McInerney, P., Johnson, A., Katz, F., and O'Donnell, M. (2007). Characterization of a triple DNA polymerase replisome. *Molecular Cell* 27, 527–538.
- Meyer, R.R., and Laine, P.S. (1990). The single-stranded DNA-binding protein of *Escherichia coli*. *Microbiological Reviews* 54, 342–380.
- Mok, M., and Marians, K.J. (1987). The *Escherichia coli* preprimosome and DNA B helicase can form replication forks that move at the same rate. *The Journal of Biological Chemistry* 262, 16644–16654.
- Mok, M.M.K.J. (1987). Formation of Rolling-circle Molecules during phix 174 Complementary Strand DNA replication. *The Journal of Biological Chemistry* 262, 2304–2309.
- Molineux, I.J., and Gefter, M.L. (1974). Properties of the *Escherichia coli* in DNA binding (unwinding) protein: interaction with DNA polymerase and DNA. *Proceedings of the National Academy of Sciences of the United States of America* 71, 3858–3862.

Morimatsu, K., Wu, Y., and Kowalczykowski, S.C. (2012). RecFOR proteins target RecA protein to a DNA gap with either DNA or RNA at the 5' terminus: implication for repair of stalled replication forks. *The Journal of Biological Chemistry* 287, 35621–35630.

Naue, N., Beerbaum, M., Bogutzki, A., Schmieder, P., and Curth, U. (2013). The helicase-binding domain of *Escherichia coli* DnaG primase interacts with the highly conserved C-terminal region of single-stranded DNA-binding protein. *Nucleic Acids Research* 1–11.

Naue, N., and Curth, U. (2012). Investigation of protein-protein interactions of single-stranded DNA-binding proteins by analytical ultracentrifugation. *Methods in Molecular Biology (Clifton, N.J.)* 922, 133–149.

O'Donnell, M.E., and Kornberg, a (1985). Dynamics of DNA polymerase III holoenzyme of *Escherichia coli* in replication of a multiprimed template. *The Journal of Biological Chemistry* 260, 12875–12883.

Olson, M.W., Dallmann, H.G., and McHenry, C.S. (1995). DnaX complex of *Escherichia coli* DNA polymerase III holoenzyme. *The Journal of Biological Chemistry* 270, 29570–29577.

Pandey, M., Syed, S., Donmez, I., Patel, G., Ha, T., and Patel, S.S. (2009). Coordinating DNA replication by means of priming loop and differential synthesis rate. *Nature* 462, 940–943.

Porter, R.D., and Black, S. (1991). The single-stranded-DNA-binding protein encoded by the *Escherichia coli* F factor can complement a deletion of the chromosomal *ssb* gene. *Journal of Bacteriology* 173, 2720–2723.

Porter, R.D., Black, S., Pannuri, S., and Carlson, A. (1990). Use of the *Escherichia coli* SSB gene to prevent bioreactor takeover by plasmidless cells. *Bio/technology (Nature Publishing Company)* 8, 47–51.

Pritchard, A.E., Dallmann, H.G., Glover, B.P., and McHenry, C.S. (2000). A novel assembly mechanism for the DNA polymerase III holoenzyme DnaX complex: association of $\delta\delta'$ with DnaX4 forms DnaX3 $\delta\delta'$. *The EMBO Journal* 19, 6536–6545.

Pritchard, A.E., Dallmann, H.G., and McHenry, C.S. (1996). In vivo assembly of the complex of the DNA polymerase III holoenzyme expressed from a five-gene artificial operon. *Biochemistry* 271, 10291–10298.

Pritchard, A.E., and McHenry, C.S. (1999). Identification of the acidic residues in the active site of DNA polymerase III. *Journal of Molecular Biology* 285, 1067–1080.

Pritchard, A.E., and McHenry, C.S. (2001). Assembly of DNA polymerase III holoenzyme: co-assembly of gamma and tau is inhibited by DnaX complex accessory

proteins but stimulated by DNA polymerase III core. *The Journal of Biological Chemistry* 276, 35217–35222.

Prusty, D., Dar, A., Priya, R., Sharma, A., Dana, S., Choudhury, N.R., Rao, N.S., and Dhar, S.K. (2010). Single-stranded DNA binding protein from human malarial parasite *Plasmodium falciparum* is encoded in the nucleus and targeted to the apicoplast. *Nucleic Acids Research* 38, 7037–7053.

Quiñones, A., and Neumann, S. (1997). The *ssb-113* allele suppresses the *dnaQ49* mutator and alters DNA supercoiling in *Escherichia coli*. *Molecular Microbiology* 25, 237–246.

Raghunathan, S., and Kozlov, A.G. (2000). Structure of the DNA binding domain of *E. coli* SSB bound to ssDNA. *Nature America* 7, 648–652.

Raghunathan, S., Ricard, C.S., Lohman, T.M., and Waksman, G. (1997). Crystal structure of the homo-tetrameric DNA binding domain of *Escherichia coli* single-stranded DNA-binding protein determined by multiwavelength x-ray diffraction on the selenomethionyl protein at 2.9-Å resolution. *Proceedings of the National Academy of Sciences of the United States of America* 94, 6652–6657.

Reems, J.A., and McHenry, C.S. (1994). *Escherichia coli* DNA polymerase III holoenzyme footprints three helical turns of its primer. *The Journal of Biological Chemistry* 269, 33091.

Reems, J.A., Wood, S., and McHenry, C.S. (1995). *Escherichia coli* DNA polymerase III holoenzyme subunits alpha, beta, and gamma directly contact the primer-template. *The Journal of Biological Chemistry* 270, 5606.

Rosenberg, S.M. (2001). Evolving responsively: adaptive mutation. *Nature Reviews. Genetics* 2, 504–515.

Rosenkranz, H., and Levy, J. (1965). Hydroxyurea: A specific inhibitor of deoxyribonucleic acid synthesis. *Biochimica Et Biophysica Acta* 95, 181–183.

Rosenkranz, H.S., Garro, A.J., Levy, J.A., and Carr, H.S. (1966). Studies with hydroxyurea. I. The reversible inhibition of bacterial DNA synthesis and the effect of hydroxyurea on the bactericidal action of streptomycin. *Biochimica Et Biophysica Acta* 114, 501–515.

Roy, R., Kozlov, A.G., Lohman, T.M., and Ha, T. (2007). Dynamic structural rearrangements between DNA binding modes of *E. coli* SSB protein. *Journal of Molecular Biology* 369, 1244–1257.

Roy, R., Kozlov, A.G., Lohman, T.M., and Ha, T. (2009). SSB protein diffusion on single-stranded DNA stimulates RecA filament formation. *Nature* 461, 1092–1097.

- Sakai, A., and Cox, M.M. (2009). RecFOR and RecOR as distinct RecA loading pathways. *The Journal of Biological Chemistry* 284, 3264–3272.
- Sanders, G.M., Dallmann, H.G., and McHenry, C.S. (2010). Reconstitution of the *B. subtilis* replisome with 13 proteins including two distinct replicases. *Molecular Cell* 37, 273–281.
- Schekman, R., Weiner, J.H., Weiner, A., and Kornberg, A. (1975). Ten proteins required to conversion of phiX174 single-stranded DNA to duplex form in vitro. *The Journal of Biological Chemistry* 250, 5859–5865.
- Schuck, P. (1998). Sedimentation analysis of noninteracting and self-associating solutes using numerical solutions to the Lamm equation. *Biophysical Journal* 75, 1503–1512.
- Shereda, R.D., Bernstein, D.A., and Keck, J.L. (2007). A central role for SSB in *Escherichia coli* RecQ DNA helicase function. *The Journal of Biological Chemistry* 282, 19247–19258.
- Shereda, R.D., Kozlov, A.G., Lohman, T.M., Cox, M.M., and Keck, J.L. (2008). SSB as an organizer/mobilizer of genome maintenance complexes. *Critical Reviews in Biochemistry and Molecular Biology* 43, 289–318.
- Shereda, R.D., Reiter, N.J., Butcher, S.E., and Keck, J.L. (2009). Identification of the SSB binding site on *E. coli* RecQ reveals a conserved surface for binding SSB's C terminus. *Journal of Molecular Biology* 386, 612–625.
- Simonetta, K.R., Kazmirski, S.L., Goedken, E.R., Cantor, A.J., Kelch, B.A., McNally, R., Seyedin, S.N., Makino, D.L., O'Donnell, M., and Kuriyan, J. (2009). The mechanism of ATP-dependent primer-template recognition by a clamp loader complex. *Cell* 137, 659–671.
- Stano, N.M., Chen, J., and McHenry, C.S. (2006). A coproofreading Zn²⁺-dependent exonuclease within a bacterial replicase. *Nature Structural & Molecular Biology* 13, 458–459.
- Stephens, K.M., and McMacken, R. (1997). Functional properties of replication fork assemblies established by the bacteriophage lambda O and P replication proteins. *The Journal of Biological Chemistry* 272, 28800–28813.
- Stukenberg, P.T., Studwell-van, P.S., and Donnell, M.O. (1991). Mechanism of the sliding beta-clamp of DNA polymerase III holoenzyme. *The Journal of Biological Chemistry* 266, 11328–11334.

Sugiura, S., Ohkubo, S., and Yamaguchi, K. (1993). Minimal essential origin of plasmid pSC101 replication: requirement of a region downstream of iterons. *Journal of Bacteriology* 175, 5993–6001.

Tanner, N. a, Loparo, J.J., Hamdan, S.M., Jergic, S., Dixon, N.E., and Van Oijen, A.M. (2009). Real-time single-molecule observation of rolling-circle DNA replication. *Nucleic Acids Research* 37, e27.

Thompson, J. a, Paschall, C.O., O'Donnell, M., and Bloom, L.B. (2009). A slow ATP-induced conformational change limits the rate of DNA binding but not the rate of beta clamp binding by the Escherichia coli gamma complex clamp loader. *The Journal of Biological Chemistry* 284, 32147–32157.

Tiranti, V., Rocchi, M., DiDonato, S., and Zeviani, M. (1993). Cloning of human and rat cDNAs encoding the mitochondrial single-stranded DNA-binding protein (SSB). *Gene* 126, 219–225.

Tougu, K., and Marians, K.J. (1996a). The extreme C terminus of primase is required for interaction with DnaB at the replication fork. *The Journal of Biological Chemistry* 271, 21391–21397.

Tougu, K., and Marians, K.J. (1996b). The interaction between helicase and primase sets the replication fork clock. *The Journal of Biological Chemistry* 271, 21398–21405.

Tsuchihashi, Z., and Kornberg, A. (1990). Translational frameshifting generates the gamma subunit of DNA polymerase III holoenzyme. *Proceedings of the National Academy of Sciences of the United States of America* 87, 2516–2520.

Turner, J., Hingorani, M.M., Kelman, Z., and O'Donnell, M. (1999). The internal workings of a DNA polymerase clamp-loading machine. *The EMBO Journal* 18, 771–783.

Umezu, K., and Kolodner, R.D. (1994). Protein interactions in genetic recombination in Escherichia coli. Interactions involving RecO and RecR overcome the inhibition of RecA by single-stranded DNA-binding protein. *The Journal of Biological Chemistry* 269, 30005–30013.

Vistica, J., Dam, J., Balbo, A., Yikilmaz, E., Mariuzza, R.A., Rouault, T.A., and Schuck, P. (2004). Sedimentation equilibrium analysis of protein interactions with global implicit mass conservation constraints and systematic noise decomposition. *Analytical Biochemistry* 326, 234–256.

Wadood, A., Dohmoto, M., Sugiura, S., and Yamaguchi, K. (1997). Characterization of copy number mutants of plasmid pSC101. *The Journal of General and Applied Microbiology* 43, 309–316.

Wieczorek, A., Downey, C.D., Dallmann, H.G., and McHenry, C.S. (2010). Only one ATP-binding DnaX subunit is required for initiation complex formation by the *Escherichia coli* DNA polymerase III holoenzyme. *The Journal of Biological Chemistry* *285*, 29049–29053.

Wieczorek, A., and McHenry, C.S. (2006). The NH₂-terminal php domain of the alpha subunit of the *Escherichia coli* replicase binds the epsilon proofreading subunit. *The Journal of Biological Chemistry* *281*, 12561–12567.

Williams, K.R., Spicer, E.K., LoPresti, M.B., Guggenheimer, R.A., and Chase, J.W. (1983). Limited proteolysis studies on the *Escherichia coli* single-stranded DNA binding protein. Evidence for a functionally homologous domain in both the *Escherichia coli* and T4 DNA binding proteins. *The Journal of Biological Chemistry* *258*, 3346–3355.

Wing, R. a, Bailey, S., and Steitz, T. a (2008a). Insights into the replisome from the structure of a ternary complex of the DNA polymerase III alpha-subunit. *Journal of Molecular Biology* *382*, 859–869.

Wing, R.A., Bailey, S., and Steitz, T.A. (2008b). Insights into the replisome from the structure of a ternary complex of the DNA polymerase III α -subunit. *Journal of Molecular Biology* *382*, 859–869.

Witte, G., Claus, U., and Curth, U. (2003). DNA polymerase III chi subunit ties single-stranded DNA binding protein to the bacterial replication machinery. *Nucleic Acids Research* *31*, 4434–4440.

Witte, G., Urbanke, C., and Curth, U. (2005). Single-stranded DNA-binding protein of *Deinococcus radiodurans*: a biophysical characterization. *Nucleic Acids Research* *33*, 1662–1670.

Wu, C.A., Zechner, E.L., Reemsll, J.A., Mchenryll, C.S., and Marian, K.J. (1992). Coordinated leading- and lagging-strand synthesis at the *Escherichia coli* DNA replication fork (V). *The Journal of Biological Chemistry* *267*, 4074–4083.

Xi, J., Zhuang, Z., Zhang, Z., Selzer, T., Spiering, M.M., Hammes, G.G., and Benkovic, S.J. (2005). Interaction between the T4 helicase-loading protein (gp59) and the DNA polymerase (gp43): a locking mechanism to delay replication during replisome assembly. *Biochemistry* *44*, 2305–2318.

Xu, L., and Marians, K.J. (2003). PriA mediates DNA replication pathway choice at recombination intermediates. *Molecular Cell* *11*, 817–826.

Yamaguchi, K., and Yamaguchi, M. The replication origin of pSC101: the nucleotide sequence and replication functions of the ori region. *Gene* *29*, 211–219.

Yang, C., Curth, U., Urbanke, C., and Kang, C. (1997). Crystal structure of human mitochondrial single-stranded DNA binding protein at 2.4 Å resolution. *Nature Structural Biology* 4, 153–157.

Yang, J., Nelson, S.W., and Benkovic, S.J. (2006). The control mechanism for lagging strand polymerase recycling during bacteriophage T4 DNA replication. *Molecular Cell* 21, 153–164.

Yang, J., Trakselis, M. a, Roccasacca, R.M., and Benkovic, S.J. (2003). The application of a minicircle substrate in the study of the coordinated T4 DNA replication. *The Journal of Biological Chemistry* 278, 49828–49838.

Yao, N., Hurwitz, J., and O'Donnell, M. (2000). Dynamics of beta and proliferating cell nuclear antigen sliding clamps in traversing DNA secondary structure. *The Journal of Biological Chemistry* 275, 1421–1432.

Yuan, Q., and McHenry, C.S. (2009). Strand displacement by DNA polymerase III occurs through a tau-psi-chi link to single-stranded DNA-binding protein coating the lagging strand template. *The Journal of Biological Chemistry* 284, 31672–31679.

Yuzhakov, a, Kelman, Z., and O'Donnell, M. (1999). Trading places on DNA--a three-point switch underlies primer handoff from primase to the replicative DNA polymerase. *Cell* 96, 153–163.

Zechner, E.L., Wu, C.A., and Marians, K.J. (1992a). Coordinated leading- and lagging-strand synthesis at the *Escherichia coli* DNA replication fork (II). *The Journal of Biological Chemistry*.

Zechner, E.L., Wu, C.A., and Marians, K.J. (1992b). Coordinated leading- and lagging-strand synthesis at the *Escherichia coli* DNA replication fork. II. Frequency of primer synthesis and efficiency of primer utilization control Okazaki fragment size. *The Journal of Biological Chemistry* 267, 4045–4053.

Zechners, E.L., Wu, C.A., and Marianssb, K.J. (1992). Coordinated leading- and lagging-strand synthesis at the *Escherichia coli* DNA replication fork (III). *The Journal of Biological Chemistry* 4054–4063.

Zhou, R., Kozlov, A.G., Roy, R., Zhang, J., Korolev, S., Lohman, T.M., and Ha, T. (2011). SSB Functions as a Sliding Platform that Migrates on DNA via Reptation. *Cell* 146, 222–232.

APPENDIX 1

Supplemental material for Chapter III

Cycling of the *E. coli* Lagging Strand Polymerase is Triggered Exclusively by the Availability of a New Primer at the Replication Fork

S1.1 Supplemental Results

S1.1.1 Establishing a coupled rolling circle replication system on a mini-circle template

In order to establish a coupled rolling circle replication system, all protein components required for *E. coli* rolling circle reactions were titrated in the presence of 1, 10, or 20 nM mini-circle DNA templates (Figure S1.1, S1.2, S1.3). Titration began with PriA, because it eliminated an unfavorable background originating from Pol III HE's strand displacement activity (Xu and Marians, 2003; Yuan and McHenry, 2009). First, a level of PriA was determined that blocked the strand displacement activity of Pol III HE in reactions performed in the absence of DnaB₆ (Figure S1.1-3A). When the selected level of PriA was used in the presence of DnaB₆, partial inhibition was observed at lower template concentrations, presumably because of blocking a DnaB₆-independent background reaction (Figure S1.1B, S1.2B). Then DnaG, PriB₂, DnaT₃, β_2 , and SSB₄ were titrated and the optimal level selected for further experiments (Figure S1.1-3 C-G). Once a concentration of a component was selected, that concentration was used in subsequent titrations of other components. Since the optimal concentration of the DnaC helicase loader varies depending on the

DnaB₆ concentration, DnaC was titrated against various concentrations of DnaB₆ (Figure S1.1-3 H-J). In reactions containing 10 and 20 nM templates, a substoichiometric level of DnaB₆ was selected for further experiments. Pol III* was titrated last (Figure S1.1-3K). Again, a substoichiometric level was selected for further experiments with the 10 and 20 nM templates. At the lowest (1 nM) template concentration, it was not possible to obtain adequate synthesis with substoichiometric helicase and Pol III*.

For 20 nM mini-circle DNA templates, the optimized concentrations of components were 0.5 μ M SSB₄, 2.5 nM Pol III*, 100 nM β_2 , 160 nM PriA, 50 nM PriB₂, 333 nM DnaT₃, 12 nM DnaB₆, 108 nM DnaC, and 25 nM DnaG (Figure S1.3). For 10 nM mini-circle DNA templates, the optimized concentrations of components were 0.13 μ M SSB₄, 1.25 nM Pol III*, 50 nM β_2 , 65 nM PriA, 50 nM PriB₂, 333 nM DnaT₃, 6 nM DnaB₆, 100 nM DnaC, and 17 nM DnaG (Figure S1.2). For 1 nM mini-circle DNA template, 0.25 μ M SSB₄, 2.5 nM Pol III*, 25 nM β_2 , 20 nM PriA, 50 nM PriB₂, 333 nM DnaT₃, 6 nM DnaB₆, 72 nM DnaC, and 17 nM DnaG were selected. However, Pol III* and DnaB₆ were required in excess of a molar ratio to DNA to obtain adequate synthesis (Figure S1.1).

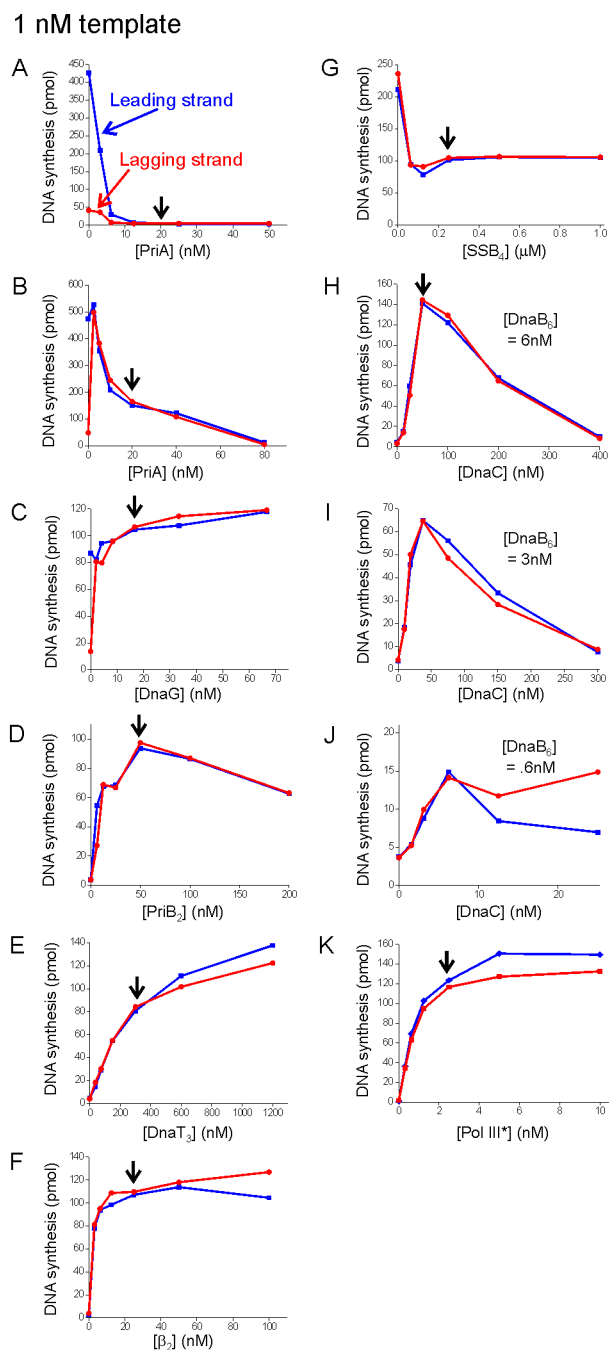


Figure S1.1 Protein requirements for *E. coli* rolling circle reactions on 1 nM mini-circle DNA template.

(A) Titration with PriA in the absence of DnaB₆. 0.25 μ M SSB₄, 25 nM β_2 , 2.5 nM Pol III*, 50 nM PriB₂, 300 nM DnaT₃, 100 nM DnaC, and 50 nM DnaG and varying amounts of PriA were incubated with 1 nM mini-circle template, 0.2 mM UTP, 0.2 mM CTP, 0.2 mM GTP, 1.2 mM ATP, 100 μ M dNTPs, and α -[³²P] dCTP or dGTP (2000 cpm/pmol) at 30°C in 25 μ l. The reaction buffer was 10 mM magnesium acetate, 70 mM KCl, 50 mM Hepes (pH 7.5), 100 mM potassium glutamate, 20 % glycerol, 200 μ g/ml bovine serum albumin, 0.02% Nonidet P-40,

and 10 mM dithiothreitol. Reaction was terminated by addition of EDTA to 20 mM final concentration after 19 min. Black arrows indicate the concentrations chosen for the subsequent titrations in all titrations.

(B) Titration with PriA in the presence of DnaB₆. Reactions were conducted as in panel A except 6 nM DnaB₆ was added with other protein components.

(C) Titration with DnaG. Reactions were conducted as in panel B except 20 nM PriA was used.

(D) Titration with PriB₂. Reactions were conducted as in panel C except 17 nM DnaG was used.

(E) Titration with DnaT₃. Reactions were conducted as in panel D except 50 nM PriB₂ was used.

(F) Titration with β₂. Reactions were conducted as in panel E except 333 nM DnaT₃ was used.

(G) Titration with SSB₄. Reactions were conducted as in panel F except 25 nM β₂ was used.

(H) Titration with DnaC in the presence of 6 nM DnaB₆. Reactions were conducted as in panel G except 250 nM SSB₄ and 6 nM DnaB₆ were used.

(I) Titration with DnaC in the presence of 3 nM DnaB₆. Reactions were conducted as in panel G except 250 nM SSB₄ and 3 nM DnaB₆ were used.

(J) Titration with DnaC in the presence of 0.6 nM DnaB₆. Reactions were conducted as in panel G except 250 nM SSB₄ and 0.6 nM DnaB₆ were used.

(K) Titration with Pol III*. Reactions were conducted as in panel H except 72 nM DnaC and 6 nM DnaB₆ were used.

10 nM template

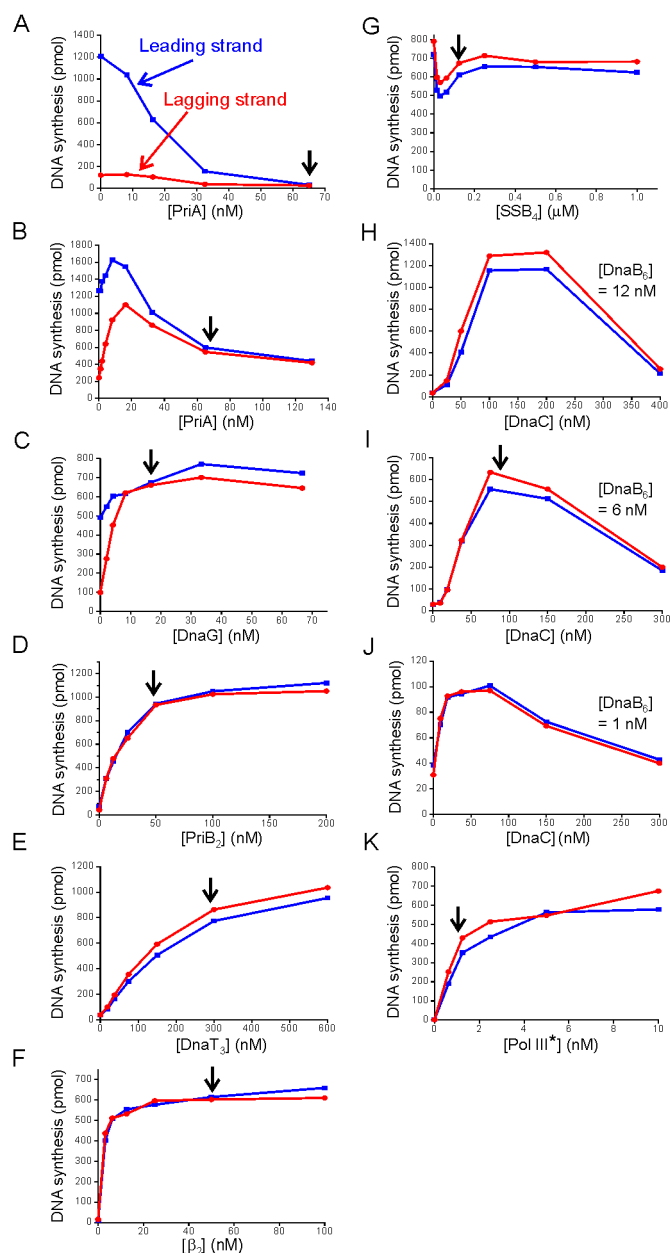


Figure S1.2 Protein requirements for *E. coli* rolling circle reactions on 10 nM mini-circle DNA template.

(A) Titration with PriA in the absence of DnaB₆. Reactions were conducted as described under the legend to Figure S1A except that the initial concentrations of protein components were 0.5 μM SSB₄, 50 nM β_2 , 10 nM Pol III*, 50 nM PriB₂, 300 nM DnaT₃, 100 nM DnaC, and 33.3 nM DnaG, and reactions were terminated after 12 min.

(B) Titration with PriA in the presence of 6 nM DnaB₆. Reactions were conducted as in panel A except 6 nM DnaB₆ was added with other protein components.

(C) Titration with DnaG. Reactions were conducted as in panel B except 65 nM PriA was used.

- (D) Titration with PriB₂. Reactions were conducted as in panel C except 17 nM DnaG was used.
- (E) Titration with DnaT₃. Reactions were conducted as in panel D except 50 nM PriB₂ was used.
- (F) Titration with β_2 . Reactions were conducted as in panel E except 333 nM DnaT₃ was used.
- (G) Titration with SSB₄. Reactions were conducted as in panel F except 50 nM β_2 was used.
- (H) Titration with DnaC in the presence of 12 nM DnaB₆. Reactions were conducted as in panel G except 130 nM SSB₄ and 12 nM DnaB₆ was used.
- (I) Titration with DnaC in the presence of 6 nM DnaB₆. Reactions were conducted as in panel G except 130 nM SSB₄ and 6 nM DnaB₆ was used.
- (J) Titration with DnaC in the presence of 1 nM DnaB₆. Reactions were conducted as in panel G except 130 nM SSB₄ and 1 nM DnaB₆ was used.
- (K) Titration with Pol III*. Reactions were conducted as in panel I except 100 nM DnaC and 6 nM DnaB₆ was used.

20 nM template

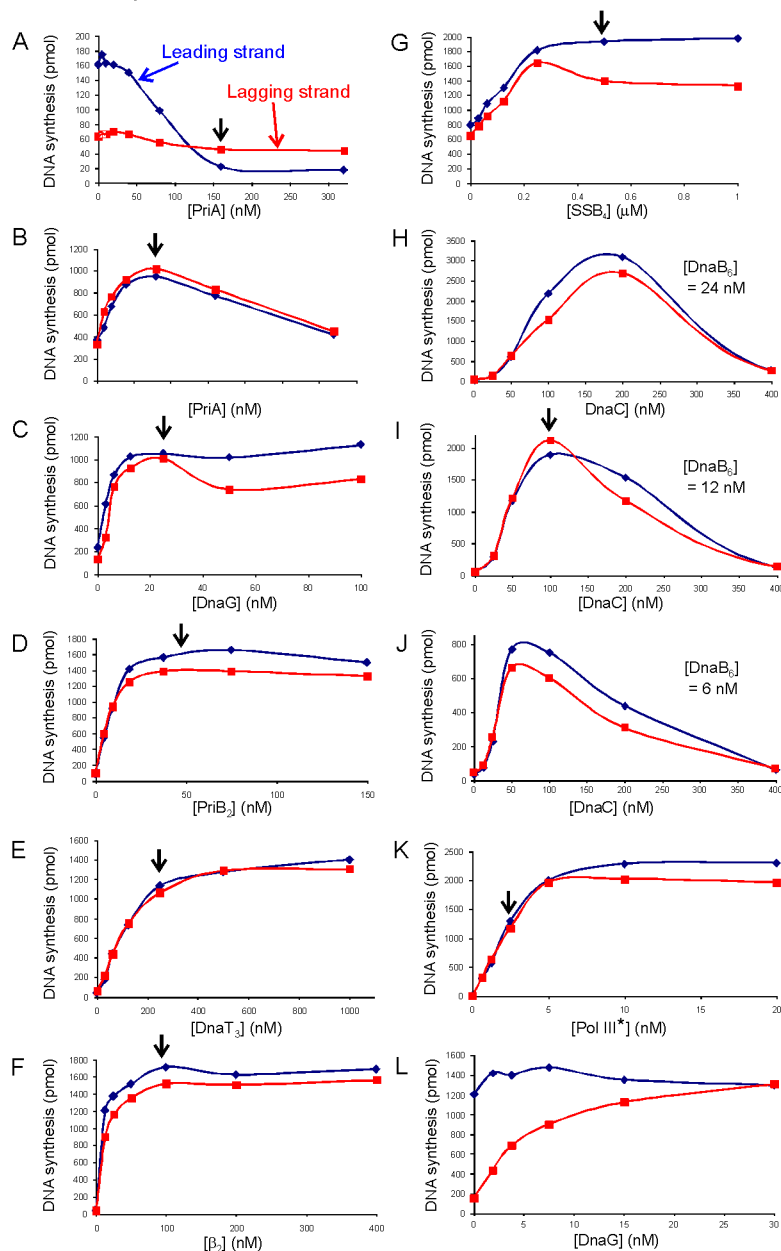


Figure S1.3 Protein requirements for *E. coli* rolling circle reactions on 20 nM mini-circle DNA template.

(A) Titration with PriA in the absence of DnaB₆. Reactions were conducted as described under the legend to Figure S1A except that the initial concentrations of protein components were 0.13 μ M SSB₄, 50 nM β_2 , 5 nM Pol III*, 50 nM PriB₂, 333 nM DnaT₃, 12 nM DnaB₆, 78 nM DnaC, and 50 nM DnaG, and reactions were terminated after 12 min.

(B) Titration with PriA in the presence of 12 nM DnaB₆. Reactions were conducted as in panel A except 12 nM DnaB₆ was added with other protein components.

(C) Titration with DnaG. Reactions were conducted as in panel B except 160 nM PriA was used.

(D) Titration with PriB₂. Reactions were conducted as in panel C except 25 nM DnaG was used.

(E) Titration with DnaT₃. Reactions were conducted as in panel D except 12 nM PriB₂ was used.

(F) Titration with β_2 . Reactions were conducted as in panel E except 333 nM DnaT₃ was used.

(G) Titration with SSB₄. Reactions were conducted as in panel F except 100 nM β_2 was used.

(H) Titration with DnaC in the presence of 24 nM DnaB₆. Reactions were conducted as in panel G except 500 nM SSB₄ and 24 nM DnaB₆ was used.

(I) Titration with DnaC in the presence of 12 nM DnaB₆. Reactions were conducted as in panel G except 500 nM SSB₄ and 12 nM DnaB₆ was used.

(J) Titration with DnaC in the presence of 6 nM DnaB₆. Reactions were conducted as in panel G except 500 nM SSB₄ and 6 nM DnaB₆ was used.

(K) Titration with Pol III*. Reactions were conducted as in panel I except 108 nM DnaC and 12 nM DnaB₆ was used.

(L) Titration with DnaG. Reactions were conducted as in panel K except 2.5 nM Pol III* was used. Note that the dependency on DnaG for leading strand synthesis observed under suboptimal conditions (panel C) is no longer observed under the fully optimized conditions represented in this panel.

S1.1.2 Preincubation of reaction components minimizes the lag phase and permits synchronization of the rolling circle reaction

Simply mixing all components together leads to a rolling circle reaction with a lag phase at the beginning due to unsynchronized DNA synthesis. To minimize this problem, a pre-initiation complex of all protein components was assembled on the template in the presence of ATP γ S, CTP, GTP, and UTP. Omitting ATP from the pre-incubation stage ensures that helicase can be loaded but not translocated. Once dNTPs and ATP were added, synthesis of each strand initiates with a reduced lag phase (Figure S1.4). 5 μ M ATP γ S was required for reactions containing 20 nM and 10 nM templates with the pre-

incubation time of 5 and 11 min, respectively. 10 μM $\text{ATP}\gamma\text{S}$ was required for reactions containing 1 nM template with 17 min incubation time.

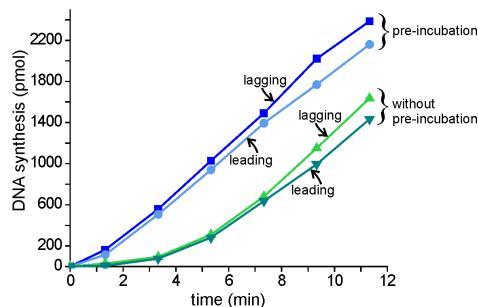


Figure S1.4 Preincubation of reaction components in the presence of $\text{ATP}\gamma\text{S}$ supports formation of a preinitiation complex and elimination of a lag phase. The data shown was obtained using 20 nM template.

S1.1.3 Increasing concentrations of ddGTP result in decreased levels of radioactive nucleotide incorporation in the lagging strand, but permit maintenance of linear synthesis rates

As the concentration of ddGTP is increased beyond the level shown in Figure 3.2C in Chapter III, the level of incorporation of dNTPs in the lagging strand product decreases (Figure S1.5). This is, in part, the result of the synthesis of shorter Okazaki fragments (Figure 1.2A). But, there is a reduction of the overall molar level of Okazaki fragment synthesis, indicating some level of perturbation.

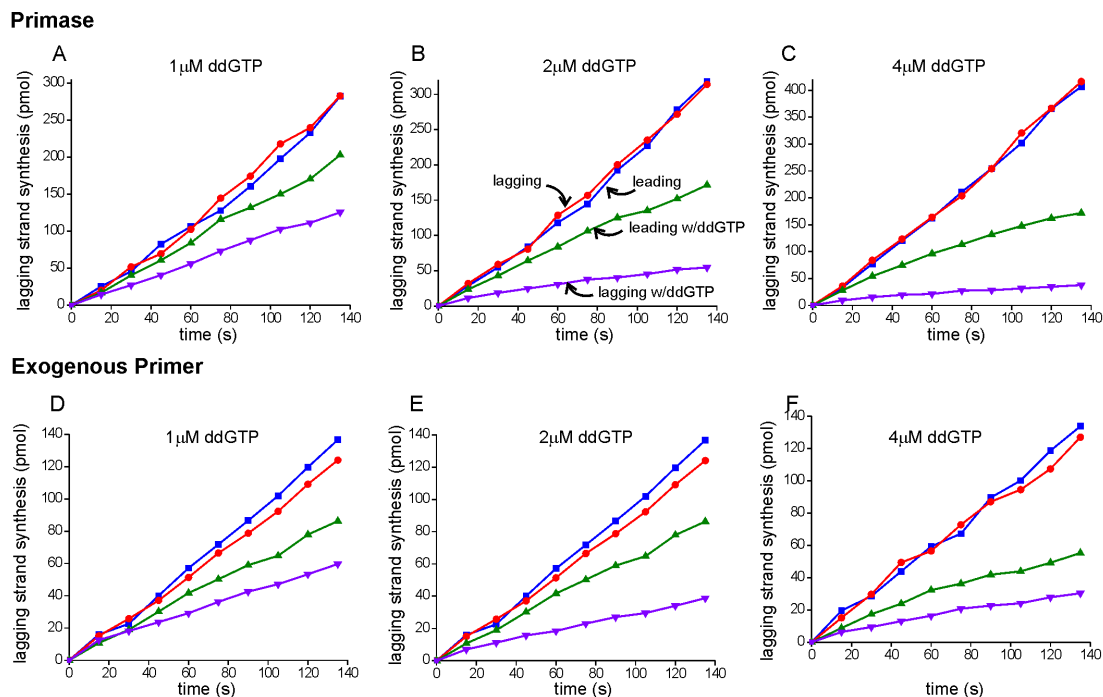


Figure S1.5 A linear rate of Okazaki fragment synthesis is maintained as the concentration of ddGTP increases.

(A-C) Reactions were performed under conditions of the optimized rolling circle reaction with 1, 2, and 4 μ M ddGTP added at the same time as radiolabeled nucleotide. The amount of leading and lagging strand synthesis in the absence (leading-blue; lagging-red) and presence (leading-green; lagging-purple) of ddGTP was quantified.

(D-F) The same experiments as A-C were performed except 120 nM exogenous synthetic 15-mer primers (TGATAGGGGGTATGG) replaced primase, GTP, UTP and CTP.

S1.1.4 dGDPNP displays a higher apparent K_m for the DNA polymerase III holoenzyme-catalyzed reaction and can be used to modulate the elongation rate

The DNA Pol III HE incorporates dGDPNP with a 20-fold higher apparent K_m than dGTP (Figure S1.6A,B). The K_m for dGDPNP (40 μ M) is sufficiently high that reactions can be conducted at sub- K_m concentrations without danger of depleting nucleotides. This allowed modulation of the rate of elongation on

cytosine-containing templates and allowed us to selectively slow the rate of lagging strand synthesis when templates with an asymmetric G:C distribution were used. The measured K_m is an estimate and expressed as an apparent value, because the reaction kinetics monitored included both initiation complex formation and elongation stages.

On a template containing approximately 25% C, the rate of elongation in the presence of near-saturating dGDPNP was reduced to 57 nt/s, 10-fold slower than the 570 nt/s measured in the presence of saturating dGTP (Figure S1.6C). Thus, dGDPNP may also be slowing the chemistry step of the reaction sufficiently that it becomes rate-limiting. Decreasing dGDPNP to a level of 0.75 K_m decreased the observed elongation rate about 25-fold. In contrast, the rate of leading strand elongation on a mini-circle template containing only two G residues is not slowed significantly (Figure S1.6D).

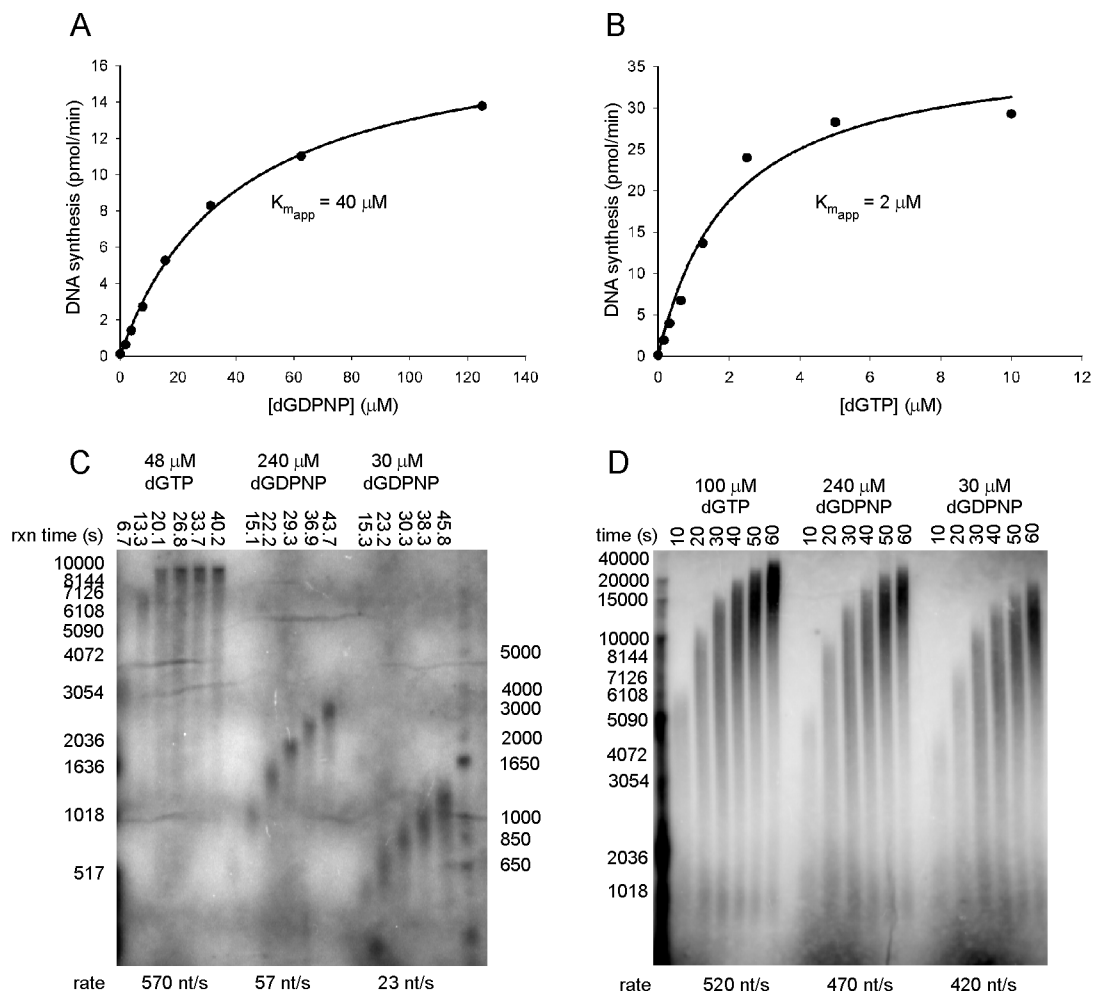


Figure S1.6 dGDPNP can be used to modulate the rate of elongation on cytosine-containing templates.

(A,B) The apparent K_m for dGTP and dGDPNP, are 40 μM and 2 μM , respectively. Reactions containing 0.6 μM SSB₄, 15 nM β_2 , 10 nM Pol III*, and 2.3 nM primed M13Gori DNA (Glover and McHenry, 2001), 100 μM ATP, 18 μM dTTP, 48 μM dATP, 48 μM dCTP, ³H-dTTP (760 cpm/pmol) and varying amounts of dGTP or dGDPNP were incubated at 30°C for 2 min (dGTP) or 5 min (dGDPNP). dNTP incorporation was determined by scintillation counting. The titration curves were fit to the Michaelis-Menton equation, $v = v_{max}[S]/(K_m + [S])$, by SigmaPlot's nonlinear regression. [S] was the concentration of dGTPs or dGDPNPs, and v was the rate of dNTP incorporation.

(C) Elongation rate on the primed M13Gori DNA template in the presence of indicated amount of dGTP or dGDPNP. Reactions were monitored on a 0.9% alkaline agarose gel. Products with dGTP at 6.7 s, 13.3 s, and 20.1 s and products with dGDPNP at all time points were used to determine the elongation rate.

(D) Rate of leading strand synthesis at 20 mM mini-circle templates in the presence of indicated amount of dGTP or dGDPNP. Time course of the reaction

was monitored on a 0.5% alkaline agarose gel, and products taken at 10 s, 20 s, and 30 s were used to determine the rate of leading strand synthesis.

S1.1.5 dGDPNP does not severely perturb the processivity of Pol III*

In order to eliminate the possibility that the shortened Okazaki fragments arise from the decreased processivity of Pol III* on the lagging strand due to dGDPNP, processivity of Pol III* was measured on primed ssDNA circular template. In the presence of dGTP and dGDPNP, the processivity was 2700 bp and 1600 bp, respectively. Although the processivity decreased, it was still longer than the shortest Okazaki fragment product (820 bp). Thus, the shortened product is not likely to result from the processivity. It has been measured that the dissociation rate of Pol III* on the Okazaki fragment with dideoxynucleotide as the last nucleotide was 10 min (Dohrmann et al., 2011), which indicated that Pol III* was very stable on the Okazaki fragment in the presence of the dNTP analog. In addition, due to some secondary structures, Pol III* paused at certain sites on the template, which caused the processivity to be underestimated to some extent (Figure S1.7).

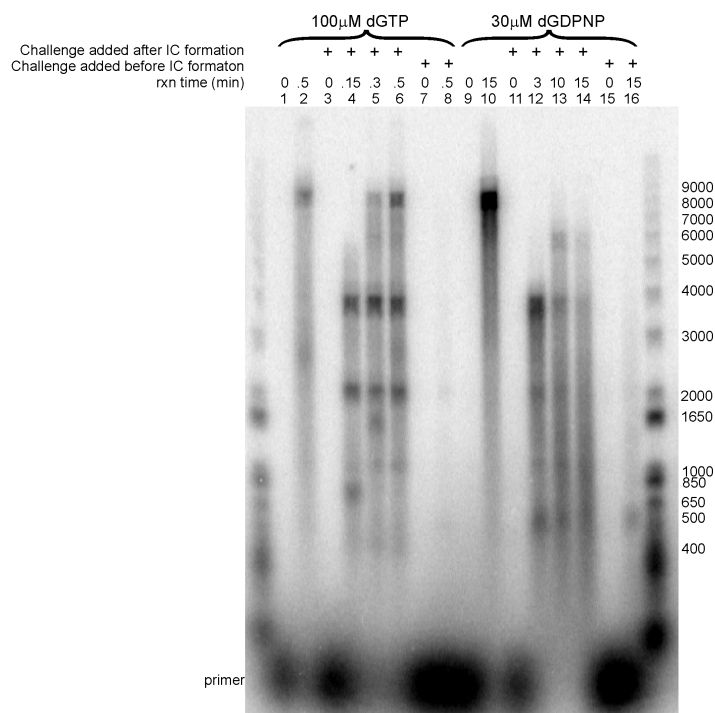


Figure S1.7 The processivity of Pol III* is about 2700 bp in the presence of dGTP and 1600 bp in the presence of dGDPNP.

The processivity of Pol III* was determined on an M13Gori template in the presence of dGTP (lane 1-8) and dGDPNP (lane 9-16). 1 nM M13Gori template annealed with 5'-³²P-labeled 30 mer (5' ATA ACG TGC TTT CCT CGT TGG AAT CAG AGC), 3 nM Pol III*, 10 nM β_2 , 800 nM SSB₄, 100 μ M ATP, 100 μ M dCTP, dATP, and dTTP were assembled to form the initiation complex for 3 min at 30°C. Then 100 μ M dGTP or 30 μ M dGDPNP was added to initiate the reaction. Where indicated 0.6 mg/ml of activated calf thymus DNA was added together with dGTP or dGDPNP to prevent reinitiation of elongation once polymerase dissociated. In control reactions (lane 7,8,15,16) calf thymus DNA was added before initiation complex formation to demonstrate the efficacy of the challenge. At indicated time points, 25 μ l reactions were stopped by addition of an equal volume of stop mix, subjected to digestion with protease K (25 μ g/ml, 30 min), and precipitated by the addition of 5.5 μ l of 3 M sodium acetate and 130 μ l of ethanol. The pellet was dissolved in 20 μ l (10% v/v glycerol, 50 mM NaOH, 1 mM EDTA, and 0.1% w/v bromocresol green) and loaded onto 0.8% alkaline agarose gels containing 5 mM NaOH and 1 mM EDTA in a running buffer of 50 mM NaOH and 2 mM EDTA. Average processivity of Pol III* in the presence of dGTP and dGDPNP was determined as describe in (Yuan and McHenry, 2009) using lane 5 and 6, and lane 13 and 14, respectively. Density between 400-10,000 nt was quantified. Analysis was complicated by major pause sites at 2000, 3800, and 5900 bp. Lane 1 and 9 contain unannealed radioactive labeled primer.

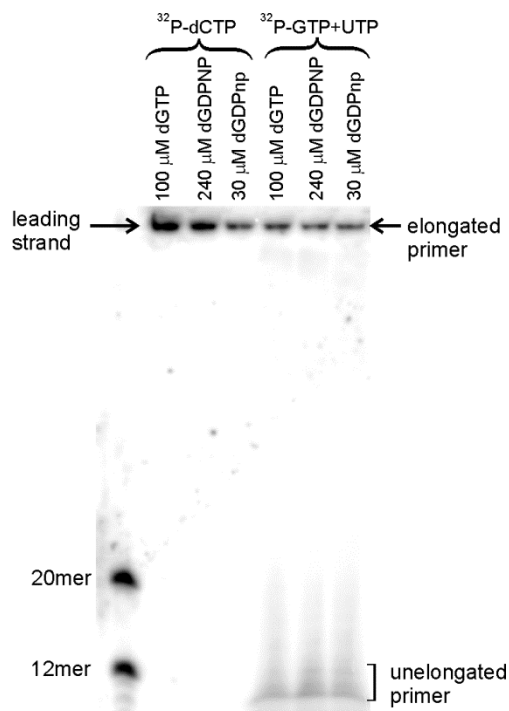


Figure S1.8 dGDPNP does not perturb the frequency of primer synthesis or the primer utilization.

Two identical sets of optimized rolling circle reactions with 20 mM templates were carried out in the presence of dGTP or dGDPNP, except the reactions were stopped at 10 min after the addition of α -[^{32}P] dCTP or dGTP. α -[^{32}P] dCTP (ca. 350 cpm/pmol) was employed in the left set to reveal leading strand products, and α -[^{32}P] GTP and UTP (ca. 12,000 cpm/pmol) in the right set to indicate RNA primers.

S1.2 Supplemental Materials and Methods

Buffers:

All reactions on mini-circle templates were conducted with buffer containing 10 mM magnesium acetate, 20 mM NaCl, 50 mM Hepes (pH 7.5), 100 mM potassium glutamate, 20% glycerol, 200 $\mu\text{g/ml}$ bovine serum albumin, 0.02% Nonidet P-40, and 10 mM dithiothreitol (DTT). Buffer T contains 50 mM Tris (pH 7.5), 10% glycerol, 0.5 mM EDTA, and 5 mM DTT. Buffer B contains 50 mM Tris

(pH 8), 20% glycerol, 1 mM EDTA, 5 mM DTT, and 0.01% NP-40. Buffer C contains 50 mM Tris (pH 8), 10% glycerol, 1 mM EDTA, 5 mM DTT, 0.01% NP-40, and 50 mM NaCl. Buffer A contains 50 mM Tris (pH 7.5), 20% glycerol, and 5 mM DTT. Buffer F contains 50 mM HEPES (pH 7.5), 100 mM NaCl, 10% glycerol, 0.25 mM EDTA, 0.01% NP-40, and 5 mM DTT. Stop mix used for stopping DNA replication reactions contained 40 mM Tris (pH 8), 0.2% SDS, 100 mM EDTA, and 50 μ g/ml proteinase K.

Mini-circle DNA template preparation:

The fragment containing linear mini-circle DNA was amplified by running 4000 x 100 μ l PCR reactions containing 100 ng of plasmid pBsRC3 DNA (Sanders et al., 2010), 2 μ M each of forward primer (5'Biotin-TGT GGA ATT GTG AGC GGA TA) and reverse primer (5'Biotin-GTT TTC CCA GTC ACG ACG TT), 200 μ M dNTPs, and 2.4 U of *Pfu* polymerase (Source). (One unit is defined as the amount of enzyme required to catalyze the incorporation of 10 nmol of dNTPs into acid-insoluble material in 30 minutes at 75°C). The PCR reaction was performed at 94°C for 3 min, followed by 30 cycles at 94°C for 25 s, 60°C for 15 s, and 72°C for 30 s, and an extra 10 min at 72°C at the end. 1.5% agarose gel showed that more than 95% amplified products were the target DNA (Figure S1.9A lane 1, Figure S1.10 step 1). The PCR product (80 mg) was extracted with one volume of phenol/chloroform/isoamyl alcohol (25: 24:1) and one volume of chloroform, and precipitated by the addition of 0.5 volumes of 5 M ammonium acetate and 1.5 volumes of isopropyl alcohol. The pellet was washed with 70%

ethanol and dissolved in 10 mM Tris-HCl buffer (pH 8) to 1 $\mu\text{g}/\mu\text{l}$. The purified PCR product (40 mg) was digested with *EcoRI* (666 U/mg DNA) at 37°C for 9 h, and the digestion was stopped by heating at 65°C for 40 min. Digestion was >90% completed (Figure S1.9A lane 2, Figure S1.10 step 2a). The linear mini-circle DNA was separated from biotin-containing terminal fragments created by *EcoRI* digestion by passing the digested DNA over a high capacity streptavidin resin (Pierce, 10 ml). 1.5% agarose gel showed that more than 95% product was the linear mini-circle DNA (Figure S1.9B lane 2, Figure S1.10 step 2b). The purified linear DNA (27 mg) was diluted to 2.5 $\mu\text{g}/\text{ml}$ and ligated using ligase (0.4 U/ml DNA solution, Epicentre), in 33 mM Tris-acetate (pH 7.8), 66 mM potassium acetate, 10 mM magnesium acetate, 5 mM DTT, and 1 mM ATP at 16°C for 20 h (Figure S1.9C lane 2, S1.8 step 3a). The unligated fragment and linear multi-ligated product were digested completely from both 3' and 5' ends by the combination of lambda exonuclease (0.3 U/ml ligation mixture), exonuclease I (0.3 U/ml ligation mixture), and exonuclease III (1 U/ml ligation mixture) at 37°C for 8 h. All enzymes were thermally inactivated at 80°C for 20 min. 2% agarose gel showed that more than 90% of product was the ligated mini-circle DNA (Figure S1.9C lane 3, Figure S1.10 step 3b). NaCl was added to the ligation reaction mixture to 0.5 M final concentration. Then the ligated mini-circle DNA was loaded onto three QIAGEN-tip 10000 columns. The column was washed with Qiagen Buffer QC and the DNA eluted with Qiagen Buffer QF. DNA was precipitated by adding 0.7 volumes of isopropanol, washed with 70% ethanol, and dissolved in TE buffer to 1 $\mu\text{g}/\mu\text{l}$ (Figure S1.10 step 3c). The purified product

(7 mg) was nicked at the single recognition site with Nt. BstNBI nicking enzyme (2 U/ μ g DNA) at 55°C for 3 h. Nt. BstNBI was thermally inactivated at 80°C for 30 min (Figure S1.10 step 4). The nicked DNA was incubated with Vent polymerase (0.75 U/ μ g DNA) and 300 μ M dATP, dCTP, and dTTP at 75°C for 2 h to form a 394-bp-long DNA flap (5). EDTA was added to a final concentration of 25 mM. The tailed DNA was purified by phenol chloroform extraction and isopropyl alcohol purification as described above. 2% agarose gel electrophoresis indicated a yield > 80% (Figure S1.9D lane 2, Figure S1.10 step 5).

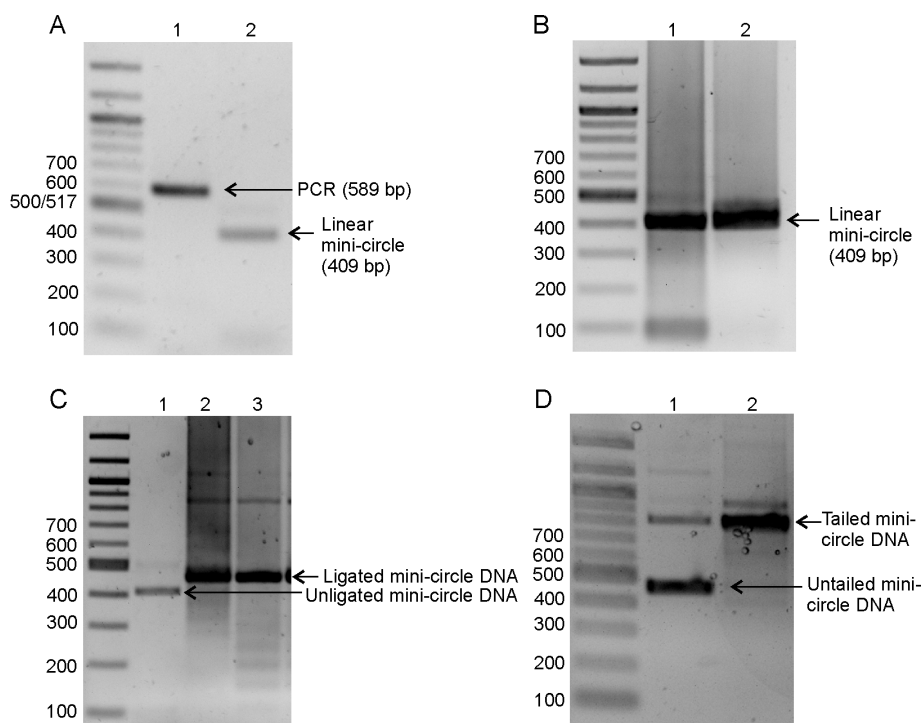


Figure S1.9 Important intermediate products and final product of mini-circle template preparation.

(A) Lane 1: The PCR product (589 bp); Lane 2: EcoRI digested products. The band of 409 bp is the linear fragment.

(B) Lane 1: EcoRI digested products; Lane 2: Linear mini-circle fragment (409 bp) after Straptavidin purification.

(C) Lane 1: Purified unligated linear mini-circle fragment; Lane 2: Ligated mini-circle DNA; Lane 3: Ligated mini-circle DNA after exonuclease clean up. (d) Lane 1: Purified untailed circular mini-circle fragment; Lane 2: tailed mini-circle DNA template after purification.

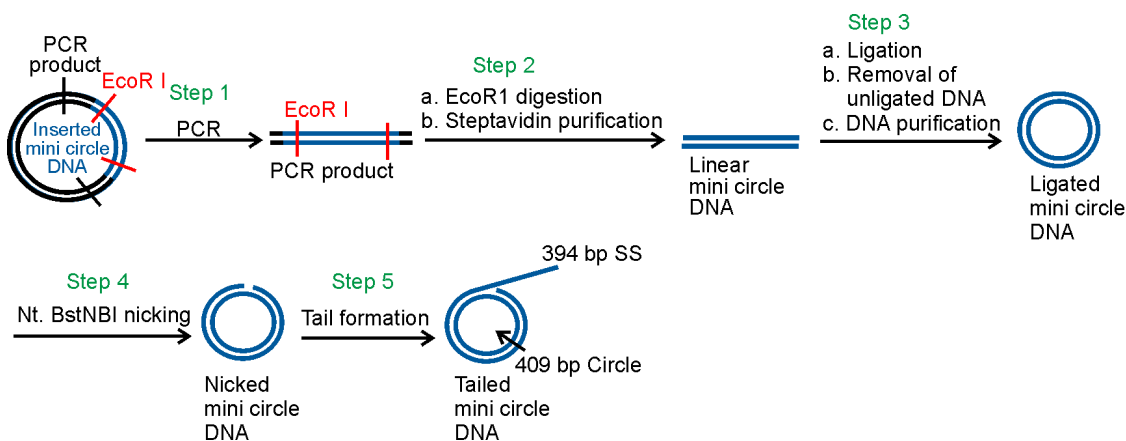


Figure S1.10 Preparation of mini-circle DNA template.

Protein Purifications:

Cells were grown in a 250 l fermentor in F-medium (Kim and McHenry, 1996) supplemented with 1% glucose at 37°C in the presence of ampicillin (100 mg/l for PriA, DnaT and Pol III*, 200 mg/l for PriB, 50 mg/l for DnaC) and chloramphenicol (25 mg/l for PriA, PriB, and DnaT, 10 mg/l for DnaC). When $OD_{600}=0.5-0.6$, IPTG was added to 1 mM. Another 100 mg/l ampicillin was added at induction for PriA and DnaT, and 200 mg/l ampicillin was added at induction and 1 h post-induction for PriB. For Pol III*, when $OD_{600}=0.83$, 200 mg/l ampicillin was added and additional 200 mg/l ampicillin was added at 2 h post-induction. Cells expressing PriA and PriB were harvested after 2 h of induction, and cells

expressing DnaT, DnaC, and Pol III* after 3 h of induction. Harvested cells were lysed to form Fr I (Cull and McHenry, 1995). Proteins were precipitated with indicated concentrations of ammonium sulfate and centrifuged at 23,000 g for 60 min. The resuspended pellet was Fr II.

PriA and other primosomal proteins were performed by modifications of published procedures (Marians, 1995). Fr II was prepared by addition of ammonium sulfate to 50% saturation to Fr I (generated from 50 g cells). The pellet was resuspended in Buffer T to conductivity equivalent to that of Buffer T+100 mM NaCl. The solution was loaded onto an SP Sepharose column (80 ml) equilibrated with Buffer T+100 mM NaCl. The column was washed with 6 volumes of the same buffer, and proteins were eluted with 10 volumes of Buffer T with a 100 mM-800 mM NaCl gradient. PriA eluted with Buffer T+400 mM and was pooled and precipitated by addition of solid ammonium sulfate to 50% saturation. The pellet was resuspended in 4 ml of Buffer T+150 mM NaCl and 20% glycerol, and loaded onto a Sephacryl 200 column (130 ml) equilibrated with Buffer T+150 mM NaCl. The eluate containing PriA (16 mg) was collected, aliquoted, frozen in liquid N₂, and stored at -80°C.

PriB Fr II was prepared by addition of ammonium sulfate to 50% saturation to Fr I (generated from 40 g cells). The pellet was resuspended in Buffer T and the conductivity of the resulting solution was adjusted to that of Buffer T+200 mM NaCl. The resulting solution was loaded onto an SP Sepharose column (80 ml) equilibrated with Buffer T+100 mM NaCl. The column was washed with 5 volumes of Buffer T+200 mM NaCl, and proteins were eluted with

12.5 volumes of Buffer T with a 200 mM-700 mM NaCl gradient. PriB eluted with Buffer T+330 mM NaCl and was pooled and loaded onto a Heparin Sepharose column (40 ml) equilibrated with Buffer T+200 mM NaCl. The column was washed with 5 volumes of the same buffer, and proteins were eluted with 10 volumes of Buffer T with a 200 mM-700 mM NaCl gradient. PriB eluted in Buffer T+420 mM NaCl and was pooled, diluted with Buffer T to make the conductivity equivalent to that of Buffer T+100 mM NaCl, and loaded onto a Hi-TRAP SP Sepharose XL column (5 ml) as a concentration step. Proteins were step eluted with Buffer T+700 mM NaCl. The concentrated proteins were loaded onto Hi-Load 16/60 Superdex 200 column equilibrated with Buffer T+300 mM NaCl. The eluate containing PriB (40 mg) was collected, aliquoted, frozen in liquid N₂, and stored at -80°C.

DnaT Fr II was prepared by addition of ammonium sulfate to 50% saturation to Fr I (generated from 150 g cells). The pellet was resuspended in Buffer T and the conductivity of the resulting solution was adjusted to that of Buffer T+100 mM NaCl. The resulting solution was loaded onto a Q Sepharose column (70 ml) equilibrated with Buffer T+100 mM NaCl. The column was washed with 6 volumes of Buffer T+100 mM NaCl, and proteins were eluted with 14 volumes of Buffer T with a 100 mM-450 mM NaCl gradient. DnaT eluted in Buffer T+220 mM NaCl and was pooled and loaded onto a Heparin Sepharose column (110 ml) equilibrated with Buffer T+100 mM NaCl. The column was washed with 7 volumes of Buffer T+100 mM NaCl, and proteins were eluted with 12 volumes of Buffer T with a 100 mM-500 mM NaCl gradient. DnaT eluted with

Buffer T+280 mM NaCl was pooled and precipitated by addition of ammonium sulfate to 65% saturation. The pellet was resuspended by 2 ml of Buffer T+150 mM NaCl and 30% glycerol, and loaded onto a Sephacryl 200 column (105 ml) equilibrated with Buffer T+150mM NaCl and 30% glycerol. The eluate containing DnaT (35 mg) was collected, aliquoted, frozen in liquid N₂, and stored at -80°C.

DnaC Fr II was prepared by addition of 0.075% polyethyleneimine and 50% saturated ammonium sulfate to Fr I (generated from 110 g cells). The pellet was resuspended in Buffer B and the conductivity of the resulting solution was similar to that of Buffer B+20 mM NaCl. The resulting solution was loaded onto a Q Sepharose column (210 ml) equilibrated with Buffer B+20 mM NaCl. The column was washed with 3 volumes of Buffer B+20 mM NaCl, and the flow through was collected and loaded onto a phosphocellulose column (40 ml) equilibrated with Buffer B+20 mM NaCl. The column was washed with 3 volumes of Buffer B+20 mM NaCl, and proteins were eluted with 10 volumes of Buffer B with a 20 mM-300 mM NaCl gradient. DnaC eluted with Buffer B+180 mM NaCl was pooled and loaded onto a hydroxyapatite column (11 ml) equilibrated with Buffer B+50 mM NaCl. The column was washed with 6 volumes of Buffer B+50 mM NaCl, and proteins were eluted with 15 volumes of Buffer C with a 0 mM-300 mM ammonium sulfate gradient. DnaC eluted with Buffer C+90 mM ammonium sulfate was pooled and dialyzed against Buffer B+150mM NaCl and 30% glycerol. Purified DnaC (10 mg) was collected, aliquoted, frozen in liquid N₂, and stored at -80°C.

Pol III* Fr II was prepared by addition of ammonium sulfate to 40% saturation to Fr I (generated from 125 g cells). The pellet was resuspended in Buffer A and the conductivity of the resulting solution was adjusted to that of Buffer A+20 mM NaCl. The resulting solution was loaded onto an SP Sepharose column (100 ml) equilibrated with Buffer A+20 mM NaCl. The column was washed with 3 volumes of Buffer A+20 mM NaCl, and proteins were eluted with 10 volumes of Buffer A with a 20 mM-200 mM NaCl gradient. Pol III* eluted with Buffer A+110 mM NaCl and was pooled and precipitated by addition of ammonium sulfate to 55% saturation. The pellet was resuspended by 0.85 ml of Buffer F, and loaded onto a Sephacryl S-300 column (10 ml) equilibrated with Buffer F. The eluate containing Pol III* (3.8 mg) was collected, aliquoted, frozen in liquid N₂, and stored at -80°C.

Concentration of all proteins was measured with a Bradford protein assay and Albumin Standard from Pierce was used (Bradford, 1976).

Filling Gaps between Incomplete Okazaki Fragments:

Gaps between incomplete Okazaki fragments were filled by thermophilic polymerases to minimize issues that might result from secondary structure within gaps. To obtain accurate quantification of gap size, we needed to assure that the polymerase used did not catalyze strand displacement synthesis through the downstream Okazaki fragment. Under the reaction conditions we employed, Pfu catalyzed an unacceptable level of strand displacement synthesis. We pursued additional polymerases and tried Phusion since the supplier (New England

Biolabs) indicated it did not strand displace. We observed moderate strand displacement (<150 nt) above one unit of polymerase per 20 μ l reaction, but not at lower levels (Figure S1.11A). 0.2 U of Phusion was chosen for gap filling of purified products resulting from rolling circle replication.

After the rolling circle product from each 25 μ l reaction was extracted with phenol-chloroform and precipitated with isopropanol, it was incubated with 100 μ M dNTPs, 0.2 U Phusion polymerase, and 32 P-dATP (2 μ Ci/reaction) at 72°C for 15 min. Gap filling products with 0.2 U and 1 U of Phusion were compared side by side, and no difference was found. Thus 0.2 U was chosen. According to the supplier, Phusion extends DNA at a rate of 15-30 s/kb, which is 10 times faster than Pfu. Since 30 min was chosen for gap filling reactions with Pfu (Yang et al., 2006), 15 min should be long enough to fill all gaps with Phusion.

Normalizing the lengths of gap filled Okazaki fragments requires the same specific activity of the radioactive nucleotides as in the original Okazaki fragments with gaps between them. Without addition of radioactivity in the gap filling reaction, the lengths might be biased towards the lower molecular weight. However, we also need to make sure that not too many unused primers are elongated during gap filling, which may obscure the true size of gaps. Therefore, a comparison of gap filling was made in the presence and absence of the same amount of 32 P-dATP as the rolling circle reaction. No significantly different lengths in two conditions were found, which relieved our concerns (Figure S1.11B).

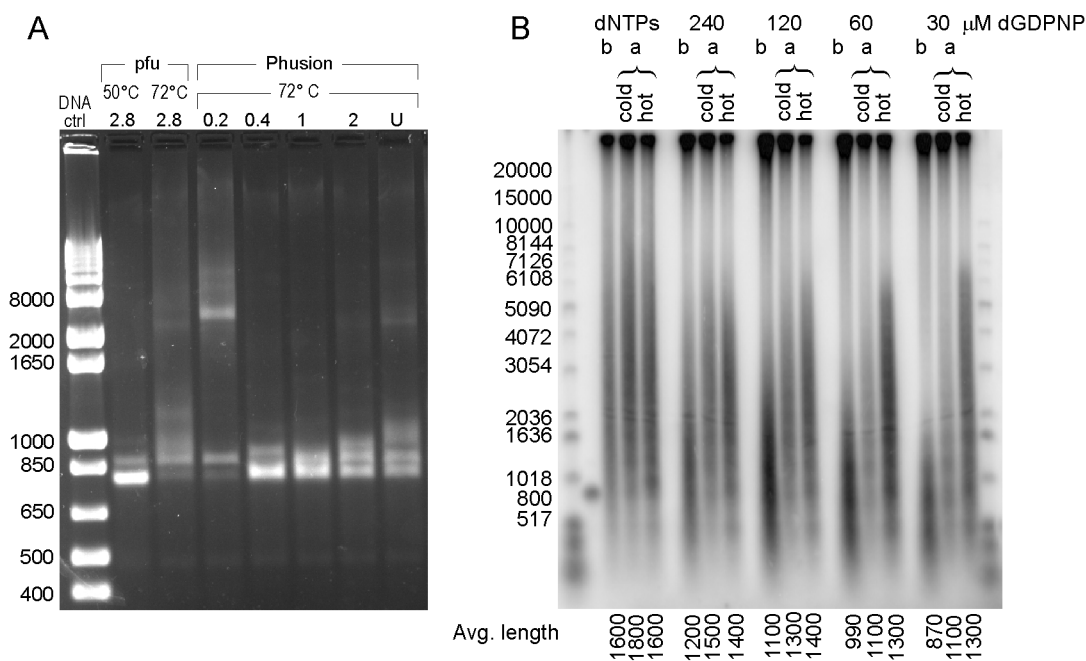


Figure S1.11 Conditions of the gap filling assay were explored.

(A) Strand displacement activity of Pfu (sources) and Phusion polymerase (New England Biolabs) with different conditions. 28 nM minicircle template, 250 μ M dNTPs, and indicated amount of Pfu or Phusion polymerase were incubated in a total of 20 μ l for 30 min at certain temperatures. “DNA ctrl” lane contains the 800 bp long mini-circle template without any polymerase. Products were monitored on an ethidium bromide stained 2% agarose gel.

(B) Adding radioactivity does not affect gap filling products. The first lane labeled as “b” in each panel is the rolling circle reaction product with indicated dGDPNP or dGTP; the second and third lanes labeled as “a” are the gap filling products without (labeled cold) and with (labeled hot) additional 32 P-dATP, respectively.

S1.3 Supplemental References

Bradford, M.M. (1976). A rapid and sensitive method for the quantitation of microgram quantities of protein utilizing the principle of protein-dye binding. *Anal Biochem* 72, 248–254.

Cull, M.G., and McHenry, C.S. (1995). Purification of *Escherichia coli* DNA polymerase III holoenzyme. *Methods in Enzymology* 262, 22–35.

Dohrmann, P.R., Manhart, C.M., Downey, C.D., and McHenry, C.S. (2011). The rate of polymerase release upon filling the gap between Okazaki fragments is inadequate to support cycling during lagging strand synthesis. *Journal of Molecular Biology* 414, 15–27.

Glover, B.P., and McHenry, C.S. (2001). The DNA polymerase III holoenzyme: an asymmetric dimeric replicative complex with leading and lagging strand polymerases. *Cell* 105, 925–934.

Kim, D.R., and McHenry, C.S. (1996). Biotin tagging deletion analysis of domain limits involved in protein-macromolecular interactions. *Biochemistry* 271, 20690–20698.

Marians, K.J. (1995). Phi X174-type primosomal proteins: purification and assay. *Methods in Enzymology* 262, 507–521.

Sanders, G.M., Dallmann, H.G., and McHenry, C.S. (2010). Reconstitution of the *B. subtilis* replisome with 13 proteins including two distinct replicases. *Molecular Cell* 37, 273–281.

Xu, L., and Marians, K.J. (2003). PriA mediates DNA replication pathway choice at recombination intermediates. *Molecular Cell* 11, 817–826.

Yang, J., Nelson, S.W., and Benkovic, S.J. (2006). The control mechanism for lagging strand polymerase recycling during bacteriophage T4 DNA replication. *Molecular Cell* 21, 153–164.

Yuan, Q., and McHenry, C.S. (2009). Strand displacement by DNA polymerase III occurs through a tau-psi-chi link to single-stranded DNA-binding protein coating the lagging strand template. *The Journal of Biological Chemistry* 284, 31672–31679.

APPENDIX 2¹

Supplemental material for Chapter IV

Multiple C-terminal tails within a single *E. coli* SSB homotetramer coordinate
DNA replication and repair²

S2.1 Supplemental Material and Methods

Cloning of Linked SSBs: Using site-directed mutagenesis (QuikChange kit, Agilent Technologies, CA) we inserted three additional restriction sites before the stop codon of the gene (Agel, NheI and KpnI). This version of the protein called *ssb-S₁* has an additional 6 amino acids (TGASGT) coded by the nucleic acid sequence of the three restriction sites. We then cloned three separate copies of the SSB genes (called SSB- β , SSB- γ and SSB- δ) with unique pairs of restriction sites flanking the 5' and 3' regions into a Topo TA vector (Invitrogen, CA). In each of these SSB clones, we removed the stop codons and also included an Agel restriction site at the 3' end of the coding sequence to be able to change the length of the individual linkers if required. SSB- β has a 5' KpnI site and 3' Agel, NcoI and ClaI sites. This step added an additional 6 amino acids (TGPWID) before the stop codon. SSB- γ has a 5' ClaI and 3' Agel, AatII and AvrII restriction sites and results in the addition of 6 amino acids (TGDVPR) after the third SSB subunit. SSB- δ was amplified using 5' AvrII and 3' BamHI sites. To generate the SSB-LD construct, we cut the SSB- β -Topo plasmid with KpnI and BamHI and

¹ The experimental work presented in this appendix was performed by the co-authors of the corresponding publication that is in preparation. This is included as a companion for the work in Chapter 4.

² The contents of this chapter are in preparation for publication in collaboration with Tim Lohman's lab at Washington University and are presented here with few modifications.

inserted it into the SSB- α -pET21a vector followed by insertion of a stop codon at the end of the C-terminus using site-directed mutagenesis. Hence the C-terminus of the corresponding SSB-LD protein has the correct sequence at its C-terminus (MDFDDDIPF) required for binding of the SSB interacting proteins (SIPs).

Similarly, the SSB-LT construct was generated by splicing together the SSB- α , SSB- β , SSB- γ and SSB- δ fragments. To generate the SSB-LD-Drl construct, we designed a linker based on the sequence of *Deinococcus radiodurans* SSB protein (QLGTQPELIQDAGGGVRMSGGA). Using a primer that carried the coding sequence for these residues, we PCR amplified the SSB- α clone to end at position 112 followed by this linker sequence. The resulting product was pasted before the SSB- β gene yielding the SSB-LD-Drl construct. To generate the SSB-LT-Drl construct, we PCR amplified the SSB-LD-Drl sequence with flanking BamHI sites and pasted it onto to the end of the SSB-LD-Drl gene, followed by removal of the internal STOP codon. The individual deletion constructs were generated using site-directed mutagenesis. For the deletions in the linked dimers, PCR primers containing the appropriate ending sequences for the a subunit were used as primers in a PCR reaction containing wt SSB as template. The resulting PCR product was then cloned into the position of the SSB-LD pET21a plasmid. Plasmids for the *in vivo* bumping experiments were generated by cloning the entire *E. coli* SOS promoter region that controls the expression of the SSB and *UvrA* genes (Brandsma et al, 1985) and in front of the 5' ATG of the appropriate SSB coding sequence using flanking NdeI restriction sites. All the clones were confirmed by sequencing.

Purification of linked-SSB proteins: The SSB-LD, SSB-LT, SSB-LD-Drl and SSB-LT-Drl proteins were overexpressed in BL21(DE3) cells and purified using a procedure similar to that described for *E. coli* SSB (Bujalowski & Lohman, 1991; Lohman, 1986). All further steps were carried out at 4 °C. 30 g of cell paste was resuspended in 150 mL lysis buffer (50 mM Tris-Cl, pH 8.0, 1 mM EDTA, 10 % sucrose, 0.2 M NaCl, 15 mM spermidine, 1 mM PMSF and 2x protease inhibitor cocktail) and lysed using an Avestin cell disrupter (Avestin Inc., Canada) and the lysate was clarified by centrifugation. The linked SSB protein and DNA in the clarified lysate were precipitated by adding polyethyleneimine (PEI) to 0.2% (final). The protein was resuspended from the PEI pellet using 200 ml of buffer T^{0.4} (50 mM Tris-Cl, pH 8.0, 10 % glycerol, 1 mM EDTA, 0.4 M NaCl, 1 mM PMSF and 2x protease inhibitor cocktail). SSB from the PEI-resuspension was precipitated by adding solid ammonium sulfate (144 g/L) (25% saturation) and the pellet containing >90 % pure SSB was resuspended in 200 ml buffer T^{0.3} (50 mM Tris-Cl, pH 8.0, 15 % glycerol, 1 mM EDTA, 0.3 M NaCl, 1 mM PMSF and 2x protease inhibitor cocktail). The resuspended protein was loaded onto a ssDNA cellulose column (50 mL resin with ~3 mg/mL binding capacity) and eluted using 200 ml buffer T² (50 mM Tris-Cl, pH 8.0, 15 % glycerol, 1 mM EDTA, 2 M NaCl, 1 mM PMSF and 2x protease inhibitor cocktail). The linked SSB protein in the eluate was precipitated with 30.8% ammonium sulfate (170 g/L). The resulting precipitate was resuspended in 20 mL of storage buffer (30 mM Tris-Cl, pH 8.0, 50 % glycerol, 2 mM EDTA, 0.5 M NaCl, and 1x protease inhibitor cocktail) and stored as 5 mL aliquots at – 20°C. Before performing experiments, these proteins

were further fractionated over a S200 size exclusion column in buffer T^{0.5} (30 mM Tris-Cl, pH 8.0, 10 % glycerol, 1 mM EDTA, 0.5 M NaCl and 1x protease inhibitor cocktail). 3 ml fractions were collected throughout the procedure and the linked SSBs separate into distinct peaks. For the SSB-LD and SSB-LT, three distinct peaks are observed. The first peak corresponds to a higher order oligomeric species, the middle peak corresponds to an octamer and the last peak corresponds to a tetramer. For the SSB-LD-Drl and SSB-LT-Drl only the octameric and tetrameric species are observed. Once separated, the proteins do not redistribute into the higher order species at room temperature (Fig. S2.4). The tetrameric species was used for all the experiments described in this study. The fractions containing the tetramer were dialyzed into storage buffer (30 mM Tris-Cl, pH 8.0, 50 % glycerol, 2 mM EDTA, 0.5 M NaCl, and 1x protease inhibitor cocktail) and stored at -20 °C. The concentration of SSB was determined spectrophotometrically using the following extinction coefficients (ϵ_{280} for 4-OB folds): SSB-WT, SSB-S1, SSB-LD and SSB-LT = $1.13 \times 10^5 \text{ M}^{-1}\text{cm}^{-1}$; SSB-LD-Drl = $1.08 \times 10^5 \text{ M}^{-1}\text{cm}^{-1}$ and SSB-LT-Drl = $9.53 \times 10^5 \text{ M}^{-1}\text{cm}^{-1}$.

smFRET: The single-molecule fluorescence resonance energy transfer (smFRET) experiments were conducted with an objective-type total internal reflection (TIRF) microscope (Olympus IX71, IX2_MPITIRTL). A biotinylated DNA duplex/ssDNA having a SSB binding site (dT)₆₅ and a short hairpin containing a donor (cy3) and an acceptor (cy5) was generated by annealing a 5'-GCCTCGCTGCCGTCGCCA-biotin-3' with a 5'-TGGCGACGGCAGCGAGGC(T)₆₅-Cy3-TGTGACTGAGACAGTCACTT-Cy5-T-

3') and immobilized onto the NeutrAvidin coated glass cover slip. The prepared slide was kept on a slide holder (Model BC-300A, 20/20 Technology, Canada) and its temperature was controlled by a Bionomic Controller BC-110 (20/20 Technology, Canada). The objective temperature was controlled by an objective heater system, Rev. 4 (Bioprotechs, Inc., PA). The data collection and processing were done with software packages kindly provided by the Taekjip Ha (University of Illinois, Urbana Champaign) using IDL v.7.1 (Exelis Visual Information Solutions, CO) and Matlab v. 7.13 (MathWorks). The SSB binding site (dT)₆₅ was saturated with an 0.1 mM SSB solution (in 10 mM Tris pH 8.1, 0.1 mM Na₂EDTA, 0.5M NaCl - a salt concentration at which a single SSB protein is bound to (dT)₆₅) onto the channel and incubated for 5 to 10 minutes. Unbound (excess) SSB was removed by washing the channel with 200 ul or 20 channel volumes of an oxygen-deficient imaging buffer (10mM Tris (pH 8.1), 0.5 M NaCl, 0.1 mM Na₂EDTA, 2.5 mM Trolox (6-hydroxy-2,5,7,8-tetramethylchroman-2-carboxylic acid, Sigma Aldrich), 0.8% w/v D-glucose, 0.1 mg/ml glucose oxidase (Type VII, from *Aspergillus*, Sigma Aldrich), 0.02mg/ml catalase (from bovine liver, Sigma Aldrich)). At every spot, 2000 frames were collected with an exposure of 30 ms/frame at 25 C. Ten to forty spots were recorded all together. After corrections for leakage (from donor to acceptor) and detection efficiency, FRET traces for individual molecules were calculated. Molecules exhibiting anti-correlation changes in both donor and acceptors (FRET changes) were chosen for hidden Markov model (HMM) analysis to extract the transition rates between the FRET states. A histogram was created from the FRET traces (60 traces of SSB, 244

traces of SSB-LD-Drl, or 69 traces of SSB-LT-Drl) with a FRET efficiency bin-size of 0.01 and normalized to an area of 1.

Cy5.5 and Cy3 fluorophores were incorporated into the base of a hairpin DNA substrate positioned at the end of a (dT)₆₅ ssDNA (Fig. S2.5). We excite the Cy3 fluorophore and monitor the change in Cy5.5 fluorescence. As SSB diffuses onto the ssDNA formed by transiently fluctuations (breathing) of the base pairs at the base of the hairpin, a decrease in FRET signal is observed due to an increase in the distance between the fluorophores. Three FRET states are observed for the DNA when bound to WT SSB, SSB-LD-Drl and SSB-LT-Drl proteins. Previous studies (Roy et al, 2007; Roy et al, 2009; Zhou et al, 2011) suggest that each FRET state corresponds to roughly 2-3 bp melted in a two-step three-state pathway for SSB diffusion and hairpin melting. We designate the three states as A, B and C; where A and C are the end states depicting low FRET (fully melted) and high FRET (fully base paired) states, respectively, and B denotes the partially melted intermediate state (Fig. S2.5). A schematic of the probable states during the hairpin melting reaction is shown in Figure S2.5. These data indicate that the reduced number of C-terminal tails does not affect the ability of SSB to diffuse along ssDNA.

Transition states of SSB sliding: Using Hidden Markov Model analysis (HMM), we identified the distinct FRET states and calculated the rate of the transitions among the states which reflects SSB diffusion and DNA melting (Roy et al, 2007). The rates of the transitions among the three states are comparable for the SSB-LD-Drl [$k_{CB} = 1.1 \pm 0.6$, $k_{BA} = 0.8 \pm 0.4$, $k_{AB} = 0.6 \pm 0.3$ and $k_{BC} = 0.3 \pm 0.2$

respectively (Fig. S2.5)] and SSB-LT-Drl [$k_{CB} = 1 \pm 0.5$, $k_{BA} = 1 \pm 0.6$, $k_{AB} = 0.6 \pm 0.5$ and $k_{BC} = 0.2 \pm 0.1$ complexes (Fig. S2.3)]. However, they are slightly slower than the rates measured for wt SSB [$k_{CB} = 2.1 \pm 1$, $k_{BA} = 1.7 \pm 1.1$, $k_{AB} = 1.2 \pm 0.3$ and $k_{BC} = 0.6 \pm 0.2$ (Fig. S2.3)]. These data indicate that the reduced number of C-terminal tails does not affect the ability of SSB to diffuse along ssDNA, although the rates are reduced slightly.

Amino Acid Composition of the various SSB proteins used in this study:

(Note: The dotted lines denote deletions and the underlined sequence denote the various linkers. The amino acids in bold are the last 9 residues found in the C-terminus of the wild-type SSB protein).

SSB-WT

MASRGVNKVLVGNLGDPEVRYMPNGGAVANITLATSESWRDKATGEMKEQ
TEWHRVVLFGKLAEVASEYLRKGSQVYIEGQLRTRKWTDQSGQDRYTTEVVV
NVGGTMQMLGGRQGGGAPAGGNIGGGQPQGGWGQPQQPQGGNQFSGGA
QSRPQQSAPAAPSNEPP**MDFDDDIPF**

SSB-S1

MASRGVNKVLVGNLGDPEVRYMPNGGAVANITLATSESWRDKATGEMKEQ
TEWHRVVLFGKLAEVASEYLRKGSQVYIEGQLRTRKWTDQSGQDRYTTEVVV
NVGGTMQMLGGRQGGGAPAGGNIGGGQPQGGWGQPQQPQGGNQFSGGA
QSRPQQSAPAAPSNEPP**MDFDDDIPFTGASGT**

SSB-D120-166

MASRGVNKVLVGNLGQDPEVRYMPNGGAVANITLATSESWRDKATGEMKEQ
 TEWHRVVLFGKLAEVASEYLRKGSQVYIEGQLRTRKWTDQSGQDRYTTEVVV
 NVGGTMQMLGGRQGGG-----PP**MDFDDDIPF**

SSB-D130-166

MASRGVNKVLVGNLGQDPEVRYMPNGGAVANITLATSESWRDKATGEMKEQ
 TEWHRVVLFGKLAEVASEYLRKGSQVYIEGQLRTRKWTDQSGQDRYTTEVVV
 NVGGTMQMLGGRQGGGAPAGGNIGGG-----PP**MDFDDDIPF**

SSB-D151-166

MASRGVNKVLVGNLGQDPEVRYMPNGGAVANITLATSESWRDKATGEMKEQ
 TEWHRVVLFGKLAEVASEYLRKGSQVYIEGQLRTRKWTDQSGQDRYTTEVVV
 NVGGTMQMLGGRQGGGAPAGGNIGGGQPQGGWGQPQQPQGGNQFSGG---
 ----PP**MDFDDDIPF**

SSB-D162-166

MASRGVNKVLVGNLGQDPEVRYMPNGGAVANITLATSESWRDKATGEMKEQ
 TEWHRVVLFGKLAEVASEYLRKGSQVYIEGQLRTRKWTDQSGQDRYTTEVVV
 NVGGTMQMLGGRQGGGAPAGGNIGGGQPQGGWGQPQQPQGGNQFSGGA
 QSRPQQSAPA-----PP**MDFDDDIPF**

SSB-LT-Drl

MASRGVNKVILVGNLGQDPEVRYMPNGGAVANITLATSESWRDKATGEMKEQ
 TEWHRVVLFGKLAEVASEYLRKGSQVYIEGQLRTRKWTDQSGQDRYTTEVVV
 NVGGTMQMLLQGTQPELIQDAGGGVMSGAGTASRGVNKVILVGNLGQDPEV
 RYMPNGGAVANITLATSESWRDKATGEMKEQTEWHRVVLFGKLAEVASEYLR
 KGSQVYIEGQLRTRKWTDQSGQDRYTTEVVVNVGGTMQMLASHMASRGVNK
 VILVGNLGQDPEVRYMPNGGAVANITLATSESWRDKATGEMKEQTEWHRVVL
 FGKLAEVASEYLRKGSQVYIEGQLRTRKWTDQSGQDRYTTEVVVNVGGTMQM
LQGTQPELIQDAGGGVMSGAGTASRGVNKVILVGNLGQDPEVRYMPNGGA
 VANITLATSESWRDKATGEMKEQTEWHRVVLFGKLAEVASEYLRKGSQVYIEG
 QLRTRKWTDQSGQDRYTTEVVVNVGGTMQMLGGRQGGGAPAGGNIGGGQP
 QGGWGQPQQPQGGNQFSGGAQSRPQQSAPAAPSNEPP**MDFDDDIPF**

SSB-LD-Dri

MASRGVNKVILVGNLGQDPEVRYMPNGGAVANITLATSESWRDKATGEMKEQ
 TEWHRVVLFGKLAEVASEYLRKGSQVYIEGQLRTRKWTDQSGQDRYTTEVVV
 NVGGTMQMLLQGTQPELIQDAGGGVMSGAGTASRGVNKVILVGNLGQDPEV
 RYMPNGGAVANITLATSESWRDKATGEMKEQTEWHRVVLFGKLAEVASEYLR
 KGSQVYIEGQLRTRKWTDQSGQDRYTTEVVVNVGGTMQMLGGRQGGGAPA
 GGNIGGGQPQGGWGQPQQPQGGNQFSGGAQSRPQQSAPAAPSNEPP**MDF**
DDDIPF

SSB-LD

MASRGVNKVILVGNLGQDPEVRYMPNGGAVANITLATSESWRDKATGEMKEQ
 TEWHRVVLFGKLAEVASEYLRKGSQVYIEGQLRTRKWTDQSGQDRYTTEVVV
 NVGGTMQMLGGRQGGGAPAGGNIGGGQPQGGWGQPQQPQGGNQFSGGA
 QSRPQQSAPAAPSNEPPMDFDDDIPFTGASGTASRGVNKVILVGNLGQDPEVR
 YMPNGGAVANITLATSESWRDKATGEMKEQTEWHRVVLFGKLAEVASEYLRK
 GSQVYIEGQLRTRKWTDQSGQDRYTTEVVVNVGGTMQMLGGRQGGGAPAG
 GNIGGGQPQGGWGQPQQPQGGNQFSGGAQSRPQQSAPAAPSNEPP**MDFD**
DDIPF

SSB-LT

MASRGVNKVILVGNLGQDPEVRYMPNGGAVANITLATSESWRDKATGEMKEQ
 TEWHRVVLFGKLAEVASEYLRKGSQVYIEGQLRTRKWTDQSGQDRYTTEVVV
 NVGGTMQMLGGRQGGGAPAGGNIGGGQPQGGWGQPQQPQGGNQFSGGA
 QSRPQQSAPAAPSNEPPMDFDDDIPFTGASGTASRGVNKVILVGNLGQDPEVR
 YMPNGGAVANITLATSESWRDKATGEMKEQTEWHRVVLFGKLAEVASEYLRK
 GSQVYIEGQLRTRKWTDQSGQDRYTTEVVVNVGGTMQMLGGRQGGGAPAG
 GNIGGGQPQGGWGQPQQPQGGNQFSGGAQSRPQQSAPAAPSNEPPMDFD
 DDIPFTGPWIDASRGVNKVILVGNLGQDPEVRYMPNGGAVANITLATSESWRD
 KATGEMKEQTEWHRVVLFGKLAEVASEYLRKGSQVYIEGQLRTRKWTDQSGQ
 DRYTTEVVVNVGGTMQMLGGRQGGGAPAGGNIGGGQPQGGWGQPQQPQG
 GNQFSGGAQSRPQQSAPAAPSNEPPMDFDDDIPFTGDVPRASRGVNKVILV
 NLGQDPEVRYMPNGGAVANITLATSESWRDKATGEMKEQTEWHRVVLFGKLA
 EVASEYLRKGSQVYIEGQLRTRKWTDQSGQDRYTTEVVVNVGGTMQMLGGR

QGGGAPAGGNIGGGQPQGGWGQPQQPQGGNQFSGGAQSRPQQSAPAAPS

NEPPMDFDDDIPF

S2.2 Supplementary Table and Figures

Number	Plasmid Name	Ability to Complement
1	pEW-WT- <i>t</i>	Helper plasmid
2	pEW-WT- <i>a</i>	Positive Control - YES
3	pEW-SSB-S1- <i>a</i>	Negative Control - NO
4	pEW-SSB-LD-Drl- <i>a</i>	YES
5	pEW-SSB-LD- <i>a</i>	YES
6	pEW-SSB-LT-Drl- <i>a</i>	Dominant Negative
7	pEW-SSB-LT- <i>a</i>	Dominant Negative
8	pEW-SSB-D120-166- <i>a</i>	YES
9	pEW-SSB-D130-166- <i>a</i>	YES
10	pEW-SSB-D151-166- <i>a</i>	YES
11	pEW-SSB-D162-166- <i>a</i>	YES
12	pEW-SSB-LD- <i>a</i> -D120-177- <i>a</i>	NO
13	pEW-SSB-LD- <i>a</i> -D130-177- <i>a</i>	Dominant Negative
14	pEW-SSB-LD- <i>a</i> -D145-177- <i>a</i>	Dominant Negative
15	pEW-SSB-LD- <i>a</i> -D162-177- <i>a</i>	Dominant Negative
16	pEW-Dr-SSB- <i>a</i>	YES

Table S2.1 Plasmids used in this study. (-a or -t denotes plasmids carrying resistance to either ampicillin or tetracycline respectively)

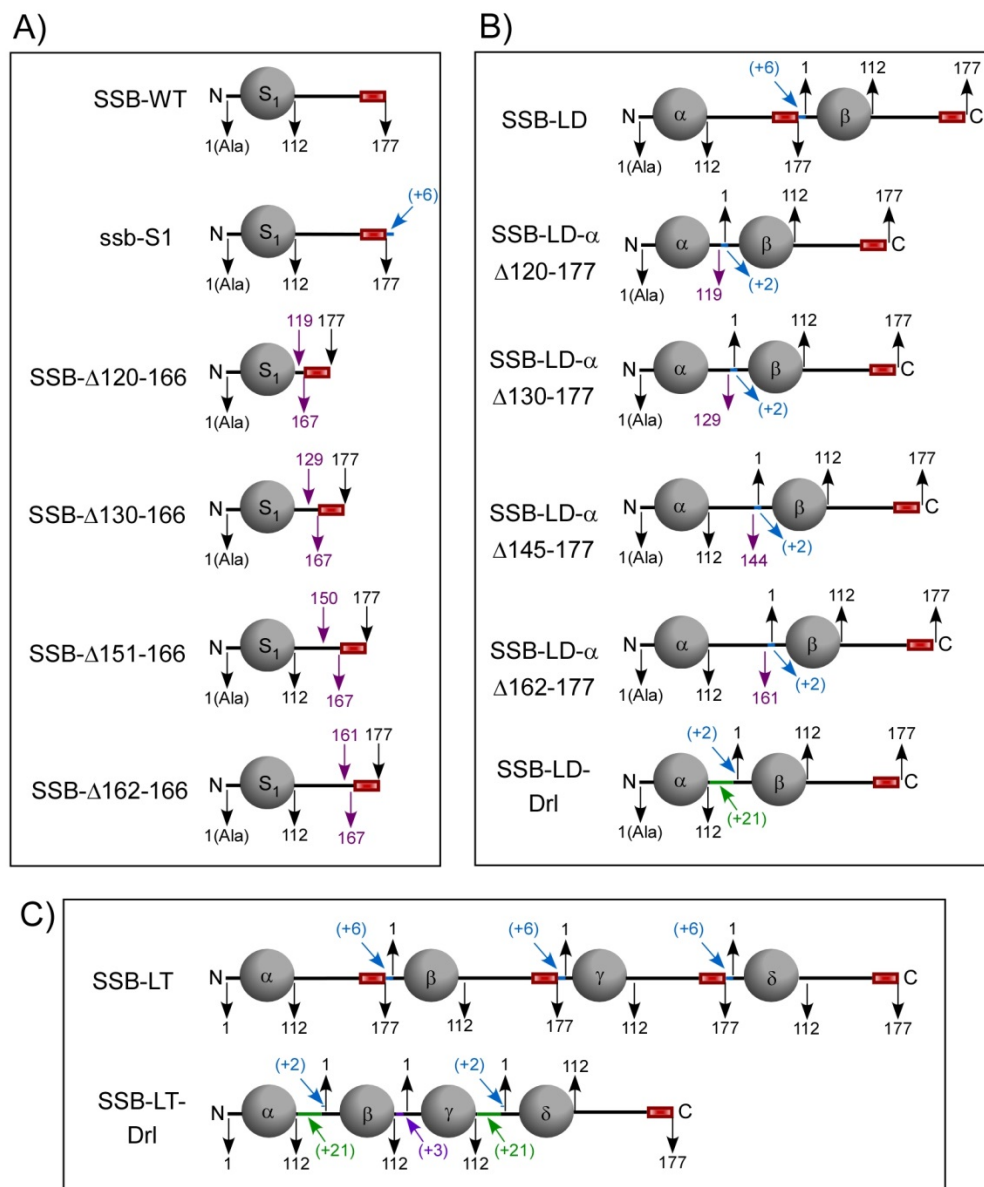


Figure S2.1 Schematic representation of the various SSB constructs used in this study. A) Constructs in which the linker region between the DNA binding core and the SIP interaction motif (C-terminal 11 amino acids) have been deleted to various lengths. B) Linked dimers with various linkers between the two linked DNA binding domains. C) Linked tetramers with either the full length linker or the Drl linker between the DNA binding domains. The number in green denotes the Drl linker and the number in blue denotes the amino acids introduced due to the unique restriction sites used to clone the linked versions. The purple numbers

and the corresponding arrows denote the missing amino acid residues in the deletion constructs and denote the linker between the SSB- β and SSB- γ subunits in the SSB-LT-Drl version.

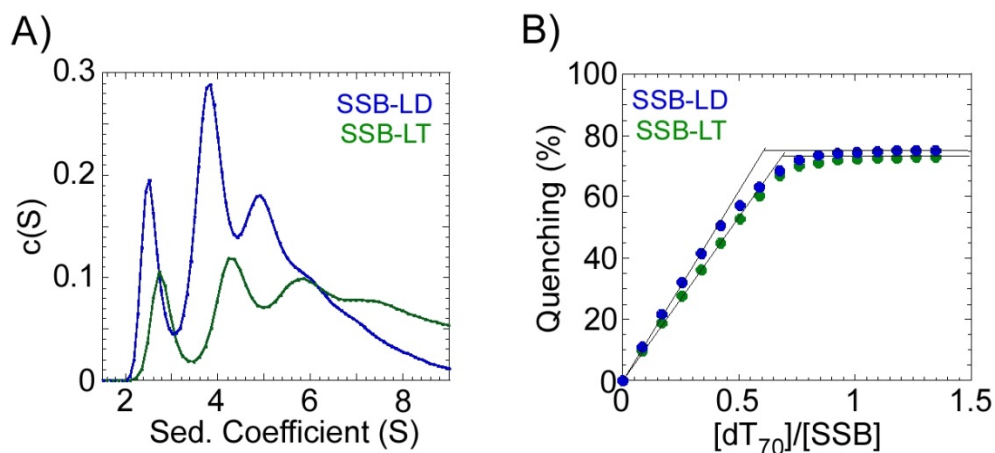


Figure S2.2 A) Analytical sedimentation experiments showing the presence of three or more species in the SSB-LD and SSB-LT protein preparations. The predicted molecular weights correspond to tetrameric, octameric and higher species in the reaction. B) Binding of the SSB-LD and SSB-LT proteins to $(dT)_{70}$. Protein preps containing a mixture of tetramers, octamers and higher order species are able to bind almost stoichiometrically to a $(dT)_{70}$ DNA substrate. These experiments were carried out in buffer containing 10 mM HEPES, pH 8.1, 0.1 mM EDTA, 500 mM NaCl and 10% v/v glycerol at 25 °C.

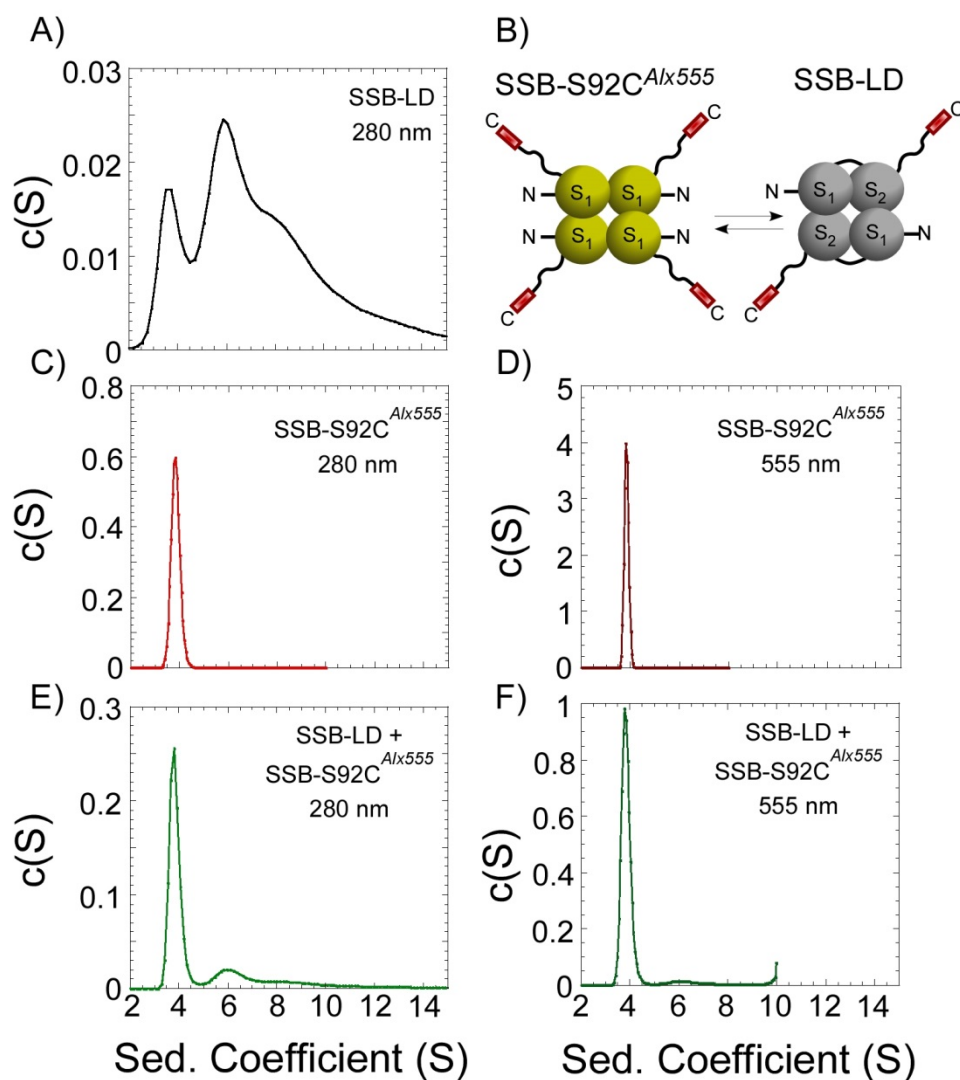
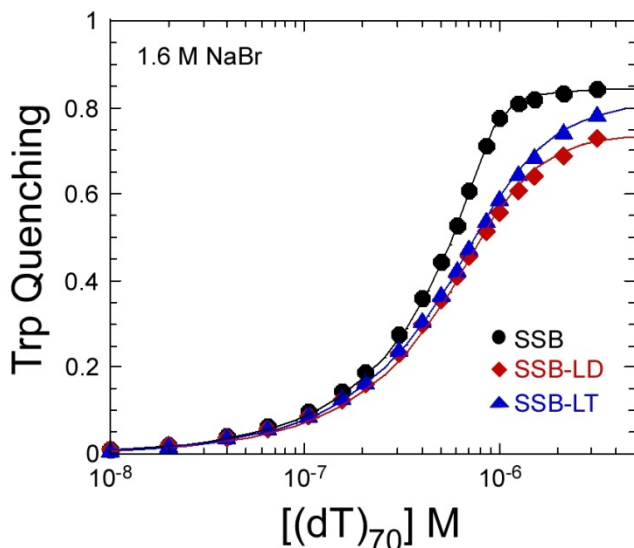


Figure S2.3 Stability of linked SSB tetramers. The mixed oligomeric pool of the purified linked SSB proteins were mixed with unlinked SSB proteins labeled with alexa-555 at position S92C. After 3 to 10 days of incubation at 25 °C, we tested the stability of the oligomeric proteins by analyzing the mixture using sedimentation velocity and monitoring the absorbance at both 280 nm and 555 nm. A) Shows the various oligomeric states of the SSB-LD protein. B) Is a schematic for the mixing experiment. C) and D) show a single tetrameric species for the labeled unlinked SSB protein at 280 nm and 555 nm respectively. E) and F) are the 280 nm and 555 nm absorbance profiles for the mixed experiment showing that the labeled-unlinked SSB subunits do not exchange with SSB-LD protein oligomeric mixtures.



SSB	K_{obs}
SSB-wt	$9.0 \pm 1.6 \times 10^7 \text{ M}^{-1}$
SSB-LD-Drl	$9.6 \pm 1.4 \times 10^6 \text{ M}^{-1}$
SSB-LT-Drl	$6.6 \pm 0.4 \times 10^6 \text{ M}^{-1}$

Figure S2.4 Binding affinity of SSB to $(\text{dT})_{70}$ in NaBr. Since all the SSB proteins bound to DNA stoichiometrically, we measured their binding affinity to a $(\text{dT})_{70}$ molecule in buffer containing NaBr (10 mM Tris-Cl, pH 8.1, 0.1 mM EDTA and 1.6 M NaBr). SSB-WT binds tightly with a $K_{\text{obs}} = 9 \pm 1.6 \times 10^7 \text{ M}^{-1}$ as previously reported (Bujalowski & Lohman, 1989). The SSB-LD-Drl and SSB-LT-Drl proteins also bind tightly to $(\text{dT})_{70}$, but with a ten-fold lower affinity ($K_{\text{obs}} = 9.6 \pm 1.4 \times 10^6 \text{ M}^{-1}$ & $6.6 \pm 0.4 \times 10^6 \text{ M}^{-1}$ for SSB-LD-Drl and SSB-LT-Drl respectively) compared to the SSB-WT protein (Bujalowski & Lohman, 1989). The data were fit as described (Bujalowski & Lohman, 1989).

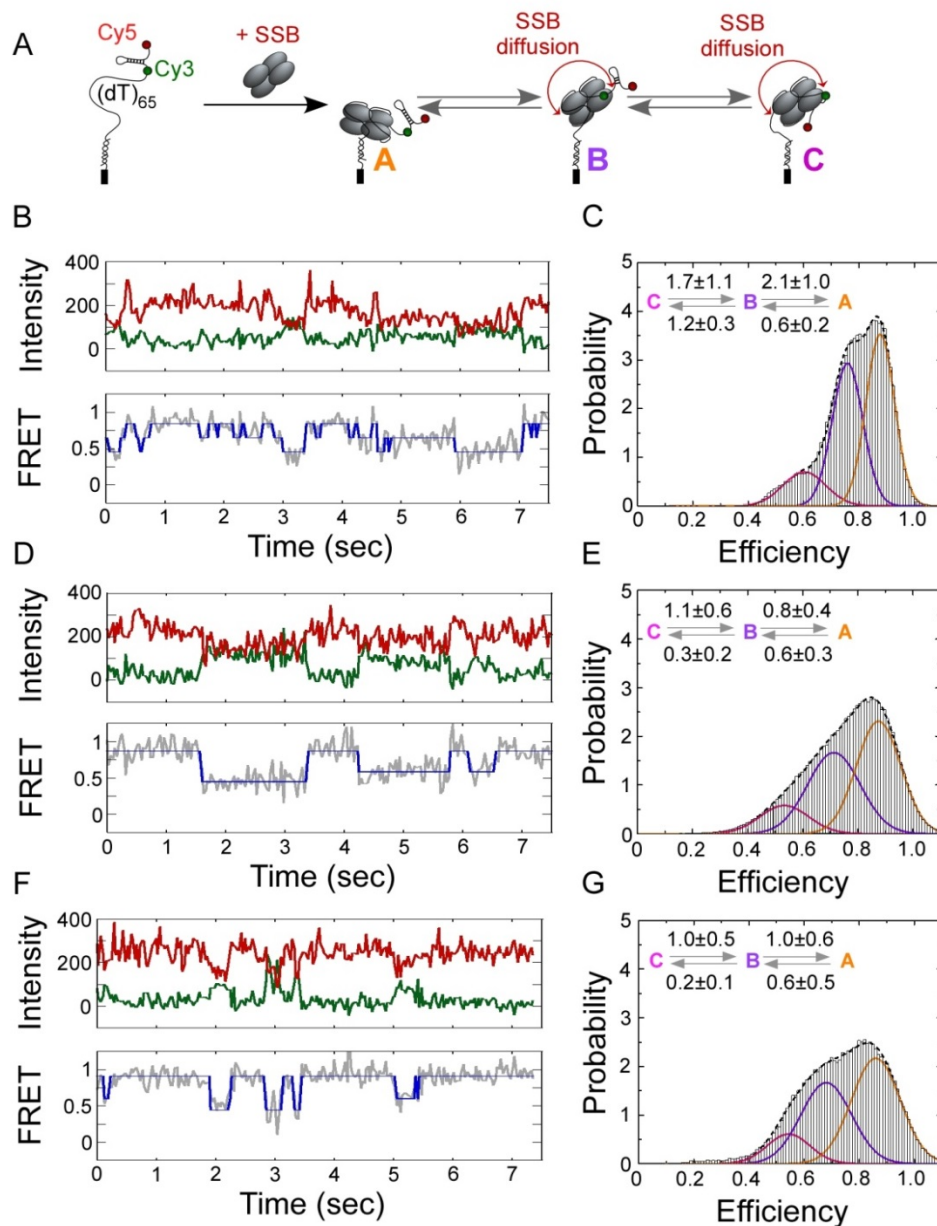


Figure S2.5 smFRET analysis showing diffusion and duplex melting activities of SSB tetramers. A) Schematic of the DNA substrate used to monitor DNA melting associated with diffusion of SSB on ssDNA. The three predicted FRET states are also shown as A, B and C. Individual fluorescence changes in the donor (green) and acceptor (red) are shown along with the resulting change in FRET (grey) for SSB-WT (B), SSB-LD-Drl (D) and SSB-LT-Drl (F). The blue line denotes a Hidden Markov Model analysis of the FRET traces to identify distinct states upon SSB diffusion and melting of the hairpin. C, E and G are histograms showing the presence of various FRET efficiencies for the SSB-WT, SSB-LD-Drl and SSB-LT-Drl tetramers respectively. The forward and backward rates for the transitions between the three states for each experiment are also depicted.

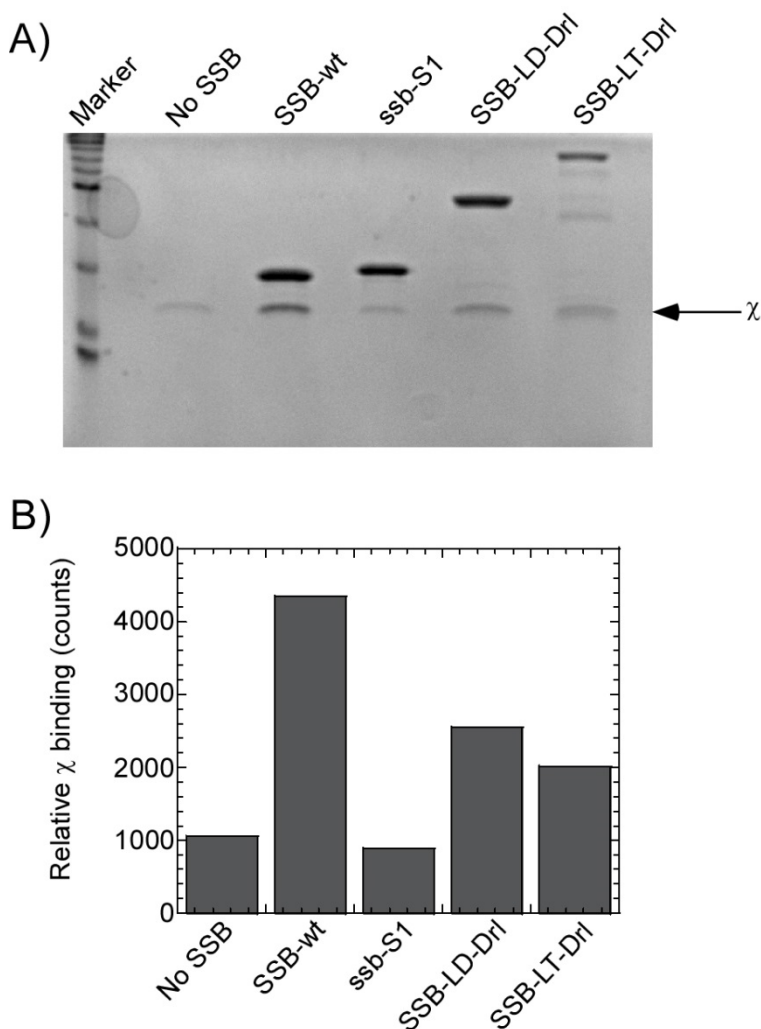


Figure S2.6 Interaction between SSB and χ monitored using ammonium sulfate precipitation analysis. Interaction between SSB and χ was measured using the ammonium sulfate precipitation protein pull down technique (Shereda et al, 2007). SSB is selectively precipitated when incubated with 0.15 g/L ammonium sulfate and any interacting χ also co-precipitates. A) SDS-PAGE gel showing the resuspended precipitate of ammonium sulfate precipitation done in the absence (No SSB lane) or presence of 5 μ M each (total concentration of OB-folds) of SSB-WT, ssb-S1, SSB-LD-Drl or SSB-LT-Drl. All the experiments had 20 μ M χ in the reaction. B) The amount of χ pulled down was quantified using ImageJ (Schneider et al, 2012) and the plot shows that the amount of χ binding to the SSB proteins is proportional to the number of C-terminal tails associated with the respective construct. SSB-WT (4 tails) has the highest amount of χ pulled down compared to the SSB-LD-Drl (2 tails) and the SSB-LT-Drl (1 tail) proteins. Background χ binding to ssb-S1 (no functional tails) and χ precipitated in the absence of any SSB in the reaction is also shown.

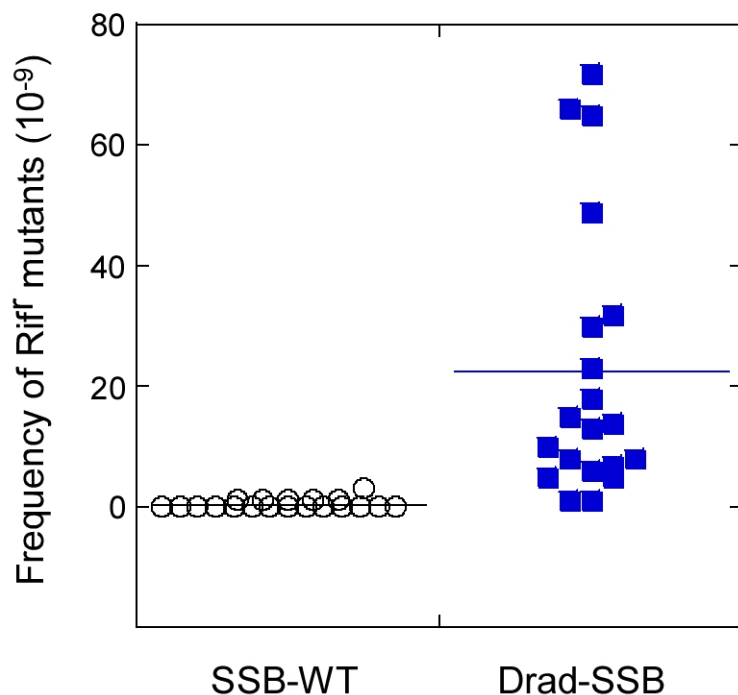


Figure S2.7 Rate of spontaneous mutagenesis in *E. coli* cells carrying the SSB protein from *Deinococcus radiodurans* (*Drad*-SSB). Cells were derived from the bumping experiment where the native *E. coli* SSB protein was functionally replaced by the *Drad*-SSB protein. These cells were treated with rifampicin and the surviving colonies were counted. The data show that these cells possessing *Drad*-SSB with two C-terminal tails has a high frequency of mutagenesis similar to cells with the SSB-LD-Drl version (Fig. 4.7A).

S2.3 Supplemental References

Brandsma JA, Bosch D, de Ruyter M, van de Putte P (1985) Analysis of the regulatory region of the *ssb* gene of *Escherichia coli*. *Nucleic acids research* **13**: 5095-5109

Bujalowski W, Lohman TM (1989) Negative co-operativity in *Escherichia coli* single strand binding protein-oligonucleotide interactions. II. Salt, temperature and oligonucleotide length effects. *Journal of molecular biology* **207**: 269-288

Bujalowski W, Lohman TM (1991) Monomers of the *Escherichia coli* SSB-1 mutant protein bind single-stranded DNA. *Journal of molecular biology* **217**: 63-74

Lohman TM (1986) Kinetics of protein-nucleic acid interactions: use of salt effects to probe mechanisms of interaction. *CRC Crit Rev Biochem* **19**: 191-245

Roy R, Kozlov AG, Lohman TM, Ha T (2007) Dynamic structural rearrangements between DNA binding modes of E. coli SSB protein. *Journal of molecular biology* **369**: 1244-1257

Roy R, Kozlov AG, Lohman TM, Ha T (2009) SSB protein diffusion on single-stranded DNA stimulates RecA filament formation. *Nature* **461**: 1092-1097

Schneider CA, Rasband WS, Eliceiri KW (2012) NIH Image to ImageJ: 25 years of image analysis. *Nature methods* **9**: 671-675

Shereda RD, Bernstein DA, Keck JL (2007) A central role for SSB in Escherichia coli RecQ DNA helicase function. *The Journal of biological chemistry* **282**: 19247-19258

Zhou R, Kozlov AG, Roy R, Zhang J, Korolev S, Lohman TM, Ha T (2011) SSB Functions as a Sliding Platform that Migrates on DNA via Reptation. *Cell* **146**: 222-232

Appendix 3

Investigation on *E. coli* Pol III exchange at the replication fork

S3.1 Introduction

Wild-type DNA polymerase (wt gp43) in the bacteriophage T4 system exhibits high processivity (Kaboord and Benkovic, 1995). However, gp43 within the replisome can be readily replaced by an exogenous mutant gp43 (gp43-D408N). gp43 D408N is incapable of elongating primers but retains the ability to form an initiation complex at the replication fork (Yang et al., 2004). Therefore, gp43-D408N can compete with gp43 and serve as a trap to inhibit both leading and lagging strand synthesis. It was observed that both leading and lagging strand synthesis in a coupled reaction initiated by gp43 were inhibited by the addition of gp43-D408N within a time period shorter than the dissociation rate of gp43. These results suggest that gp43-D408N actively displaces gp43, rather than passively binding template after dissociation of wt gp43. It was proposed that the C-terminus of the incoming polymerases binds the interdomain loop of one subunit of the clamp and displaces the polymerase at the replication fork (Yang et al., 2004).

Similarly, in the bacteriophage T7 system, a complex of wild-type DNA polymerase (gp5) and its processivity factor, *E. coli* thioredoxin (trx), can readily exchange with excess mutant gp5-thioredoxin complexes (gp5-Y526F/trx) without affecting high processivity. Replacing tyrosine 526 with phenylalanine in the nucleotide binding site made the mutant gp5 resistant to inhibition of ddNTPs but does not affect its ability to bind to other protein components and elongate primers. Both strand

displacement synthesis and leading strand synthesis in a coupled reaction initiated by gp5-Y526F/trx are inhibited upon addition of gp5/trx and ddNTPs, which indicates that wild-type polymerase exchanges (Johnson et al., 2007). Exchange was not observed in a ssDNA replication reaction where helicase was not included. To explain why the T7 polymerase retains high processivity, yet exchanges with other polymerases, it was proposed that more than one copy of polymerase binds different subunits of the hexameric T7 helicase and exchanges with polymerase that transiently dissociates (Johnson et al., 2007).

eYFP-tagged *E. coli* Pol III α proteins were detected by a whole-cell single molecule technique when they bound near the replication fork (Xie et al., 2008). Repetitive bursts of fluorescence intensity were obtained in living cells with fluorescent Pol III α , which indicates that new polymerases continuously bind to the replication fork. Otherwise, no signal would be seen after fluorescent proteins on the originally bound Pol III α photobleached. It was proposed that either a free polymerase directly replaced the polymerase within the replisome on the lagging strand (Lia et al., 2012).

S3.2 Results

S3.2.1 Exogenous D403E Pol III does not exchange with Pol III at the replication fork

To test whether the *E. coli* Pol III at the replication fork dynamically exchanges with free Pol III in solution as Lia et al. proposed (Lia et al., 2012), I employed a dominant negative mutant *E. coli* Pol III α (α -D403E) that is able to form an initiation complex at the replication fork, but cannot elongate (Pritchard and McHenry, 1999;

Downey and McHenry, 2010). When D403E Pol III was pre-mixed with wild-type *E. coli* Pol III to form an initiation complex, rolling circle DNA replication was inhibited in proportion to the concentration of D403E Pol III as expected (Fig. S3.1A). When D403E Pol III was added to an ongoing rolling circle DNA replication reaction, I discovered that the amount of leading and lagging strand synthesis did not change (Fig. S3.1B). This result shows that exogenous Pol III does not exchange with Pol III within the replisome (Lia et al., 2012).

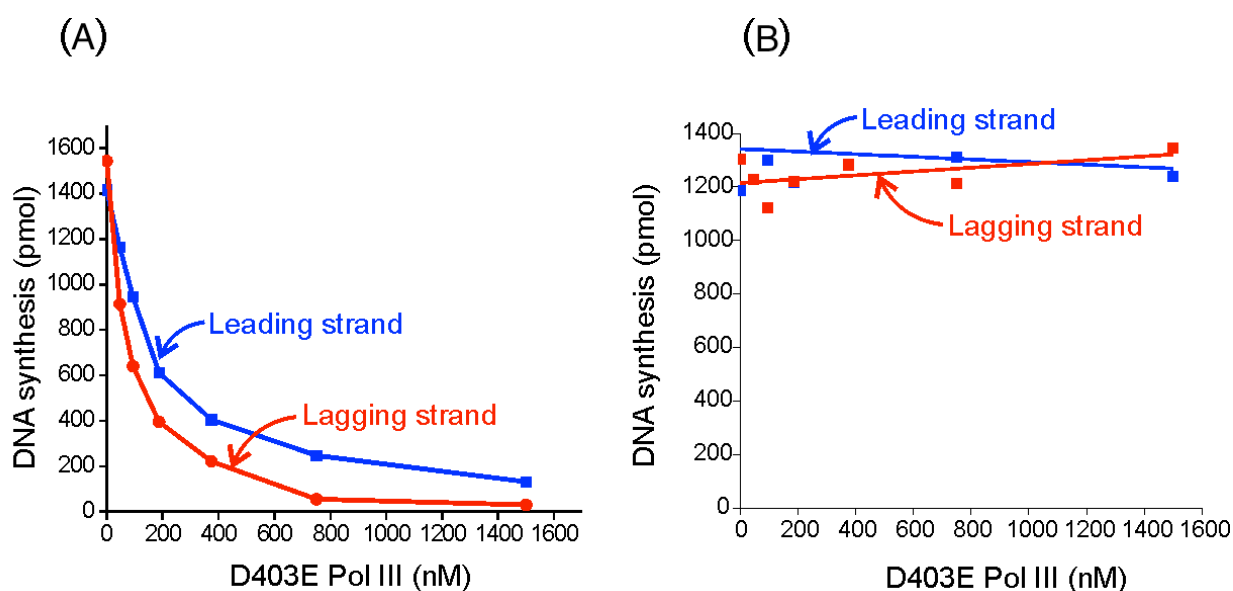


Figure S3.1 *E. coli* Pol III at the replication fork is resistant to inhibition by D403E Pol III. (A) Protein components required for a rolling circle reaction were added to a pre-mixed solution of wild-type Pol III and D403E Pol III. After initiation complex formation, rolling circle replication reaction was started by the addition of 1 mM ATP, 100 μ M dNTPs, and α -[32 P]-dCTP/dGTP. (B) D403E Pol III was added to an ongoing rolling circle DNA reaction.

S3.2.2 Exogenous D403E *E. coli* Pol III* exchanges with Pol III* at the replication fork

I also tested whether exogenous D403E Pol III* was able to compete with wild-type Pol III* at the replication fork. In a control reaction, D403E Pol III* inhibited a rolling circle reaction when pre-mixed with wild-type Pol III* to form initiation complex (Fig.

S3.2A). Surprisingly, D403E Pol III* also inhibited an ongoing rolling circle reaction. Lagging strand synthesis could be fully inhibited with sufficient D403E Pol III*, but leading strand synthesis was only reduced about two-fold (Fig. S3.2B).

This result may reconcile the conflict between our finding that free polymerase cannot exchange with Pol III at the replication fork (Fig. S3.2) and the single molecule experiments that were interpreted to indicate that free Pol III could dynamically exchange at replication fork (Lia et al., 2012). I believe that the bursts of fluorescence they observed may result from Pol III* exchange at the replication fork, since it is not possible to distinguish between Pol III and Pol III* from the fluorescence assay they conducted. They could also have observed exogenous Pol III required for other processes associated with the nascent replication product, such as mismatch repair. Involvement of the DnaX complex in Pol III* exchange indicates that interactions via the DnaX complex are important for polymerase exchange. Because τ interacts with both Pol III and helicase, multiple copies of the DnaX complex containing the τ subunit and attached Pol III might bind helicase as a Pol III* repository awaiting exchange at the replication fork as proposed in the T7 system (Johnson et al., 2007). Intact Pol III* might replace Pol III* at the replication fork.

Greater inhibition of lagging strand synthesis than leading suggests that the lagging strand polymerase is more labile to exchange. Because a lagging strand polymerase must frequently dissociate from Okazaki fragments, it might be subject more frequent exchange.

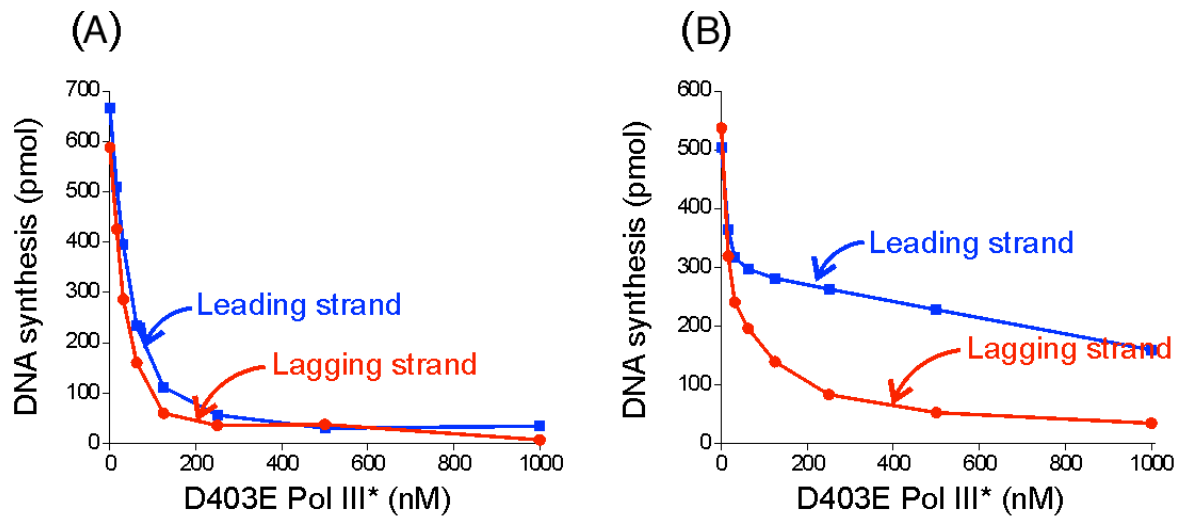


Figure S3.2 D403E Pol III* outcompetes the Pol III* at the replication fork. (A) The initiation complex was formed by pre-mixing both wild-type Pol III* and D403E Pol III*. Rolling circle replication reaction was then started by the addition of 1 mM ATP, 100 μ M dNTPs, and α -[32 P]-dCTP/dGTP. (B) D403E Pol III* was added to an ongoing rolling circle DNA reaction.

S3.2.3 DnaX complex with one inactive ATPase is not competent for rolling circle DNA replication

In order to explore how one inactive DnaX ATPase affects coupled leading and lagging strand synthesis, a rolling circle reaction was conducted with reconstituted Pol III* containing either one wild-type γ DnaX subunit (Pol III_{2 τ 2 γ 1 $\delta\delta'$ $\chi\psi$) or one mutant K51E γ DnaX subunit (Pol III_{2 τ 2 γ 1* $\delta\delta'$ $\chi\psi$). The mutation occurs within the Walker A motif abolishing ATP binding (Wieczorek et al., 2010). ATP binding changes the conformation of the DnaX complex, leading to clamp opening and enhanced affinity of the DnaX complex for β_2 and template (Ason et al., 2000; Jeruzalmi et al., 2001). One inactive ATPase causes the rate of initiation complex formation on ssDNA to be 30-fold lower (Wieczorek et al., 2010; Downey et al., 2011). In a rolling circle replication reaction, an initiation complex must be formed before each new Okazaki fragment is synthesized.}}

Therefore, it is expected that a DnaX complex containing one inactive ATPase may cause delayed initiation of Okazaki fragment elongation. In order to study whether an inactive ATPase affects the polymerase cycling process, dGDPNP was used in a rolling circle reaction, as dGDPNP slows the rate of lagging strand polymerase, leading to short Okazaki fragments and gaps between them (Chapter III). Defect of ATP binding may give rise to shorter fragments and longer gaps.

In the presence of Pol III* containing mutant γ , no Okazaki fragments was observed on an alkaline agarose gel, and the amount of total DNA synthesis was about 20-fold less than in the presence of Pol III* containing wt γ (Fig. S3.3). This result demonstrates the significance of ATPase for both leading and lagging strand synthesis. Because of the frequent initiation complex formation on the lagging strand in a rolling circle reaction, slowing the rate of initiation complex formation by the inactive ATPase should exert much more severe effect than in a ssDNA replication reaction.

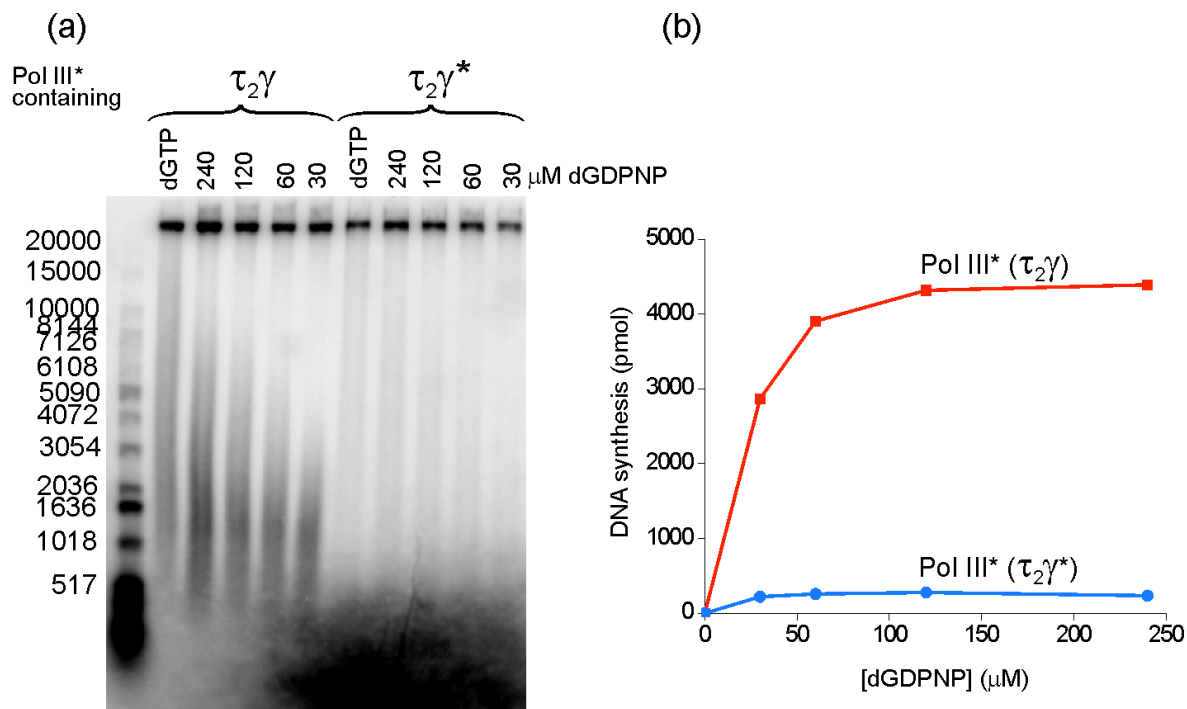


Figure S3.3 Pol III* with the DnaX complex ($\tau_2\gamma$) containing an inactive ATPase cannot support the rolling circle reaction as Pol III* with DnaX complex ($\tau_2\gamma$). (A) 32 P-dATP labeled reaction products were loaded onto alkaline agarose gel. The samples were loaded with similar amount of radioactivity in each lane or the largest quantity that I was able to obtain (from left to right: 0.7 μ l/146 kcpm, 1.9 μ l/154 kcpm, 2.0 μ l/154 kcpm, 2.2 μ l/152 kcpm, 2.9 μ l/148 kcpm, 25 μ l/74 kcpm, 25 μ l/106 kcpm, 25 μ l/124 kcpm, 25 μ l/116 cpm, 25 μ l/98 kcpm). (B) The amount of total DNA synthesis in the rolling circle reaction corresponding to (A) was quantified using scintillation counting.

S3.3 Materials and Methods

Proteins: Wild-type overexpressed Pol III* (Chapter III, Materials and methods), reconstituted Pol III* (Pol III $_{2\tau_2\gamma\delta\delta'\chi\psi}$) (Chapter III, Materials and methods), wild-type Pol III (Kim and McHenry, 1996), D403E Pol III α (Pritchard & McHenry, 1999), ϵ (Scheuermann and Echols, 1984), θ (Carter et al., 1993), τ -complex (Pritchard et al., 2000), DnaX complex with wild-type γ ($\tau_2\gamma\delta\delta'\chi\psi$) (Pritchard et al., 2000), DnaX complex with mutant γ ($\tau_2\gamma^*\delta\delta'\chi\psi$) (Wieczorek et al., 2010) were purified as described. All other protein components for rolling circle DNA replication was prepared as described in

Appendix 1, supplement for Chapter III. D403E Pol III was assembled by incubating D403E Pol III α , ϵ , and θ at a ratio of 1:1:1 on ice for 15 min. D403E Pol III* was assembled by incubating D403E Pol III α , ϵ , θ and τ -complex at a ratio of 3:3:3:1 on ice for 15 min. Pol III* (Pol III₂ $\tau_2\gamma^*\delta\delta'\chi\psi$) was assembled by incubating Pol III and the DnaX complex ($\tau_2\gamma^*\delta\delta'\chi\psi$) at a ratio of 4:1 at room temperature for 5 min and purified by Mono-S column.

Competition experiments with D403E Pol: A rolling circle reaction was conducted as described in Chapter III in the section of “optimized rolling circle reaction with 20 nM mini-circle template” except that 2.5 nM overproduced Pol III* was replaced with 10 nM wild-type Pol III and 2.5 nM τ -complex. 100 nM DnaG was replaced with 25 nM DnaG, and varied amounts of D403E Pol III was added at the same time with α -[³²P]-dCTP or α -[³²P]-dGTP. In the control experiment to test inhibition of D403E Pol III, wild-type Pol III and varied D403E Pol III were combined first and then mixed with other components to form an initiation complex. After 5 min, 1 mM ATP, 100 μ M dNTPs, and α -[³²P]-dCTP or α -[³²P]-dGTP were added to start the reaction. After another 8 min, the reaction was quenched with 83 mM EDTA final concentration.

Competition experiments with D403E Pol III:* A rolling circle reaction was conducted as described in Chapter III in the section of “optimized rolling circle reaction with 20 nM mini-circle template” except 100 nM DnaG was replaced with 25 nM DnaG and varied amounts of D403E Pol III* was added at the same time with α -[³²P]-dCTP or α -[³²P]-dGTP. A control experiment was conducted as described in “Competition

experiments with D403E Pol III”, except D403E Pol III* was combined with other component to form an initiation complex.

Rolling circle replication assay with Pol III containing wild-type and mutant γ DnaX subunits:* Optimized rolling circle reactions in the presence of dGTP and dGDPNP were performed as described in Chapter III except Pol III* reconstituted with wild-type γ (Pol III_{2 τ 2 γ $\delta\delta'$ $\chi\psi$) or mutant γ (Pol III_{2 τ 2 γ^* $\delta\delta'$ $\chi\psi$) were substituted for the overexpressed Pol III*, and α -[³²P]-dATP was substituted for α -[³²P]-dCTP and α -[³²P]-dGTP to allow simultaneous labeling of leading and lagging strand products.}}

S3.4 References

- Ason, B., Bertram, J.G., Hingorani, M.M., Beechem, J.M., Donnell, M.O., Goodman, M.F., and Bloom, L.B. (2000). A model for Escherichia coli DNA polymerase III holoenzyme assembly at primer/template ends. *The Journal of Biological Chemistry* 275, 3006–3015.
- Carter, J., Franden, M.A., Aebersold, R., Kim, D.R., and McHenry, C.S. (1993). Isolation, sequencing and overexpression of the gene encoding the θ subunit of DNA polymerase III holoenzyme. *Nucleic Acids Research* 21, 3281–3286.
- Downey, C.D., Crooke, E., and McHenry, C.S. (2011). Polymerase chaperoning and multiple ATPase sites enable the E. coli DNA polymerase III holoenzyme to rapidly form initiation complexes. *Journal of Molecular Biology* 412, 340–353.
- Downey, C.D., and McHenry, C.S. (2010). Chaperoning of a replicative polymerase onto a newly assembled DNA-bound sliding clamp by the clamp loader. *Molecular Cell* 37, 481–491.
- Jeruzalmi, D., O'Donnell, M., and Kuriyan, J. (2001). Crystal structure of the processivity clamp loader gamma (gamma) complex of E. coli DNA polymerase III. *Cell* 106, 429–441.
- Johnson, D.E., Takahashi, M., Hamdan, S.M., Lee, S.-J., and Richardson, C.C. (2007). Exchange of DNA polymerases at the replication fork of bacteriophage T7. *Proceedings of the National Academy of Sciences of the United States of America* 104, 5312–5317.

Kaboord, B.F., and Benkovic, S.J. (1995). Accessory proteins function as matchmakers in the assembly of the T4 DNA polymerase holoenzyme. *Current Biology : CB* 5, 149–157.

Kim, D.R., and McHenry, C.S. (1996). In vivo assembly of overproduced DNA polymerase III. *The Journal of Biological Chemistry* 271, 20681–20689.

Lia, G., Michel, B., and Allemand, J.-F. (2012). Polymerase exchange during Okazaki fragment synthesis observed in living cells. *Science* 335, 328–331.

Pritchard, A.E., Dallmann, H.G., Glover, B.P., and McHenry, C.S. (2000). A novel assembly mechanism for the DNA polymerase III holoenzyme DnaX complex: association of $\delta\delta'$ with DnaX4 forms DnaX3 $\delta\delta'$. *The EMBO Journal* 19, 6536–6545.

Pritchard, A.E., and McHenry, C.S. (1999). Identification of the acidic residues in the active site of DNA polymerase III. *Journal of Molecular Biology* 285, 1067–1080.

Scheuermann, R.H., and Echols, H. (1984). A separate editing exonuclease for DNA replication: the epsilon subunit of Escherichia coli DNA polymerase III holoenzyme. *Proceedings of the National Academy of Sciences of the United States of America* 81, 7747–7751.

Wieczorek, A., Downey, C.D., Dallmann, H.G., and McHenry, C.S. (2010). Only one ATP-binding DnaX subunit is required for initiation complex formation by the Escherichia coli DNA polymerase III holoenzyme. *The Journal of Biological Chemistry* 285, 29049–29053.

Xie, X.S., Choi, P.J., Li, G.-W., Lee, N.K., and Lia, G. (2008). Single-molecule approach to molecular biology in living bacterial cells. *Annual Review of Biophysics* 37, 417–444.